TESIS DE LA UNIVERSIDAD DE ZARAGOZA

2024

437

Eduardo Martínez Carrasco

Distance protection function under high penetration of renewable energies based on power electronics. Development of an enhanced faulted phase selector

Director/es
Comech Moreno, María Paz

ISSN 2254-7606

Prensas de la Universidad
Universidad Zaragoza

Universidad de Zaragoza
Servicio de Publicaciones

ISSN 2254-7606

Universidad Zaragoza
1542

Tesis Doctoral

DISTANCE PROTECTION FUNCTION UNDER HIGH PENETRATION OF RENEWABLE ENERGIES BASED ON POWER ELECTRONICS. DEVELOPMENT OF AN ENHANCED FAULTED PHASE SELECTOR

Autor

Eduardo Martínez Carrasco

Director/es

Comech Moreno, María Paz

UNIVERSIDAD DE ZARAGOZA
Escuela de Doctorado

Programa de Doctorado en Energías Renovables y Eficiencia Energética

2022

Distance protection function under high penetration of renewable energies based on power electronics. Development of an enhanced faulted phase selector

Eduardo Martínez Carrasco

Universidad de Zaragoza

PhD Program: Renewable Energies and Energy Efficiency

Universidad Zaragoza

Supervised by: María Paz Comech

Contents

List of abbreviations

APE	Actual PE penetration
AVR	Automatic Voltage Regulator
AVR	Automatic Voltage Regulator
CBF	Circuit breaker failure
CCT	Critical clearing time
COI	Centre of inertia
CT	Current Transformer
DC	Direct Current
DFIG	Doubly Fed Induction Generator
DRF	Double Reference Frame
FC	Full Converter
FPI	Front Panel Interface
FRT	Fault Ride Through
FT	Frequency threshold
FCWT	Full Converter Wind Turbine
GSCC	Grid Side Converter Control
GSVSC	Grid-Side Voltage Source Convertor
H_{APE}	Inertia time constant of the system under actual PE penetration
HiL	Hardware in the Loop
H_{PPE}	Inertia time constant of the system under presumed PE penetration
HVDC	High Voltage Direct Current
HVFPI	High Voltage Front Panel Interface
IGBT	Insulated-Gate Bipolar Transistor
LL Fault	Line to line fault
LLG Fault	Line to line to ground fault
LLL Fault	Three phase fault
LSA	Load shedding amount
LVRT	Low voltage ride through
LVRT	Low Voltage Ride Through
MPPT	Maximum Power Point Tracking
PCC	Point of Common Coupling
P_{Dist}	Active power lost due to outage of generation unit(s)
PE	Power Electronics

PF	Power factor
PI	Proportional-Integral
PLL	Phase Locked Loop
PMSG	Permanent Magnet Synchronous Machine
P_{PE}	Active power generated by PE-devices
PPE	Presumed PE penetration
PSB	Power swing blocking
P_{SG}	Active power generated by synchronous generators
PST	Power swing tripping
PV	Photovoltaic
PV	PhotoVoltaic
RSCC:	Rotor Side Converter Control
RTDS	Real-Time Digital Simulator
SG	Syncrhonous Generator
SLG Fault	Single line to ground fault
SRF	Single Reference Frame
TOWI	Trip-on-the-way-in
TOWO	Trip-on-the-way-out
UC	Unit commitment
UFLS	Under-frequency load shedding
UVLS	Under-voltage load shedding
VSC	Voltage Source Convertor
WT	Wind Turbine

List of figures

List of tables

Resumen y conclusiones

Los objetivos asociados con la transición energética llevan consigo un importante incremento del nivel de penetración de la generación renovable basada en electrónica de potencia en la red eléctrica. Existen numerosas diferencias entre el comportamiento de este tipo de generación y la generación síncrona convencional, lo que puede afectar al control y operación del sistema. Entre estas diferencias, destacan las relacionadas con la aportación de corriente durante faltas producidas en el sistema eléctrico de potencia, lo que puede afectar al correcto funcionamiento de los sistemas de protección.

En esta tesis se aborda el funcionamiento de los sistemas de protección en redes de transporte ante la creciente penetración de energías renovables. El análisis se realiza mediante el ensayo de equipos de protección comerciales en las condiciones de aportación de corriente proveniente mayoritariamente de fuentes renovables mediante simulaciones HiL (Hardware in the Loop), con el objetivo de comprobar la problemática que puede encontrarse en un futuro cercano. A partir de los resultados se realizó el diseño de soluciones prácticas e implementables en los equipos de protección actualmente presentes en el mercado.

La realización de este trabajo vino motivada por la necesidad que los TSOs (Transmission System Operators) europeos de estudiar el efecto que las energías renovables pueden tener en la operación y seguridad de la red. Para satisfacer estas necesidades, entre otras iniciativas, surgió el proyecto H2020 MIGRATE (https://www.h2020-migrate.eu/), donde se desarrolló el estudio que se presenta en esta tesis doctoral, centrada en el estudio del impacto de las energías renovables en los sistemas de protección de la red eléctrica.

Para alcanzar este objetivo, se distribuyó el trabajo en diferentes fases que en esta tesis corresponden a cada uno de los capítulos de este documento.

En un primer capítulo se incluye el modelado de generadores renovables para su simulación en RTDS (Real Time Digital Simulator) y, posteriormente realizar los ensayos HiL. Se desarrolló un modelo EMT (transitorios electromagnéticos) de un generador solar fotovoltaico y un generador eólico de tipo 4 teniendo en cuenta su comportamiento según el código de red para la simulación de cortocircuitos y el análisis de protecciones. Estos modelos contemplan el desacoplo entre el control

de las intensidades de secuencia positiva y de secuencia negativa ante faltas desequilibradas. Además, incluyen el control para limitación de la intensidad de secuencia negativa y pueden proporcionar intensidad de secuencia negativa de forma proporcional a la tensión de secuencia negativa durante la falta.

En la segunda fase, se realizaron pruebas de laboratorio mediante estudios HIL con el simulador RTDS. En los estudios HIL, se produce la interacción entre los resultados de la simulación y los equipos reales. En este estudio, los equipos reales empleados son dos protecciones comerciales de dos fabricantes diferentes. En la simulación, se emplean los modelos desarrollados en la primera etapa descrita anteriormente.

Para la realización de estas simulaciones, se desarrolló un protocolo de pruebas que permite realizar un análisis exhaustivo del comportamiento de estos equipos y que considera las funciones de protección de distancia (21), diferencial de línea (87L) y sobreintensidad direccional de neutro (67N) como las tres funciones principales y más importantes empleadas actualmente en líneas de transporte de energía eléctrica. De esta etapa se obtienen los resultados mostrados en el capítulo 2. Estos resultados permitieron detectar necesidades de mejora en la detección de faltas por parte de la función de distancia cuando la aportación de corriente proviene de sistemas de generación basados en electrónica de potencia. Sin embargo, las funciones de protección 87L y 67N no presentaron un mal comportamiento, por lo que quedaron fuera del estudio posterior de propuestas de mejora.

En el tercer capítulo se describe la propuesta desarrollada en esta tesis para la mejora del funcionamiento de la protección de distancia en redes con elevada penetración de energías renovables. Se desarrolló un algoritmo de selector de fases en falta que mejora sensiblemente el comportamiento global de la función de distancia ante este tipo de aportaciones. Este desarrollo se realizó mediante un algoritmo multicriterio que combina, adapta y mejora el funcionamiento de conceptos de protección tradicionales adaptándolos a la aportación de la generación renovable, siempre con el objetivo de que sea implementable en un equipo de mercado.

En la cuarta fase de este trabajo se implementó la solución del selector de fase en falta propuesto en un equipo de protección real para la prueba de concepto en laboratorio. La solución del selector de fases en falta desarrollada se integra dentro de la función de distancia del equipo (medida de impedancia, recepción de medidas de tensión e intensidad, generación de disparos, ajustes, etc.). Este paso, el de implementar la solución desarrollada en un equipo real pudo realizarse gracias a la colaboración con Schneider Electric. Sobre este equipo, en el que se implementa la solución propuesta, se realizan de nuevo ensayos siguiendo el protocolo desarrollado para la segunda fase, verificando la mejora en los resultados obtenidos en cerca del 100% de los casos. Además de realizar pruebas en la red con una alta penetración de energía renovable, también se probó la solución en base al estándar de protección IEC 60255:121 para la función de distancia, con objetivo de comprobar la solución propuesta sigue siendo válida para redes tradicionales basadas en generación síncrona, obteniendo buenos resultados en cuanto a la detección y tiempos de actuación medios cercanos a los de las protecciones comerciales actuales.

Con todo ello, el principal resultado de esta tesis ha sido el de un selector de fases que mejora el funcionamiento de la protección de distancia ante elevada penetración de renovables, contribuyendo de esta manera a mantener los niveles de seguridad en la red. Este desarrollo se realizó con el objetivo de que fuera implementable en un equipo comercial, lo cual fue logrado de forma satisfactoria y demostrado en laboratorio. Además de ser una solución válida para redes con elevada penetración de energías renovables, también se ha demostrado que funciona correctamente en redes tradicionales con generación síncrona.

Las principales conclusiones a las que se ha llegado gracias al cumplimiento de las etapas de desarrollo comentadas anteriormente son:

- La aportación de intensidad a la falta por parte de los generadores renovables basados en electrónica de potencia difiere respecto a la aportación a la falta por parte de los generadores síncronos, lo que hace que algunas de las funciones de la protección de distancia se vean afectadas. Las funciones con un comportamiento incorrecto fueron:
    - El selector de fases en falta no detecta correctamente las fases afectadas por la falta en caso de faltas desequilibradas.
    - La detección de direccionalidad no es correcta. Muchas veces es un algoritmo que se encuentra muy relacionado con el selector de fases en falta y la medida de impedancia.
    - La medida de impedancia resultaba oscilante o errática, principalmente en el transitorio tras la inyección, y puede provocar sobrealcance de zona 1 o disparos retrasados en el tiempo.

- Las funciones de protección diferencial de línea y sobreintensidad direccional de neutro no se ven apenas afectadas por el cambio en la aportación de corriente de cortocircuito, salvo por algunos retrasos observados en la actuación de la 67N debido a la reducida aportación de intensidad a la falta.

- Es posible conseguir un correcto funcionamiento de la protección de distancia en redes con elevada penetración de renovables usando algoritmos multicriterio de selección de fase en falta. Estos algoritmos multicriterio, a su vez se basan en criterios de protección actuales modificados para tener en cuenta la generación renovable. Este punto es importante para que la solución pueda ser implementable en un equipo.

- Las comunicaciones fiables entre elementos de la red serán importantes de cara a la fiabilidad de la red en un futuro con una elevada penetración de energías renovables, ya que son necesarias para las funciones de protección diferencial de línea y para los esquemas de comunicación de la protección de distancia.

- Además de la mejora propuesta en esta tesis, existe la posibilidad de seguir desarrollando e implementado soluciones para un funcionamiento mejorado de las protecciones ante elevada penetración de energías renovables mediante algoritmos que mejoren la medida de la impedancia.

Durante esta tesis se han realizado las siguientes contribuciones:

1. Patente presentada para el algoritmo de protección en el año 2020: E. Martínez, S. Borroy and M. T. Villén, "Protection method of an electrical distribution and/or transmission network against short-circuits". European Patent Office Patent PCT/EP2020/053877, 2nd September 2020. PCT/EP2020/053877 Page 450, bulletin 2036: https://www.epo.org/archive/epo/pubs/bulletin/2020/bulletin2036.pdf https://patentscope.wipo.int/search/en/detail.jsf?docId=WO2020178006&tab=PCTBIBLIO (Accesible marzo 2022)

2. Presentación de artículo de revista: E. Martínez Carrasco, M. P. Comech Moreno, M. T. Villén Martínez and S. Borroy Vicente, "Improved Faulted Phase Selection Algorithm for Distance Protection under High Penetration of Renewable Energies," *Energies,* vol. 13, no. 3, p. 558, 2020.

3. Participación en la conferencia CIRED 2019 en Madrid, los días 3 a 6 de junio de 2019 con un artículo y una presentación en sesión de poster: E. Martinez, S. Borroy, M. T. Villén, D. López, M. Popov and H. Grasset, "New faulted phase selector solution for dealing with the effects of type-4 wind turbine on present protection relaying algorithms,"

4. Dos presentaciones orales en el congreso "Workshop H2020 MIGRATE 2019 Working package 4" (https://www.tennet.eu/fileadmin/user_upload/Events/migrate/Agenda/Roadshow_Agenda_WP4.pdf) en Madrid los días 20 y 21 de noviembre de 2019 sobre los resultados explicados en los capítulos 1 y 3 de esta tesis:

    a. Mesa redonda 1: "Short-circuit behaviour of Power Electronics Based Generators vs. Synchronous generators" con la presentación "*Control systems for Type-4 wind turbines and PV generation systems during short circuit"*.

        - Moderada por: Luis Coronado (Red Eléctrica de España)

        - Compartiendo mesa redonda con: Marjan Popov (Delft University of Technology), Oriol Gomis (Universidad Politécnica de Cataluña) y José Luis Rodríguez (Universidad Carlos III de Madrid).

    b. Mesa redonda 4: "New protection enhancements and technologies for a future scenario with high shares of renewables with the presentation" con la presentación "*Proposal of and enhanced distance protection*".

        - Moderada por: David López (Red Eléctrica de España)

        - Compartiendo mesa redonda con: Marjan Popov (Delft University of Technology), Henri Grasset (Schneider Electric, Francia), Jorge Cárdenas (General Electric), George Mikhael (ABB España), Matías Kereit (Siemens Alemania) y Jean Leon Eternod (SEL México).

5. Participación en el grupo de trabajo B5.65 de CIGRE que comenzó en Agosto de 2018 (actualmente activo) con el título *"Enhancing Protection System Performance by Optimising the Response of Inverter-Based Sources".*

6. Participación en las "Jornadas técnicas CIGRE Madrid 2018" el 27 y 28 de noviembre con un artículo: Borroy, S.; Martínez, E.; Villén, M.; Popov, M.; Chavez, J.; López, D.; Andrino, R.; Pindado, L.; López, S.; Grasset, H.; Guibout, C.; Watare, A.; Terzija, V.; Azizi, S.; Sun, M.; Kilter, J.; Reinson, A.; Tealane, M. "Análisis experimental del comportamiento de los sistemas de protección actuales ante elevada penetración de energías renovables por medio de plataforma Hardware In the Loop"

7. Participación en "III Congreso Smart Grid" los días 18 y 19 de octubre de 2016 con artículo y presentación oral:
    a. Martínez, E.; Borroy, S; Abad, M.; Giménez, L.: *"Validación mediante RTDS de equipo de protección de redes inteligentes"* https://www.smartgridsinfo.es/comunicaciones/validacion-mediante-rtds-equipo-proteccion-redes-inteligentes
    b. Martínez, E.; Borroy, S; Abad, M.; López, D.; Andrino, R.; Pindado, L.;"*Impacto de la conexión masiva de energías renovables y electrónica de potencia en la seguridad de la red".* https://www.smartgridsinfo.es/comunicaciones/comunicacion-impacto-conexion-masiva-energias-renovables-electronica-potencia-seguridad-red

Summary and complementary activities

The energy transition is coming with a significant increase in renewable energy penetration based on power electronics. Among the differences between this type of generation and conventional synchronous generation, it is worth highlighting those related to the current contribution during short circuit faults, which may affect the correct operation of the protection systems.

This thesis deals with the operation of protection systems in transmission networks under the growing penetration of renewable energies. The analysis is carried out by testing real protection equipment and designing practical and implementable solutions in the protection equipment currently present on the market.

This work was motivated by the need of European TSOs (Transmission System Operators) to study the effect that renewable energies may have on the operation and security of the network. To meet these needs, among other initiatives, the H2020 MIGRATE project (https://www.h2020-migrate.eu/) focused on studying the impact of renewable energies in the protection systems of the electrical network. The study presented in this doctoral thesis was developed under the frame of the MIGRATE project.

The developed work was distributed in different phases that correspond to the chapters of this document.

The first chapter includes modelling renewable generators for their simulation in RTDS (Real-Time Digital Simulator). An EMT (electromagnetic transients) model of a photovoltaic generator and a Type-4 wind generator was developed, taking into account their behaviour according to the grid code for the simulation of short circuits and the analysis of protections. These models contain the decoupling between the control of the positive sequence and negative sequence currents in the event of unbalanced faults. They include control for negative sequence current limitation and provide negative sequence current proportional to the negative sequence voltage during the fault.

In the second phase, laboratory tests were carried out using HIL (Hardware in the Loop) studies with the RTDS simulator. In HIL studies, simulation results interact with real equipment. In this phase of

the study, two commercial protections from two different manufacturers were tested. The models developed in the first stage described above are used in the simulation.

A test protocol was developed to carry out these simulations. This protocol allows an exhaustive analysis of the behaviour of these protection devices with the three main functions currently used in electric power transmission lines: distance protection (21), line differential (87L) and ground directional overcurrent (67N). From this stage, the results shown in chapter 2 are obtained. These results allowed for improvements in fault detection by the distance function when the current contribution comes from generation systems based on power electronics. However, the 87L and 67N protection functions behave correctly, so they were left out of the subsequent study of improvement proposals.

The third chapter describes the proposal developed in this thesis to improve the operation of distance protection in networks with a high penetration of renewable energies. A faulted phase selector algorithm was developed that significantly enhances the global behaviour of the distance function in networks with high penetration of renewable energy. This proposal uses a multicriteria algorithm that combines and improves the operation of traditional protection concepts, adapting them to renewable generation.

In the fourth phase of this work, the proposed faulted phase selector solution was implemented in a real protection device for a proof of concept in the laboratory. The developed phase selector solution is integrated within the distance function of the equipment (impedance measurement, reception of voltage and current measurements, trigger generation, settings, etc.). The implementation of the algorithm in a real device was possible thanks to the collaboration with Schneider Electric. The protocol developed in the second step was applied to the equipment, verifying the improvement in nearly 100% of the cases with high penetration of renewable energy. In addition, the solution was tested based on the IEC 60255:121 protection standard for the distance function. The objective was to verify that the proposed solution is still valid for traditional networks based on synchronous generation, obtaining good results in detection and average tripping times close to those of current commercial protections.

With all this, the main result of this thesis is a faulted phase selector that improves the operation of the distance protection against high penetration of renewables, thus contributing to maintaining security levels in the network. This development was implemented in a commercial equipment, which was successfully achieved and demonstrated in the laboratory. In addition to being a valid solution for networks with a high penetration of renewable energies, it has also been shown to work correctly in traditional networks with synchronous generation.

The main conclusions that have been reached thanks to the fulfilment of the development stages are:

- The difference between the current contribution to the fault from renewable generators based on power electronics and synchronous generators causes distance protection function behaviour problems in terms of:
    - Faulted phase selection does not detect correctly.
    - Directionality detection fails. This algorithm is closely related to the faulted phase selector and impedance measurement.
    - The impedance measurement was oscillating or erratic mainly in the transient period after the injection and may cause zone 1 overreach or trigger in delayed time for both zone 1 and zone 2.

- The neutral directional overcurrent and line differential protection functions were hardly affected during the study. Only some delays were observed in the 67N actuation due to the reduced contribution to the fault.
- It is possible to achieve a correct operation of distance protection with high penetration of renewables using multicriteria faulted phase selection algorithm. This algorithm is based on modified current protection criteria to consider renewable generation behaviour. This point is important because the solution must be implementable in commercial equipment.
- Reliable communications between network elements will be essential for the network's reliability in the future with high penetration of renewable energies because it allows the operation of line differential protection functions and distance protection communication schemes.
- Further steps could be focused on continuously developing and implementing solutions for improved protections against high penetration of renewable energies. These new proposals can be based methods that improve impedance measurement.

During this Thesis; following training courses, collaborations for teaching, publications, conference assistance and workshops have been done:

1. Patent presented in 2020 for the developed algorithm: E. Martínez, S. Borroy and M. T. Villén, "Protection method of an electrical distribution and/or transmission network against short-circuits". European Patent Office Patent PCT/EP2020/053877, 2nd September 2020. PCT/EP2020/053877 Page 450, bulletin 2036: https://www.epo.org/archive/epo/pubs/bulletin/2020/bulletin2036.pdf https://patentscope.wipo.int/search/en/detail.jsf?docId=WO2020178006&tab=PCTBIBLIO

2. Paper presentation in Energies Journal in January 2020 E. Martínez Carrasco, M. P. Comech Moreno, M. T. Villén Martínez and S. Borroy Vicente, "Improved Faulted Phase Selection Algorithm for Distance Protection under High Penetration of Renewable Energies," *Energies,* vol. 13, no. 3, p. 558, 2020.

3. Participation in CIRED conference 2019 in Madrid, on 3rd-6th June 2019 with a paper and a presentation in a poster session: E. Martinez, S. Borroy, M. T. Villén, D. López, M. Popov and H. Grasset, "New faulted phase selector solution for dealing with the effects of type-4 wind turbine on present protection relaying algorithms"

4. Two oral presentations in "Workshop H2020 MIGRATE 2019 Working package 4" in Madrid on November 20th and 21st, 2019 about the results explained in chapter 1 and chapter 3 of this Thesis:
    a. Roundtable 1: Short-circuit behaviour of Power Electronics Based Generators vs. Synchronous generators with the presentation "*Control systems for Type-4 wind turbines and PV generation systems during short circuit"*.
        - Chairman: Luis Coronado (Red Eléctrica de España)
        - Sharing roundtable with: Marjan Popov (Delft University of Technology), Oriol Gomis (Universidad Politécnica de Cataluña) and José Luis Rodríguez (Universidad Carlos III de Madrid).
    b. Roundtable 4: New protection enhancements and technologies for a future scenario with high shares of renewables with the presentation "*Proposal of and enhanced distance protection*".
        - Chairman: David López (Red Eléctrica de España)

- Sharing roundtable with: Marjan Popov (Delft University of Technology), Henri Grasset (Schneider Electric, Francia), Jorge Cárdenas (General Electric), George Mikhael (ABB España), Matías Kereit (Siemens Alemania) y Jean Leon Eternod (SEL México).

5. Participation in CIGRE Working Group B5.65 from August 2018 (currently ongoing) with the title *"Enhancing Protection System Performance by Optimising the Response of Inverter-Based Sources".*

6. Participation in "Jornadas técnicas CIGRE Madrid 2018" on November 27th and 28th with a paper: Borroy, S.; Martínez, E.; Villén, M.; Popov, M.; Chavez, J.; López, D.; Andrino, R.; Pindado, L.; López, S.; Grasset, H.; Guibout, C.; Watare, A.; Terzija, V.; Azizi, S.; Sun, M.; Kilter, J.; Reinson, A.; Tealane, M. "Análisis experimental del comportamiento de los sistemas de protección actuales ante elevada penetración de energías renovables por medio de plataforma Hardware In the Loop"

8. Participation in "III Congreso Smart Grid" on 18th and 19th October 2016 with paper and oral presentation:
   a. Martínez, E.; Borroy, S; Abad, M.; Giménez, L.: *"Validación mediante RTDS de equipo de protección de redes inteligentes"*
   b. Martínez, E.; Borroy, S; Abad, M.; López, D.; Andrino, R.; Pindado, L.;"*Impacto de la conexión masiva de energías renovables y electrónica de potencia en la seguridad de la red".*

Chapter 0 Introduction

The increase in renewable-type generation connected to the electrical power system displaces conventional generation, on which the control and management criteria of the traditional network are based. In particular, the difference in the current contribution during the short-circuit by the renewable generators based on power electronics (PE) can cause failure to detect short-circuits and, therefore, affect the network stability. The motivation of this work comes from the interest of European TSOs, Universities, Research Institutions and Technology Companies about how increasing penetration of renewable energies may affect the operation, security and reliability of electrical networks in the near future.

The starting point of this Thesis is the H2020 MIGRATE Project (Massive Integration of Power Electronic Devices). This Project aimed to find solutions for the technological challenges arising from the essential and increasing role of power electronics and renewable energies in power systems. The Project started in January 2016 and lasted four years until December 2019.

This Thesis aims to analyse how the modified dynamic behaviour (regarding the synchronous generation) of the power system caused by the control systems and power electronics (PE) affects the performance protection systems. The massive connection of PE-based renewable sources is expected to weaken the existing protection system and change the short circuit dynamics. Consequently, such protection systems, which were developed taking into account short-circuit currents from synchronous machines, may no longer respond or respond incorrectly to the new short-circuit dynamics. This document shows the study of the ability of existing protection devices to operate under system disturbances generated by PE correctly and the analysis of technical and technological requirements for future protection systems to keep current levels of reliability. Firstly, accurate models for protection studies and HiL tests are developed to assess the existing protection functions/solutions under high PE penetration. Secondly, new protection solutions for 100% PE-based renewable generation are designed and tested by performing HiL tests with real protection equipment supplied by Schneider Electric to check the technical feasibility of the proposed solutions. The outputs of this thesis also contain a set of recommendations for the design of protection schemes for power systems with high penetration of PE.

The objective that completes this thesis is the proposal of solutions for improving the behaviour of protections under high penetration of renewables, which must be implementable in commercial protection relays.

These objectives were considered strategic both by the European Commission and the different TSOs involved in the project. These chapters are organized to deal with all the objectives and compose this Thesis:

- Chapter 1: Benchmark Grid Modelling:
    - Definition of a relevant grid for the study with nodes and lines where the equipment under test reads current contribution from 100% penetration of PE.
    - Development of PE models according to representative grid code for the analysis of present protection algorithms considering positive and negative sequence current control.
- Chapter 2: Assessment of Short Circuit Protection under high PE level:
    - Evaluation of a representative sample of commercial protection relays. In this work, the tests of two protection relay manufacturers are shown.
    - For these relays, three protection functions commonly used in transmission lines are tested and studied: line differential current (87-L), distance (21) and ground directional overcurrent (67N).
    - Assessment of which problems appear for these protection functions because of the current contribution of renewable energies.
- Chapter 3: Development of faulted phase selector algorithm:
    - Based on the results and observed in chapter 2, a solution is investigated and design to improve the behaviour of present protection algorithms with renewables while the behaviour with traditional synchronous generator is still correct.
- Chapter 4: Implementation of the algorithm in MICOM P544:
    - The solution developed in chapter 3 is programmed in a commercial protection relay and tested to check:
        - The applicability of the solution in a real and commercial protection platform.
        - If the solution implemented in the relay works correctly with current contribution to the fault coming from renewable energies.
        - If the solution accomplishes the commercial protection standards to ensure correct behaviour with synchronous generators.

Including additional information in appendix:

Appendix 1: Parameters of the grid model:

- About the grid model defined in chapter 1

Appendix 2: FCWT model test results:

- About the tests applied to commercial protection relays in chapter 2. Analysis of behaviour of the protection relay with current contribution coming from Full Converter.

Appendix 3: PV model test results:

- About the tests applied to commercial protection relays in chapter 2. Analysis of behaviour of the protection relay with current contribution coming from PV generator.

Appendix 4: Test protocol for the assessment of protection relays behaviour under high penetration of power electronic devices:

- Definition of the tests applied to commercial protection relays in Chapter 2.

0.1 Renewable energy penetration in European countries

The energy mix is the share or combination between different sources of generation, as primary energy sources, to accomplish the energy needs in a specific region. These primary energies are nuclear, coal, oil, gas, wind, sun, water, etc.

European TSOs are studying the increasing penetration of renewables since it causes two main effects that affect the behaviour of protection systems: reduction of system inertia and reduction/modification of short-circuit contribution.

The following figure summarizes the installed capacity in different European countries based on TSO data from Spain [1], France [2], Italy [3], Germany [4] [5] [6], Switzerland [7], Slovenia [8] [9], The Netherlands [10], Ireland [11], Scotland [12], Finland [13] and Estonia [14]. It shows the significant installed renewable power in European countries; for example, the sum of the percentages of wind and solar in Germany is 53.83 %, 41.80 % in Spain or 40.91 % in the Netherlands. These generators are typically based on power electronic converters, so this figure shows the increasing importance of analyzing the behaviour of the system protection before their short circuit current in high penetration levels scenarios.

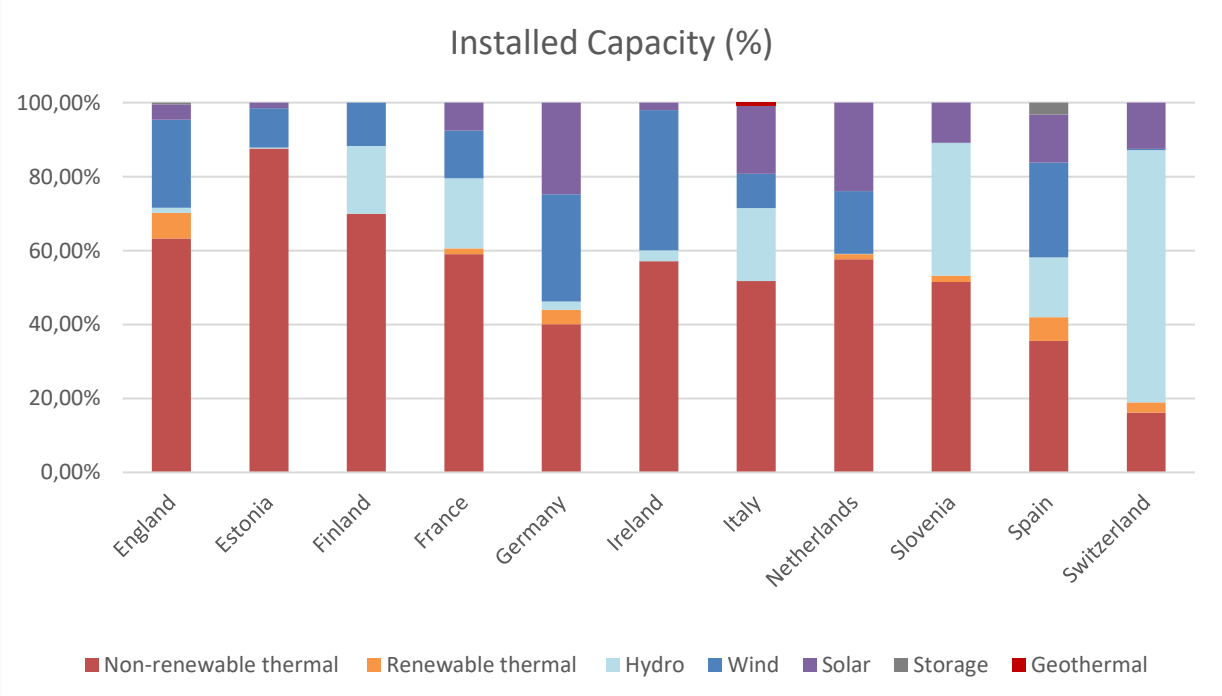

Figure 1. Installed capacity in European countries at the end of 2020.

0.2 Protection functions

The high penetration of renewable energies in the different countries analyzed in section 0.1 may affect the behavior of protection algorithms [15] [16]. Some papers have already analyzed different effects on terms of different current injection of renewable energies during the fault [17] [18] and its possible effect on protection relays [19].

This thesis analyses the behavior of protection relays at transmission level. For that, main protection functions used in transmission networks are studied in laboratory to find possible problems caused by renewable energy integration and propose solutions.

To investigate the possible impact of power electronics on protection systems installed at the transmission level, it is necessary to consider what are the main functions used in these protections and how they behave. In this research, the protection functions analysed are:

- Segregated line differential current (87-L).
- Distance (21)
- Ground Directional Overcurrent (67N)

For analysing how commercial protections can be affected, in this thesis laboratory tests will be applied to physical protection relays.

The numbers in brackets indicate the abbreviated designation by their ANSI (American National Standards Institute) [20]. These abbreviations are commonly used during this work for referring to the protection functions. This section summarizes the theory of these protection functions analyzed in the following chapters.

0.2.1 Line differential current (87L)

Line differential protection is widely used as primary protection in transmission lines. Its operation relies on fast communication between both sides of the protected line and first Kirchoff Law. 87L protects the line but does not provide backup for the rest of the system. Thus, all the faults produced out of the line are not covered by the line differential protection and must be detected by other protection functions such as distance or ground directional overcurrent.

Line differential protection needs communication between both sides of the line to exchange current measurements and calculate the differential current. If the communication link fails, this protection becomes automatically unavailable. Digital protection relays can detect this kind of communication failure to avoid a maloperation of the protection functions.

Typically, line differential protection performance is based on the representation of differential current (I_{diff}) and the bias current (I_{bias}), also called restraint current, which can be calculated by using the following expressions [21]

$$\overline{\boldsymbol{I_{diff}}} = \sum_{i=1}^{N} \overline{\boldsymbol{I_{side_i}}} \quad (1)$$

$$\boldsymbol{I_{bias}} = \sum_{i=1}^{N} \boldsymbol{abs}(\overline{\boldsymbol{I_{side_i}}}) \quad (2)$$

An example of this characteristic can be observed in Figure 2. If the combination of calculated currents I_{diff} and I_{bias} is above the characteristic represented by the blue line, a fault is detected inside the line, but if the combination of I_{diff} and I_{bias} is below this characteristic, the protection considers normal conditions in the line. The ramp in the characteristic from Figure 2 avoids maloperation of

the line differential protection when the I_{bias} increases because of different load conditions and due to errors in current transformer measurements.

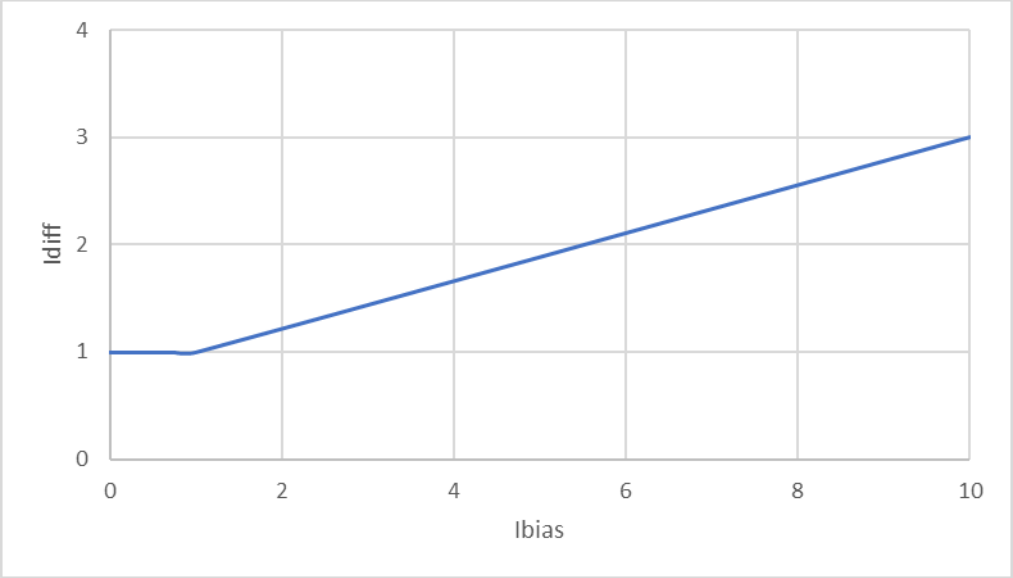

Figure 2. Typical 87-L characteristic in p.u. [22]

Figure 3 represents the single line diagram of the protected line in normal conditions. The green arrows represent the current through the line from side A to side B. In this conditions, differential current (I_{diff}) is near to zero (it is not zero due to the capacitive effect of the line). In transmission networks the power can be bi-directional, flowing from side A to side B or from side B to side A. Since I_{diff} is near to zero and I_{bias} is defined by the load current of the line, the relation between both currents is below the 87-L characteristic from Figure 2.

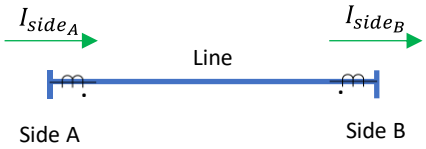

Figure 3. Single line diagram of the protected line with two terminals. Normal conditions.

In Figure 4, the same line is represented when a fault inside the line is produced. In this case, fault current contribution comes from sides A and B to the fault. This fault current is much higher than the load current, which causes a significant increase in the I_{bias} current. Since the fault contribution direction goes towards the fault, the I_{diff} also increases. This combination of ents I_{diff} and I_{bias} is above the characteristic from Figure 2 and cause the trip of the 87L function.

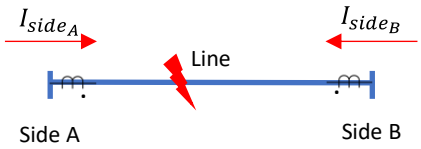

Figure 4. Single line diagram of the protected line with two terminals. Fault inside the line.

In Figure 5, the current is outside the line so I_{bias} current can be as significant as the case of the fault inside the line but, I_{diff} is much lower because the fault current enters the line by side A and goes

out by side B. This combination of I_{bias} and I_{diff} currents is below the 87L characteristic from Figure 2 and the protection does not send a tripping signal.

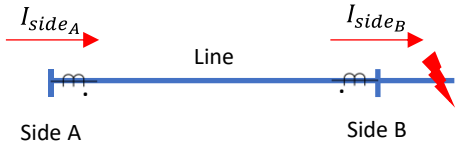

Figure 5. Single line diagram of the protected line with two terminals. Fault outside the line.

0.2.2 Distance (21)

Distance protection is typically used in transmission and distribution systems as the primary protection function when communications are not available between both sides of the line to be protected as backup protection when these communications are available and 87L is working as primary protection. In addition, unlike the line differential protection that protects only the line, distance is a backup protection of the system thanks to the use of different protection zones covering beyond the line.

Distance protection identifies fault conditions by impedance measurement and, therefore, it is its main algorithm to determine a fault condition. The impedance is proportional to the line length, so it is possible to know the location of a fault (in the line, in the adjacent line, etc.) by using three-phase voltage and current measurements at one side of the line. Additionally, two more complementary algorithms support the correct identification of the fault. These algorithms are in charge of identifying the directionality and the faulted phase.

There are different impedance calculation loops which activation depends on the fault type.

- Phase to ground impedance loops are calculated according to [23]:

$$\bar{Z}_A = \frac{\bar{U}_{ph_A}}{\bar{I}_{ph_A} - k_0 \cdot \bar{I}_{earth}} \quad (3)$$

$$\bar{Z}_B = \frac{\bar{U}_{ph_B}}{\bar{I}_{ph_B} - k_0 \cdot \bar{I}_{earth}} \quad (4)$$

$$\bar{Z}_C = \frac{\bar{U}_{ph_C}}{\bar{I}_{ph_C} - k_0 \cdot \bar{I}_{earth}} \quad (5)$$

Where $\bar{k}_0 = \frac{\bar{Z}_{Earth}}{\bar{Z}_{line}}$

- Phase to phase impedace loops are calculated according to:

$$\bar{Z}_{AB} = \frac{\bar{U}_{ph_A} - \bar{U}_{ph_B}}{\bar{I}_{ph_A} - \bar{I}_{ph_B}} \quad (6)$$

$$\bar{Z}_{BC} = \frac{\bar{U}_{ph_B} - \bar{U}_{ph_C}}{\bar{I}_{ph_B} - \bar{I}_{ph_C}} \quad (7)$$

$$\bar{Z}_{CA} = \frac{\bar{U}_{ph_C} - \bar{U}_{ph_A}}{\bar{I}_{ph_C} - \bar{I}_{ph_A}} \quad (8)$$

Figure 6 represents a line protected by distance protection located in bus A. The adjacent line and the protection zones are also shown in the figure. Usually, three distance protection zones are defined associated with tripping times for forwarding actuation and one protection zone for reverse actuation:

- Zone 1 forward: Ideally, this zone is in charge of protecting the entire line where the protection is located. However, possible measurement errors in current and voltage transformers can produce overreach problems detecting faults in Zone 1 when the fault is in the adjacent line. Then, it is not recommended to set this zone beyond 85% of line impedance. Usually, the delay for the actuation of this zone is between 0 and 100 ms maximum.
- Zone 2 forward: This zone covers the portion of the protected line that Zone 1 does not cover, and it provides backup protection for the busbar of the remote bus (bus B in the figure). Typically, the reach of this zone is set to 120% of the protected line from bus A. Since this protection zone covers part of the adjacent line, it must coordinate its actuation with the distance protection of the adjacent line. For this cause, normally, the delay for the actuation of this zone is between 200 and 400 ms.
- Zone 3 forward: This zone acts as backup protection for the system. Typically, the reach of this zone is set to 110% of the longest line connected to the remote bus (bus B in the figure). It must coordinate its actuation with the distance protection of the adjacent lines to avoid malfunctioning operation. For this cause, usually, the delay for the actuation of this zone is between 800 and 1 s.
- Reverse zone: This zone is not represented in the graph, but it is mainly located in the third sector of the impedance plane shown in Figure 7. It is usually used as backup protection to cover the local busbar. The recommendation to set this zone is to use the criterion of 65% of the impedance of the shortest line connected to the protected line. The delay for the actuation of this zone depends on the application.

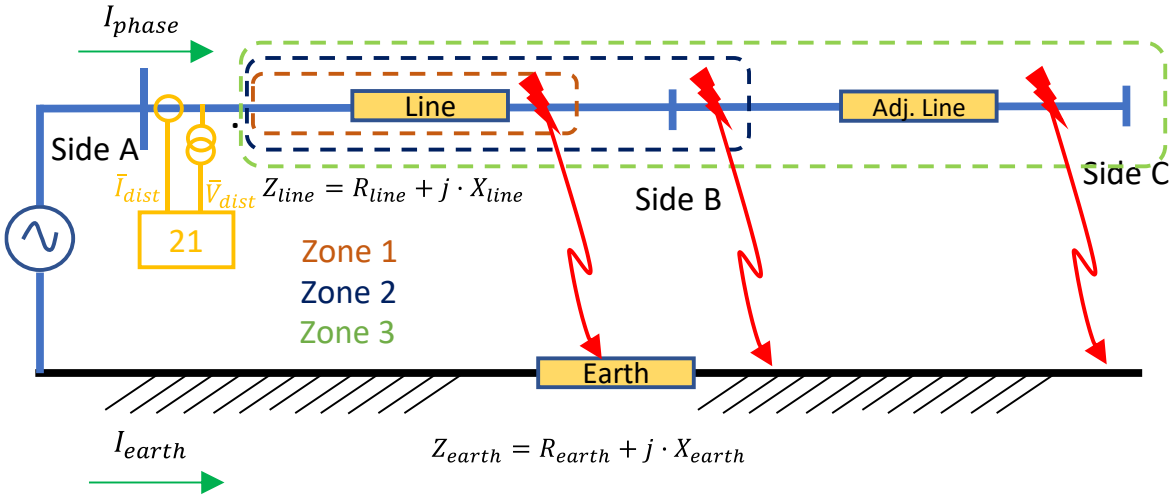

Figure 6. Protection zones represented in a line diagram.

Figure 7 represents quadrilateral characteristics. This characteristic is calculated with a reactive reach (Y-axis) and a resistive reach (X-axis) to deal with resistive faults in each protection zone. It is typical to set the resistive reach at four times the reactive reach of the impedance. This type of characteristic, due to its nonlinearity, was started to use in modern protection relays [24].

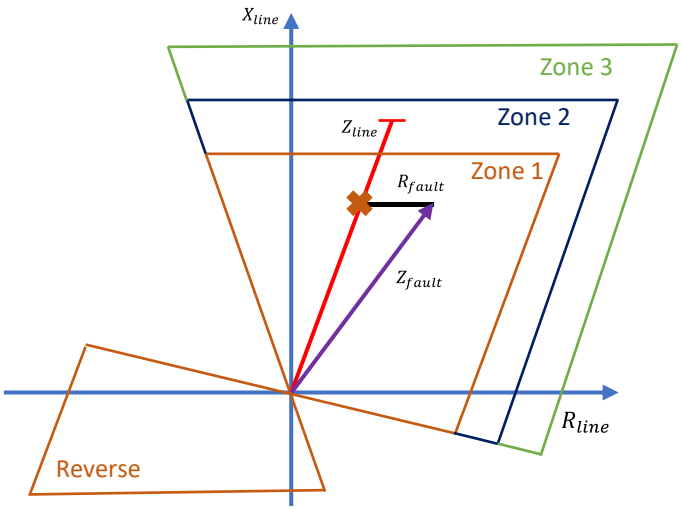

Figure 7. Protection zones represented in impedance plane with quadrilateral characteristic.

Another traditional characteristic used for phase-to-phase faults is the "mho" characteristic [25]. It was present already in old protection relays, but with the use of digital relays, it is considered less versatile than quadrilateral for resistive faults. This protection characteristic has not been used in the study of this thesis because of the versatility of settings provided by quadrilateral characteristic, so its explanation is not included here.

Although impedance loops can identify where the fault is located, two more algorithms work parallel with the fault impedance calculation: faulted phase selector and directionality.

- Faulted phase selection identifies in which phase or phases the fault is located using a different principle than the one used for impedance measurement. Then, if both algorithms, impedance measurement and faulted phase selection indicate the same phases in fault, the actuation of the distance protection becomes more reliable.
- Directionality can distinguish if the fault is located forward or backwards regarding the location of the distance protection and its measurement transformers.

These two algorithms complement the actuation of the impedance loops and provide additional reliability to the fault detection to generate a breaker trip when a fault exists and avoid detecting if the fault is not located in the protected zones.

In addition to these algorithms, whose operation will be analyzed throughout this work, the following algorithms make distance protection operation even more reliable:

- Fuse fail algorithm: Avoids maloperation due to loss of the voltage measurement.
- Power swing and out of step: Avoid maloperation due to the travel of the impedance inside the protection zone in a non-fault situation.
- Load encroachment: Avoids maloperation due to the entrance of the protection zone in the load zone of the impedance.
- Switch onto fault: Accelerates the trip of time-delayed zones when a fault appears when the breaker is closed after a manual close, or a reclose cycle.
- Communication schemes: In this section, distance protection has been explained as a stand-alone protection algorithm. However, it is also possible to increase its reliability and actuation speed if the protection on one side of the line is connected to the protection on the other side. Communications between these two protections allow implementing different communication schemes such as permissive overreach transferred trip (POTT), permissive underreach transferred trip (PUTT), block or current inversion.

These algorithms are out of the scope of this work.

0.2.3 Ground directional overcurrent (67N)

Ground directional overcurrent usually works as backup protection of distance and line differential protection in transmission and meshed distribution networks. 67N is the main protection function for grounded faults only in medium voltage feeders. As backup of distance protection, it allows the detection of high impedance faults that cannot be detected because the impedance measured falls out the characteristic of the protection.

67N does not cover all the fault types, but it detects those faults that involve ground, i.e., single line to ground faults and line to line to ground faults. Line to line and three-phase faults are not detected by 67N because of the lack of current circulating by ground.

The algorithm principle is based mainly on two phasors: neutral voltage and neutral current. One of the phasors is used as a polarizing phasor, and the other one as an operation phasor. In this section, the option of using neutral voltage for polarizing (3V0) and neutral current for actuation (3I0) is explained, but negative sequence voltage could be used (3V2) for polarization when zero-sequence voltage is too low.

The operation magnitude is the current that circulates by ground defined by 3I0. The angle of the polarization phasor is compared with the angle of the operation phasor. If the difference between these angles enters the operation zone and the threshold of the operation quantity is reached by the operation phasor, the relay trips.

The characteristic shown in Figure 8 has been inherited from the operation of electromechanical relays, using the “maximum torque angle” defined by the line angle (setting of the relay in digital relays). The operational zones with the directionality backwards and forward are determined based on the maximum torque angle as defined in the figure.

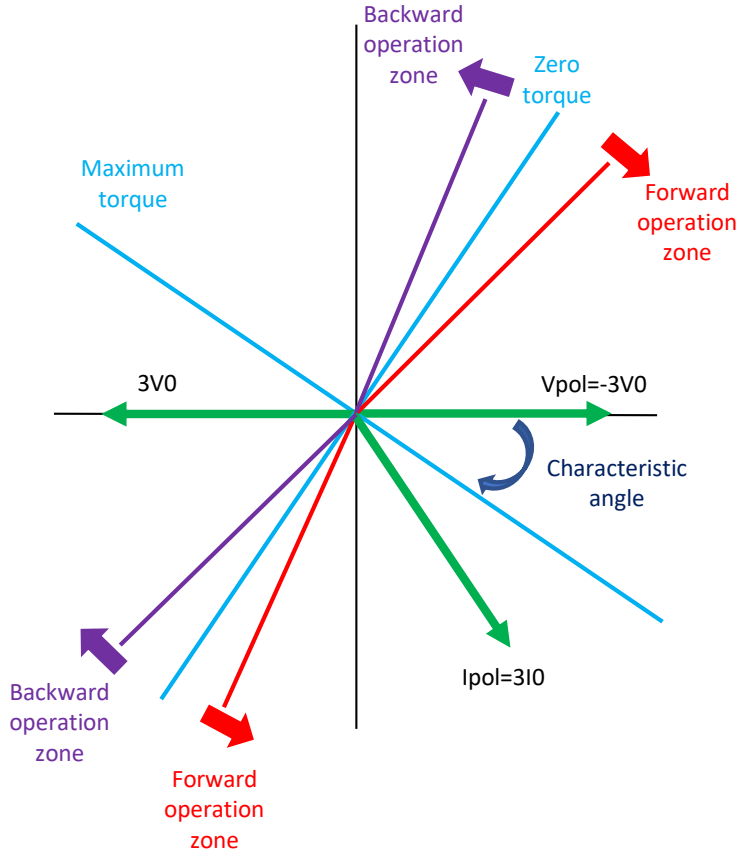

Figure 8. Ground directional overcurrent characteristic.

Chapter 1 The benchmark grid model

The analysis of commercial protection equipment and the algorithms developed throughout this work have been carried out using Hardware in the Loop (HiL). In HiL experiments, the real devices interact with a benchmark network modelled in RSCAD interface (detailed explanations about the test infrastructure are in Appendix 4).

In this research work, a full converter wind turbine (FCWT) and a photovoltaic generator (PV) model have been developed and integrated successfully into the benchmark grid. The developed models represent the behaviour of these devices during balanced and unbalanced short circuits. With this objective, several strategies for crowbar protection, low voltage ride through, negative sequence injection, active and reactive power injection have been implemented. The models of both the generators and the benchmark grid have been developed to easily modify the parameters that could influence the response of protective devices.

Moreover, different scenarios have been defined and simulated in the benchmark grid to verify protection system behaviour and the adequacy of the proposed solutions.

This chapter describes the benchmark grid model and generator models of the PV generator and the FCWT.

1.1 The Benchmark Grid Model

The objective of this grid model is to allow the study of system protection behaviour in high penetration of renewable energies scenarios considering protection functions commonly used in high-voltage transmission networks (distance, line differential and ground directional overcurrent protection).

The benchmark model consists of a full-converter wind turbine generator, a photovoltaic generator and conventional synchronous generation. The model includes an infinite grid equivalent with the possibility of modifying its strength to represent two scenarios: a "strong network" with high short circuit power and a "weak network" with low short circuit power. The parameters of this equivalent appear in Appendix 1.

The network for the study is selected so that different elements can be considered: network equivalent, renewable energies, synchronous generation and different lines where fault studies can be applied at 400 kV level. The benchmark model is shown in Figure 9. The parameters of the benchmark model are available in Appendix 1.

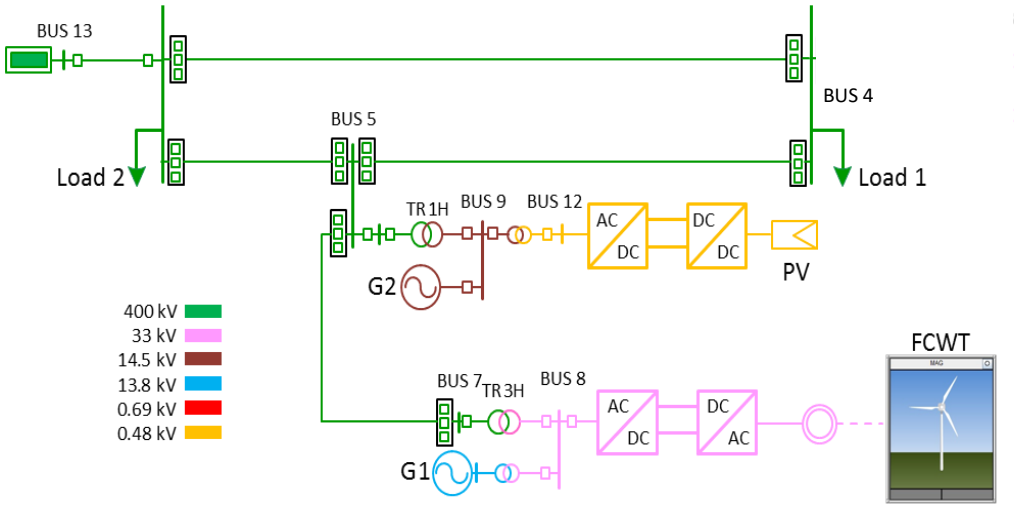

Figure 9. Benchmark model.

Within this network, the generators that have been used for the analysis of short circuit protection behaviour are:

- Type-4 wind turbine with full-converter Permanent Magnet Synchronous Generator (PMSG).
- Solar PV panel connected to the system through a full converter, making a photovoltaic generator.
- Conventional synchronous generators connected in parallel with these elements.

The capability of these models under different disturbances has been further analyzed and upgraded to improve present protection system performance under high penetration of PE. This chapter describes additional capabilities of the converters (FCWT, PV) studied in this work, such as providing negative sequence current in unbalanced faults.

The following sections describe the Type-4 WT and the PV generator modelling. Conventional synchronous generators have been modelled in parallel with PE-based generators to compare the response of the protection equipment within different generation scenarios. These synchronous generators are indicated as G1 and G2 in Figure 9, and Figure 10 shows its RSCAD block. The parameters of these generators are summarized in Appendix 1.

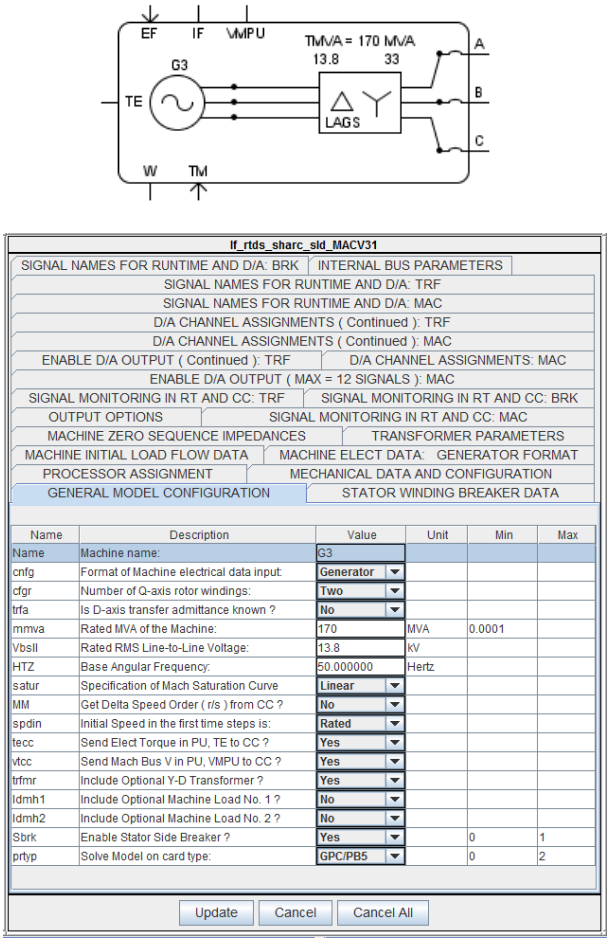

Figure 10. RTDS Synchronous generator model.

Transmission lines have been represented using the Bergeron model [26]. Figure 11 shows the transmission line, controllable switches located at both sides and the fault logic box. The controls (opening and closing breakers, fault model control) used for the transmission lines are implemented with the standard library components of RSCAD.

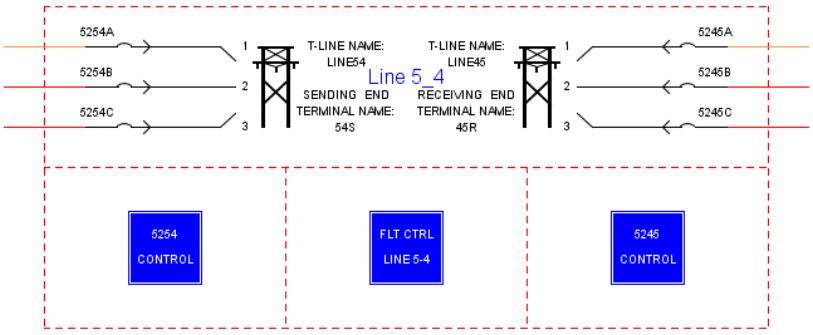

Figure 11. RTDS Transmission line model.

Figure 12 shows fault control boxes used in the simulations. They are based on the fault logic blocks to simulate these fault types:

- Single-phase faults:
  - Phase A to ground
  - Phase B to ground

- Phase C to ground
- Line to line to ground:
  - Phase AB to ground
  - Phase BC to ground
  - Phase CA to ground
- Three-phase fault to ground:
  - Phase ABC to ground
- Solid and resistive faults
- Evolutive faults

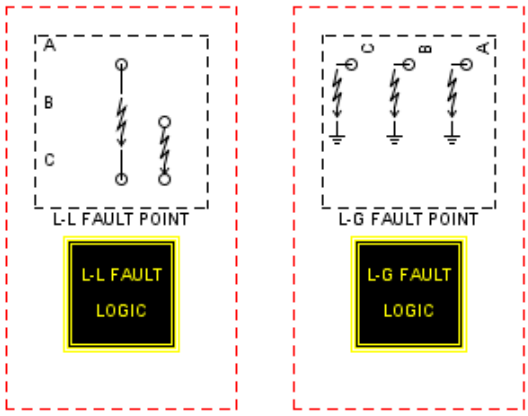

Figure 12. RTDS Fault logics blocks.

1.2 General control structure principles

The classic control structure of the power converter control is based on vector current and is developed in two levels. Figure 13 shows the general structure of the control loops involved. The inner control loop deals with controlling the currents (active and reactive), while the outer control loop deals with the control of the voltages (active and reactive).

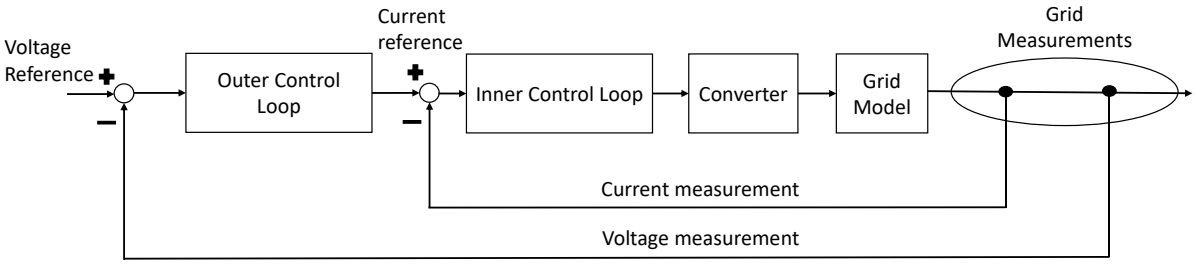

Figure 13. General control structure used for the control of dq components.

On the one hand, during the steady-state, the active current control is in charge of dealing with DC voltage at the DC bus of the power converter and dealing with the active power delivered by the generators. Besides, the reactive current control manages the voltage at the PCC of the converter or fixes the reactive power provided to the grid.

On the other hand, during the fault state, the control system applied to VSCs provides voltage support (through the control of reactive current and defined by the grid codes) and limits the

maximum current supplied by the converter to avoid undesirable damage to the equipment. The maximum current limit of the converter considers both reactive and active current.

The two-dimensional *dq-frame* is introduced here to transform the problem of controlling three sinusoidal signals to control of two DC ones, which simplifies the problem. Next sections 1.2.1 to 1.2.5 explain generalities, based on the state of the art, about the control systems to be implemented in Type-4 WT and PV generator. Section 1.2.6 analyses the different possibilities of control systems to be applied to type-4 WT and PV generator.

1.2.1 Stationary reference frame

Three arbitrary waveform signals (e.g. $f_a, f_b, \text{and } f_c$), whose sum is zero can be represented in a two-axis orthogonal stationary reference frame using the Clarke transformation [27].

$$f_a + f_b + f_c \equiv 0 \quad (9)$$

The associated space vector to these signals is defined as

$$\overline{F}(t) = F_\alpha(t) + jF_\beta(t) = \frac{2}{3}\left[e^{j0}f_a(t) + e^{j\frac{2\pi}{3}}f_b(t) + e^{j\frac{4\pi}{3}}f_c(t)\right] \quad (10)$$

The matrix representation would be

$$\begin{bmatrix}F_\alpha(t)\\F_\beta(t)\end{bmatrix} = \frac{2}{3}C\begin{bmatrix}f_a(t)\\f_b(t)\\f_c(t)\end{bmatrix} \quad (11)$$

Where

$$C = \begin{bmatrix}1 & -\frac{1}{2} & -\frac{1}{2}\\ 0 & \frac{\sqrt{3}}{2} & -\frac{\sqrt{3}}{2}\end{bmatrix} \quad (12)$$

Consequently, the mentioned three signals can be derived back by inverting equation (11) and considering the real part of obtained components:

$$f_a(t) = R_e\{\overline{F}(t)e^{-j0}\} \quad (13)$$

$$f_b(t) = R_e\left\{\overline{F}(t)e^{-j\frac{2\pi}{3}}\right\} \quad (14)$$

$$f_c(t) = R_e\left\{\overline{F}(t)e^{-j\frac{4\pi}{3}}\right\} \quad (15)$$

In the case of a balanced three-phase sinusoidal signal, the above equations can be represented as:

$$f_a(t) = F(t)\cos[\theta(t)] \quad (16)$$

$$f_b(t) = F(t)\cos\left[\theta(t) - \frac{2\pi}{3}\right] \quad (17)$$

$$f_c(t) = F(t)\cos\left[\theta(t) - \frac{4\pi}{3}\right] \quad (18)$$

where

$$\theta(t) = \theta_0 + \int_0^t \omega(\tau)d\tau \quad (19)$$

where $\theta(t)$, $\omega(t)$, and $F(t)$ are the instantaneous phase angle, frequency, and magnitude of the three-phase signal, respectively. Besides, θ_0 is the initial phase angle. The space phasor of these signals is:

$$\overline{F}(t) = F(t)e^{j\theta(t)} \quad (20)$$

This equation can be represented graphically in the following complex plane

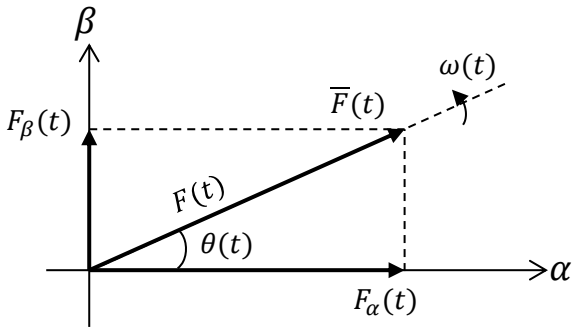

Figure 14. Space vector in stationary reference frame.

1.2.2 Rotating reference frame

According to the concept of stationary reference frame, the space vector of a balanced three-phase sinusoidal signal rotates at an instantaneous angular velocity of $\omega(t)$ in $\alpha\beta$ frame. Although the magnitude $\overline{F}(t)$ is constant, its projections on α- and β- axes are time-variant. From the control point of view, a rotating Cartesian frame (dq frame in Figure 15) can be introduced so that its instantaneous angular velocity $(\omega_r(t))$ is set equal to the angular velocity of $\overline{F}(t)$, that is $\omega(t)$. Consequently, the projections of $\overline{F}(t)$ on the two axes of this rotating frame would be time-invariant.

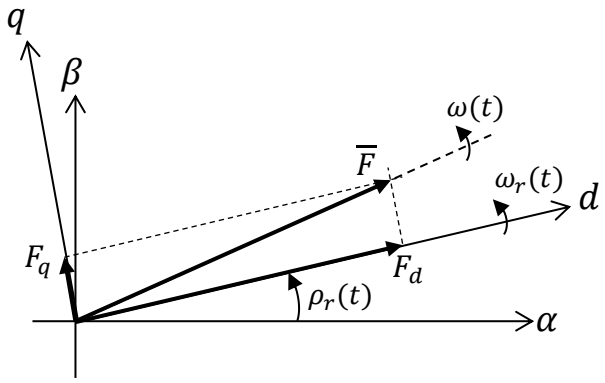

Figure 15. Space vector in rotating reference frame [28].

The correlation between the stationary and rotating reference frames can be represented through Park transformation:

$$\begin{bmatrix} F_d \\ F_q \end{bmatrix} = \begin{bmatrix} \cos\rho_r(t) & \sin\rho_r(t) \\ -\sin\rho_r(t) & \cos\rho_r(t) \end{bmatrix} \begin{bmatrix} F_\alpha \\ F_\beta \end{bmatrix} \quad (21)$$

To consider the dynamic behaviour of the PE-based component, the three-phase electrical signals are vectorised in the rotating reference frame to decouple control strategy for positive and negative sequence components. This frame rotates clockwise at the same angular speed as that of $\overline{F}(t)$. Figure 16 shows these two positive and negative rotating reference frames.

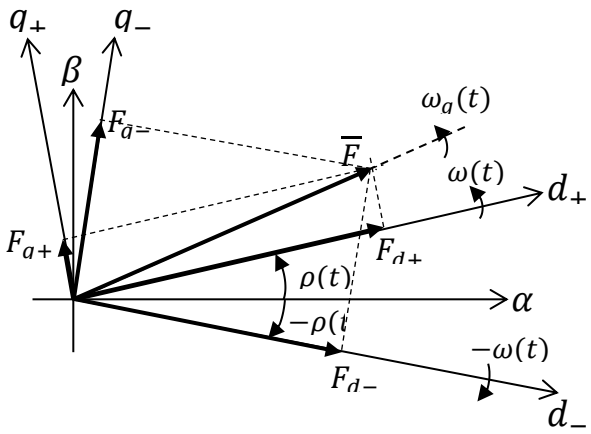

Figure 16. Space vectors in both positive and negative rotating reference [28].

The two-axis orthogonal stationary reference frame components are correlated to the negative rotating reference frame through the following transformation:

$$\begin{bmatrix} F_{d-} \\ F_{q-} \end{bmatrix} = \begin{bmatrix} \cos\rho_r(t) & -\sin\rho_r(t) \\ \sin\rho_r(t) & \cos\rho_r(t) \end{bmatrix} \begin{bmatrix} F_\alpha \\ F_\beta \end{bmatrix} \quad (22)$$

In addition to this, the transformation between $(dq+)$ and $(dq-)$ reference frames are given by:

$$F_{dq+} = F_{dq-}.\, e^{-j2\omega_s t} \quad (23)$$

$$F_{dq-} = F_{dq+}.\, e^{j2\omega_s t} \quad (24)$$

As said before, three-wire three-phase AC system can be analyzed and more easily controlled using the space vector concept. The active and reactive powers in the *dq* rotating frame are obtained from:

$$P = \frac{3}{2}(V_d I_d + V_q I_q) \quad (25)$$

$$Q = \frac{3}{2}(-V_d I_q + V_q I_d) \quad (26)$$

Now, if the *d*-axis is aligned to the signal at phase A, V_q takes a zero value. In that case the above equations would reduce to the following:

$$P = \frac{3}{2} V_d I_d \quad (27)$$

$$Q = -\frac{3}{2} V_d I_q \quad (28)$$

This means active and reactive powers can be independently controlled when V_d is around unity by simply changing the *d*- and *q*-axes currents injected by the VSC.

1.2.3 Outer Current Control

In normal operation conditions, voltage level is kept around one per unit, so only I_d and I_q can effectively control active and reactive power, which provide two degrees of freedom. To securely operate any VSC-based system, at least one controller must be responsible for preserving the DC voltage of the converter within a permissible range. Furthermore, the system frequency and AC voltage level can be controlled by injecting the proper amount of active and reactive power. The selection of control signals depends on the grid topology and the system operator plan. The set values of voltage are finally translated to current set values, i.e., those implying the currents to be injected by the VSC. Moreover, the time constants of the outer controller loops are typically slower

than inner current controller constants to avoid system instability produced by the inner and outer controllers.

The outer control loops provide references to the inner control loop. The electrical variables incorporated in these control loops are the DC voltage (regarding active power control), the injected current by the VSC and the AC voltage at the PCC. The current references are generated to provide the desired active and reactive power flows using the outer control loop. These controllers must act suitably both steady-state and fault conditions.

a DC Voltage Control Loop in Steady-State Conditions

The DC voltage control loop accounts for maintaining the DC voltage at the DC side of the VSC. This controller is one of the active power controls and provides the setpoint for I_d current (active current). Accordingly, it maintains the balance between the active power injected toward the DC capacitor from the DC grid and the power delivered to the AC grid by the converter. During the steady-state conditions, this control makes the full active power provided by the DC grid be injected into the AC grid. In transient conditions, the DC voltage plays a critical role as an indicator of the active power balance in the DC part of the system.

The basis for controlling V_{DC} concerning power balance is the following equation:

$$\frac{dW_{C_{DC}}}{dt} = V_{DC}\, I_l - P_g \qquad (29)$$

where $W_{C_{DC}}$ is the energy stored in the capacitor, and I_l is the DC current toward the capacitor. In this equation, the power delivered from the generator to the VSC is assumed to be equal to the one injected to the grid. Equation can be rewritten as below:

$$\left(\frac{C_{DC}}{2}\right)\frac{dV_{DC}^2}{dt} = V_{DC}\, I_l - \frac{3}{2}V_g I_{td} \qquad (30)$$

Figure 17 shows how the DC link voltage is regulated using the above equations.

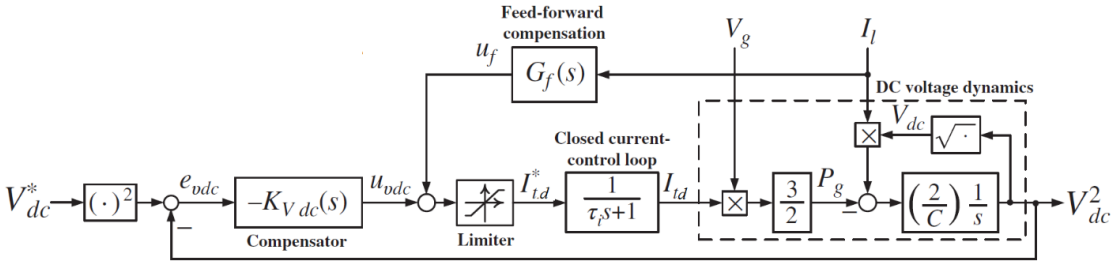

Figure 17. DC-link voltage regulator [28].

b AC Voltage Control Loop

The AC voltage controller deals with the voltage magnitude at the point of common coupling (PCC). This control system appropriately adjusts the reactive power delivered to or absorbed from the grid by the VSC. Figure 18 shows the schematic block diagram of AC voltage control used to control the AC grid voltage in the benchmark.

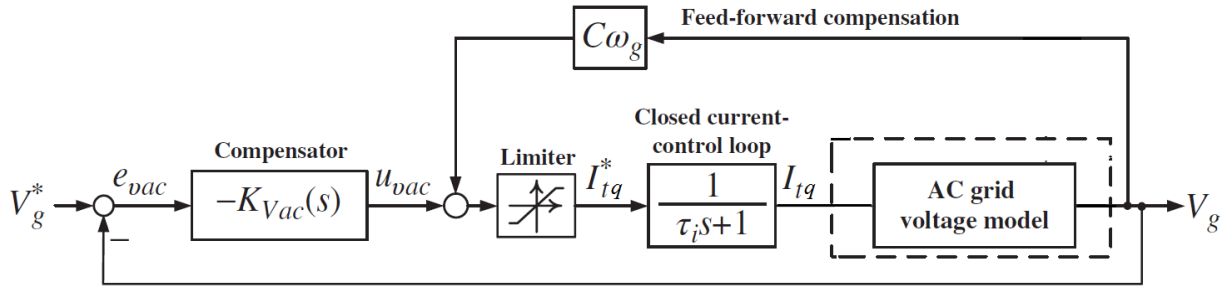

Figure 18. AC voltage regulator [28].

1.2.4 Inner control loop

The inner current controller is the essential part of the control systems associated with VSCs to control the current output of the VSC. Suitable currents to generate the desired voltage are calculated considering the circuit equations between the VSC terminal and the PCC voltages.

Regarding to Figure 19, the relation between the voltage at the VSC terminal and the grid can be obtained as follows:

$$L\frac{di_{ta}}{dt} = -Ri_{ta} + v_{ta} - v_{ga} \quad (31)$$

$$L\frac{di_{tb}}{dt} = -Ri_{tb} + v_{tb} - v_{gb} \quad (32)$$

$$L\frac{di_{tc}}{dt} = -Ri_{tc} + v_{tc} - v_{gc} \quad (33)$$

By converting the above set of equations to the *dq-frame*, the expressions are:

$$L\frac{dI_{td}}{dt} = -RI_{td} + L\omega I_{tq} + V_{td} - V_{gd} \quad (34)$$

$$L\frac{dI_{tq}}{dt} = -RI_{tq} - L\omega I_{td} + V_{tq} - V_{gq} \quad (35)$$

From these two equations, it can be gathered that the I_{td} and I_{tq} currents have additional cross-terms that relates values in D and Q axes, so they are not completely independent. That is why in the control system shown in Figure 19, $L\omega$ branches are used to decouple I_{td} and I_{tq}. In this way, the injected currents at the VSC terminal would follow the associated set values in the inner control loop. In the VSC shown in Figure 19, the current setpoint values are denoted as I_{td}^* and I_{tq}^*.

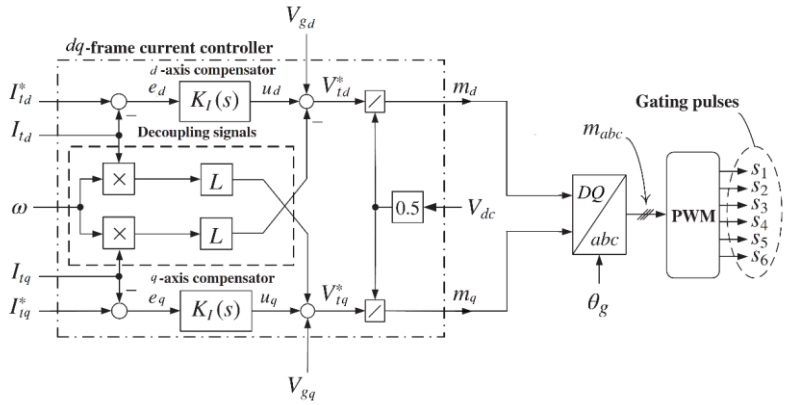

Figure 19. Inner current controller and generated gating pulses [28].

1.2.5 Grid Code Requirements for Fault Ride Through

Grid codes are used for the Transmission System Operators (TSOs) of the different countries to regulate the requirements for connection to their grids. Among such requirements, Low-Voltage Ride Through (LVRT) establishes the conditions for the disconnection and the rules for the voltage support and current injection during these voltage dips for renewable generators.

LVRT establishes that generator units must remain connected to the grid and continue stable operation for voltages above the voltage limit established in the LVRT profile, as shown in the next figure.

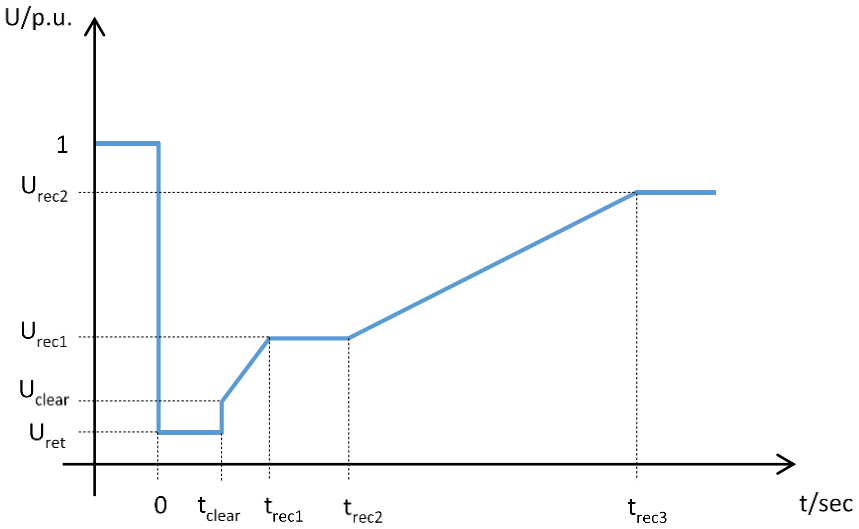

Figure 20. LVRT profile applied to PE generators.

In addition, the reactive power supply is a requirement during the voltage dips. The corresponding voltage control characteristic is shown in the figure. Accordingly, PE-based components have to inject at least 1.0 p.u. reactive current when the voltage drops below 50%. A dead-band of 10% is considered to avoid undesirable control actions.

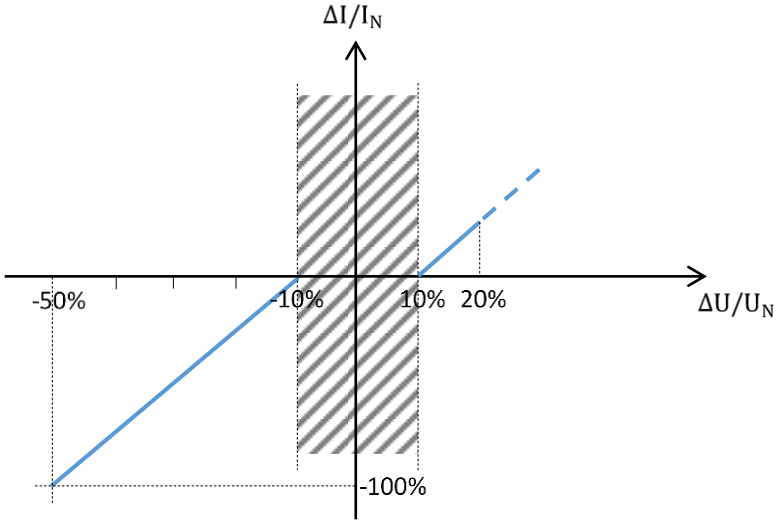

Figure 21. Increment of reactive current defined by the Tennet grid code [29].

The control system calculates the increment of reactive current according to the positive sequence voltage measured. Tennet grid code was used as an example for the study, since it did not consider the injection of negative sequence current and, therefore, it implies symmetrical current injection during asymmetrical faults. This situation is considered, at the early stage of this work, as the most problematic for present protection algorithms to correctly identify a fault.

Taking into account this grid code, the increment of the reactive power is given by the following equation:

$$\frac{\Delta I_B\,(A)}{I_N(A)} = k \cdot \frac{\Delta U(V)}{U_N(V)} - b = k \cdot \Delta U(p.u.) - b \qquad (36)$$

Where,

ΔI_B is the increment of reactive current, in Ampere.

I_N is the nominal current of the system, in Ampere. In the practice, this current will be the current buffered previously to the fault.

ΔU is the voltage drop, in Volt

U_N is the nominal voltage, in Volt

$\Delta U\ (p.u.)$ is the voltage drop, in per unit

b is the compensating factor due to the presence of the dead band until a voltage drop of 10 %.

1.2.6 Negative sequence current contribution control

There are different criteria regarding the negative sequence contribution during unbalance fault. For example, Spanish grid code already includes injecting negative sequence current during unbalanced faults [30] to provide a behaviour similar to synchronous generators, according to sequence networks. However, there are still other TSOs [31] like in Netherlands that do not have this requirement which could be favourable for detection of faults by protection relays. For this reason, the behaviour of the protection system with only positive sequence current and with the influence of negative sequence current injection is studied in the following chapters.

When positive and negative sequence values are present, active and reactive powers contain a constant and two sinusoidal terms as shown below [32] [33]:

$$P = P_0 + P_{cos} \cdot \cos(2\omega t) + P_{sin} \cdot \sin(2\omega t) \qquad (37)$$

$$Q = Q_0 + Q_{cos} \cdot \cos(2\omega t) + Q_{sin} \cdot \sin(2\omega t) \qquad (38)$$

where $P_0$and Q_0 are the constant values of the active and reactive powers, and P_{cos}, P_{sin}, Q_{cos}, Q_{sin} are the sinusoidal power terms at 2ω frequency. Active and reactive power indicated in the previous equations can be written in terms of voltages and currents in the *dq-frame* in both positive and negative sequence networks as:

$$\begin{pmatrix} P_0 \\ Q_0 \\ P_{cos} \\ P_{sin} \\ Q_{cos} \\ Q_{sin} \end{pmatrix} = \frac{3}{2} \cdot \begin{pmatrix} U_d^p & U_q^p & U_d^n & U_q^n \\ U_q^p & -U_d^p & U_q^n & -U_d^n \\ U_d^n & U_q^n & U_d^p & U_q^p \\ U_q^n & -U_d^n & -U_q^p & U_d^p \\ U_q^n & -U_d^n & U_q^p & -U_d^p \\ -U_d^n & -U_q^n & U_d^p & U_q^p \end{pmatrix} \cdot \begin{pmatrix} I_d^p \\ I_q^p \\ I_d^n \\ I_q^n \end{pmatrix} \quad (39)$$

The above equation system relates power terms and current injection setpoints from the VSC. In this system, the number of control variables (four current variables) is less than the number of power terms on the right-hand side (six values). Thus, only four power terms can be controlled directly, leaving the other two terms as linear functions of current set values.

If the system is balanced, components with the superscript "*n*" disappear (negative sequence components) because sinusoidal terms $P_{cos}, P_{sin}, Q_{cos}, Q_{sin}$ depend on the presence of negative sequence values in the system. It occurs in steady-state conditions, or during balanced faults, that is three-phase faults.

During asymmetrical faults or any unbalance in the system, terms with superscript "n" (negative sequence) play a very important role in the behaviour of active and reactive powers. Below, different strategies to control active and reactive powers are shown:

a Negative sequence current equal to zero

This strategy is the most straightforward. In this strategy, the positive sequence currents (I_d^p, I_q^p) are calculated using the grid code requirements according to 1.2.5, and the negative sequence currents (I_d^n, I_q^n) are set equal to zero. This strategy aims to inject only positive sequence current during grid faults, even in non-symmetrical faults. With this method, the entire current capacity of the VSC is used to deliver reactive power demanded by the grid code requirements and the maximum active power with the remaining current capability of the power converter.

b Minimizing 2ω oscillations in active power

In this case, the objective is to control the constant terms of active and reactive power (P_0, Q_0) and eliminate the sinusoidal terms of active power (P_{cos}, P_{sin}). In this way, (42) is simplified to the following system of equations:

$$\begin{pmatrix} P_0 \\ Q_0 \\ P_{cos} \\ P_{sin} \end{pmatrix} = \frac{3}{2} \cdot \begin{pmatrix} U_d^p & U_q^p & U_d^n & U_q^n \\ U_q^p & -U_d^p & U_q^n & -U_d^n \\ U_d^n & U_q^n & U_d^p & U_q^p \\ U_q^n & -U_d^n & -U_q^p & U_d^p \end{pmatrix} \cdot \begin{pmatrix} I_d^p \\ I_q^p \\ I_d^n \\ I_q^n \end{pmatrix} \quad (40)$$

This system has to be solved to find out the setpoint values for currents, according to the intended values for different power terms.

$$\begin{pmatrix} I_d^p \\ I_q^p \\ I_d^n \\ I_q^n \end{pmatrix} = \frac{2}{3} \cdot \begin{pmatrix} U_d^p & U_q^p & U_d^n & U_q^n \\ U_q^p & -U_d^p & U_q^n & -U_d^n \\ U_d^n & U_q^n & U_d^p & U_q^p \\ U_q^n & -U_d^n & -U_q^p & U_d^p \end{pmatrix}^{-1} \cdot \begin{pmatrix} P_0 \\ Q_0 \\ P_{cos} \\ P_{sin} \end{pmatrix} \quad (41)$$

Removing active power 2ω oscillations means that the sinusoidal terms of active power should be set equal to zero:

$$P_{cos} = 0\,, P_{sin} = 0 \qquad (42)$$

Besides, the positive sequence currents are dictated by the National Grid Codes. The positive set values provide voltage support during fault and deliver as maximum active power from the remainder of VSC current capacity.

c Negative sequence current proportional to the negative sequence voltage

This strategy is based on synchronous generators behaviour. Positive sequence voltages and currents are independent of negative sequence voltages and currents. This allows separating the active and reactive power constant terms (P_0, Q_0) into two components:

$$P_0 = P_0^{positive} + P_0^{negative} \qquad (43)$$

$$Q_0 = Q_0^{positive} + Q_0^{negative} \qquad (44)$$

$$\begin{pmatrix} P_0^{positive} \\ Q_0^{positive} \\ P_0^{negative} \\ Q_0^{negative} \end{pmatrix} = \frac{3}{2} \cdot \begin{pmatrix} U_d^p & U_q^p & 0 & 0 \\ U_q^p & -U_d^p & 0 & 0 \\ 0 & 0 & U_d^n & U_q^n \\ 0 & 0 & U_q^n & -U_d^n \end{pmatrix} \cdot \begin{pmatrix} I_d^p \\ I_q^p \\ I_d^n \\ I_q^n \end{pmatrix} \qquad (45)$$

In the positive sequence network, since the voltage in *q*-axes is almost zero, it is possible to approximate the active current with I_d^p and the reactive current with I_q^p. The references for the positive sequence currents in the *dq-frame*, as seen before, are specified by the grid code requirements.

$$\begin{pmatrix} I_d^p \\ I_q^p \\ I_d^n \\ I_q^n \end{pmatrix} = \frac{2}{3} \cdot \begin{pmatrix} U_d^p & U_q^p & 0 & 0 \\ U_q^p & -U_d^p & 0 & 0 \\ 0 & 0 & U_d^n & U_q^n \\ 0 & 0 & U_q^n & -U_d^n \end{pmatrix}^{-1} \cdot \begin{pmatrix} P_0^{positive} \\ Q_0^{positive} \\ P_0^{negative} \\ Q_0^{negative} \end{pmatrix} \qquad (46)$$

However, for the negative sequence network, both voltages in *d* and *q* axes are significant during faults. Hence, the relation between the currents and the active and reactive power in negative sequence are the result of solving the matrix:

$$\begin{pmatrix} I_d^n \\ I_q^n \end{pmatrix} = \frac{2}{3} \cdot \begin{pmatrix} U_d^n & U_q^n \\ U_q^n & -U_d^n \end{pmatrix}^{-1} \cdot \begin{pmatrix} P_0^{negative} \\ Q_0^{negative} \end{pmatrix} = \frac{2}{3} \cdot \begin{pmatrix} \frac{P_0^n \cdot U_d^n}{U_d^{n2} + U_q^{n2}} + \frac{Q_0^n \cdot U_q^n}{U_d^{n2} + U_q^{n2}} \\ \frac{P_0^n \cdot U_q^n}{U_d^{n2} + U_q^{n2}} - \frac{Q_0^n \cdot U_d^n}{U_d^{n2} + U_q^{n2}} \end{pmatrix} \qquad (47)$$

Then, once the references are provided to active and reactive power in the negative sequence, it is possible to calculate the set values for negative sequence currents through this formula.

The separated use of positive and negative reference is based on decoupling the control into parallel and independent control loops, generating a Double Reference Frame (DRF). These separated control loops allow working in the permanent state by using of the positive sequence. Besides, DRF control also manages positive and negative components of the current during a fault situation.

The proposed control structure is shown in the capture seen in Figure 22:

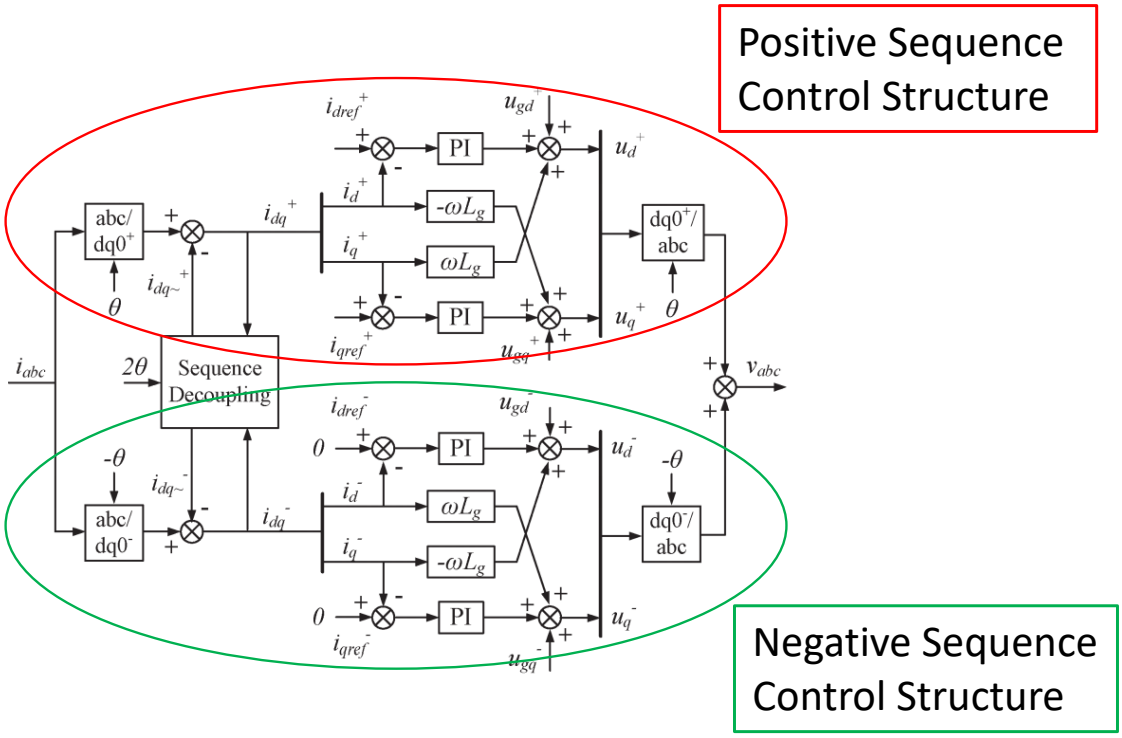

Figure 22. Decoupled control for active and reactive current. Source [34].

1.3 Full Converter - Permanent Magnet Synchronous Generator Wind Turbine Model

This model aims to represent the behaviour of the FCWT, also named as Type-4 wind turbine, in normal conditions and before short circuit events. It consist of the turbine, the generator and the converter physical models, and the control models of the generator-side converter and the grid-side converter. The general theory of control shown in section 1.2 is applied to developing the Type-4 wind turbine control systems. The base model is the library model shown in Figure 23, and it was adapted a described in this section.

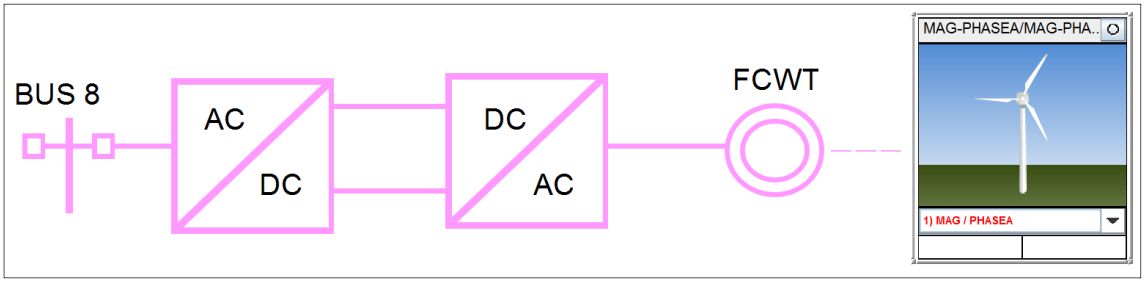

Figure 23. Full-Converter Scheme.

The following sections explain the different components of the model and the control system. Besides, the grid code requirements for wind turbines, the design and implementation of the negative control systems and the detection of fault situations are explained. Wind turbine model, parameters of the generator and generator-side converter were used as library models. On the other hand, the chopper model and the grid side converter control were developed by the author for the studies oh this thesis.

1.3.1 Wind turbine model

The model of wind turbine included in RSCAD is shown in Figure 24. It considers wind speed, air density, altitude above the sea level, turbine power and parameters of the Cp-Lambda curve. The inertia of the mechanical system, number of pole pairs and electrical parameters are also set in the generator model.

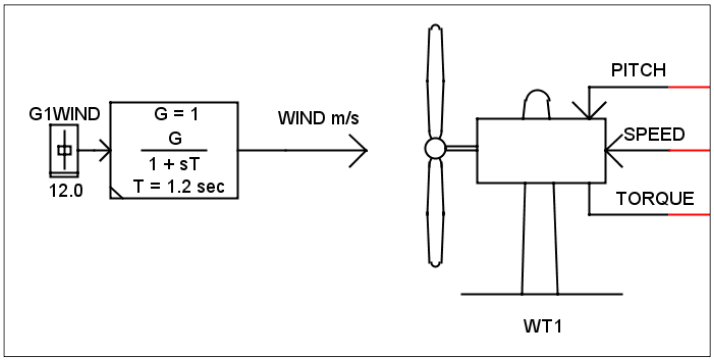

Figure 24. Wind turbine model.

1.3.2 Generator model

Figure 25 shows the generator model, and the parameters from the library model in RSCAD are summarized in Table 1. A 2.5 MW PMSG is used as base and scaled to obtain the installed power in the simulated scenarios in the benchmark grid model.

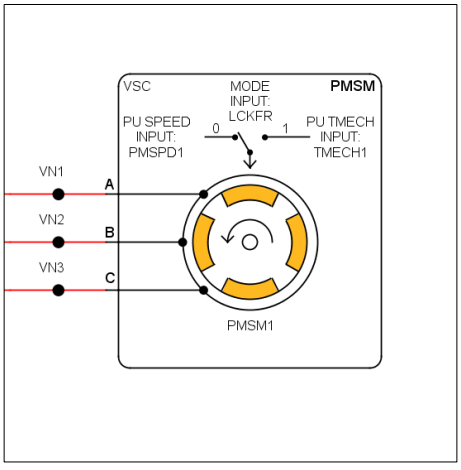

Figure 25. Permanent Magnet Synchronous Generator.

Table 1. Parameters of PMSG.

Description	Value	Unit
Rated Stator Voltage (LL)	4	kV
Rated Apparent Power	2.5	MVA
Rated frequency	3.77	Hz
Stator Leakage Reactance	0.1	p.u.
D-axis Unsaturated Magnetization Reactance	0.65	p.u.
D-axis Damped Leakage Reactance	2.5	p.u.
Q-axis Magnetizing Reactance	1.0	p.u.
Q-axis Damper Leakage Reactance	2.5	p.u.
Stator Resistance	0.01	p.u.
D-axis Damper Resistance	2.0	p.u.
Q-axis Damper Resistance	2.0	p.u.
Magnetic Strength	1.3	p.u.
Inertia Constant	3.5	p.u.

1.3.3 Generator-Side converter and control

Generator-Side converter manages the control of the operating conditions of the PMSG. Figure 26 shows the generator-side converter connected to the PMSG.

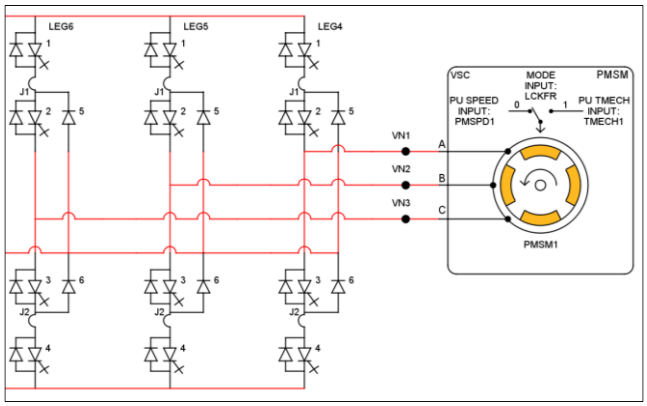

Figure 26. Generator-Side Converter .

Figure 27 hows the diagram of the FCWT detailing the control loops applied to the generator-side converter. These control loops are in charge of tracking the maximum active power generated by the PMSG and the magnetizing current needed (i.e. reactive power or voltage control) by controlling the rotating speed and the voltage at generator terminals.

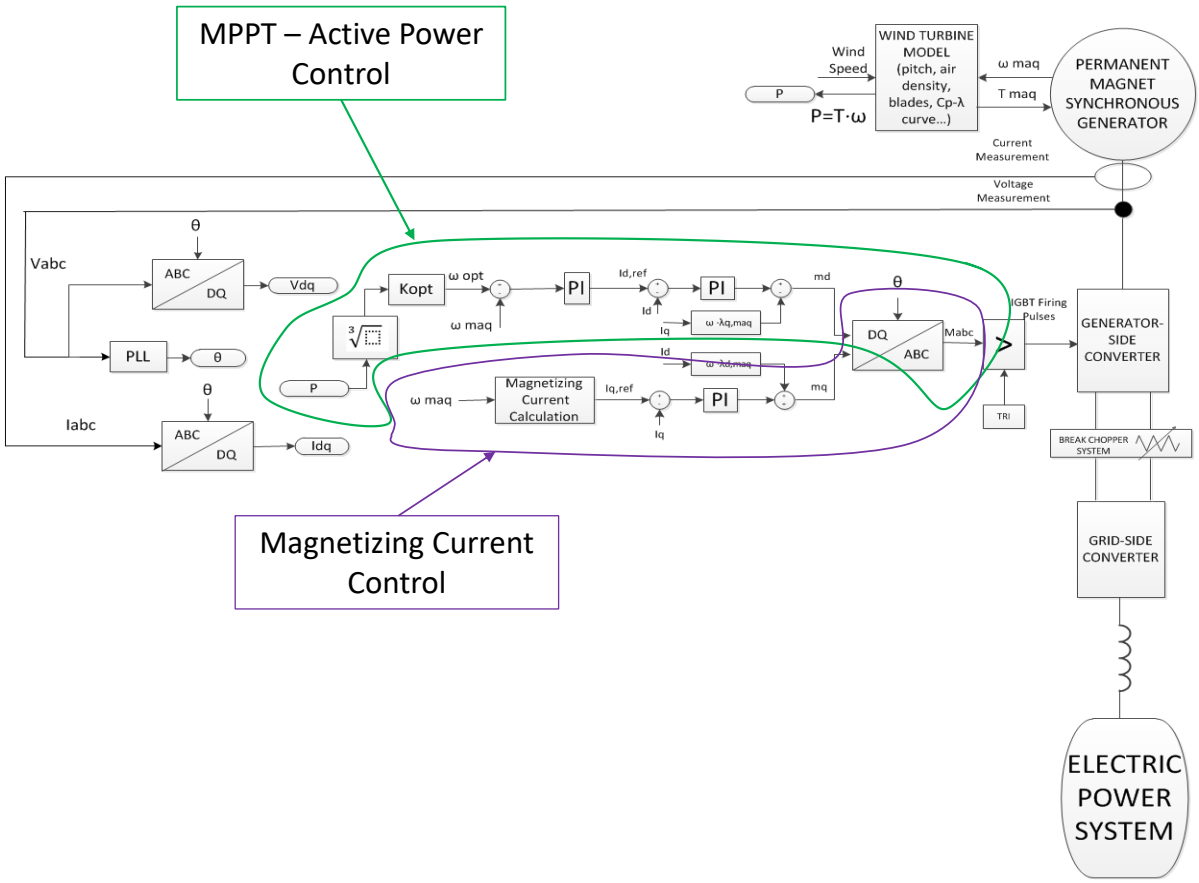

Figure 27. General Diagram for Generator-side converter.

For the active power control loop (emphasized in green in Figure 27), the generator speed reference is calculated according to the well-known equation of the optimum rotating speed (ω_{opt}) regarding the active power and the optimum k_{opt} factor:

$$\omega_{opt} = \sqrt{\frac{P}{k_{opt}}} \text{ [35]} \quad (48)$$

$$k_{opt} = \frac{0.5 \cdot \rho \cdot A \cdot r^3 \cdot C_{p,max}}{\lambda_{opt}^3} \text{ [35]} \quad (49)$$

where: ρ is the air density, A is the area swept by the blades, r is the blade radius, $C_{p,max}$ and λ_{opt} are the optimum parameters of the Cp-Lambda curve of the wind turbine.

Once the optimum rotating speed is calculated, the control system generates an active current setpoint by comparing the rotating speed measured on the generator and the optimum speed calculated by the equation shown above. The active current is directly related to the electromagnetic torque through the equation:

$$T_e = \frac{3}{2} \cdot N_{pp} \cdot \hat{\psi} \cdot I_q \text{ [35]} \quad (50)$$

where T_e is the electromagnetic torque, N_{pp} is the number of pairs of poles, $\hat{\psi}$ is the permanent magnetic flux, and I_q is the active current.

Therefore, controlling the active current using the control of the generator rotating speed, the electromagnetic torque of the generator is controlled.

1.3.4 Chopper model

The chopper system is used in power converters to dissipate the excess of active power during faults and control the voltage in the DC bus in case of a fault event. In these events, the grid side converter can not evacuate power from the generator to the grid, increasing the DC bus voltage. The RSCAD library model does not include a chopper system, so the voltage at the DC bus rises very fast during a fault situation. Since this element is usually installed in commercial FCWT for FRT capability, a chopper system model has been designed and included. Figure 28 shows the chopper system merged between the grid-side and the generator-side converters.

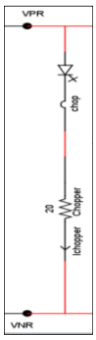

Figure 28. Chopper System.

1.3.5 Grid-Side converter and control

Next figure shows the three-level grid side converter of the Type-4 wind turbine model. The grid side converter control is in charge of synchronizing the wind turbine generator to the power grid, and controlling the active and reactive power injection during normal operation conditions or during faults.

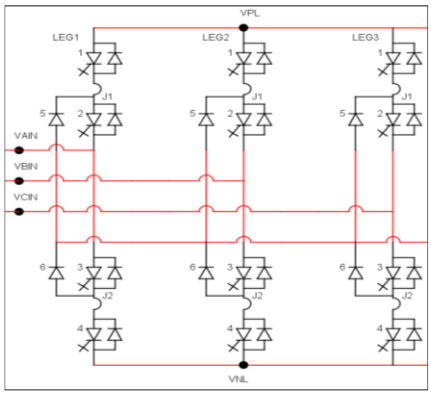

Figure 29. Three-level, grid side converter.

The grid-side control system available in the RTDS library model is not suitable during transient phenomena, such as faults in the power system, because it does not represent the behaviour of FCWT before these events. The developed control model for Type-4 wind turbine incorporates the following new features with regard to the library model:

- Provides a realistic behaviour during permanent and transient phenomena
- Can limit the current during fault transients in the grid (to 1.3 pu maximum, according to ([36] [27] [37] [38]).
- Is adapted to the grid code requirements, so the Type-4 WT remains connected during transient voltage dips and provides voltage support.

- Can control the negative sequence current injection

The control diagram applied for the implementation of the control strategies at the grid side converter in the positive and negative sequence is in Figure 30.

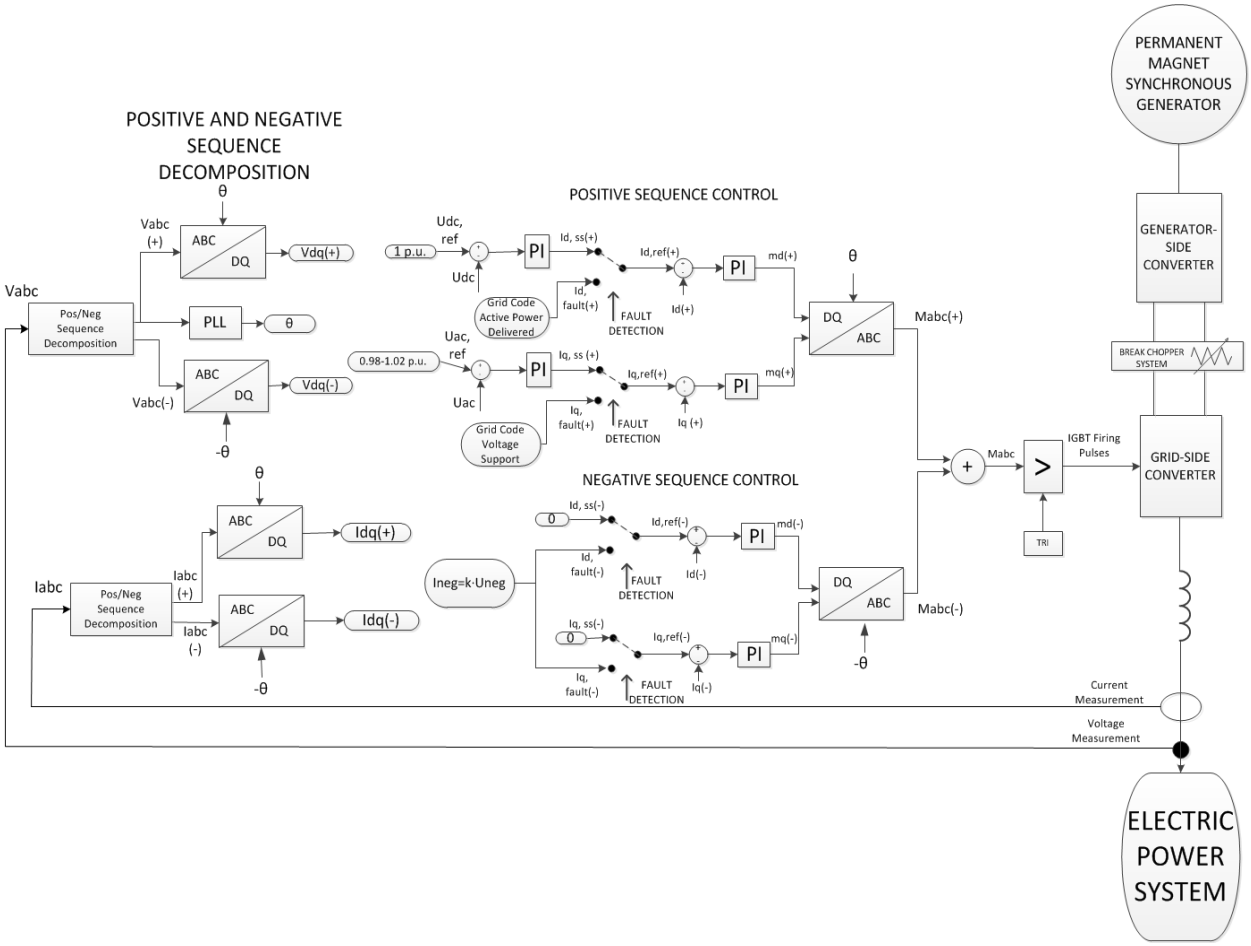

Figure 30. General diagram for grid-side converter control.

Diagram from the figure shows:

- Grid synchronization by PLL
- Voltage and current decomposition
- The control loops for the steady-state and the fault state
- Control loops for positive and negative sequence

The control of the grid side converter is essential for the work developed in this thesis. Therefore, the following sections explain each of the parts indicated above in detail.

a Grid synchronization and voltage and current decomposition

A first step to control the grid side converter is to decouple the real current and voltage waveforms into positive and negative sequence current and voltage waveforms. Red circle from the next figure indicates the positive and negative sequence decomposition and the grid synchronization through the PLL ([39] [33] [40] [41]).

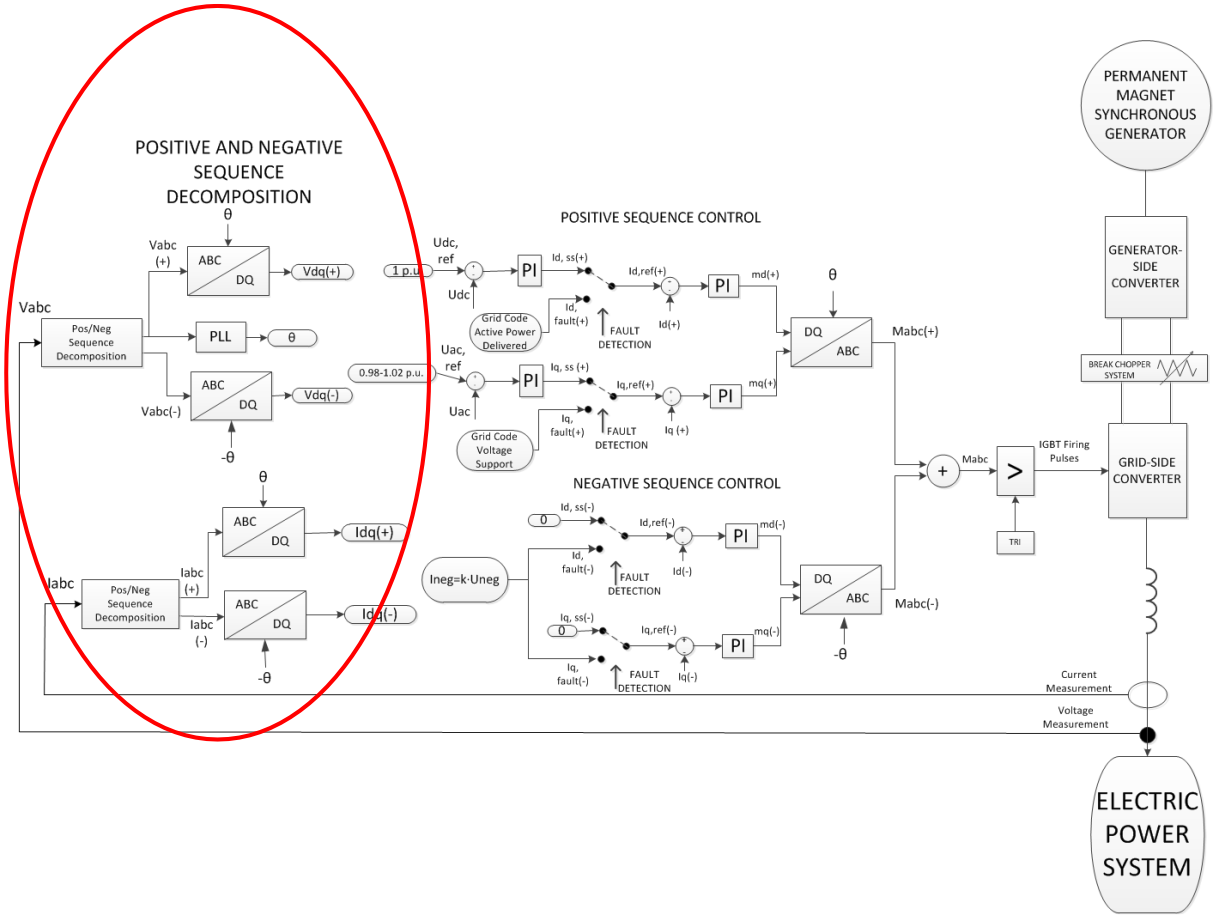

Figure 31. Voltage and current decomposition and grid synchronization.

Clark transformation (1.2.1) and 90º lagging have been used to decompose the voltage and current waveforms into positive and negative sequence. Figure 32 shows the process to decompose current waveforms.

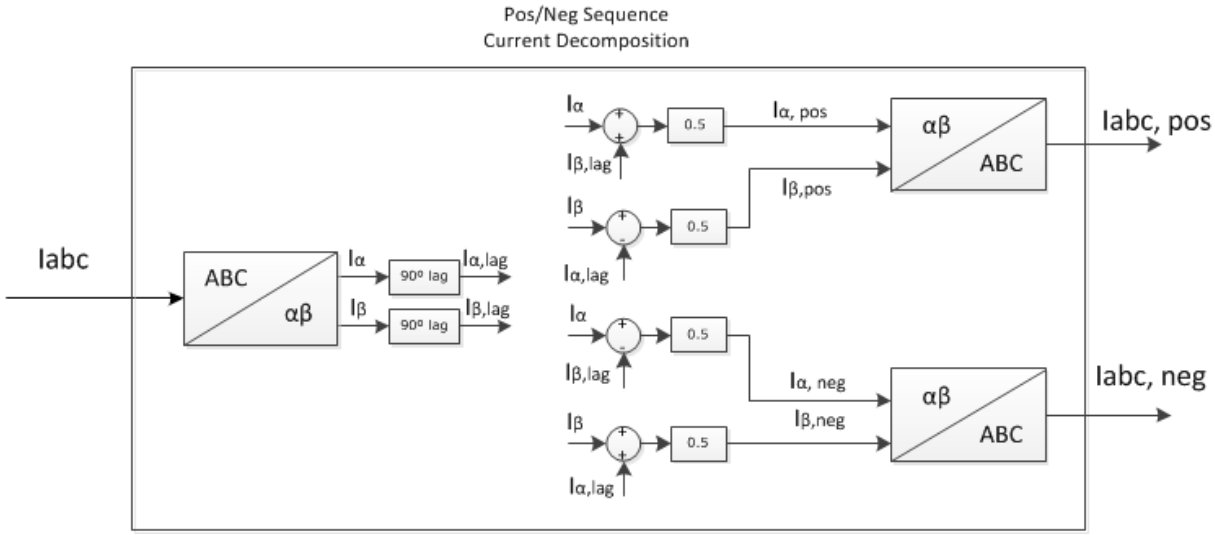

Figure 32. Current decomposition into positive and negative voltage.

In the first stage, shown on the left side of Figure 32, the Clark Transformation is applied to the instantaneous current values. The current waveforms are transformed into alpha-beta waveforms

(I_α, I_β). A lag of 90º is used to these alpha-beta currents using a transfer function, obtaining $I_{\alpha_{90}}, I_{\beta_{90}}$. The following equations are applied to decompose the currents in positive and negative sequence:

- For the positive sequence:

$$I_{\alpha_{pos}} = \frac{1}{2} \cdot (I_\alpha + I_{\beta_{90}}) \quad (51)$$

$$I_{\beta_{pos}} = \frac{1}{2} \cdot (I_\beta - I_{\alpha_{90}}) \quad (52)$$

- For the negative sequence:

$$I_{\alpha_{neg}} = \frac{1}{2} \cdot (I_\alpha - I_{\beta_{90}}) \quad (53)$$

$$I_{\beta_{neg}} = \frac{1}{2} \cdot (I_\beta + I_{\alpha_{90}}) \quad (54)$$

Applying the inverse of the Clark Transformation to ($I_{\alpha_{pos}}$, $I_{\beta_{pos}}$) and to ($I_{\alpha_{neg}}$, $I_{\beta_{neg}}$) separately, positive and negative sequence currents are obtained.

Following the same process for the voltage decomposition provides the values of positive and negative voltages as shown in the following figure.

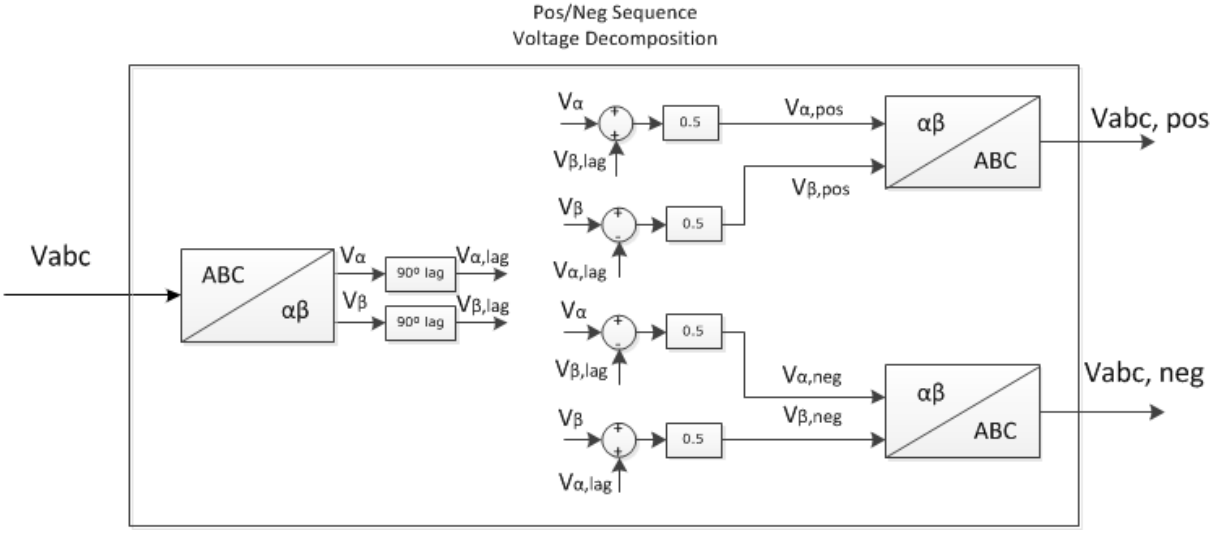

Figure 33. Voltage decomposition into positive and negative sequence.

To avoid oscillations in the angular frequency (ω) and position (θ), the positive sequence voltage signals are provided to the Phase Locked Loop (Figure 34) to obtain the synchronization with the grid.

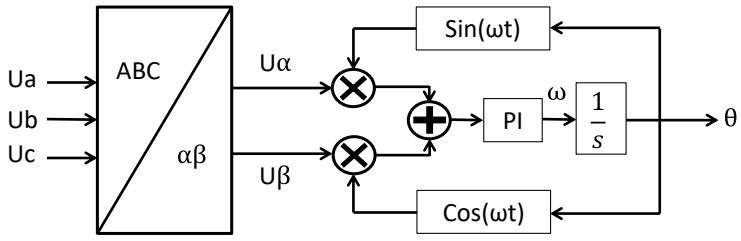

Figure 34. Phase Locked Loop block applied to voltage signals in positive sequence.

Negative sequence voltage and current are negligible during normal operation conditions because the system is balanced but the appear only during unbalance situations. When the negative sequence comes up, oscillations at 2ω frequency appear and are transmitted to the voltage and currents in the *dq* reference if Single Reference Frame PLL is used [33]. To avoid having these 2w oscillations in currents and voltages, the calculation of the position of the grid voltage is done with the positive sequence, using a decoupled calculation of the positive and negative sequence, using in this way a double reference frame [33]. In this way, these oscillations do not affect the behaviour of the Park transformations.

b Grid-Side converter: positive sequence control loops

The positive sequence control is indicated by the red circle in Figure 35.

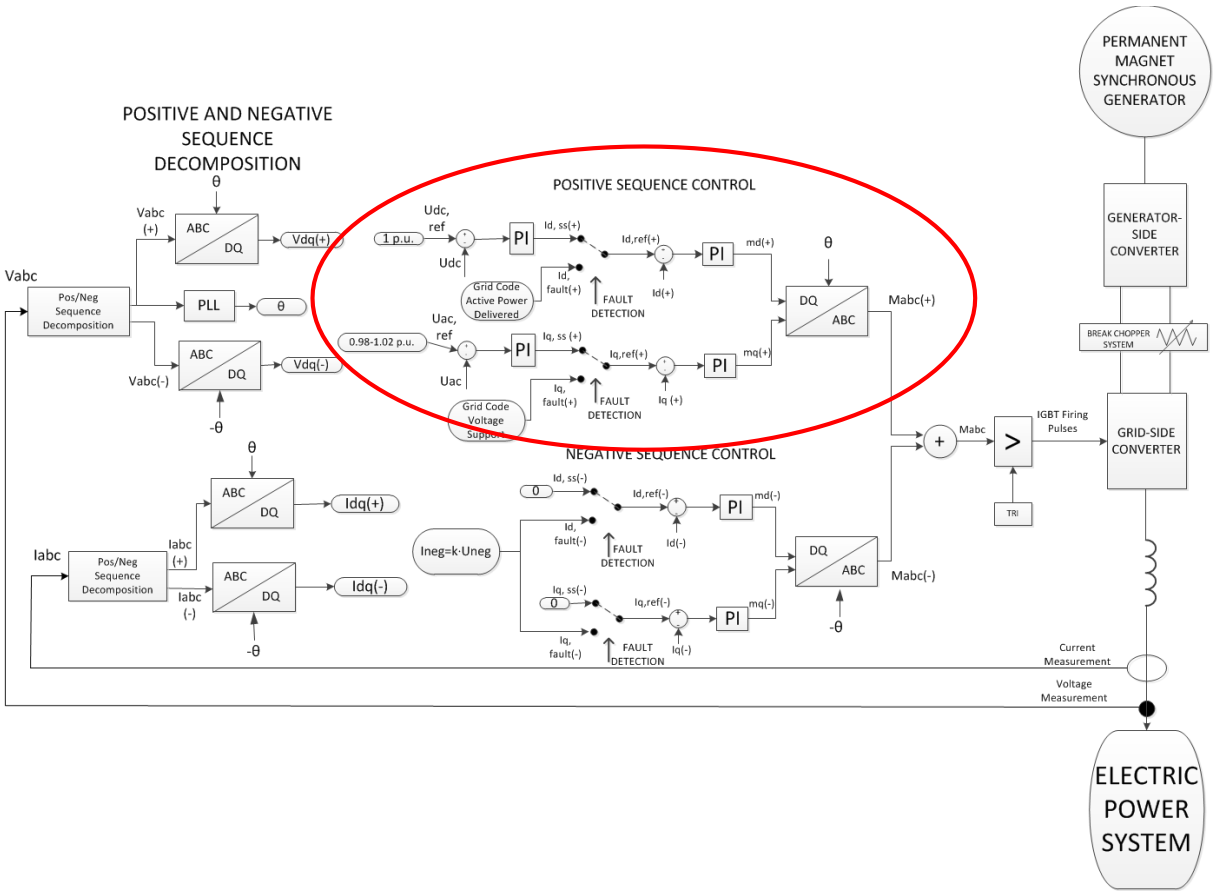

Figure 35. Positive sequence control. DC and AC voltage control/Fault control.

The electrical variables managed in the outer control loops are the DC voltage (active power control) and the AC voltage at the PCC (reactive power control). The outer control loops generate the current references to manage the active and reactive power flows and provide them to inner control loops.

These outer control loops act during the steady-state conditions and during faults, and are briefly described below.

DC Voltage Control Loop in steady-state

The DC voltage control loop is in charge of keeping constant the DC voltage at the power electronic DC bus. This control corresponds to the active power control loop, and provides the I_d setpoint (active current) to balance the active power injected into the DC bus by the generator-side converter and the power delivered to the network by the grid-side converter.

Thus, DC voltage becomes a key indicator of the active power balance in the DC bus.

AC Voltage Control Loop in steady-state

The base of this control system is the management of the reactive power delivered or absorbed by the power electronic converter to control the AC voltage at the PCC. The output of the AC Voltage control loop provides the I_q setpoint, considered as the reactive current reference.

Positive Sequence current loops for fault control

The control system detects the fault situation if the positive sequence voltage falls below 0.9 p.u. and enters the voltage support working mode. According to the TenneT grid code [29] (applied to the grid-side control), the implemented algorithm is:

a. First, the algorithm buffers the total and the reactive current delivered before the fault. The maximum current can be limited with a slider by the user (between 1.0 p.u. and 1.3 p.u.([37]) to define different scenarios in the protection performance studies ([38] [42] [43] [44]). The goal of this adjustable limit is to change the maximum positive sequence current limit and provide the negative sequence current.

b. The control calculates the increment of reactive current, according to equation 28 from section 1.2.5.

c. The active current in positive sequence during the fault is calculated as the vectorial difference between the maximum current value and the reactive current based on the grid code. Being able to evacuate active power during the fault is important because the wind turbine continues generating power during the voltage dip. This active power generated by the wind turbine is injected into the DC bus by the generator-side converter. Therefore, the more power that the grid side converter can deliver to the network during the grid fault, the less active power the chopper will have to dissipate in heat.

To soften the voltage transients after the fault, the voltage support mode is maintained for 500 ms after the control system detects that the fault is cleared. After that, the normal AC voltage regulation takes control again.

In addition, according to the grid code, active power must be increased with a rate between 15-20 % after the fault. To meet this requirement, a ramp has been applied to the reference current from the value established during the fault to the value the DC voltage control. Once final setpoint of the active power is reached, the normal DC voltage control is working again and the voltage dip is finally considered overtaken.

Inner control loops for the Grid-Side converter in positive sequence. Id and Iq control loops

Once the outer control loops generate the currents setpoints in *dq* axes (in steady-state conditions or in the fault conditions), the inner control loops receive these, and the modulation indexes for the positive sequence are generated (m_d^{pos}, m_q^{pos}). The ABC modulation indexes for positive sequence ($m_a^{pos}, m_b^{pos}, m_c^{pos}$) are calculated with the Park Transformation and the positive value of the theta angle provided by the Phase-Locked Loop.

c Grid side converter: negative sequence current control loops

A negative sequence current control has been applied to the FCWT grid side converter control model. The negative sequence control is remarked by the red circle in Figure 36.

During the normal state, the system is balanced, and the references provided by the outer control loop to the negative current are equal to zero. This fact makes the output current of the converter to be symmetrical during the regular operation of the grid, i.e. the only positive sequence current is provided. Nevertheless, if an unbalanced fault is produced, the control system needs to deal with the negative sequence voltages during such faults and provide a negative sequence current.

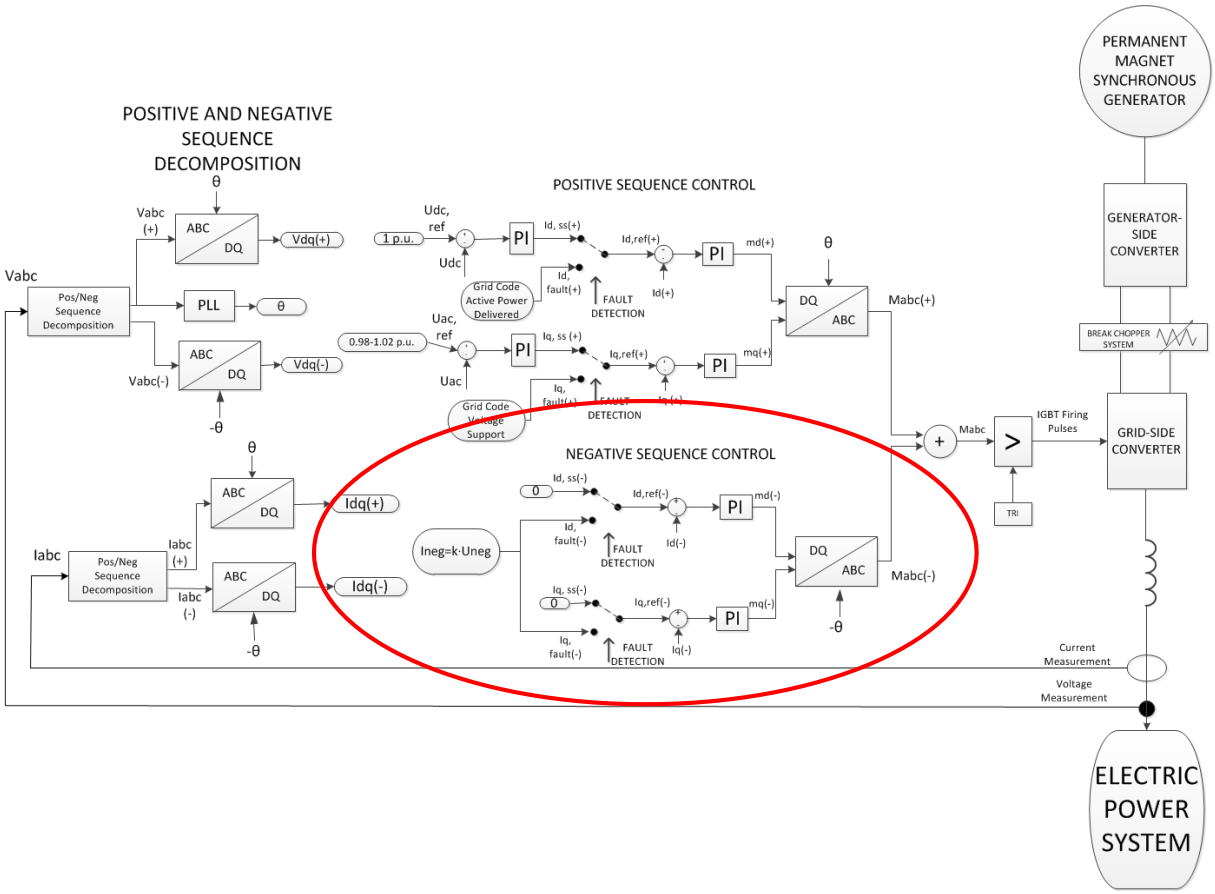

Figure 36. Negative current control. Current proportional to the voltage.

The control of negative sequence has been developed during the first phase of this Thesis. It represents a significant part of the model to study the operation of the protection system, and its theoretical basis has been explained in section 1.2.6. Three different strategies have been considered:

- **Minimization of 2ω oscillations in active power**

  According to the explanations seen in section 1.2.6, with this strategy, it is possible to eliminate the oscillations in active power flow by selecting these parameters:

  $$P_{cos} = 0\,, P_{sin} = 0 \qquad (55)$$

  $$I_d^p, I_q^p, \text{ fixed by the grid code} \qquad (56)$$

  This method has been studied to be applied in the model. Initially, it seems interesting because it avoids or reduces as much as possible the oscillations in the active power coming from the full converter during faults. However, as previously explained, all the oscillations cannot be totally removed because the sinusoidal terms of reactive power (Q_{cos}, Q_{sin}) cannot be fixed seeing that they are a linear combination of voltage and current values in positive and negative sequence.

This method can be beneficial to reduce the torque oscillations during faults in generators directly coupled to the grid such as DFIG machines and, therefore, to increase their lifetime. For this reason, in Type-3 wind turbine, where the stator of the induction generator is directly connected to the grid, can take advantage of this strategy to avoid that the generator receives these oscillations, that may be problematic due to the associated generated torque on it. However, in Type-4 wind turbines, the PMSG is decoupled from the grid, and the benefits regarding the reduction of the oscillations in the active power do not seem so necessary.

Therefore, for Type-4 wind turbines, and taking into account that the models are focused on the protection studies, this strategy has been discarded, and strategies described in the following subsections have been tested in the developed model to check different behaviours of the protection during faults([38] [42] [43] [44]).

- **Negative sequence current equal to zero**

This strategy injects only positive sequence currents during the grid fault, even in asymmetrical faults. This control action is near the performance of the currently installed Type-4 wind turbines during faults, so it has been implemented in the control system to check protections performance.

- **Negative sequence current proportional to the negative sequence voltage**

This strategy considers that the positive sequence voltages and currents are separated from negative sequence voltages and currents. This separation makes it possible to decouple the active and reactive power constant terms (P_0, Q_0) into two components for each one.

This strategy is based on synchronous generator behaviour, where the negative sequence network is defined by the expression [45]:

$$V_a^{(2)} = Z_2 \cdot I_a^{(2)}. \quad (57)$$

The control follows these steps:

1. Measurement of negative sequence voltage U_{neg} (three-phase value, using the decomposition of positive and negative sequence voltage previously explained in 1.3.5).
2. Calculation of negative sequence current I_{neg}, according to the expression $I_{neg} = k \cdot U_{neg}$. Since the goal of this algorithm is to obtain a similar behaviour to a synchronous generator, it is necessary to consider that the relationship between $Uneg$ and $Ineg$ is given by the negative sequence impedance $Zneg$ ($Uneg = Zneg \cdot Ineg$). Thus, the expression of the voltage in negative sequences is applied with the following expression:

$$U_{neg} = Z_{neg} \cdot I_{neg} \rightarrow I_{neg} = \frac{1}{Z_{neg}} \cdot U_{neg} \rightarrow I_{neg} = k \cdot U_{neg} \quad (58)$$

In terms of the currents and voltages used by the control and measured from the electrical system

$$\sqrt{I_d^{n^2} + I_q^{n^2}} = k \cdot \sqrt{U_d^{n^2} + U_q^{n^2}} \quad (59)$$

"*k*" factors can be adjusted by the user to check the behaviour of protections during faults.

Moreover, the limits in the current due to the maximum ratings of the power electronic converter do not allow to provide as much negative sequence current as the synchronous generators (SG) during an asymmetrical fault due to the maximum current limit of the

PE. SG behaviour is analysed below to set the priority between the different components of the current during unbalanced conditions.

In SG, the proportional relation between negative sequence voltage and current in rms is accomplished during the fault.

Therefore, once the apparent power is calculated for the negative sequence, active and reactive power are calculated with a power factor set by the user by a slider. This power factor allows to distribute the apparent power into different amount of active and reactive power in negative sequence. However, the relation between $Ineg$ and $Uneg$, remains constant as in synchronous generators.

The relation between the references for $Pneg$ and $Qneg$ and the voltages and currents in *dq* are given by the matrix expression

$$\begin{pmatrix} I_d^n \\ I_q^n \end{pmatrix} = \frac{2}{3} \cdot \begin{pmatrix} U_d^n & U_q^n \\ U_q^n & -U_d^n \end{pmatrix}^{-1} \cdot \begin{pmatrix} P_0^{negative} \\ Q_0^{negative} \end{pmatrix} = \frac{2}{3} \cdot \begin{pmatrix} \frac{P_0^n \cdot U_d^n}{U_d^{n\,2} + U_q^{n^2}} + \frac{Q_0^n \cdot U_q^n}{U_d^{n\,2} + U_q^{n^2}} \\ \frac{P_0^n \cdot U_q^n}{U_d^{n\,2} + U_q^{n^2}} - \frac{Q_0^n \cdot U_d^n}{U_d^{n\,2} + U_q^{n^2}} \end{pmatrix} \quad (60)$$

Inner control loops for the Grid-Side converter in negative sequence. Id and Iq control loops

The negative sequence current control loop provides the values of current setpoints, according to the strategy chosen in the outer control loop, depending on the study to be done over the protection system ([38] [42] [43] [44]). The inner current control loop for the negative sequence provides the modulation indexes for the negative sequence (m_d^{neg}, m_q^{neg}).

The ABC modulation indexes for negative sequence ($m_a^{neg}, m_b^{neg}, m_c^{neg}$) are calculated with the Park Transformation and the negative value of the theta angle provided by the PLL.

d Final modulation indexes

The final modulation indexes are calculated based on the values of modulation indexes in positive and negative sequence, obtaining the final value for the modulation index on each phase ($m_a = m_a^{pos} + m_a^{neg}, m_b = m_b^{pos} + m_b^{neg}, m_c = m_c^{pos} + m_c^{neg}$).

e Zero Sequence currents

The zero-sequence current cannot flow in the grid converter of the Type-4 wind turbine due to the delta connection of the low voltage side of the transformer (33 kV side). However, the high voltage side (400 kV) of this transformer has the wye grounded. Then, in faults involving the neutral in the 400 kV side, this connection of the transformer allows zero-sequence current circulation, but not from the power electronic converter that is connected in the 33 kV side.

f LVRT Disconnection

An additional control system is needed to disconnect the wind farm if the voltage at the PCC is lower than the Grid Code LVRT profile shown in section 1.2.5. This algorithm checks the voltage at the PCC once the fault appears and acts over a switch that disconnects the wind farm, so that there is no current contribution from this generator during the fault.

1.4 Photovoltaic System

The basis of the strategies applied to the control system for PV converter is very similar to the controls already explained in detail for the wind turbine model. Therefore, in the next section, only the new concepts regarding the PV system elements are explained, and the common control systems are referenced to the previous wind turbine controls, mainly to the grid-side converter controls.

1.4.1 PV generator

The photovoltaic solar model of the library includes a 2 MVA and 480 V PV system, connected to a 13.2 kV network through a power transformer. The elements that are included in the library model are the PV panel model and the DC/AC converter.

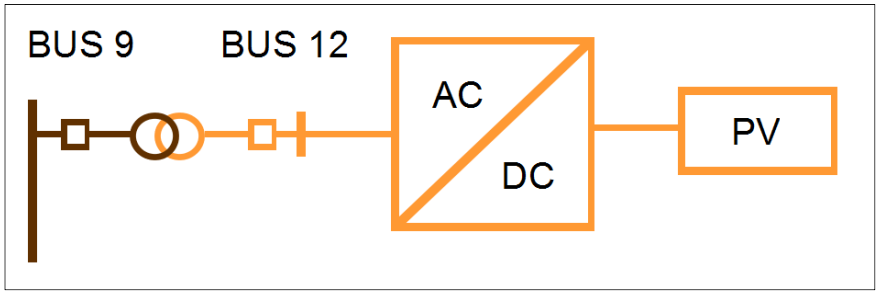

Figure 37. PV system model.

1.4.2 PV panel model

RSCAD provides a very complete solar cell model, including the following options to choose:

- Semiconductor
- Number of series and parallel connected cells
- Open circuit voltage and short circuit current
- Short circuit current temperature coefficient and open circuit voltage temperature coefficient
- Open circuit series resistance and short circuit shunt resistance

The model also brings the option to calculate directly the maximum power point tracking by means of two methods: Lambert function and Fractional open circuit voltage [46].

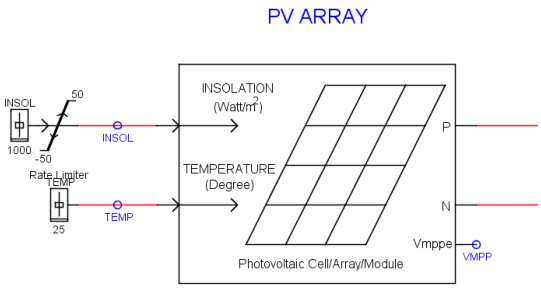

Figure 38. PV Array model. Source: RSCAD library.

The model provides a 2 MVA solar system, connected in low voltage (480 V) to an external grid of 13.2 kV. Scaling factor (like in the case of the Type-4/FCWT) is used to reach the active power values defined: 40, 80, 120 and 200 MW of power delivery from the renewable generators.

1.4.3 Chopper model

Figure 39 shows the general diagram of the PV system. As it can be seen in this figure, no break chopper is connected. Unlike the case of the full converter applied to the wind turbine, the PV system does not need to include a breaking resistor to dissipate the excess of power during a fault condition in the external network and avoid the increase of the DC bus voltage. In the extreme case that no power can be delivered to the grid during a fault, the current in the DC side of the PV generator would be equal to zero, which would lead to an open circuit working condition. This condition is not dangerous for the system since the maximum voltage of the PV panel is the open-circuit voltage (V_{oc}), known from the datasheet of the equipment and used for converted sizing in the design stage of the plant.

1.4.4 Grid-Side converter and control

This power converter is in charge of the grid synchronization of the PV system with the external network. Its control system must deal with normal conditions and fault situations in the grid. The analysis of this converter and its controls is very similar to the grid-side converter analyzed for the PMSG-FC from section 1.3: the active power exchange between the solar panel and the grid is controlled by keeping constant the DC voltage and the AC voltage at the PCC is applied to reactive power management.

As it happened in the PMSG-FC library model, the library control system is designed for working in steady-state situations, but the operation under voltage dips or faults in the system is not adequate. That is the reason why it is needed to use a more advanced control system than which is made in the library.

For this goal, similar strategies and control design regarding the PMSG-FC system has been applied for the grid-side control structure of the PV system (adapting the parameters for PI controllers at each design). Since the grid codes impose the same requirements for solar and wind power installations, and the same potential problems are expected for both full converters, it seems appropriate to use the same development for both cases.

The basis and the structure for the controls applied to the PV system are the same than applied for the Type-4 wind turbine, explained in section 1.3.5.

The control diagram implemented for grid side converter in positive and negative sequence in the PV generator appears in Figure 39.

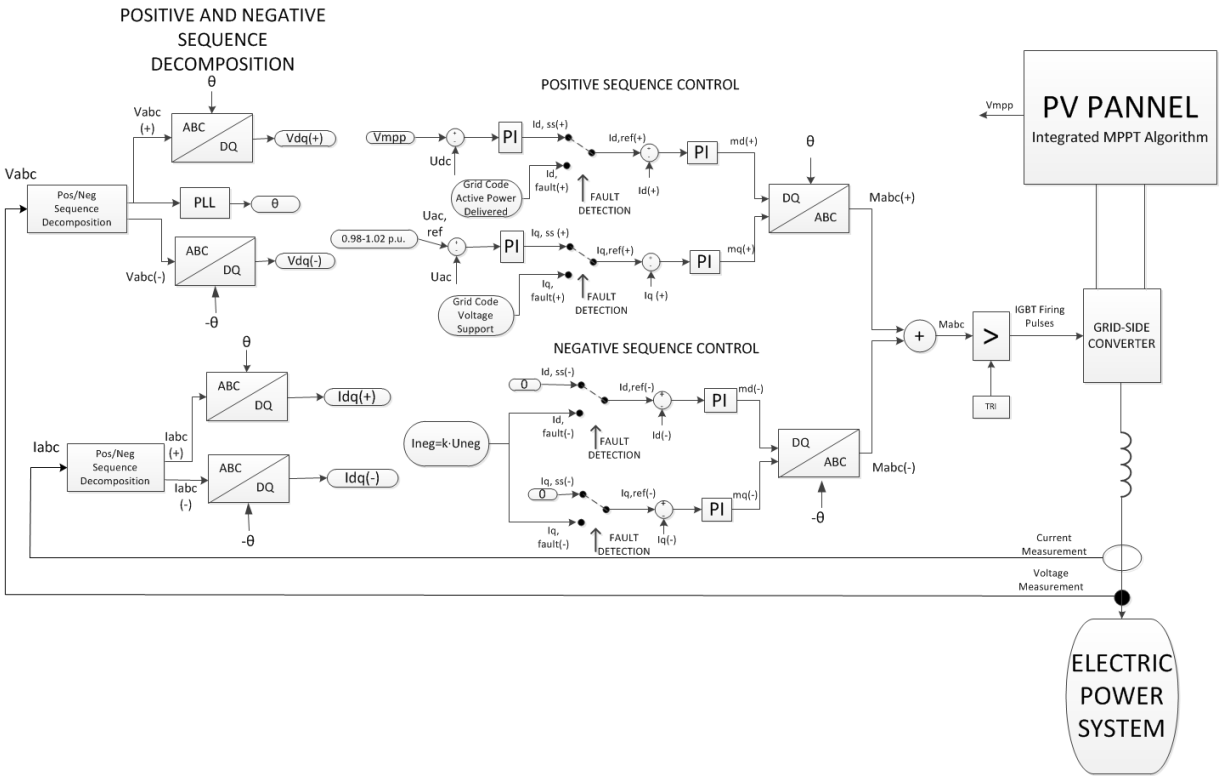

Figure 39. General Control Diagram for PV system.

a Grid synchronization and voltage and current decomposition

The voltage and current decomposition into positive and negative sequence are obtained in the same way than the full converter, previously explained in section 1.3.5 a. The same philosophy of decoupling the positive and negative sequence for voltage and current is applied here and also the same PLL for synchronizing the system.

b Grid-Side converter: positive sequence control loops

Figure 40 shows the control loops for the positive sequence embedded into the general control diagram of the PV system. It is based on the same strategy than the previously explained for the WT system.

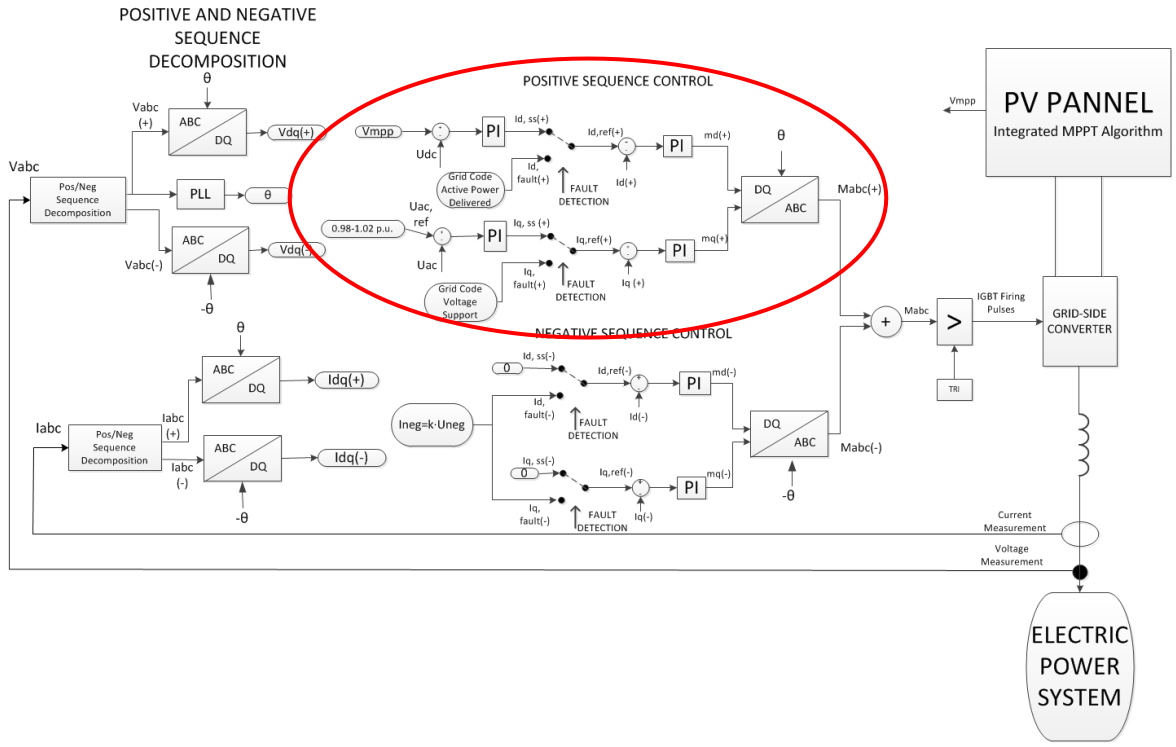

Figure 40. Positive sequence control into the full model.

As explained before, outer control loops provide the current reference for controlling the active and reactive power flow that the grid-side converter exchanges with the network. The generation of these references depends on the state of the system. In the case of a system working on the normal operation mode, the current setpoints are provided by the DC bus voltage control and AC voltage control at the PCC of the grid-side converter. In grid fault conditions, the current references considering the fault control mode. The same logic than in the case of the Type-4 WT has been followed.

DC Voltage Control Loop in steady state

The DC voltage control is essential for PV system operation. The PV panels array is sized to generate a voltage in the range of the DC voltage needed to inject power into the AC network, taking into account the variable conditions of the solar irradiance. The DC voltage provided by the solar panel at its maximum operating point is around 2.0 kV. This voltage is enough to inject power into a power system of 480 Vrms line to line without any additional DC/DC converter. Besides, DC/DC converters do not take part in fault ride through algorithms, so no supplementary DC/DC converter modelling is needed for the protection studies developed in this work.

The MPPT techniques calculate the DC voltage that gets the maximum power depending on the electrical parameters and the environmental conditions in each moment. This value is provided as a reference to the DC voltage control loop that generates the positive sequence active current setpoint (I_d^p) to deliver the maximum active power from the PV panel to the grid, completing the regulation system.

AC Voltage Control Loop in steady-state

Reactive power control loop calculates the positive sequence reactive current setpoint (I_q^p) depending on the voltage at the PCC. The limit of the reactive current depends on the maximum ratings of the power converter and the active current required by the DC Voltage Control.

Positive sequence current loops for fault control

As previously explained for Type-4/FCWT, when the control system detects a fault situation in the grid (the positive sequence voltage goes below 0.9 p.u.), the current references are generated according to the grid code requirements. In this situation, the positive sequence reactive current setpoint (I_q) is calculated depending on the voltage dip level and the reactive current injected before the fault. The active current is calculated taking into account the current available considering the maximum ratings of the converter and the reactive current from the requirements.

Inner control loops for the Grid-Side converter in positive sequence. Id and Iq control loops

Once the outer control loops generate the currents setpoints in *dq* axes (in steady-state conditions or in the fault conditions), the inner control loops generate the modulation indexes for the positive sequence in the *dq*-frame (m_d^{pos}, m_q^{pos}). The ABC modulation indexes for positive sequence ($m_a^{pos}, m_b^{pos}, m_c^{pos}$) are calculated with the Park Transformation and the positive value of the theta angle provided by the Phase-Locked Loop.

c Grid side converter: negative sequence current control loops

Figure 41 shows the negative sequence control loops into the general control diagram of the PV system. Same explanation than given for the FCWT is valid for this control system.

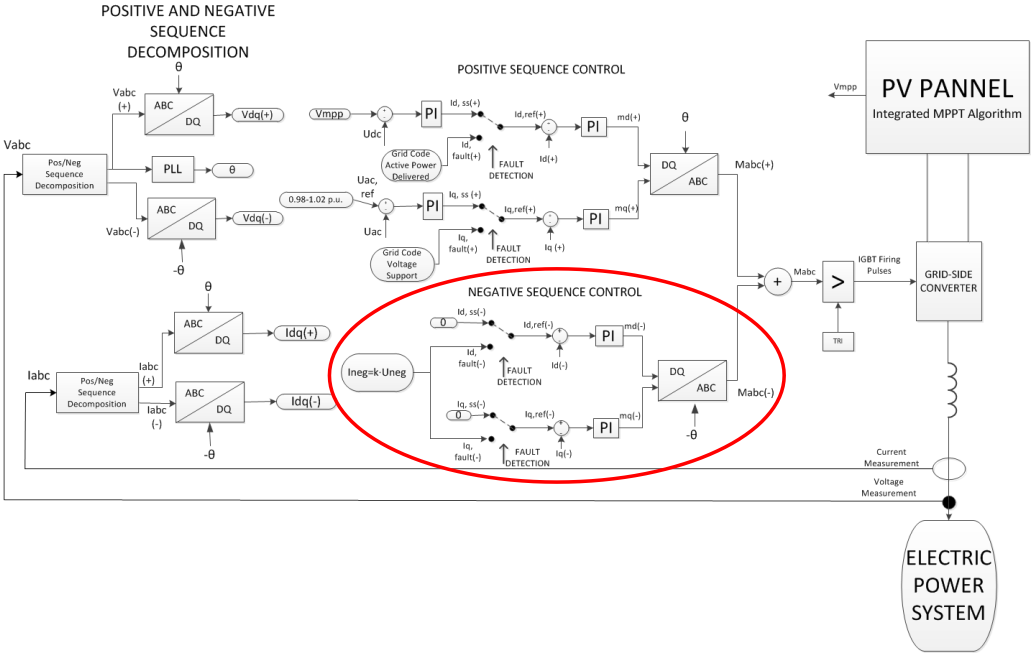

Figure 41. Negative sequence control into the full model.

Outer control loops for the Grid-Side converter in negative sequence

During the normal state, the system is balanced, and the references provided by the outer control loop to the negative current in the dq-frame are equal to zero. This fact makes the output current of the converter to be symmetrical during the normal operation of the grid. Nevertheless, in unbalanced faults, the system needs to deal with the negative sequence voltages that appear during the unbalanced faults. In this case, two options have been implemented for negative sequence current generation:

- **The negative sequence currents are equal to zero**

  This behaviour imitates the behaviour of currently installed PV systems. During faults, these generators only inject positive sequence current, even in unbalanced faults.

- **The negative sequence current is proportional to negative sequence voltage.**

  Approximating the relationship between the negative voltage and current shown in the sequence network for negative sequence as described in section 1.3.5 c.

Inner control loops for the Grid-Side converter in negative sequence. Id and Iq control loops

The inner current control loop for negative sequence provide the modulation indexes for negative sequence (m_d^{neg}, m_q^{neg}) considering the negative sequence current setpoints from the outer control loop.

The ABC modulation indexes for negative sequence ($m_a^{neg}, m_b^{neg}, m_c^{neg}$) are calculated with the Park Transformation and the negative value of the theta angle provided by the PLL.

d Final modulation indexes

The final modulation indexes are calculated based on the values of modulation indexes in positive and in negative sequence, obtaining the final value for the modulation index on each phase ($m_a = m_a^{pos} + m_a^{neg}, m_b = m_b^{pos} + m_b^{neg}, m_c = m_c^{pos} + m_c^{neg}$).

e Zero Sequence currents

The zero-sequence current cannot flow in the grid converter of the PV system due to the delta connection of the low voltage side of the transformer (14.5 kV side). However, the high voltage side (400 kV) of this transformer has a star connection with grounded neutral. Then, in the case of fault involving the neutral in the 400 kV side, this connection of the transformer supplies the zero-sequence current, but not the power electronic converter connected in the 14.5 kV side.

f LVRT disconnection

An additional control system is needed to disconnect the wind farm if the voltage at the PCC is lower than the Grid Code LVRT profile shown in section 1.2.5. This algorithm checks the voltage at the PCC once the fault appears and acts over a switch that disconnects the wind farm, so that there is no current contribution from this generator during the fault.

Chapter 2 Assessment of Short Circuit Protection under high PE level

The analysis of unexpected behaviour of protections is an essential input for generating new protection algorithms, which is expected to provide new solutions adapted to a future scenario with high penetration of renewables. This chapter aims to evaluate if present protection systems may be in trouble in future scenarios with high penetration levels of renewable energies asynchronously connected through power electronics. Therefore, general setting criteria used by TSOs with present protection relays have been used to compare the results under two different scenarios depending on the installed generation, considering synchronous generation and PE-based renewable generators.

Figure 42 summarizes the procedure followed for this work and described in this chapter and the following. The steps indicated in the green arrow are described in this chapter to reach the new solutions described in Chapter 3 and implemented in Chapter 4.

Two different protection relays from two manufacturers (called A and B to keep their confidentiality) are tested in the laboratory to analyze their behaviour under renewable energies current contribution. It was necessary to develop automatic tools for launching all the tests to the protection relays to carry out the present analysis. After analyzing the results, recommendations and conclusions arise to develop a new improved protection solution.

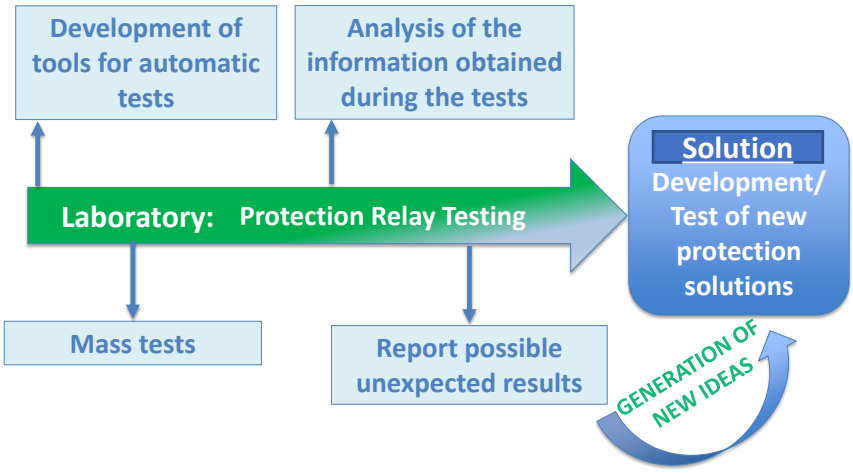

Figure 42. Chapter 2 study: General structure.

2.1 Laboratory tests methodology for Short Circuit Protection assessment

The methodology followed for the tests shown in this chapter is:

1. Protection settings are calculated according to TSO criteria [47] and uploaded in the devices from Manufacturar A and B.
2. Check the behaviour of the protection for a 100% synchronous generator scenario. Distance, differential and ground directional overcurrent protection functions are tested independently one by one in each location defined in section 2.2.
3. Apply the same tests from step 2 in renewable generation scenarios.
4. Collecting results: Analysis of tripping time/lack of trip of protection relays of both manufacturers.
5. Selection of most representative tests and results among all the tests analyzed.
6. Download and analyze oscilography for further analysis.

The values of the relay settings for each location are based on the TSO Setting Criteria [47] defined by REE. Settings are loaded to Manufacturers A and B. This nomenclature is used in this work to keep the confidentiality of the results. Distance, differential and ground directional overcurrent protection functions are tested independently one by one. A more detailed explanation of the testing procedure is included in Appendix 4.

2.2 Description of the contour variables

The Benchmark model shown in section 1.1 has been used to test commercial protections under scenarios based on high penetration levels of renewable energies and power electronic converters. Different fault types have been simulated in lines 5-7 and 4-5, indicated by blue circles in the following figure, aiming to test distance, line differential and ground directional overcurrent functions.

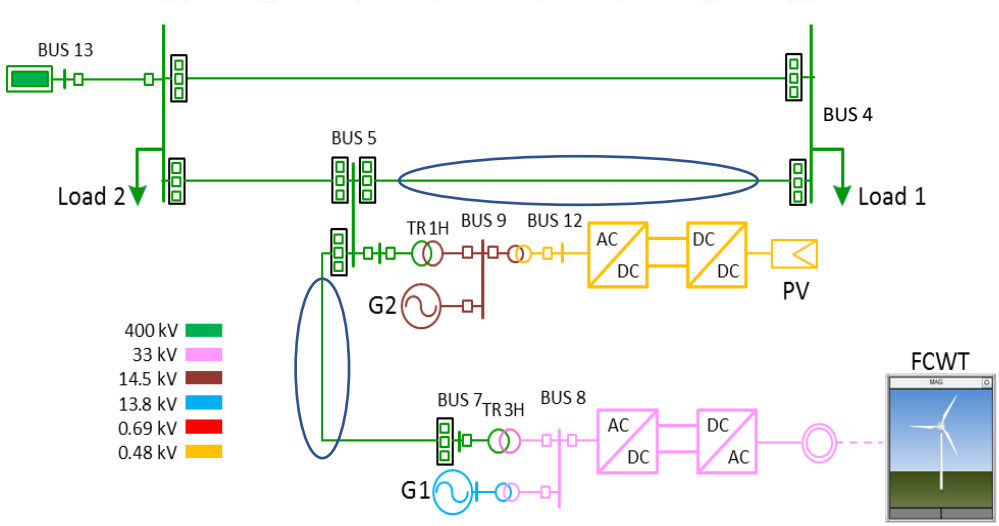

Figure 43. Benchmark model.

To differentiate the positions of each line, in the following sections, the point closest to the Thevenin equivalent of the external network connected to Node 13 is denoted as the "grid side position" of the analyzed line. Likewise, it will be designated as the "generator side position" of the surveyed line, that position that is closer to the synchronous or renewable generator whose contribution is being analyzed.

2.2.1 Breaker status at grid-side positions

The control of PE used in this work needs a voltage source reference to be synchronised with. This means that it is not possible to eliminate the traditional synchronous behaviour of the slack equivalent bus (bus 13 in the figure). Therefore, protections located at the grid-side position see a synchronous generator-based current contribution to the fault and those at the generator-side protection detect the current from the PE-based generator.

Since this study aims to analyze protection algorithms and settings criteria currently used behaviour under high penetration level of renewables, breaker at grid-side position always remains closed avoiding islanding operation during distance protection and ground directional overcurrent tests, emulating a breaker failure. Thus, protection relays at the generator-side position can see the fault contribution during all the fault duration while the renewable generator control do not lose the voltage reference provided by the slack bus.

If the protection trip from the grid-side position was not blocked, one of these two situations could occur:

1. The voltage falls below the LVRT limit of each renewable generator. In this case, the control system disconnects the renewable generator and the line protection relay stops seeing the current contribution from the renewable source. Unless line protection trips before generation disconnection, a non-trip will be obtained, and it is not possible to analyse line protection behaviour. Under this situation, the test would be considered incomplete and results not relevant.

2. The voltage drop is not enough to cause disconnection due to the LVRT control. Reactive current injection during the fault due to the voltage support requirements based on grid codes increase voltage at the point of connection of the PE-based generator. This is the sequence of events:

a) Protection relay installed at grid-side position detects the fault and trips. This trip will usually last at least 70-90 ms: 20-30 ms for the tripping decision of the protection relay and 50-60 ms for the breaker opening time.

b) During these 4 or 5 cycles, the voltage dip control mode from the PE-based generator is activated, providing voltage support according to grid code requirements. The deeper the voltage drop in the grid is, the more significant reactive current support is, according to the grid code behaviour.

c) Reactive power injection makes that voltage remains above the LVRT limit, and the PE-based generator continues connected in islanded mode. Since this situation is not in the scope of this study and controls of the generators are not configured to detect this situation, the control system would probably lose stability[1].

d) This non-controlled mode may cause non-stable current and voltage waveforms. Under these conditions, the behaviour of the protection cannot be considered relevant nor reliable because tests conditions are not controlled.

Because of the above, for the analysis of protection relays behaviour under PE current contribution, the trip of the grid side breaker has been blocked to avoid islanded operation; this means that:

- for line 5-7 protection, the relay acts over the breaker located at bus 7, and the breaker at bus 5 is blocked.
- for line 4-5 protection, the relay acts over the breaker located at bus 5, and the breaker at bus 4 is blocked.

In these cases, the current contribution measured by relays comes from Type-4 WT and PV generators, respectively. Both generators inject power into the grid with a fully rated converter topology, but the behaviour is not the same due to the difference between PMSG and PV panels [48]. The initial peak observed for the PV generator after the fault inception is not as high as in Type-4 WT, and the current reduction after this fault inception is faster, as can be observed in Appendix 2 and Appendix 3.

2.3 Settings validation for distance protection

Initial validation of the settings was applied with synchronous generation current contribution previously before testing the positions with renewable energy. This validation aims to check and compare the behaviour of correct settings for traditional synchronous generation grid and with renewable-based generation grid.

According to Appendix 4, the initial validation of the settings was applied for generation in line 5-7 of Figure 43. The results obtained are summarized in Table 2.

[1] Nevertheless, WT installed are equipped with anti-island detectors. Under this situation, the WT would be disconnected, and the fault current would disappear, so the protection may not detect the fault situation.

Table 2. Results for settings validation in grid side position based on IEC 62055-121:2014. Distance protection.

Fault type	Point of the Voltage wave	Fault resistance	Point of the line	Synch. generation level	Grid conditions	Relay A and B
SLG	0 and 90 degrees	15 ohm	0% and 50 %	40, 200 MW	Strong and weak grid, synchronous generation	Correct behaviour. Zone 1 trip in less than 35 ms.
SLG	0 and 90 degrees	15 ohm	100%	40, 200 MW	Strong and weak grid, synchronous generation	Correct behaviour. Zone 2 trip in less than 440 ms.
LL	0 and 90 degrees	10 ohm	0% and 50%	40, 200 MW	Strong and weak grid, synchronous generation	Correct behaviour. Zone 1 trip in less than 35 ms.
LL	0 and 90 degrees	10 ohm	100%	40, 200 MW	Strong and weak grid, synchronous generation	Correct behaviour. Zone 2 trip in less than 440 ms.

According to the results from Table 2, the following conclusions were obtained:

- Results obtained for grid-side position relays according to the standard conditions for testing are correct.
- Settings criteria for distance protection are considered correct.

The final validation of each line and protection function settings is done independently. Before starting to test scenarios with high penetration of renewable energies and power electronics, each protection is tested with a synchronous generation scenario. Results from these tests are used as a reference for comparison. Once the behaviour is considered correct for the synchronous generation scenario, tests with renewables can be applied with the same settings.

Fault resistances used for the tests depends on the protection tested:

- For distance protection: Solid fault.
- For line differential protection: 150 ohms fault phase to ground faults.
- For ground directional overcurrent protection: 150 ohm phase to ground faults. If the polarizing voltage is insufficient to activate the protection function, the fault resistance value can be reduced to half (75 ohms)

The output of this step are the validated settings to analyse the behaviour of protection relays with current contribution from renewables.

2.4 Distance Protection Tests

This section summarises the results obtained for distance protection testing in lines 5-7 and 4-5 from the benchmark grid described in the previous section.

Solid faults have been applied in all the tests because it is the more favourable case for distance protection. Therefore, the study is focused on the effect of renewable energy source contribution in distance protection rather than fault resistance influence, which is a well-known limitation of distance protection [49] that is not considered in this study.

Problems in the operation of distance protection are studied in this , therefore, it is analysed in the tests if they occur: overreach and/or underreach of the impedance measurement, missed trips and delayed trips.

In Appendix 4, the cases are explained in more detail.

2.4.1 Line 5-7 fault simulation results

This section shows the analysis of the simulated faults in Line 5-7 of the Benchmark grid described in Chapter 1. These simulations allow checking commercial protections before FCWT current contribution. Two generation scenarios have been tested. Below the main results are described.

a Synchronous generation scenario

As stated before, settings for distance protection are firstly validated with synchronous generation scenario with solid faults. Once the distance protection relays provide correct tripping times for zone 1 and zone 2 faults, the settings are considered accurate and suppose the starting point for the test with contribution from renewable energies. The same philosophy is followed for line 4-5.

Therefore, results obtained for line 5-7 with synchronous generation scenario can be summarized as:

- **Zone 1.** Trip times are correct (less than 45 ms) for faults in these study cases:
    - Generation level of 40 and 200 MW
    - Type of fault: Single line to ground, line to line, line to line to ground and three-phase to ground
- **Zone 2**. Trip times are correct (less than 440 ms) for faults in these study cases :
    - Generation level of 40 and 200 MW
    - Type of fault: Single line to ground, line to line, line to line to ground and three-phase to ground

b Renewable generation scenario

Once the settings are validated for the synchronous generation scenario, the renewable generation scenarios are tested, and the obtained results are presented in this section in terms of statistical results.

Results including all types of fault, point of the line and generation levels are gathered. These results have been divided into weak and strong grid conditions for 100% renewable. Results are summarized in Table 3, where results are classified using this notation:

- **No trip** means that the protection does not detect the fault, and the trip is not produced. This supposes the worst behaviour of the protection from the point of view of system security.
- **Delayed trip and overreach** shows tests with a delayed trip in zone 1, delayed trips in zone 2 or overreach of zone 1 over faults located in zone 2.

The values shown in Table 2 in the columns "No trip" and "delayed trips, overreach" indicate the percentages with respect to the total number of cases of each scenario. For example, for the 100% of cases applied for the scenario "100% RW – Strong Grid", 53.33% of the cases were "No trip", and the 20.00 % were "delayed trips, overreach". It means that in 26.67 % of tests, the behaviour of the protection was correct (100%-53.33%-20.00%=26.67%). More details about the tests applied can be checked in Appendix 4.

Table 3. Comparison of manufacturers results before faults applied to line 5-7.

Comparison: Weak vs Strong grid line 5-7			
Protection relay	**Scenario**	**No trip**	**Delayed trips, overreach**
Manufacturer A	100 % RW - STRONG GRID	53.33%	20.00%
	100 % RW - WEAK GRID	50.83%	13.33%
Manufacturer B	100 % RW - STRONG GRID	38.33%	30.83%
	100 % RW - WEAK GRID	45.83%	31.67%

According to the results from Table 3, there are no significant differences between weak and strong grid conditions in terms of unexpected behaviours of protection relays, both in the case of 100% renewable and synchronous scenarios. Thus, for the subsequent analysis, the results of both scenarios can be merged (both missed trips and delayed/overreach trips).

Next Figure 44 and Figure 45 show these results classified by type of fault for each manufacturer, gathering the total faults applied with:

- Strong and weak grid conditions;
- Generation level of 40 and 200 MW;
- Points of the fault along the line: 0, 50, 70, 90 and 100%.

In these figures, along with the number of faults/percentages where the protection relays present an unexpected behaviour, it is also interesting to observe the distribution of the bar chart for the different manufacturers. Figure 44 a) shows the missed trips percentage for Manufacturer A protection for the fault types tested. As it is displayed, this protection obtains the worst result for single line to ground faults (SLG) and line to line faults (LL). Figure 44 b) shows the delayed trips and overreach malfunction for Manufacturer A protection finding the maximum percentage for the line to line fault (LL) with 5.42 % of malfunctioning tests and the minimum for the single line fault (SLG) with 2.92 %.

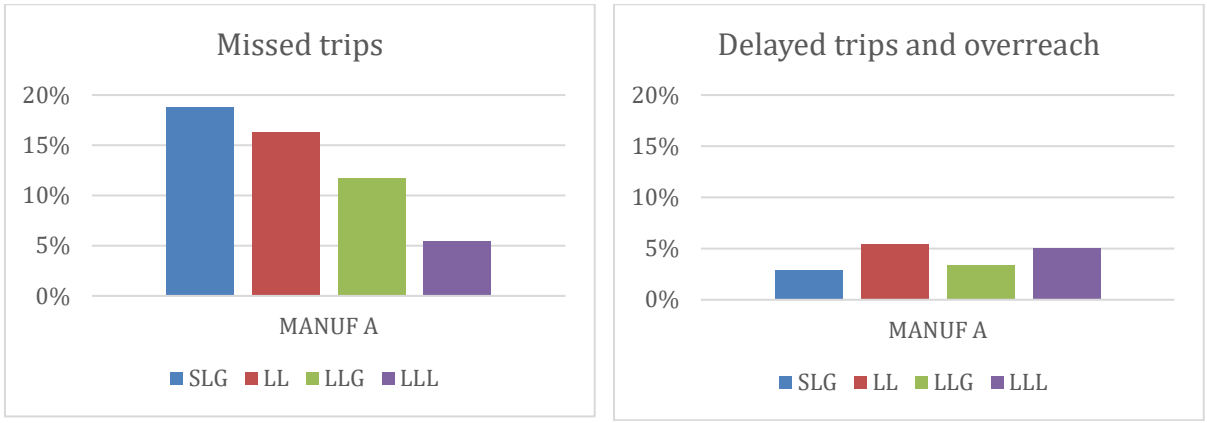

a) *b)*

Figure 44. Manufacturer A protection missed trips (a) and delayed trips and overreach (b).

Figure 45 shows the missed trips in Manufacturer B protection for the fault types tested. In this case, line to line (LL) and three-phase faults (LLL) missed trip percentages are greater than those defects involving the ground. However, the trend is the opposite for the delayed trips and overreach, where the maximum value is obtained for the line to line to ground (LLG) and the single line to ground (SLG) faults.

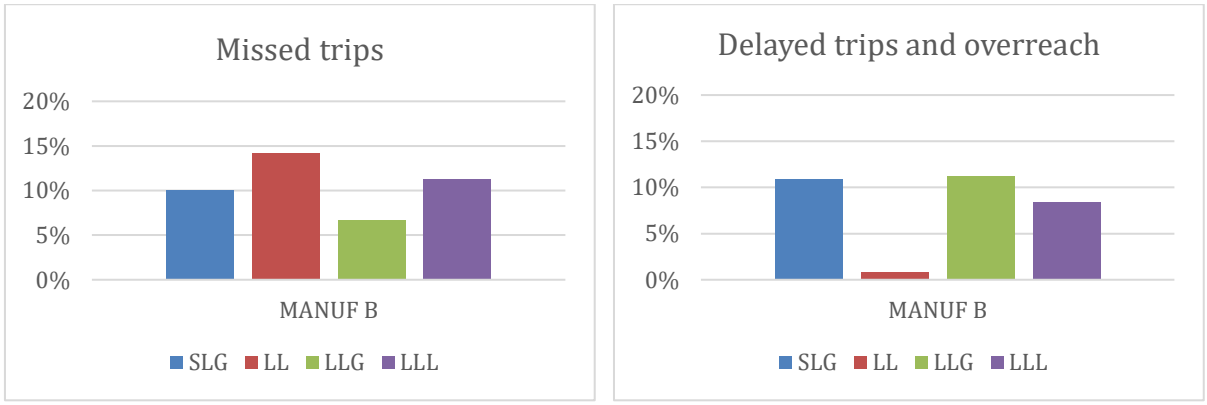

a) *b)*

Figure 45. Manufacturer B protection missed trips (a) and delayed trips and overreach (b).

After analyzing the results observed for these two relays, these initial conclusions can be drafted:

- The implementation of distance protection function differs between manufacturers. This fact is clearly noticeable in this study since each manufacturer protection presents a different bar distribution for the same tests and settings loaded in the equipment.
- Considering global results of the protection relays, line to line faults (LL) present worse results regarding the missed trips, the most problematic behaviour. It is essential to remind that, in these tests, Type-4 WT [50] [51] only injects positive sequence current during faults, even in asymmetrical faults, as shown below in the oscillography analysis from section 2.4.3 [52]. Therefore, this control mode of the generator during asymmetrical faults (negative sequence current equal to zero) is especially problematic for protections when there is no zero-sequence current such as in the line to line faults, isolated from the ground.

- According to the observed results, faults involving ground (SLG and LLG) were generally less problematic than the isolated LL fault. In this case, the zero-sequence current flowing through the neutral of the transformer helps to detect the fault.

Given these results, further analysis of the causes of the malfunction in the commercial protection must be performed, taking into account the oscillography files recorded in the simulations. This analysis is described in section 2.4.3.

2.4.2 Line 4-5 fault simulation results

A similar analysis to the one in the previous section has been performed in Line 4-5 of the Benchmark grid described in section 2.2. In this case, these simulations allow checking commercial protections before PV current contribution. The Test Protocol detailed in Appendix 4 shows test grid configurations used for testing line 4-5.

a Synchronous generation scenario

As explained in the previous section, settings for distance protection are firstly validated with synchronous generation scenario with solid faults. The settings are considered correct once the protection relays provide precise tripping times for zone 1 and zone 2 faults. It supposes the starting point for testing the protection before the current contribution from renewable generation.

Results obtained for line 4-5 in synchronous generation scenario can be summarized as:

- **Zone 1.** Trip times are correct (less than 45 ms) for faults in these study cases:
    - Generation level of 40 and 200 MW
    - Type of fault: Single line to ground, line to line, line to line to ground and three-phase to ground
- **Zone 2.** Trip times are correct (less than 440 ms) for faults in these study cases:
    - Generation level of 40 and 200 MW
    - Type of fault: Single line to ground, line to line, line to line to ground and three-phase to ground

b Renewable generation scenario

Once the settings are validated for the synchronous generation scenario, the renewable generation scenarios are tested, and the obtained results are presented in this section in terms of statistical results.

Table 4 summarizes such results, classifying them according to the manufacturer protection analyzed, the network strength and the renewable generation penetration level. Again, the percentages do not differ between the strong and the weak grid conditions. Therefore, the following results shown in the different bar charts below gather weak and strong grid conditions in the same graph to analyze each manufacturer's behaviour against each type of fault.

Table 4. Comparison of manufacturers results before faults applied to line 4-5.

Comparison: Weak vs Strong grid line 4-5			
Protection relay	**Scenario**	**No trip**	**Delayed trips, overreach**
Manufacturer A	100 % RW - STRONG GRID	60.12 %	17.26 %
	100 % RW - WEAK GRID	59.52 %	17.86 %
Manufacturer B	100 % RW - STRONG GRID	29.77 %	32.74 %
	100 % RW - WEAK GRID	35.71 %	21.43 %

Figure 46 and Figure 47 show these results classified by type of fault for each manufacturer, gathering the total faults applied. When these results are analyzed, the first important issue is the surprisingly high number of missed trips obtained. Nevertheless, despite the exceptionally high percentage of faults, the distribution of missed trips between the different fault types from Figure 46 a) and Figure 47 a) are similar to FCWT results from the previous section. This statistic makes sense since full converter control systems associated with PV and Type-4 WT generators were developed with the same philosophy (see Chapter 1).

Manufacturer A presents the highest number of missed trips for single line to ground faults (SLG) and similar behaviour between the rest of the events (LL and LLG and LLL) as shown in Figure 46 a). Regarding Manufacturer B, Figure 47 a) expose that the highest number of missed trips are obtained for LL, and LLL and the percentage of missed trips for faults involving ground (SLG and LLG) are lower.

Results for delayed trips and overreach situations can be observed in from Figure 46 b) and Figure 47 b). Again, there is a strong relationship between the missed trips shown and the rest of the non-expected results (such as delayed trips in zone 1 and zone 2 and overreach of zone 1 over faults located in zone 2). This fact can be seen, for example, in manufacturer A. Single line to ground faults were especially problematic, with the highest number of missed trips in comparison to the other three types of events. However, Figure 46 b) shows that single line to ground (SLG) does not produce delayed or overreach trips, but it is due to the high number of missed trips found for this type of fault and presented in Figure 46 a). Regarding the rest of the faults, line to line (LL) is the most problematic in terms of delayed or overreach trips, followed by line to line to ground (LLG) and three-phase faults (LLL) in manufacturer A.

The high level of missed trips obtained for line to line (LL) and three-phase faults (LLL) affects Manufacturer B delayed trips results. In this case, a higher percentage is found in line to line to ground (LLG) and single line faults (SLG).

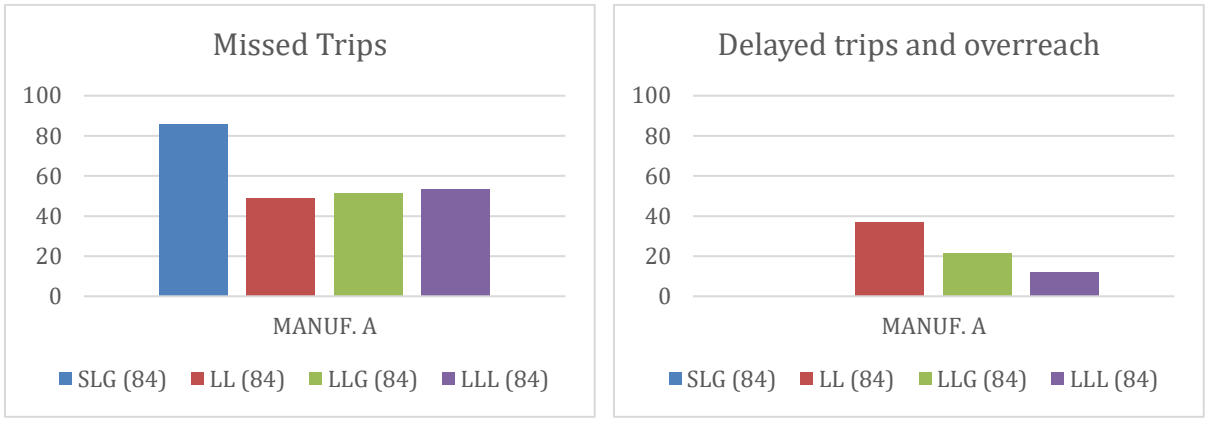

a) *b)*

Figure 46. Manufacturer A protection missed trips (a) and delayed trips and overreach (b).

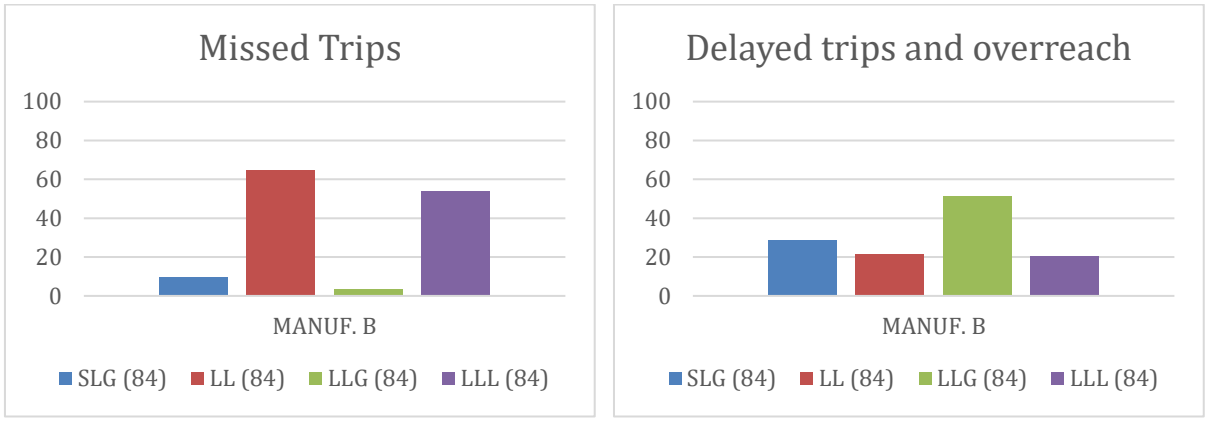

a) *b)*

Figure 47. Manufacturer B protection missed trips (a) and delayed trips and overreach (b).

2.4.3 Protection oscillography analysis

This section shows the oscillography results recorded in the simulations described above to analyze the causes of the malfunction observed in the figures above.

Next, the current evolution during line to line fault (LL) in line 5-7 is analysed. This fault type was the most problematic according results from section 2.4.1. Figure 48 indicates states starting from a pre-fault situation with type-4 wind turbine current contribution:

- Prefault state: Standard symmetrical current injection previously to the fault.
- Initial current contribution with positive and negative sequence current: Before the control system reacts to the fault state controlling the current, the FCWT behaviour is similar to a synchronous generator, injecting both positive and negative sequence current to the fault. The duration of this state is about 8-15 ms.
- Transition period: The control action starts and progressively reduces the negative sequence current injection. This period has been detected as especially problematic for faulted phase selection algorithms and directionality declaration for the manufacturer protections tested by RTDS in the laboratory. This transition period takes around 20-30 ms.
- Steady-state period during the fault: Once the control has been achieved to eliminate the negative sequence current injection, only positive sequence current is injected during this

period, although the fault applied is line to line. This period is identified in the figure as ONLY + SEQ.

Regarding the current values observed in the oscillography, power electronics can provide peak current values up to three times the nominal value during the first moments after the fault inception [53], but these currents are rapidly damped until the steady-state of the fault, where the value is limited to around 1.1 pu.

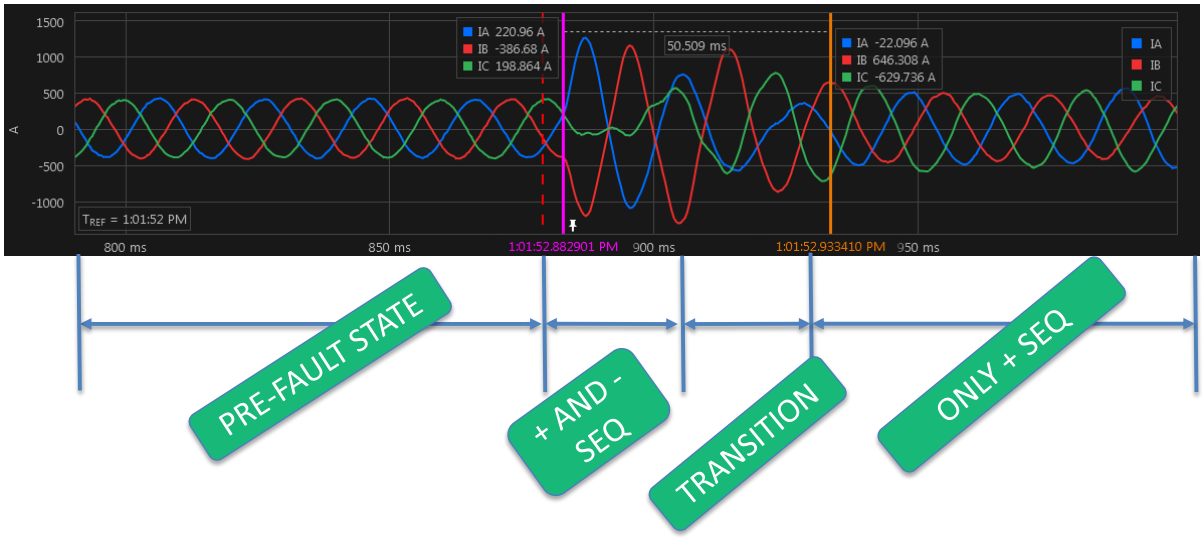

Figure 48. Currents measured by protections during LL fault for type-4 wind turbine.

Figure 49 shows the results recorded in the oscillography files when fault current contribution comes from synchronous generation. The event is simulated in line 5-7, at 70% of the line length involving phases A and B, and the generation level is 200 MW for a type (LL).

These are the parameters present in the figure, along with the denomination displayed in the graph:

- Analogic signals:
  - Current for phases A, B and C (*IA_A, IB_A* and *IC_A*)
  - Phase voltages for phases A, B and C (*VA_KV, VB_KV* and *VC_KV*)
  - Impedance measurement (MAB_Mag)
- Digital signals:
  - Directionality declaration (*FORWARD_DIRECTIONALITY_GROUND, FORWARD_DIRECTIONALITY_PHASES, REVERSE_DIRECTIONALITY_GROUND* and *REVERSE_DIRECTIONALITY_PHASES*)
  - Selection of phase in fault *(FAULT_SELECTION_PHASE_A, FAULT_SELECTION_PHASE_B, FAULT_SELECTION_PHASE_C* and *FAULT_SELECTION_GROUND).*

In these digital signals from the figure, it can be seen that the protection relays do not have any problem correctly declaring the directionality (*FORWARD_DIRECTIONALITY_PHASES* and *FORWARD_DIRECTIONALITY_GROUND* activated) and detecting the phases in fault (*FAULT_SELECTION_PHASE_A* and *FAULT_SELECTION_PHASE_B* activated). The impedance measurement is also stable during the fault (third graph in green).

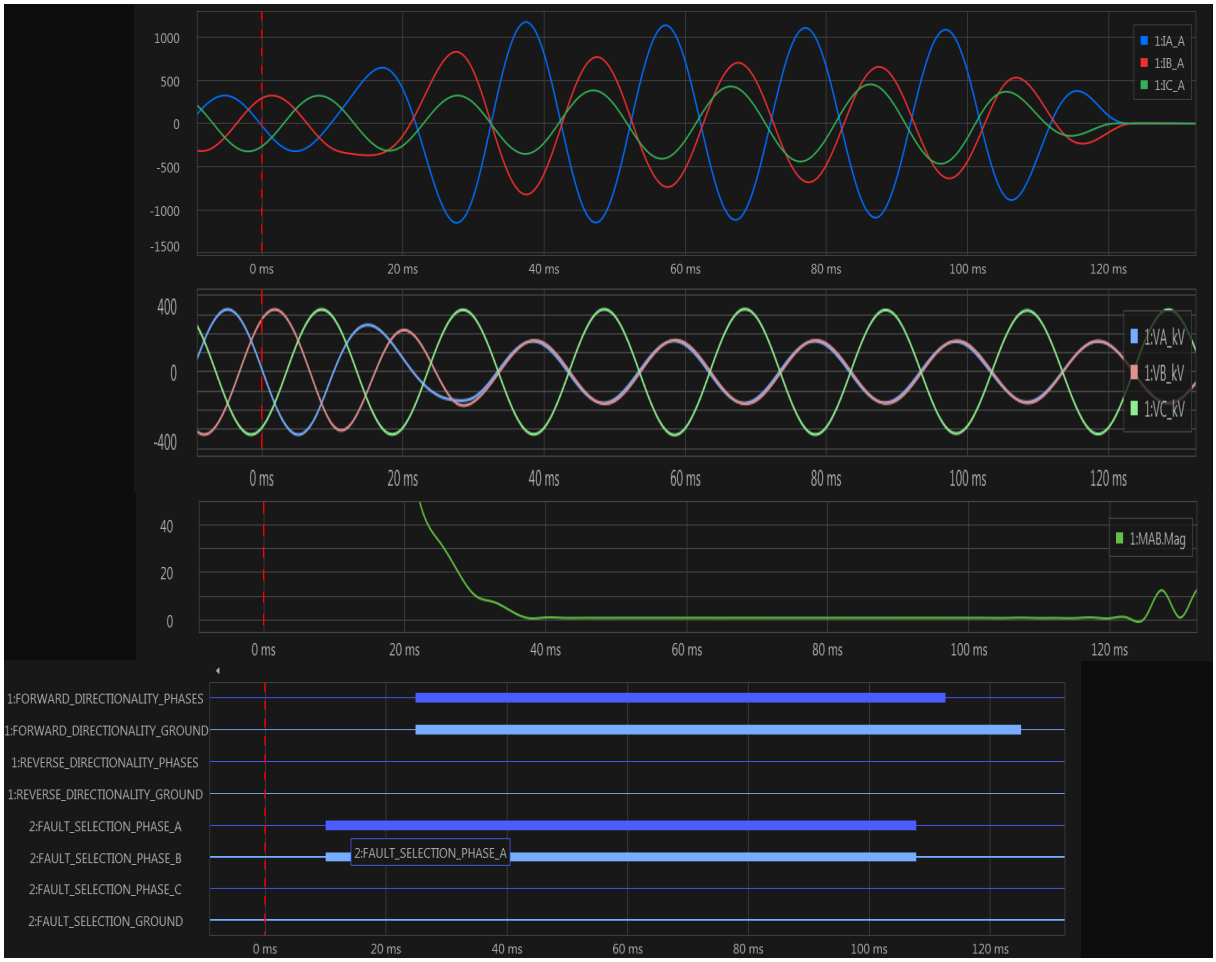

Figure 49. Protection relay oscillography: (From the top to the bottom of the graph) Current, voltage, impedance and digital signals. LL fault and Synchronous Generator current contribution.

Figure 50 shows the current, voltage and digital signals for one of the LL tests performed in line 5-7, with current contribution coming from the Type-4 WT. As in the previous figure, the fault is simulated at 70% of the line length involving phases A and B, and the generation level is 200 MW.

As it can be seen, the transition state defined before causes malfunction of distance algorithms in terms of:

- **Impedance measurement** (third graph of Figure 49, in green). As it can be noticed, it is not constant during the transition period, and this situation may lead to a non-predictable behaviour, either non-tripping or tripping of the fault. In any case, zone 1 tripping will normally experience delayed operations due to this variable impedance measurement during the transition period.
- **Directionality declaration**. As it can be observed, *REVERSE_DIRECTIONALITY_GROUND and REVERSE_DIRECTIONALITY_PHASES* bits are activated during the transition state, declaring reverse directionality. The fault injected is forward so, the forward distance elements cannot be activated and the fault is not cleared in zone 1.
- **Selection of phase in fault.** After the fault inception, the phase fault selector acts as expected, indicating phases A and B. This behaviour is due to the presence of both positive and negative sequence currents during this stage (called + *AND* - *SEQ* in Figure 48). However,

during the transition period, the fault selector does not operate correctly, inducing the wrong operation of the protection because the distance elements cannot be activated to trip the fault within the correct time.

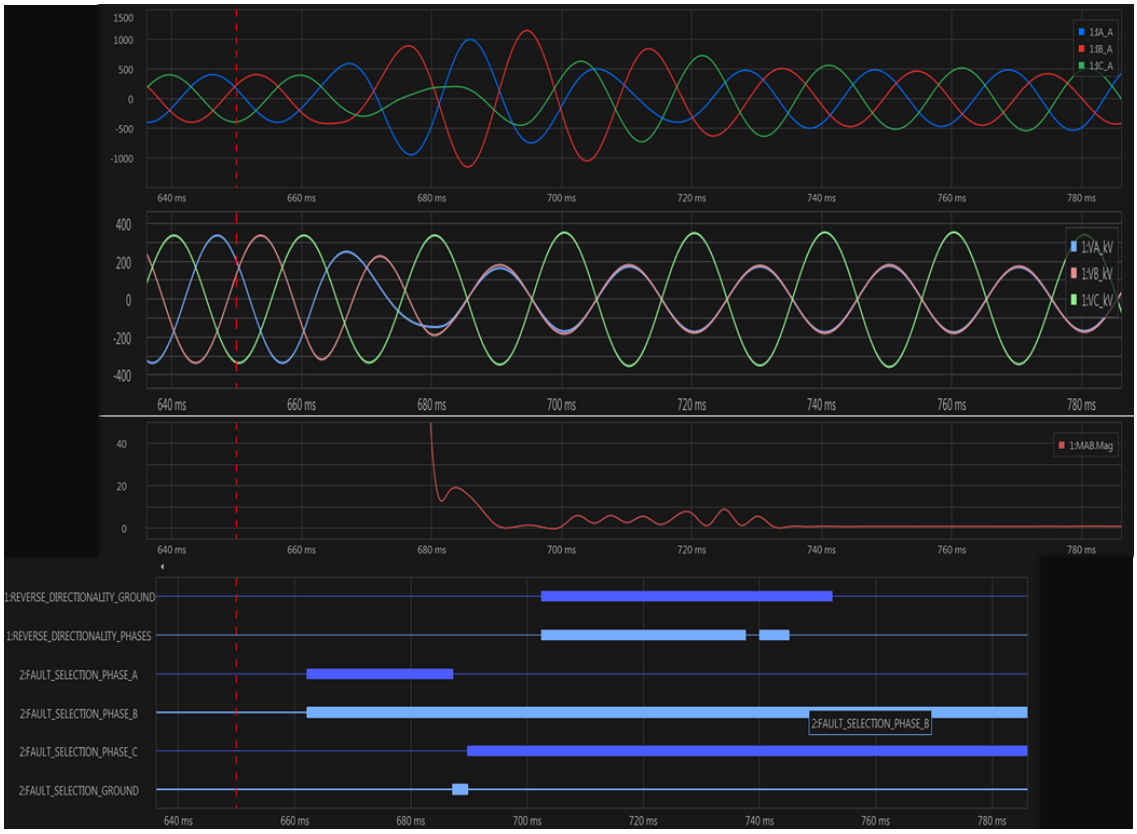

Figure 50. Protection relay oscillography: (From the top to the bottom of the graph) Current, voltage, impedance and digital signals. LL fault and Type-4 WT current contribution.

Figure 51 shows the single line to ground fault in line 4-5 without negative sequence current injection from the PV generator. In this case, the impedance measurement is correct in the steady-state, but distance elements are deactivated due to the following reasons:

- **Phase selector has not been activated adequately**. Phases A and ground are the elements involved in the fault, but phases B and C signals are activated in the oscillography. There is a mistake in the fault phase selector, so the protection does not operate correctly.
- **The directionality declaration is not correct**. Reverse directionality is activated during the transition state, as explained previously in line 5-7 results from Figure 50.

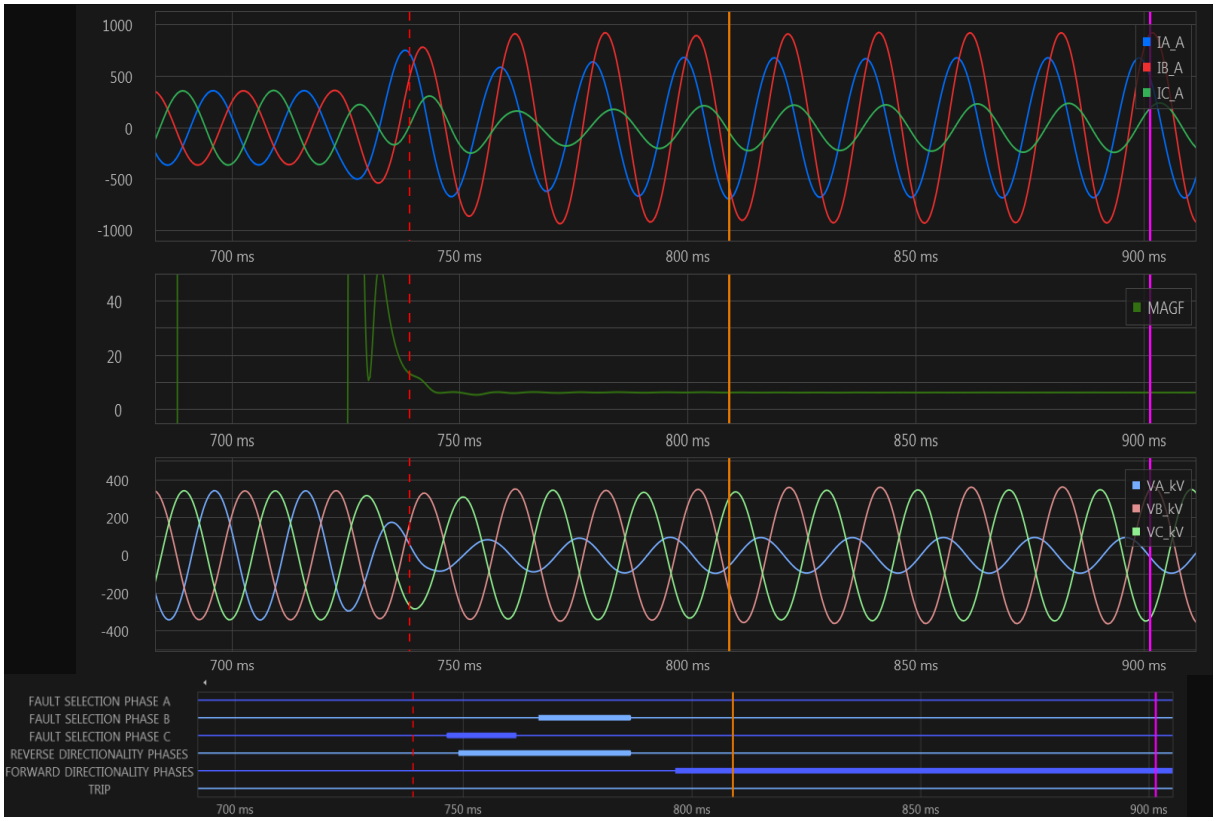

Figure 51. Protection relay oscillography: (From the top to the bottom of the graph) Current, voltage, impedance and digital signals. SLG fault and PV generator current contribution without Ineg.

On the other hand, especially in the case of the PV generator where so many missed trips have been observed, it becomes interesting to analyze the effect of negative sequence current injection. Thus, a negative sequence current has been injected to know if this injection may improve the distance function performance. As explained in section 1.2.6, there are different methods to calculate the negative sequence current contribution. In this test, negative sequence current is proportional to the negative sequence voltage as explained in subsection 1.2.6 c, with a K factor of 2.

Figure 52 shows the behaviour of the protection relay with the injection of both positive and negative sequence current from the converter of the PV generator for a single line to ground fault(SLG). In this case, it is noticeable that the fault selection is activated correctly, with no activation of the fault selectors for phases B and C. Forward directionality is activated correctly, and the trip order is emitted. So, protection algorithms dedicated to fault selection and directionality declaration take a clear benefit from the presence of negative sequence current.

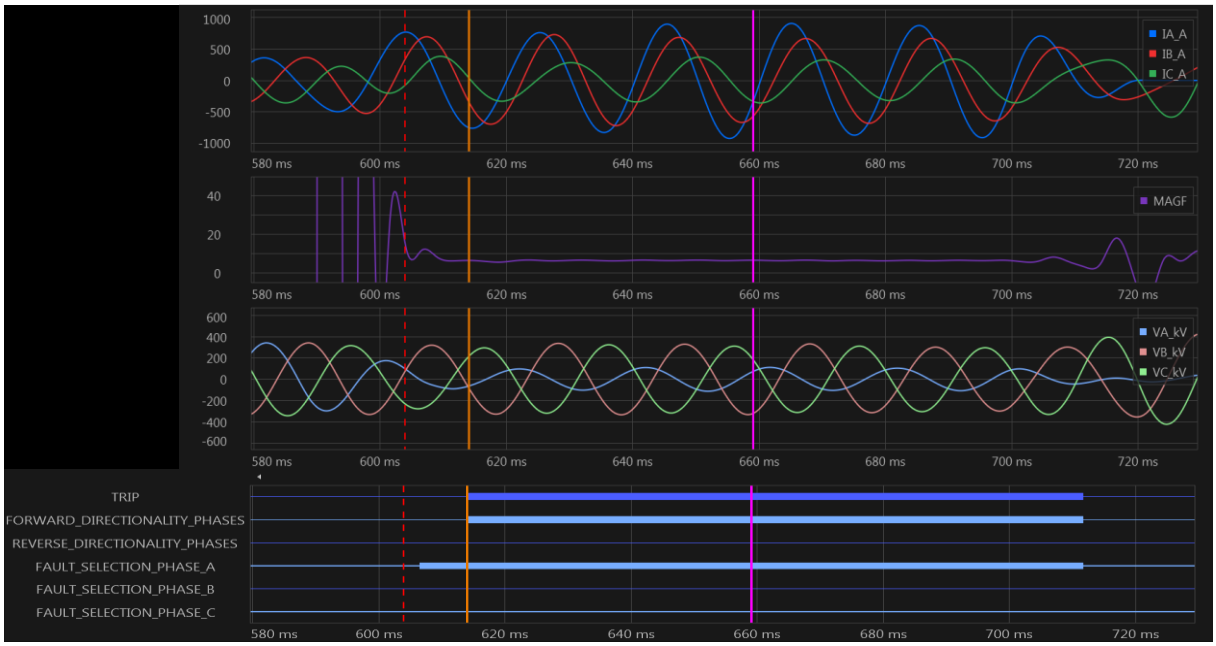

Figure 52. Protection relay oscillography: (From the top to the bottom of the graph) Current, voltage, impedance and digital signals. SLG fault and PV generator current contribution with Ineg.

The same analysis has been followed regarding the line to line fault. According to the bar charts shown in sections 2.4.1 and 2.4.2, manufacturer B presents many missed trips for the line to line faults (LL). As done previously with the SLG fault, a qualitative analysis is applied to compare protection behaviour if only a positive sequence current is injected or if anegative sequence current is also injected.

Figure 53 shows the behaviour of a protection relay in a LL fault with injection of only positive sequence. In this case, the phase selector behaviour is erratic (fault applied between phases A and B). In the first instants, phase selection works correctly after fault inception, as it was explained for the Type-4 WT. Still, both phase C and ground selectors are wrongly activated during the transient state, which makes that protection finally does not emit the trip signal.. This problem is recurrent and has been reported previously both in the PV generator and Type-4 WT.

The impedance measurement (second graph, in geen) is correct during the steady-state of the current during the fault. Still, during the transient state between fault inception and only positive sequence current injection, the measurement presents oscillations that may lead to a possible mal-operation.

Figure 54 shows the behaviour of a protection relay manufacturer with the injection of both positive and negative sequence current during the same fault. It can be seen how, after the fault inception, there is still some false activations of the fault selector (phases C and ground). Finally, in this case, with the combination of both positive and negative sequence current, the activation of phases A and B remains over the other two-phase selectors, which makes the protection finally trip.

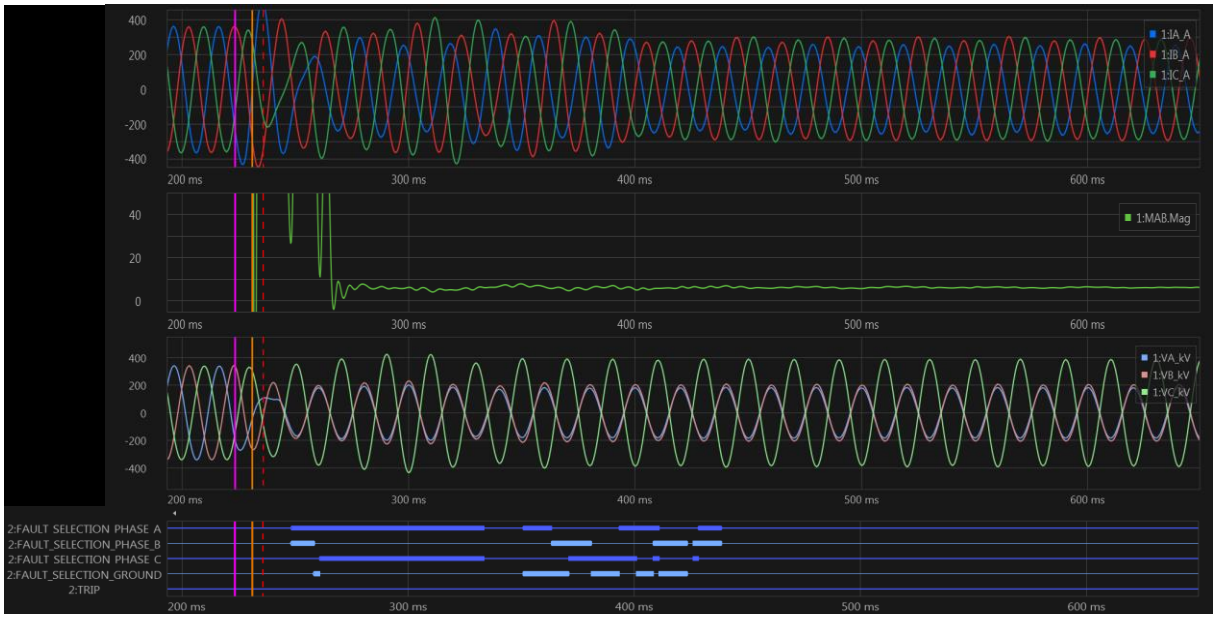

Figure 53. Protection relay oscillography: (From the top to the bottom of the graph) Current, voltage, impedance and digital signals. LL fault and PV generator current contribution without Ineg.

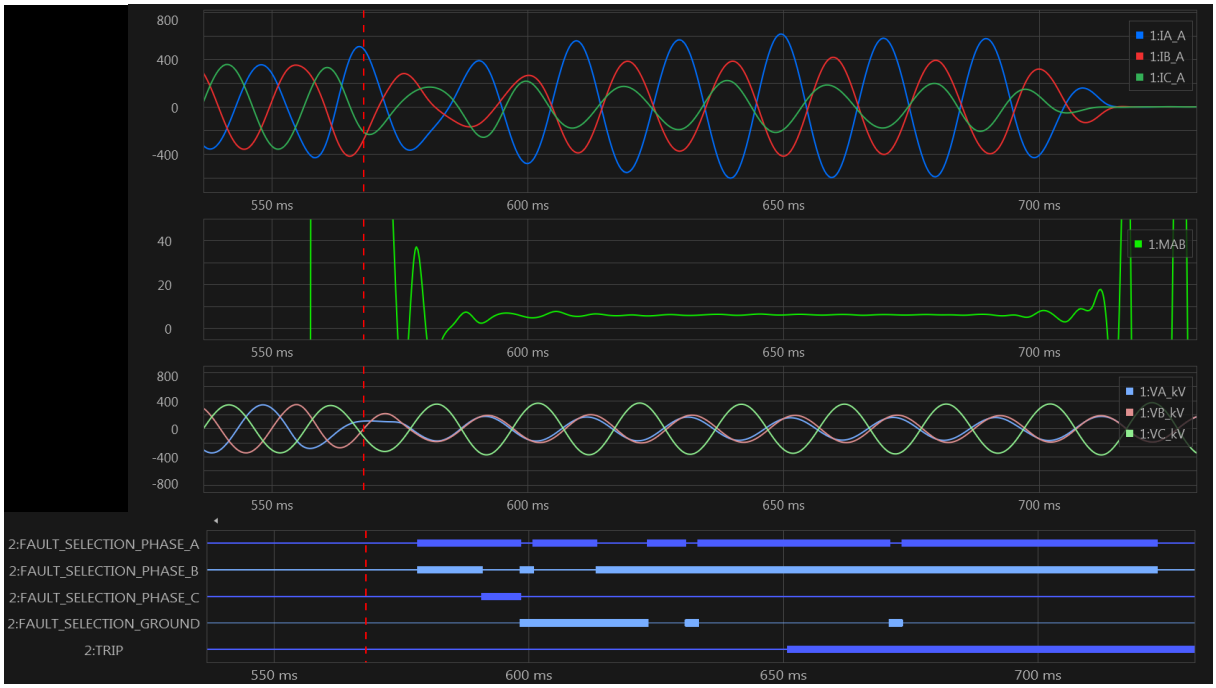

Figure 54.Protection relay oscillography: (From the top to the bottom of the graph) Current, voltage, impedance and digital signals. LL fault and PV generator current contribution with Ineg.

As in the single line to ground fault, in the line to line fault, the injection of negative sequence current improved the behaviour of the protection relays that did not emit trip order in its absence. As shown in the oscillography, the presence of negative sequence current benefits the performance of the phase selector algorithm. The improvement in the phase selector changes the final result of the tests significantly: only with positive sequence current injection there was a missed trip, but the combination of positive and negative sequence current injection a zone 1 produces the trip for the fault at 70 % of the line.

2.5 Line differential Protection Testing

The operation of line differential protection is based on calculating the difference between incoming and outgoing currents, being segregated by phase.

The same benchmark grid shown in section 2.2 has been used for the study of line differential protection. Lines 5-7 and 4-5 were under investigation. As in the case of distance protection study, these lines have a current contribution to the fault of synchronous generation on one side and renewable generation on the other side.

Acceptance criteria are defined with tripping in less than 45 ms if the fault is inside the line and no tripping if the fault is outside the line.

2.5.1 Line 5-7 Results

Results obtained are correct for all points of fault defined, scenarios, generation level and type of faults. Trip times are less than 35 ms.

2.5.2 Line 4-5 Results

Results obtained are correct for all points of fault defined, scenarios, generation level and type of faults. Trip times are less than 35 ms in general. However, some results were obtained in about 50 ms. In this case, considering the length of the line (244 km) compared to the previous line length (35.1 and 30 km), tripping times are also regarded as correct.

Line differential was shown as a robust and stable method for protecting lines with high penetration of renewables. However, it also protects the affected element and does not provide backup protection in the grid.

Therefore, distance protection will focus on the developed solution in this work because it presents most of the problems.

2.6 Ground directional overcurrent Protection (67N) Testing

Ground directional overcurrent is tested using the same procedure as the distance protection function. As explained in the test protocol, these tests aim to investigate possible problems under a non-expected behaviour of the primary protection function (distance).

The ground connection of the transformer provides an appropriate path for the zero-sequence current, allowing the correct actuation of ground directional overcurrent protection.

Acceptance criteria are defined with tripping in less than 645 ms, considering the low current contribution to the fault (only provided by the ground connection of the transformer).

2.6.1 Line 5-7 Results

Results obtained are correct for all points of fault defined, scenarios, generation level and type of faults. In general, trip times are around 620-640 ms, which corresponds to the second step of 67N settings.

In this case, single line to ground and line to line to ground faults supplies current through the neutral and, therefore, they are tripped. Line to line and three-phase faults do not provide ground current, so this protection function does not detect them.

2.6.2 Line 4-5 Results

Results obtained are correct for all points of fault defined, scenarios, generation level and type of faults. In general, trip times are around 620-640 ms, which corresponds to the second step of 67N settings.

2.7 Conclusions for the laboratory test analysis

According to the analysis made and the results obtained during the test process, the following conclusions can be highlighted:

DISTANCE PROTECTION FUNCTION

- Distance protection is the function that concentrates the higher number of non-expected results in terms of:
    - Missed trips
    - The overreach of zone 1 for faults located at zone 2
    - Delayed trips for faults found both in zone 1 and zone 2
- The implementation of distance algorithms differs in the analyzed protection; thus, each manufacturer protection presents a different distribution of non-expected results for each type of fault. Some are more in trouble with a single line to ground faults, while others find more problems with phase to phase faults.
- Despite this, distance protection has more problems detecting the line to line fault (LL).
- Ground current contribution, which is present in single line to ground (SLG) and line to line to ground (LLG) faults due to the grounding of the transformers, may help the detection of faults.
- The lack of negative sequence current (even during asymmetrical faults) due to the control algorithms implemented on PV generator and Type-4 WT has been observed as problematic for distance protection algorithm in terms of:
    - Directionality declaration
    - Fault selection
- Additional injection of negative sequence current during asymmetrical faults has improved fault detection in terms of directionality declaration and fault selection.
- Transition period associated with the PV and Type-4 WT controls between the fault inception and the steady-state of the current during the fault is critical. This transient period is especially problematic for algorithms associated with distance protection behaviour (directionality and fault selection). Correct phase selector and declaration of directionality are crucial for the performance of distance protection. Oscillography shown in the analysis of distance protection (such as the one observed in Figure 48) demonstrates that the dynamic

of the response is essential for the behaviour of faulted phase selector, directionality declaration and impedance measurement.

- According to the previous statements, these renewable generators present a different behaviour than traditional synchronous generators. They must be taken into account from the point of view of protection algorithms.
- Impedance measurement is correct during the steady-state of the fault current, but it oscillates during the transient period mentioned. This fact leads the protection to overreach in some circumstances where the impedance enters in zone 1 for some milliseconds even when the fault is located in zone 2.
- Current contribution level during the steady-state of the fault can help the fault detection, but, considering that the minimum threshold has been reached, it is not the critical factor. Initial peak of the current, transient period of the control, directionality declaration and phase selection result more important than the current level.
- Line length and distance from the renewable generator to the fault may also influence fault detection. Impedance to the fault reduces the initial peak transient current at fully rated power electronic converters. This peak value, similar to a synchronous generator behaviour in the first 8 to 15 ms after the fault inception, is quickly reduced , making the fault detection for distance protection algorithms more difficult. The more significant impedance to the fault (line length), the smaller the current peak value is.

Some publications, such as [54] , show protections problems to operate on similar cases. However, this publication does not explain the reasons and origin of this problem. In this chapter, they were analysed using real-time tools for testing the protective relays from different manufacturers. The meaningful results shown about the protection can help to find bottlenecks of the currently available protection schemes to integrate renewable generation.

Based on the above described conclusions, the next steps of this thesis are:

- Improving the fault selection and directionality algorithms during the transient state associated with full converter topologies and control systems that limit the negative sequence current.
- Improving the impedance measurement during the first moments after the fault and the called “transient” period of generators based on full converter topologies.
- Distance protection is the focus of the development of this thesis.

LINE DIFFERENTIAL FUNCTION

- Using the same benchmark as used for the distance protection testing, line differential protection has been tested.
- Line differential protection worked correctly for all the tests performed in this study, with the different kinds of renewable generators and types of fault. Then, the 87L function will not be an object of the study to improve its behaviour in this thesis.
- It was initially expected this kind of behaviour for line differential since the differential measurement at both sides of the line presents high reliability for fault detection. The tests performed tests confirm this correct behaviour.

GROUND DIRECTIONAL OVERCURRENT FUNCTION

- Using the same benchmark as used for the distance protection testing, ground directional overcurrent protection has been tested.
- Ground directional overcurrent protection works as a backup in transmission lines, and, consequently, it must trip in case of distance protection failure.
- This protection detects the current through the grounding of the system. Renewable generators are typically connected to the transmission network through a wye-grounded transformer on the high voltage side (delta connection on the low voltage side). This connection makes the circulation of current possible in case of fault involving ground. Then, the 67N function will not be an object of the study to improve its behaviour in this thesis.
- This protection behaves as expected under fault resistances of 150 ohms (75 ohms when the polarizing voltage was too reduced). Trips are generated for those faults involving ground (SLG and LLG), which is expected for this protection function.
- However, most of the trips have been produced in near 600 ms (second step of current set in protection relays). Therefore, the defect could remain un-cleared during this period because of the lack of distance protection for single line to ground and line to line to ground faults.
- Therefore, renewable generators does not affect 67N function behaviour, which depends on the connection of the neutral of the transformer.

Chapter 3 Development of faulted phase selector algorithm

Tests performed in Chapter 2 revealed problems with directionality declaration and faulted phase selection for distance protection due to symmetrical current contribution from Type-4 WTs and PV generators in the case of asymmetrical faults. This balanced current injection during asymmetrical faults represents a very different behaviour regarding the traditional fault behaviour of synchronous generators, which leads distance protection to malfunction due to the mentioned problems.

The starting point of the developed algorithm in this thesis is the current injection of PE-based generators described in section 2.4.3, which shows the different periods of current injection from a Type-4 WT before and after a line to line fault.

Figure 56 shows the behaviour of one commercial protection relay analysed in Chapter 2 under the fault condition shown in Figure 55. The faulted phase selection algorithm works appropriately during the initial period after the fault inception when the positive and negative sequence currents coexist (similar behaviour to a synchronous generator). However, the faulted phase selector and the directionality declaration do not behave correctly during the transition period. Once this error appears during this transition period, the relay algorithms cannot correctly detect the faulted phase. The action of the generator control during this transition suppresses the negative sequence current, resulting in the error in the detection of the faulted phase selection and directionality.

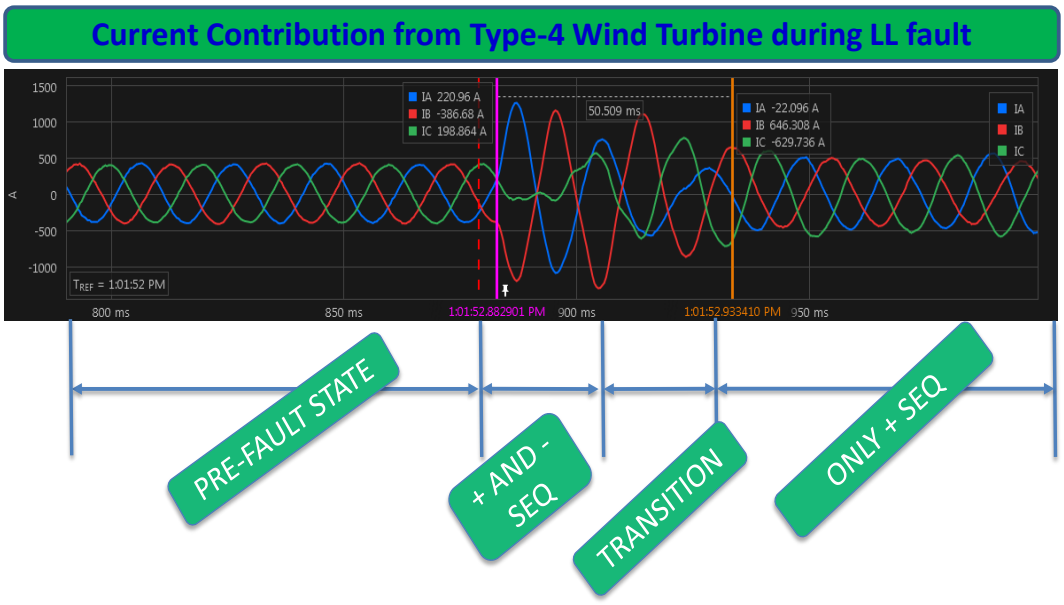

Figure 55. Fault contribution from Type-4 WT with negative sequence current suppression strategy.

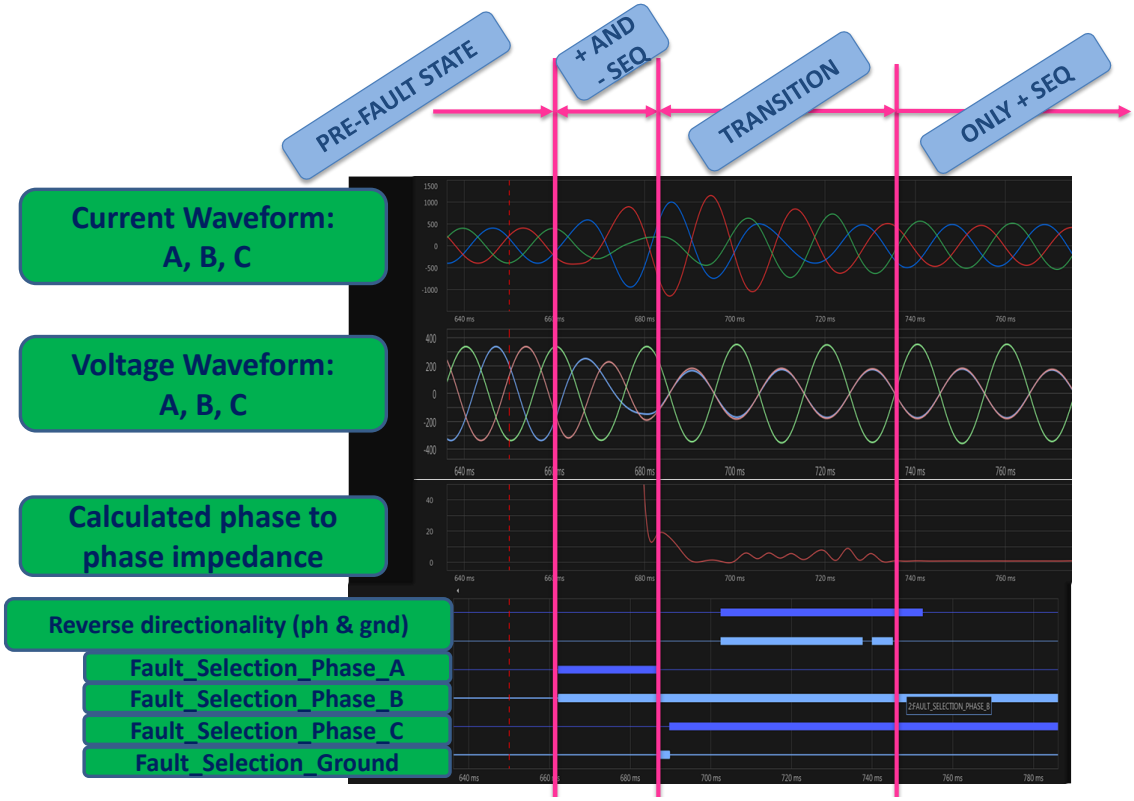

Figure 56. Relay behaviour during LL fault. Wrong faulted phase selection and directionality activations.

Based on this analysis of the tests performed in Chapter 2, an algorithm that provides an effective solution to the problem detected has been developed. This solution, presented in the following sections, can work with present distance protection algorithms implemented in commercial protection relays. The solution must deal both with fault current contribution coming from both renewable energies and synchronous generation.

3.1 Methodology

To propose a suitable solution to the problem highlighted during the tests from Chapter 2, this research sequence has been followed:

1. **Analysis of the laboratory results and its implications regarding present theory implemented on protection relays**

   The first stage of this research process is to analyze why the current contribution from Type-4 WTs and PV Generators affects present protection algorithms behaviour. However, it is a fact that protection relay manufacturers do not provide their complete solution in their user manuals about how their protection algorithms work. Though, user manuals of these protections offer interesting information about their principles, along with the results obtained in the tests, allowing obtaining initial valuable conclusions.

   Superimposed quantities theory, also called "delta quantities", "superimposed currents" or "delta currents", has been traditionally implemented and is presently used for many of the protection relay manufacturers [55] [56] [57] [58] [59] because of its operation speed, simple implementation and low computational load. Then, to solve the lack of information about faulted phase selection algorithms in the manufacturer user manuals, this study starts from a superimposed quantities algorithm based on [58], [60] and [61] , and analyzes the behaviour of this algorithm with fault current contribution from Type-4 WT and PV generator.

   Comparing the results of the behaviour of the superimposed quantities algorithm obtained for renewables with results obtained for synchronous generators is very useful for explaining the differences observed in the performance of protection relays with synchronous generators and renewables in Chapter 2.

2. **Development of the solution**

   Based on the results obtained in this analysis, an investigation on a suitable solution that permits identifying the faulted phase selection correctly even with a symmetrical current contribution to unbalanced faults has been carried out. The development of the solution is composed of different approaches and debug processes where the tests and analysis are critical to improving the algorithm behaviour.

3. **Interim solution of the algorithm: Testing and debugging process**

   The development of the solution leads to an interim solution of the proposed algorithm. This algorithm is tested under the same conditions as protection relays in Chapter 2. Parameters like fault type, distance of the fault, generation level, scenario, suppression of negative sequence current, fault resistance and repetitiveness analysis for consistency checking of the results are also applied to verify the correct behaviour of the proposed algorithm. These first runs of simulations improve and debug the behaviour of the algorithm previously to the tests with real hardware platform described in the next Chapter 4. Section 3.4 presents this phase of the development.

4. **Final solution of the algorithm**

   Once the protection study is finished and the improvements implemented on the algorithm, the final version is ready to be implemented on a physical platform, as described in Chapter 4.

3.2 Superimposed quantities algorithm

As stated in section 3.1, a superimposed quantity algorithm based on technical papers [58] [60] [61] has been used to analyze the directionality and faulted phase selection under fault current provided by Type-4 WT and PV generators. These results are compared with the performance in the case of contribution from synchronous generators.

3.2.1 Theory of superimposed quatities

Based on the theory and demonstrations seen in [58], it is possible to define the incremental impedance according to the expression:

$$\overline{\Delta Z_R} = \frac{\text{Post Fault } \overline{V_R} - \text{Pre Fault } \overline{V_R}}{\text{Post Fault } \overline{I_R} - \text{Pre Fault } \overline{I_R}} = \frac{\overline{\Delta V_R}}{\overline{\Delta I_R}} = -\overline{Z_{S1}} \quad (61)$$

where all quantities in this equation are phasors.

This expression means that the incremental impedance seen from the relay (subscript "R") is equivalent to the positive sequence source impedance. This formula can also be represented as:

$$\frac{\overline{\Delta V_R}}{\overline{\Delta I_R} \cdot (-\overline{Z_{S1}})} = 1 \quad (62)$$

This means that, according to [58], during a fault, the magnitude and phase of the incremental voltage waveform (or phasor) are equal to the magnitude and phase of the incremental current waveform (or phasor) multiplied by the negative of the source impedance behind the relay.

Superimposed quantities theory defines an element called "scalar product", defined as:

$$\text{Scalar Product} \rightarrow \text{real}\left(\overline{\Delta V_R} \cdot \text{conj}\left(\overline{\Delta I_R} \cdot (-\overline{Z_{S1}})\right)\right) = \Delta v_R \cdot \Delta i_R \cdot z_{s1} \cdot \cos\theta \rightarrow \Delta v_R \cdot \Delta i_R \cdot \cos\theta \quad (63)$$

Where z_{S1} is the value of the impedance, which is always positive, does not affect the sign of the scalar product, so it can be reduced to unity for the study. θ angle represents any phase angle mismatch that could exist in the source phase angle representation. Since θ angle is usually around 0º, $\cos\theta$ factor is near the unity and does not influence the sign of the result [58].

If the maximum peak of this scalar product is negative, forward directionality is declared, while if the maximum peak is positive, backward directionality is declared.

One scalar product (named as ΔT_{LL} in the following equation) can be defined by phase, taking into account line voltage and current measurements so that a set of three scalar products are defined as:

$$\Delta T_{AB} = \text{real}\left(\Delta V_{AB} \cdot \text{conj}\left(-\Delta I_{Ac}\right)\right) \quad (64)$$

$$\Delta T_{BC} = \text{real}\left(\Delta V_{BC} \cdot \text{conj}\left(-\Delta I_{Bc}\right)\right) \quad (65)$$

$$\Delta T_{CA} = \text{real}\left(\Delta V_{CA} \cdot \text{conj}\left(-\Delta I_{Cc}\right)\right) \quad (66)$$

Depending on the value and sign obtained for each scalar product, it is possible to classify the type of fault. Table 6 shows the relative values of each scalar product for different types of fault for traditional synchronous generation current contribution.

Table 5. Classical classification of different types of fault according to the values of scalar products according to [58].

Type of fault	ΔT_{AB}	ΔT_{BC}	ΔT_{CA}
AG	ΔT_{AB}	0	ΔT_{AB}
BG	ΔT_{AB}	ΔT_{AB}	0
CG	0	ΔT_{BC}	ΔT_{BC}
AB, ABG	ΔT_{AB}	$0.25 \cdot \Delta T_{AB}$	$0.25 \cdot \Delta T_{AB}$
BC, BCG	$0.25 \cdot \Delta T_{BC}$	ΔT_{BC}	$0.25 \cdot \Delta T_{BC}$
CA, CAG	$0.25 \cdot \Delta T_{CA}$	$0.25 \cdot \Delta T_{CA}$	ΔT_{CA}

3.2.2 Implementation on RTDS of superimposed quantities theory

As mentioned above, superimposed quantities theory is used for many of the present algorithms from protection relays. Thus, this theory has been implemented in RTDS similarly to the diagram shown in Figure 57 to analyse the potential problems of present algorithms under the current contribution of Type-4 WT and PV generator during short circuits.

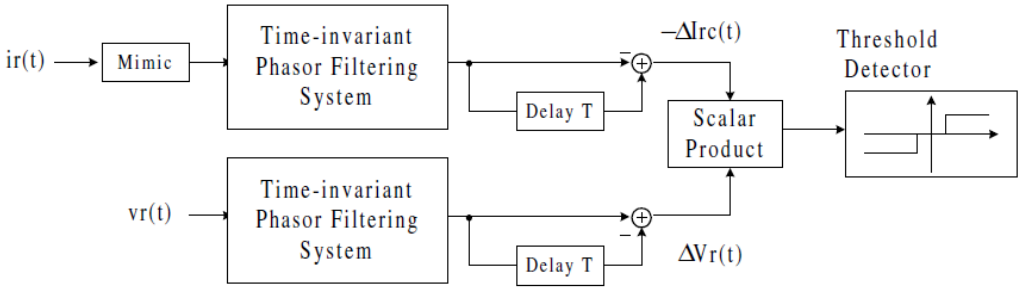

Figure 57. Block diagram implementation of superimposed quantities [58].

Figure 57 represents the calculation of scalar products. On the left side, current and voltage waveforms are received and, after a filtering phase, the delta quantity is calculated using a delay both for voltage and current. This calculation provides the current and voltage variation considering the instantaneous values, also called delta quantity. The diagram considers the scalar product between the delta quantity of current and the delta quantity of voltage.

Once implemented in RTDS, tests have been applied to this algorithm to compare its behaviour when the fault current contribution comes from synchronous generators and when it comes from Type-4 WT and PV generators. Single line to ground (AG), line to line (AB) and line to line to ground (ABG) have been applied. The procedure followed (benchmark grid, test protocol and automatic testing process) for this analysis has been the same than used for the study of distance protection in Chapter 2.

Figure 58 compares the scalar products of ΔT_{AB}, ΔT_{BC} and ΔT_{CA} obtained for a phase A to ground fault test for synchronous generator (a) and Type-4 WT (b). It can be noticed how the relationship between scalar products shown in Table 6 is accomplished for the synchronous generator case, with ΔT_{AB} equal to ΔT_{CA} and $\Delta T_{BC} = 0$. There is an initial positive peak, but the negative peak is one order magnitude larger than the positive. Therefore, directionality is declared forward (negative scalar products), and the faulted phase selector would activate the AG fault loop.

However, if the right side figure is observed, the response of the algorithm with Type-4 WT current contribution differs from the result of the synchronous source. Several interesting features are remarkable. First, the relationship between scalar products seen in Table 6 is no longer accomplished for Type-4 WT, which may associate problems in faulted phase selection. In addition, the initial positive peak is similar in magnitude to the negative peak after could result in the wrong directionality declaration. Finally, the scalar product ΔT_{BC} is not only different from zero, but it also takes negative values. These three important differences lead protections based on superimposed quantities not to work correctly under a different current contribution regarding synchronous generators in terms of directionality and faulted phase selection.

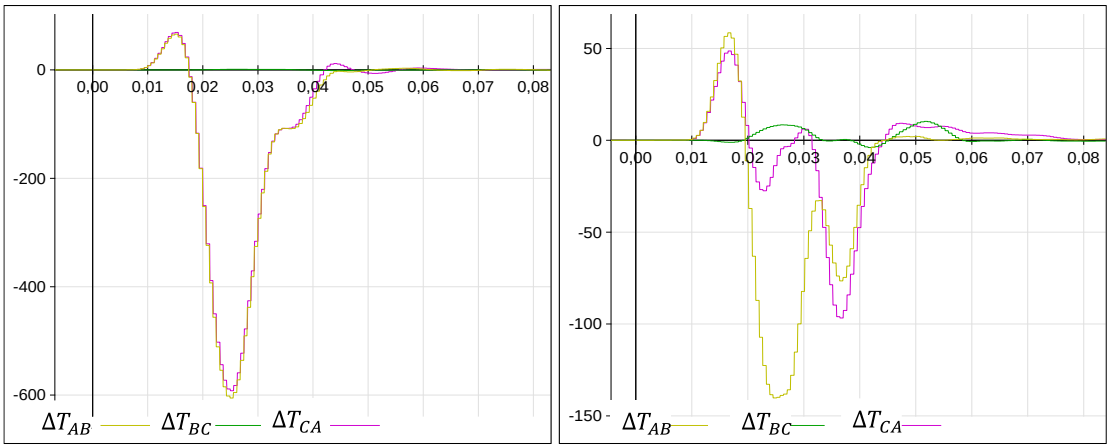

a) *b)*

Figure 58. Overlap of instantaneous values of scalar products for AG fault for synchronous generator (a) and Type-4 WT (b)[2].

Similar analysis can be applied to line to line fault involving A and B phases, shown in Figure 59. Looking at the left side figure (SG contribution), the relationship between the scalar products is accomplished again. ΔT_{BC} and ΔT_{CA} are 0.25 times ΔT_{AB}, what results in a correct fault phase selection according Table 6. The negative peak value is one order magnitude larger than the positive peak, so there is no doubt about the forward directionality and the three scalar products have the same sign during the test.

However, in the case Type-4 WT contribution shown in the right-side picture, the relationship between the scalar products is no longer accomplished, leading to a malfunction of the faulted phase selector algorithm; negative peak is similar in magnitude to the positive peak and positive and negative values of the scalar products coexist at the same time instant. The combination of these factors may cause a malfunction of the directionality declaration and faulted phase selection, thus explaining the results obtained experimentally in Chapter 2.

[2] Please note the difference between the scales of the right and left side pictures

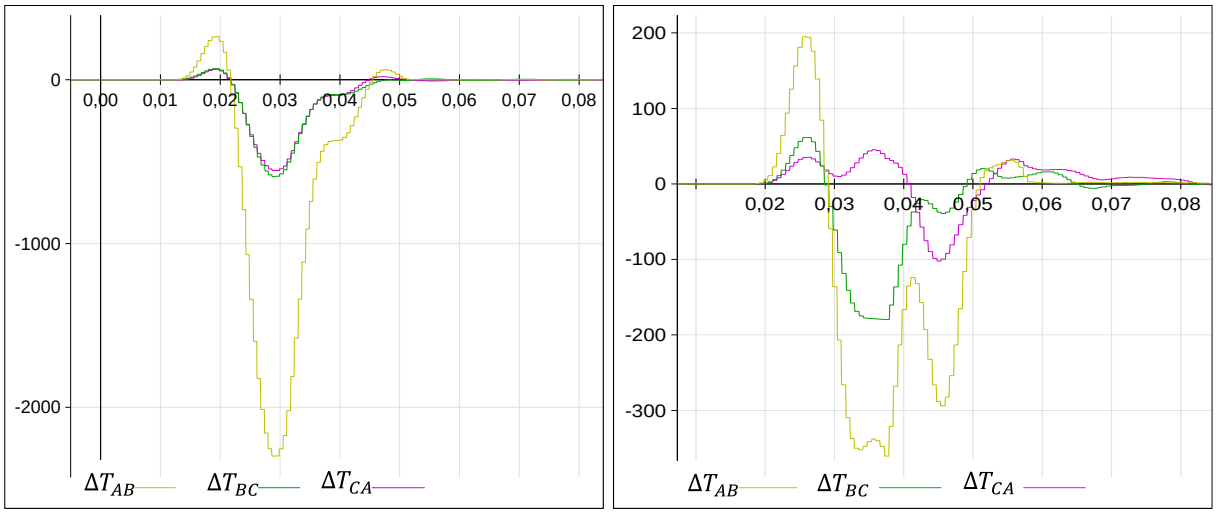

a) *b)*

Figure 59. Overlap of instantaneous values of scalar products for AB fault for synchronous generator (a) and Type-4 WT right side (b).

Figure 60 shows the behaviour for SG (left) and Type-4 WT (right).

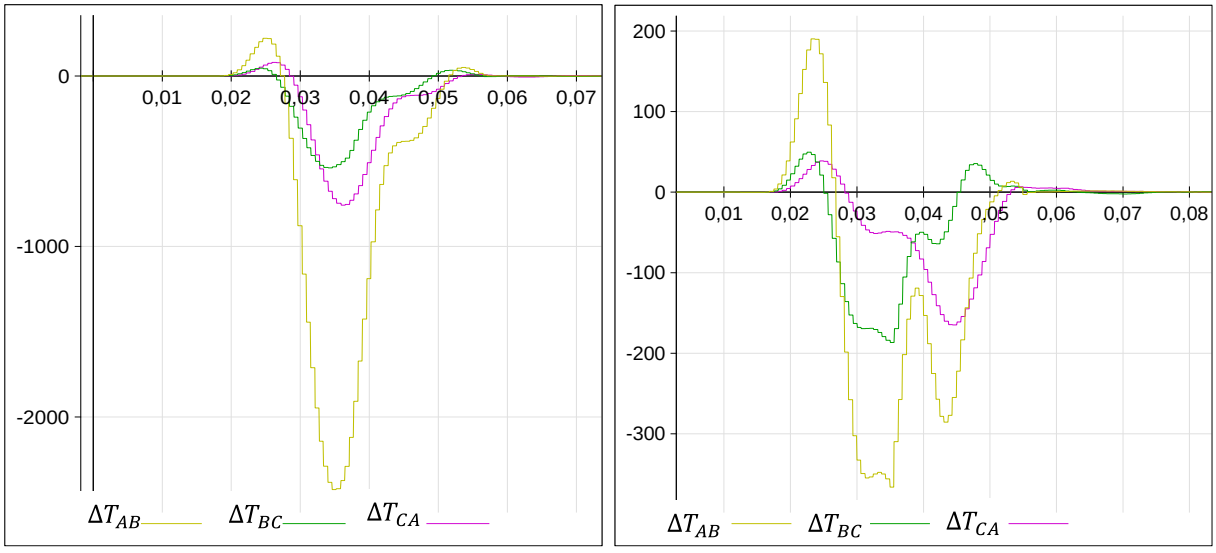

a) *b)*

Figure 60. Overlap of instantaneous values of scalar products for ABG fault for Synchronous generator (a) and Type-4 WT (b).

Scalar products applied to SG current contribution during the fault accomplish the relationships according to Table 6 with a certain margin for this type of fault. Some papers that use this method [60], indicate a margin of action of ±10%, as indicated in Figure 61. SG current behaviour is inside this margin proposed in Figure 61 so that the faulted phase selection and directionality is indicated accurately.

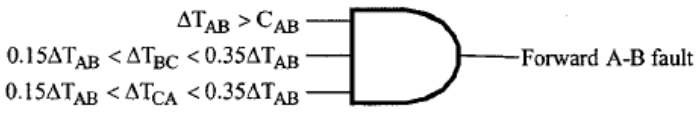

Figure 61. Margin of action for AB and ABG faults [60].

However, as in the previously analysed faults, the relationship is not accomplished again for Type-4 WT, leading to possible problems with directionality and faulted phase selection.

Therefore, this initial analysis based on superimposed quantities theory commonly used by different manufacturers for faulted phase selection and directionality declaration has shown that this principle explains graphically the problems observed in Chapter 2: wrong faulted phase selection and wrong directionality declaration.

The following section describes the new proposed algorithm developed, taking these results as a reference of the problem.

3.3 New proposed algorithm

The developed algorithm is based on the principle that Type-4 WT and PV generators behave similarly to synchronous generators during the first instants after the fault inception, according to Chapter 2 results and analysis shown in section 3.2. Further than these first milliseconds after the fault inception, faulted phase selector and directionality algorithms in present protection relays showed a wrong performance (see Figure 56).

Therefore, the initial hypothesis for the faulted phase selection is: Criteria for fault selection used for synchronous generation could be valid if applied only during the first fault moments after the fault inception, previously to the "transition period" in Figure 55. Accordingly, a concept called "valid window", relevant for the proposed algorithm, is introduced. This "valid window" is a time frame that allows classical criteria for faulted phase selection to correctly identify the faulted phase and directionality and to be immune to the transition and final period of the current contribution from Type-4 WT and PV generator during an asymmetrical fault.

Regarding this "valid window", the developed algorithm fulfils the following features:

- It identifies and indicates where the valid period to consider the criteria 1 and 2 starts and ends. More details appear in section 3.3.4.
- It adapts the "valid window" to the different time responses of the renewable control systems. Since each control system may have different control time constants, it is essential for the proper performance of the algorithm that this window is time adaptive.

Therefore, this valid window is called "adaptive window" during the rest of the document.

3.3.1 Fault detection and initial classification

A minimum threshold is required to identify unbalanced fault conditions and activate the algorithm. Thus, as the initial step, a threshold detector has been implemented for initial fault classification.

This initial classification is based on ratios of negative and zero sequence currents regarding the positive sequence current. Initial thresholds used for fault classification are shown in Figure 62, and these limits can be settable by the user.

As indicated in Figure 62, no zero sequence leads to the line to line or three-phase fault loop and, after that, the presence of negative sequence current allows to distinguish between line to line (LL) and three-phase faults (LLL).

If zero-sequence current appears, fault type can be single phase to ground (SLG) or line to line to ground (LLG). Both of these faults have negative sequence current, so it is not possible to provide further separation taking into account only negative and zero sequences current at this step.

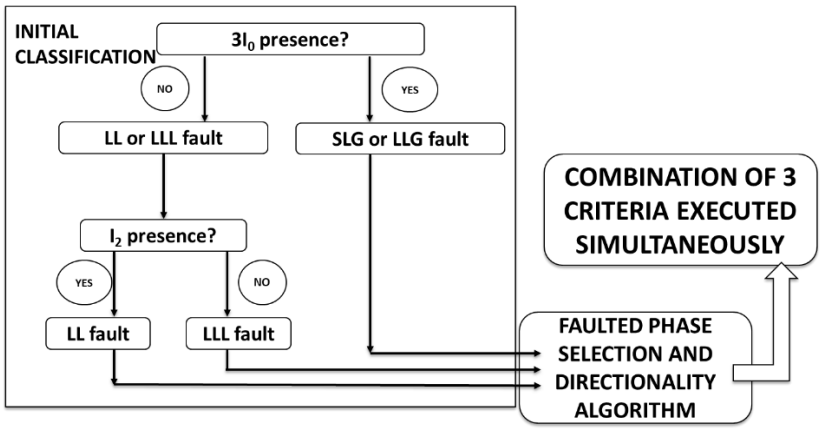

Figure 62. Initial fault classification of the algorithm.

The output of the initial classification shown in Figure 62 is redirected to the faulted phase identification algorithm. This algorithm uses three criteria simultaneously: criterion 1 and criterion 2 based on phasor angles and criterion 3 based on a modified superimposed quantities theory. Figure 63 shows the combination of different criteria employed in the algorithm. This combination of criteria is explained in the next sections.

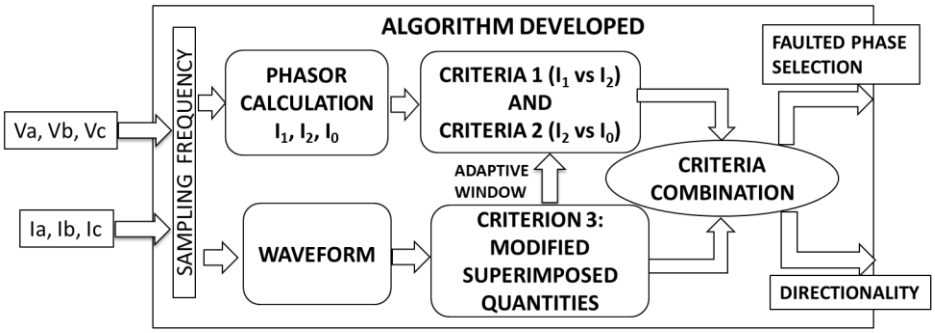

Figure 63. General diagram of the algorithm.

3.3.2 Criterion 1. Positive vs Negative sequence currents

This criterion is based on phasor angles of the positive and negative sequence currents obtained using the Fast Fourier Transform (FFT). In this step, the algorithm calculates $\delta_{criterion1}$, which represents the difference between positive and negative sequence phasor (reference with phase A). Algorithm compares this result with the angular sectors observed in Figure 64 for SLG and LLG faults or sectors from Figure 65 for LL faults to obtain the faulted phase selection. The operation principle of these figures is based on sequence networks and they have been traditionally used for synchronous network [61].

If zero sequence is detected, obtained $\delta_{criterion1}$ is compared with sectors from Figure 64. As an example, this figure shows the results of a fault between phase C and ground (CG fault). As it can be observed, the algorithm defines three zones:

- Reference operation zone: It starts at 210 degrees and finishes at 270 degrees for a CG fault.
- Dead band: The user can define a dead band zone between the adjacent zones to avoid wrong zone activations. This dead band has been set to zero degrees to evaluate its stability without needing more parameters.
- Final operation zone: The final operation zone is obtained if the dead band zone is subtracted from the reference operation zone. If the dead band is set to zero degrees, the final and the reference operation zones are equal.

These defined zones are applicable for all sectors shown in Figure 64: reference operation zone for AG faults goes from 330º to 30º, ABG from 30º to 90º, BG from 90º to 150º, BCG from 150º to 210º and CAG from 270º to 330º.

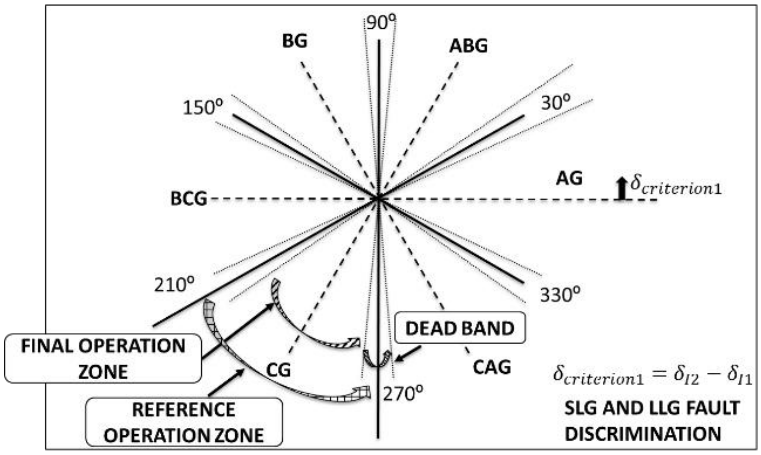

Figure 64. Criterion 1 for LG and LLG faults.

If no zero sequence current is detected in the initial fault classification step, $\delta_{criterion1}$ is compared with sectors in Figure 65 to correctly identify the type of fault among the different LL faults. In this case, AB sector starts at 0º and finishes at 120º, BC sector starts at 120º and finishes at 240º, and CA sector starts at 240º and finishes at 360º.

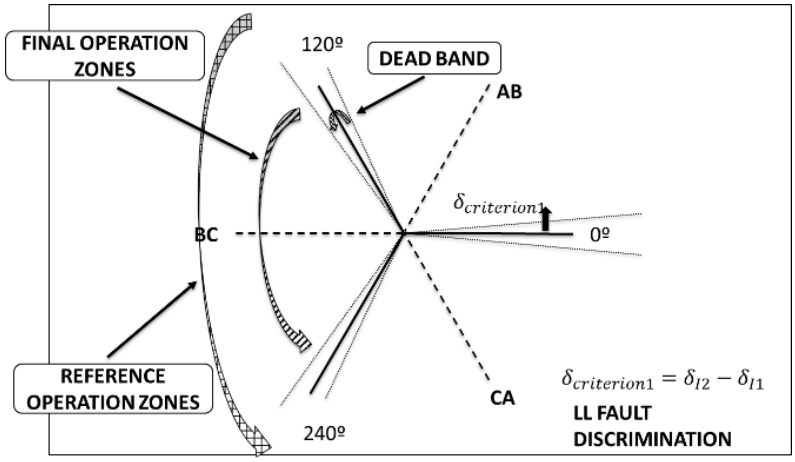

Figure 65. Criterion 1 for line to line faults.

3.3.3 Criterion 2. Negative vs zero sequence currents

Criterion 1 presents a disadvantage for grounded faults due to the proximity between adjacent sectors. For example, in an AG fault, quick activation of adjacent ABG or CAG sectors can happen

due to possible delays in calculating the phasors. Then a second criterion based on the comparison between negative and zero sequence currents [61] is used to increase the robustness of the proposed algorithm. This criterion is only valid for grounded faults but provides the advantage that the adjacent sectors seen in Criterion 1 are delayed 120 degrees in Criterion 2 as is observed in Figure 66.

To illustrate this difference, Figure 66 shows an AG fault as an example. In criterion 1, ABG and CAG are the adjacent sectors. However, in Criterion 2, ABG is 120º leading AG and CAG is 120º lagging AG.

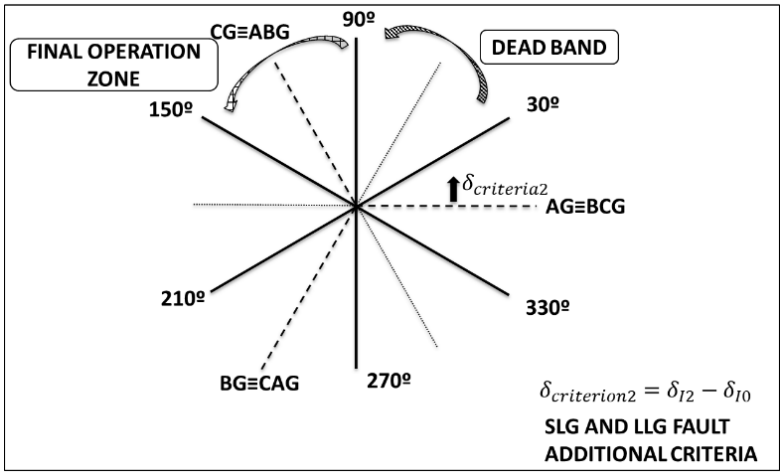

Figure 66. Criterion 2 for single line to ground and line to line to ground faults.

As it can be observed in Figure 66, AG and BCG faults share the sector 330º to 30º, CG and ABG faults share the sector 90º to 150º and finally BG and CAG faults share the sector 210º to 270º. In this case, sectors 30º to 90º, 150º to 210º and 270º to 330º are non-used sectors and considered as dead-band sectors as can be noticed in the picture.

3.3.4 Adaptive window applied to criteria 1 and 2

As explained in section 2.4 and summarized at the beginning of this chapter, bad behaviour of protection relays tested in laboratory were related to the transition period of the fault current contribution from Type-4 WT and PV generators. This transition period was especially problematic for the analyzed faulted phase selector and directional algorithms in distance protection of protection relay manufacturers.

Due to these features, it is essential to avoid calculating criteria 1 and 2 during that transition period, taking valid data from the fault inception to the last instants before such transition period. This window was already defined as "adaptive window" in section 3.3.

In addition, it is imperative to make the algorithm independent from the time response of the renewable generator. It has been observed that PV generators, whose generator is not based on rotating elements, react faster after fault inception than Type-4 WT. Therefore, the goal of this "adaptive window" is to be unaffected by different time responses and be able to adapt to possible different time responses (Figure 67).

Figure 67 shows phase to ground voltages, line currents and scalar products ΔT_{AB}, ΔT_{BC} and ΔT_{CA} waveforms in an SLG fault. Through a maximum and minimum counting of the generated waveforms, the algorithm defines this adaptive window so that only criteria 1 and 2 will be considered during this lapse of time. The number of maximum and minimums is related to the length of the adaptive

window. It is an additional setting of the protection relay that can be set as many other parameters in the relay according to the criteria of the company or the manufacturer.

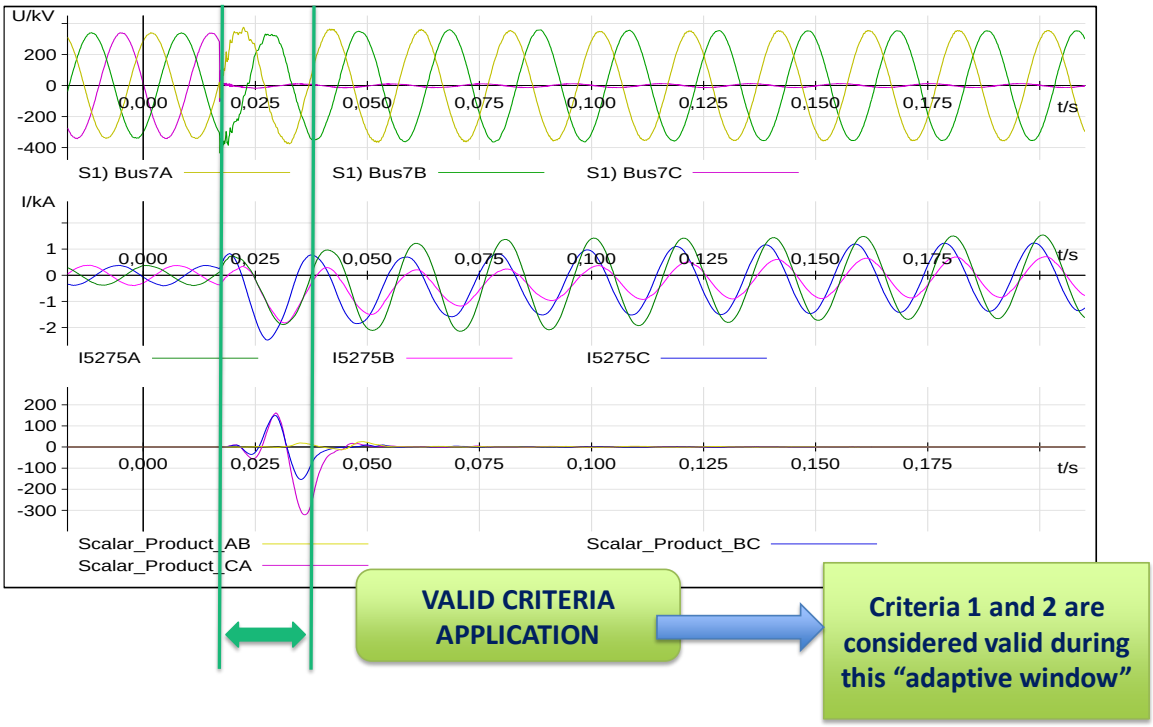

Figure 67. Adaptive window for a single line to ground fault.

3.3.5 Criterion 3: Adaptation of superimposed quantities theory

Criteria 1 and 2 are based on phasor theory jointly with the required adaptive window to ensure the correct behaviour of the algorithm.

In addition to criteria 1 and 2 applied during the adaptive window, the proposed algorithm uses the superimposed quantities theory to distinguish between the different fault types, adapting the requirements from Figure 56 to a network with a high PE penetration level where these criteria are not valid. The new criteria for dealing with fault current contribution coming from renewables is shown in Table 6. Setting proposed, as other parameters used in protection relays based on the experience and observability, were obtained on a large number of tests performed to the Type-4 WT and PV generator during Hardware in the Loop tests carried out in this research.

Making use again of the theory of superimposed quantities, additional criterion has been defined to distinguish between the different types of fault based on the large number of tests performed to the Type-4 WT and PV generator and summarized in Chapter 2. This adaptation is related to the table shown in Table 5 from section 3.2.1, defined in [58]. Setting values in this table is unsuitable for fault current contributions from Type-4 WT and/or PV generator, as observed in analysis form section 3.2.2. Therefore, a criterion of values, which could be even an adjustable setting by user, has been defined as:

Table 6. New criteria proposed.

Type of fault	ΔT_{AB}	ΔT_{BC}	ΔT_{CA}
AG	ΔT_{AB}	$<0.1 \cdot \Delta T_{AB}$	NC
BG	NC	ΔT_{BC}	$<0.1 \cdot \Delta T_{BC}$
CG	$<0.1 \cdot \Delta T_{CA}$	NC	ΔT_{CA}
AB, ABG	ΔT_{AB}	$>0.25 \cdot \Delta T_{AB}$ $<0.75 \cdot \Delta T_{AB}$	NC
BC, BCG	NC	ΔT_{BC}	$>0.25 \cdot \Delta T_{BC}$ $<0.75 \cdot \Delta T_{BC}$
CA, CAG	$>0.25 \cdot \Delta T_{CA}$ $<0.75 \cdot \Delta T_{CA}$	NC	ΔT_{CA}
NC	Not Considered		

3.3.6 Directionality

Criteria 1 and 2 based on phasors are not affected by the directionality of the fault because it influences in the same way to positive, negative and zero sequence current. Therefore, since these two criteria are based on the difference between positive and negative sequence angles (criterion 1) and negative and zero sequences (criterion 2), the directionality does not affect the behaviour of this principle of faulted phase selection. Consequently, the theory of superimposed quantities monitors the scalar products values to evaluate the directionality, as already described and used in criterion 3 for faulted phase selection. A maximum negative peak of the scalar products means forward, while a maximum positive peak means backward directionality [62].

3.3.7 Final decision

The criteria explained in sections 3.3.2 to 3.3.5 are combined to calculate the final result of the algorithm. Using three criteria running in parallel and based on different protection theories confers robustness to this final decision.

The final decision logic is depicted in Figure 68. For SLG faults and LLG faults, the algorithm uses a combination of three criteria. The fulfilment of at least criterion 1 and criterion 3 provides a reliable output. Criterion 1 and 3 were chosen in this case because they work with different protection principles. If two out of three criteria are accomplished, the corresponding type of fault would be activated in the oscillography. In addition, if the three criteria are accomplished simultaneously, the label 3/3 (three out of three) criteria corresponding to the faulted phase selector loop affected. An oscillography example is shown in section 3.4.

If different faulted phase selector loops are activated the faulted phase selector loop with the higher number of criteria accomplished would be the selected loop.

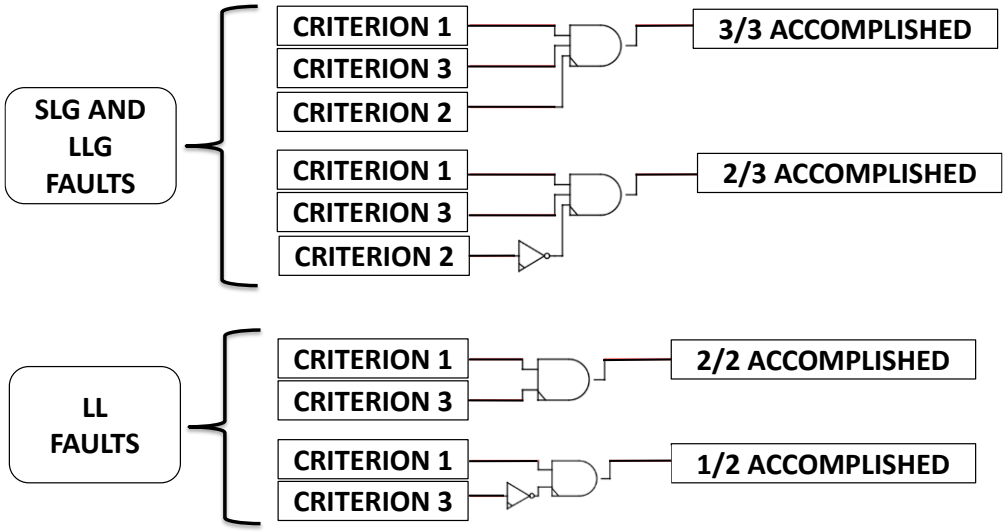

Figure 68. Logic diagram of the final decision of the algorithm.

Similar explanation can be applied to line to line faults. In this case, since there is no presence of zero sequence current, only two criteria are employed: criterion 1 and criterion 3. If criterion 1 is accomplished but criterion 3 is not accomplished, then the label 1/2 (one out of two) are activated for the faulted phase selector loop chosen (for example, for a line to line fault between phases A and B, the digital signal activated would be AB_1/2). On the other hand, if the two criteria are accomplished, the label 2/2 (two out of two) are activated for the faulted phase selector loop chosen (following with the example, for a line to line fault between phases A and B, the digital signal activated would be AB_2/2).

In case of activation of different faulted phase selector loops (for example AB_1/2 and BC_2/2) the faulted phase selector loop with the higher number of criteria accomplished would be the loop selected. Therefore, in this case the BC loop will prevail.

The algorithm presented is protected with the patent [63].

3.4 Algorithm behaviour in lab tests

The same test cases applied in Chapter 2, including additional tests to check different fault resistances and fault types, have been done to check the behaviour of the developed algorithm by RTDS. The benchmark grid used for the study was shown in Figure 43.

Accordingly, the following parameters have been modified during each simulation:

- Scenario: Renewable generation in buses 7 for line 5-7 tests and bus 5 for line 4-5 tests.
- Line under test: Line 5-7 for Type-4 WT tests and line 4-5 for PV tests.
- Distance to the fault:
    - 0%, 50%, 70%, 90%, 100% forward of the line from bus 7 for Type-4 WT for fault study in line 57;
    - 0%, 50%, 70%, 90%, 100% forward of the line from bus 5 for PV for fault study in line 4-5;
- Generation level: 40 and 200 MW. (Total of two combinations)
- Type of faults: AG, BG, CG, AB, BC, CA, ABG, BCG, CAG. (Total of nine combinations)
- Fault resistance: 0, 1 and 10 ohms. (Total of three combinations)
- Repetitiveness: Three times each fault. (Total of three combinations)

The overall number of combinations makes 270 faults per line and fault resistance value. Table 7 and Table 8 summarize the results for Type-4 WT and PV generator current contribution. Results are classified by fault resistances and type of fault. They show the summary of 30 faults per row corresponding to the combinations of two generation levels (40/200 MW), 5 types of faults (0, 50, 70, 90 and 100%) with a repetitiveness of three times each fault to check the consistency of the results [64].

Table 7. Algorithm behaviour. Summary of results obtained for different faults fed by Type-4 WT.

	R=0 ohm		**R=1 ohm**		**R=10 ohm**		**Overall results**		
Type of fault	**Correct detection**	**Wrong detection**	**Correct detection**	**Wrong detection**	**Correct detection**	**Wrong detection**	**Correct detection**	**Wrong detection**	**Correct (%)**
AG	30	0	30	0	30	0	90	0	100%
BG	30	0	30	0	29	1	89	1	99%
CG	28	2	29	1	30	0	87	3	97%
ABG	30	0	30	0	30	0	90	0	100%
BCG	27	3	27	3	29	1	83	7	92%
CAG	30	0	30	0	30	0	90	0	100%
AB	30	0	30	0	30	0	90	0	100%
BC	30	0	30	0	30	0	90	0	100%
CA	30	0	30	0	30	0	90	0	100%
TOTAL	265	5	266	4	268	2	799	11	99%

Table 8. Algorithm behaviour. Summary of results obtained for different faults fed by PV generator.

	R=0 ohm		R=1 ohm		R=10 ohm		OVERALL RESULTS		
Type of fault	Correct detection	Wrong detection	Correct detection	Wrong detection	Correct detection	Wrong detection	Correct detection	Wrong detection	Correct (%)
AG	30	0	30	0	30	0	90	0	100%
BG	30	0	30	0	30	0	90	0	100%
CG	30	0	30	0	30	0	90	0	100%
ABG	30	0	30	0	30	0	90	0	100%
BCG	30	0	30	0	30	0	90	0	100%
CAG	30	0	30	0	30	0	90	0	100%
AB	30	0	30	0	30	0	90	0	100%
BC	30	0	30	0	30	0	90	0	100%
CA	30	0	30	0	30	0	90	0	100%
TOTAL	270	0	270	0	270	0	810	0	100%

Figure 69 shows the oscillography obtained by the developed algorithm in an AG fault at line 5-7 at the 70 % of the line length with a fault resistance of 0 Ω and a total installed generation of 200 MW.

As seen at the bottom of the figure, the proposed algorithm can obtain the correct faulted phases and directionality.

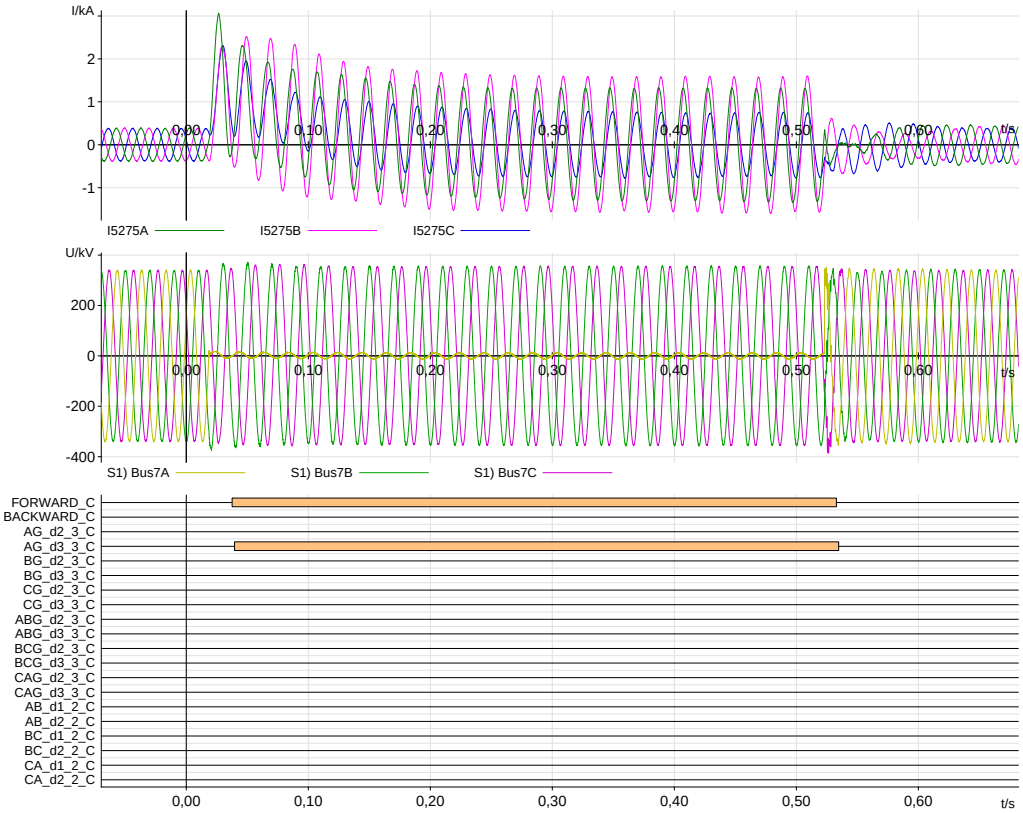

Figure 69. Phase A to ground fault, R=0 ohm, Generation=200 MW, Point of the line=70%.

In the proposed solution and according to the tests performed, faulted phase selection has been solved for Type-4 WT and PV generator current contribution, as shown in the previous tables where 100% of AG, ABG and AB faults were correctly detected by faulted phase selector algorithm. Table 9 compares missed trips obtained with the proposed algorithm and commercial protections test shown in Chapter 2 indicating an significant improvement in results.

Table 9. Comparison of missed trips with the proposed algorithm with commercial response.

	Line 5-7 (Type-4 WT contribution)			**Line 4-5 (PV generator contribution)**		
Type of fault	**Proposed Algorithm**	**Manufacturer A**	**Manufacturer B**	**Proposed Algorithm**	**Manufacturer A**	**Manufacturer B**
SLG	1.48%	18.75%	10.00%	0.00%	85.71%	9.52%
LL	0.00%	16.25%	14.17%	0.00%	48.80%	64.28%
LLG	2.59%	11.66%	6.67%	0.00%	51.19%	3.57%

Once the algorithm has been validated in laboratory, it is implemented in a protection relay. This process and its results are explained in Chapter 4.

Chapter 4 Implementation of the algorithm in MICOM P544

Faulted phase selector developed in Chapter 3 was provided to Schneider Electric so that it can be implemented in the MICOM P544 platform as a firmware upgrade in the real protection relays. The aims of this chapter is to demonstrate that the proposed algorithm can be implemented in a real protection platform and check the improvement of an existing distance protection function with the use of the adaptative window in laboratory tests. Therefore, this chapter is a *proof of concepts* in a real equipment of the algorithm developed in Chapter 3.

To achieve these goals, a collaboration with Schneider has been done for one year. After several iterations of improvements to the firmware, the faulted phase selector algorithm has been successfully implemented into the distance function of MICOM P544 protection relay for this proof of concept. It is important to note that implementing this algorithm in the firmware of the protection was a research activity. Nowadays, the developed algorithm is not available in commercial devices of Schneider.

This chapter explains the work developed by the author of this thesis in this process.

4.1 Validation of the solution

Figure 70 shows the outline of the distance function implemented in the firmware in combination with Schneider in MICOM P544 distance protection relay:

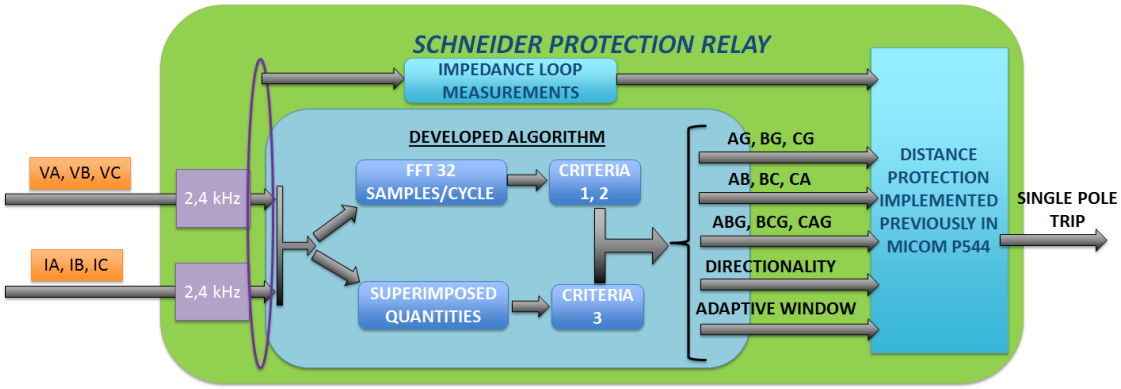

Figure 70. Performance of distance protection implemented in the Schneider MICOM P544 platform.

This Figure 70 represents the implementation of the algorithm developed in section 3.3.

The algorithm receives voltage and current measurements from the protection relay MICOM P544, which uses a 2.4 kHz sampling frequency. This sampling frequency has been taken into account during the tests. The developed algorithm works with the acquired values of voltages and currents, performing the following:

- Calculating the Fast Fourier Transform (FFT) for phasor angle estimations and sequence components calculation.
- Using the waveforms directly to create the scalar products associated with the superimposed quantity theory.

Criteria 1, 2 and 3 explained in Chapter 3 are evaluated with logical components such as comparators and set/reset blocks before obtaining the final output. The final outputs of the algorithm are composed of:

- Faulted phase selector loops: AG, BG, CG, AB, BC, CA, ABG, BCG, CAG.
- Directionality: Backward or forward.
- Adaptive window activation.

Faulted phase selector loops and directionality are provided to the algorithm already implemented in MICOM P544. The equipment generates the trip signal combining the impedance loop measurements already performed by the relay and the proposed algorithm. This new algorithm is tested in this chapter in the same conditions as commercial protection algorithms were tested in the laboratory in Chapter 2.

Implementing the algorithm in the protection relay confirms that the first objective of checking that the algorithm developed is able to run in a commercial protection relay is accomplished. Figure 71 shows the protection relay with the updated firmware version containing the faulted phase selection algorithm developed.

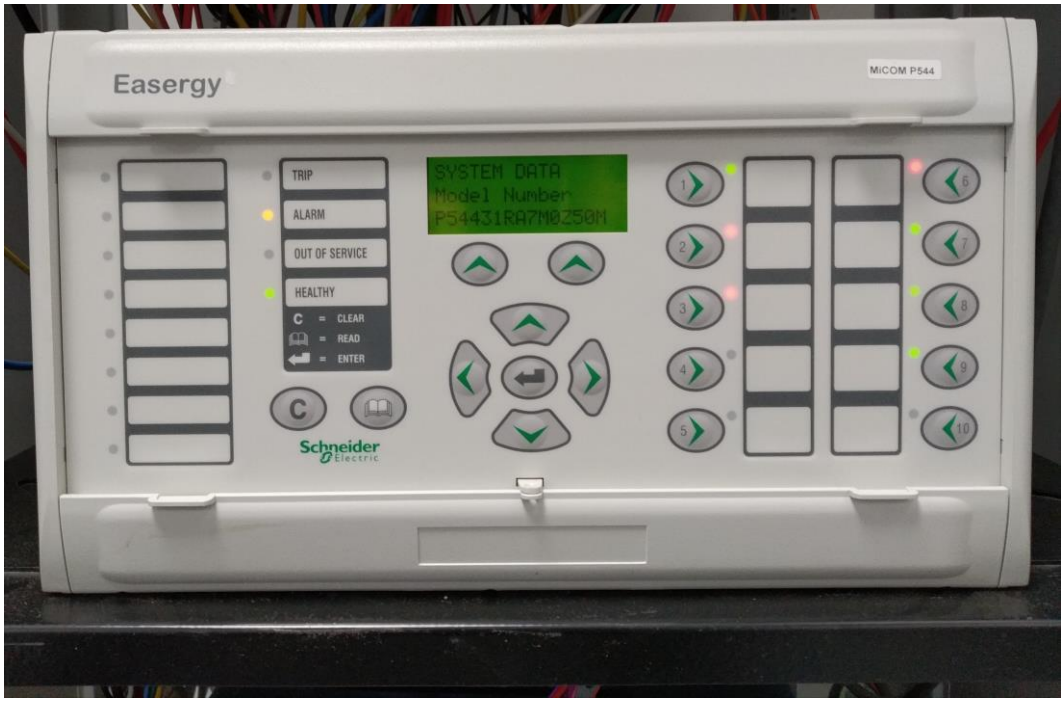

Figure 71. Schneider MICOM P544 with updated firmware version "Z5" for the proof of concepts.

The second objective is to check that the behaviour of commercial distance protection, under fault current contributions coming from renewable sources, is improved thanks to the faulted phase selector proposed.

The benchmark grid from Figure 43 has been again tested in these conditions:

- Generation level (MW): 40, 200.
- Type of generation: Type-4 WT.
- Fault resistance: 0, 1 and 10 ohms.
- Distance to the fault (%): 0, 50, 70, 90, 100.
- Type of fault: AG, BG, CG, ABG, BCG, CAG, AB, BC, CA.
- Repetitiveness: 3 times each fault.

Therefore, 810 faults have been simulated, allowing to debug the behaviour of the firmware until achieving a prosperous and stable performance. Table 10 summarizes the overall results obtained from these tests showing that the implementation of the faulted phase selection developed has significantly improved the protection behaviour compared to the behaviour observed in commercial protection relays in laboratory tests from Chapter 2.

Developed faulted phase selector acted correctly, avoiding the problems observed for distance protection in previous laboratory tests. Some overreach problems were detected and have been analysed in the sections 4.2 and 4.3. These specific cases of in Table 10 have been studied in detail for being representative of the "wrong detection" of the improved protection. The result of the analysis appears in sections 4.2 and 4.3. The correction of these identified cases are related to the impedance measurement and they were not object of the improvement proposed in this work.

Table 10. Summary of results obtained with Type-4 WT[3].

	R=0 ohm		R=1 ohm		R=10 ohm		Overall results		
Type of fault	**Correct detection**	**Wrong detection**	**Correct detection**	**Wrong detection**	**Correct detection**	**Wrong detection**	**Correct detection**	**Wrong detection**	**Correct (%)**
AG	30	0	30	0	30	0	90	0	100%
BG	30	0	30	0	30	0	90	0	100%
CG	30	0	30	0	30	0	90	0	100%
ABG (*)(**)	29	1	30	0	30	0	89	1	98.9%
BCG(*)	30	0	27	3	30	0	87	3	96.7%
CAG	30	0	30	0	30	0	90	0	100%
AB (*) (**)	27	3	27	3	27	3	81	9	90%
BC (*)	30	0	30	0	30	0	90	0	100%
CA (*)	30	0	29	1	30	0	89	1	98.9%
TOTAL	266	4	263	7	267	3	796	14	98.3%

4.2 Analysis of faults simulated in 40 MW scenario

During lab test of the solution, two malfunction cases were detected:

- Missed trips for AB and ABG faults located at 0% of the line
- Overreach of zone 1 for faults at 90% and 100% of the line

This section analyses these phenomena using the oscillography provided by the protection relay and the theoretical impedance measurement.

4.2.1 AB and ABG faults located at 0 % of the line length

Some AB and ABG faults are not tripped when the fault is applied at 0% of the line. This issue is common to the tests applied with different values of fault resistance.

In these cases, the faulted phase selection algorithm detects a fault in AB or ABG, but the impedance loop does not allow the trip of the distance protection. Then, oscillography was downloaded, and its result was studied, including the impedance estimation (X and R values).

[3] (*) Overreach of zone 1 has been detected, but they have not been marked as wrong behaviour since the faulted phase selector acted correctly and the overreach occurred due to the impedance drop in zone 1.

(**) Missed trip of faults at 0% of the line for 40 MW generation level. Although the faulted phase selector worked correctly, they were marked as wrong because it detected the impedance as backwards.

According to the information provided by the manufacturer, the impedance can be calculated by:

$$\overline{Z_{AB}} = \frac{\overline{U_A} - \overline{U_B}}{\overline{I_A} - \overline{I_B}} \quad (67)$$

Based on this equation, the phasor of the impedance is obtained. Real and imaginary components are calculated to know the reactance (X_AB in the graph) and resistance (R_AB in the graph). In Figure 72, both resistance and reactance values oscillate around zero until reactance (X_AB) remains below zero so that the protection does not trip. Furthermore, Figure 73 shows the correct actuation of the faulted phase selector, and the directionality bit indicates the backward direction. The impedance measurement, with negative reactance seen in Figure 72, also corresponds to a backward directionality.

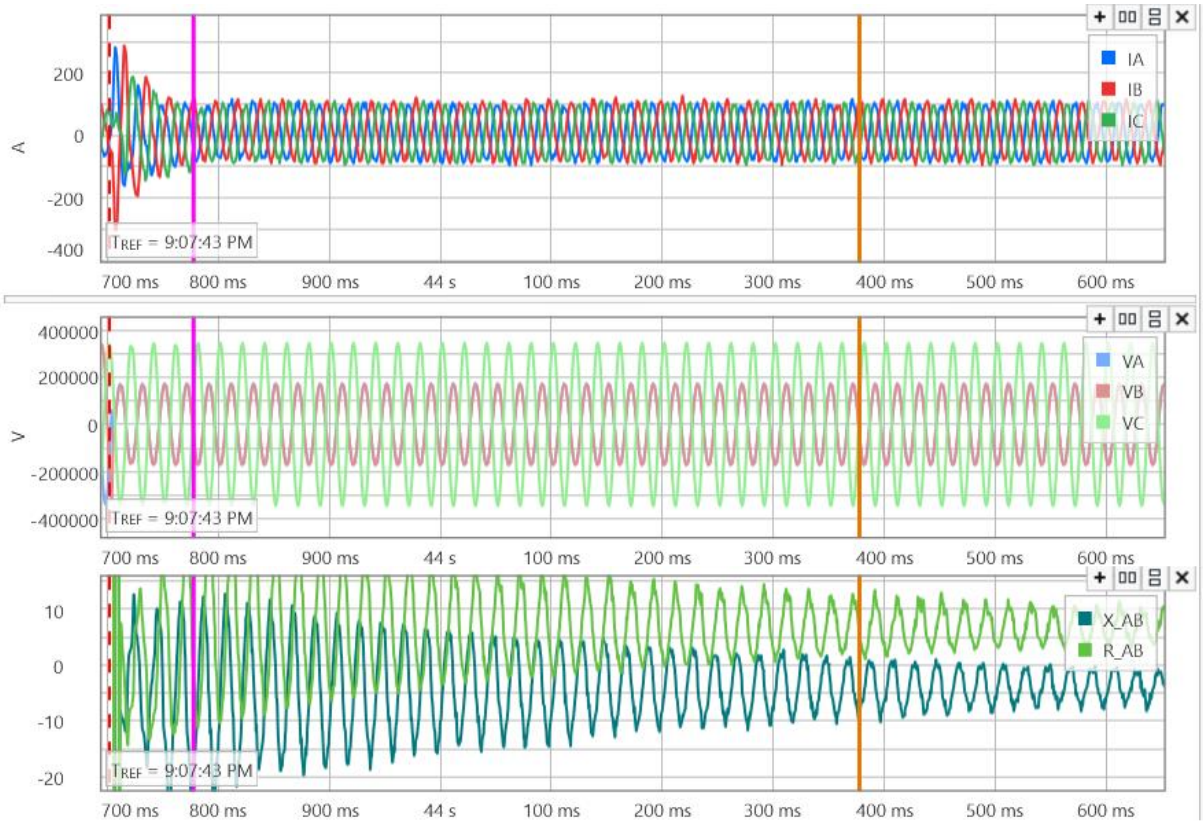

Figure 72. AB fault at 0% of the line in the 40 MW scenario. Resistance and reactance values, currents and voltages.

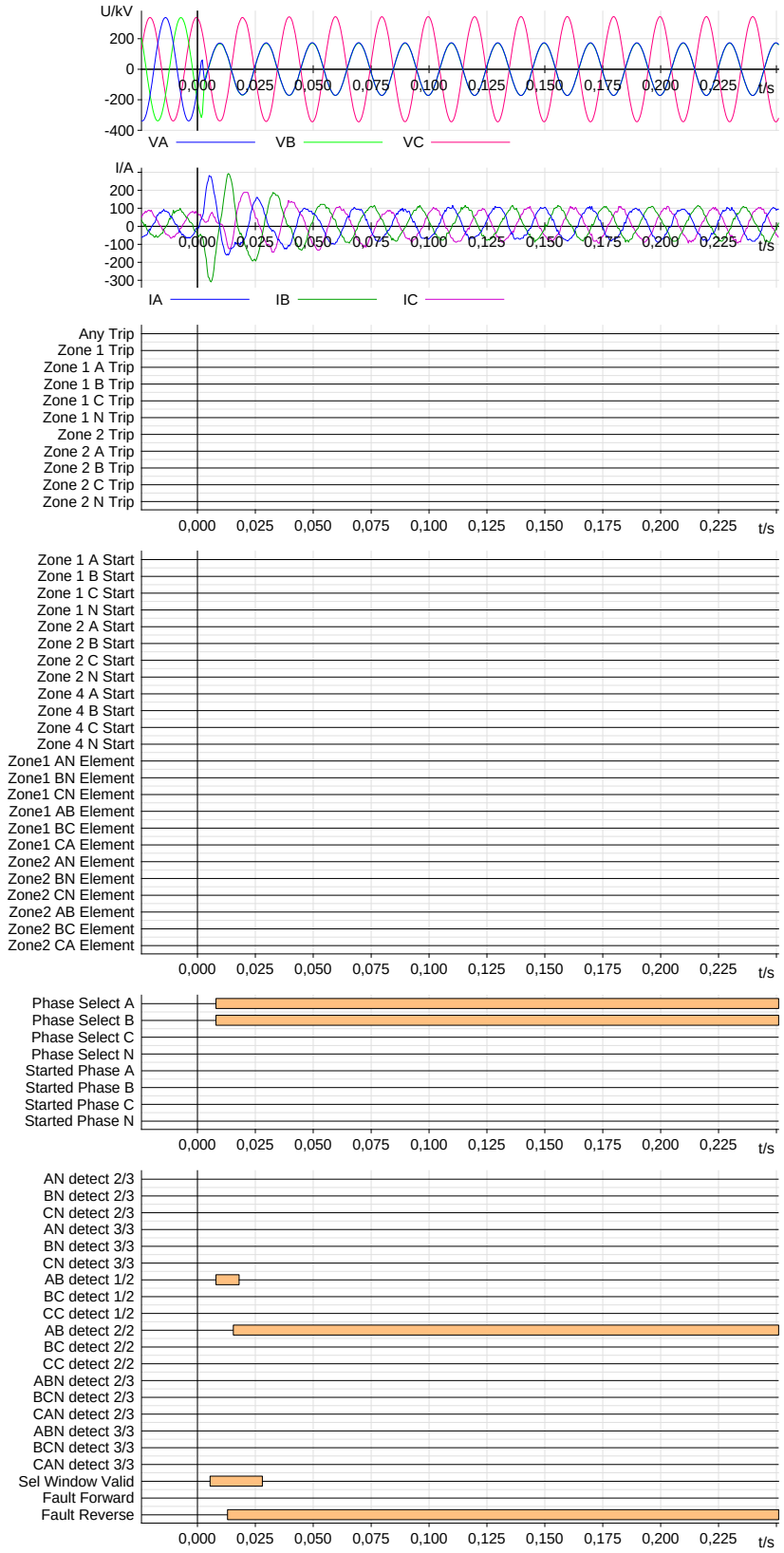

Figure 73. AB fault at 0% of the line in the 40 MW scenario. Voltage, current and digital signals.

Therefore, the conclusion is that the faulted phase selector algorithm acts correctly for this case. Still, the impedance seen by the relay for a fault at 0% of the line (fault forward) with current contribution from Type-4 WT is not in zone 1 because it is detected as backward directionality. Then, the impedance measurement, which corresponds to backward directionality, avoids the protection trip , what is a wrong behaviour of the equipment.

In the case of ABG faults, the impedance also oscillates around zero, but the impedance loop activates the trip order as shown in Figure 74 when reactance becomes positive (instant marked by the orange cursor) in an oscillography downloaded from the protection relay.

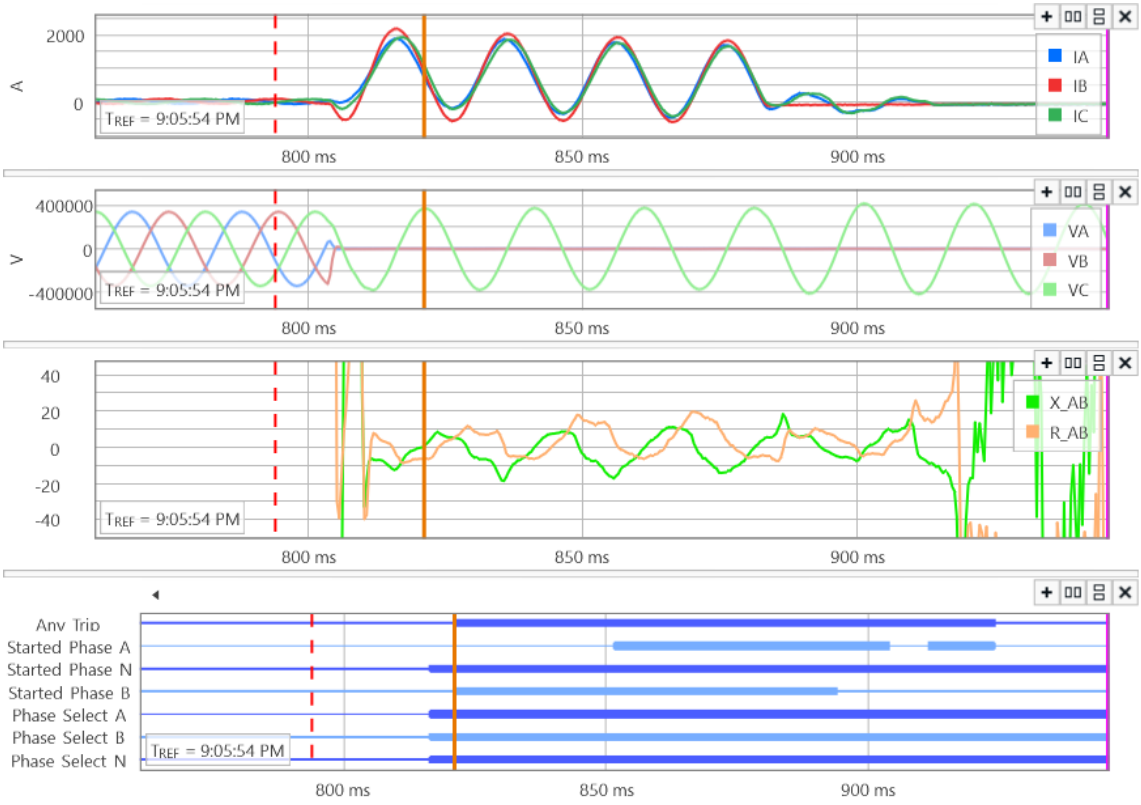

Figure 74. ABG fault at 0% of the line in the 40 MW scenario. Voltages, currents, resistance and reactance values.

Figure 75 shows the activation of faulted phase selector (ABG) and the trip command once the impedance drops in the zone. Initially, the BG impedance loop is activated; then, the AG is also activated. On the other hand, CG is not activated which is also correct for this type of fault. The faulted phase is correctly identified and the trip occurs when the impedance drops in the zone.

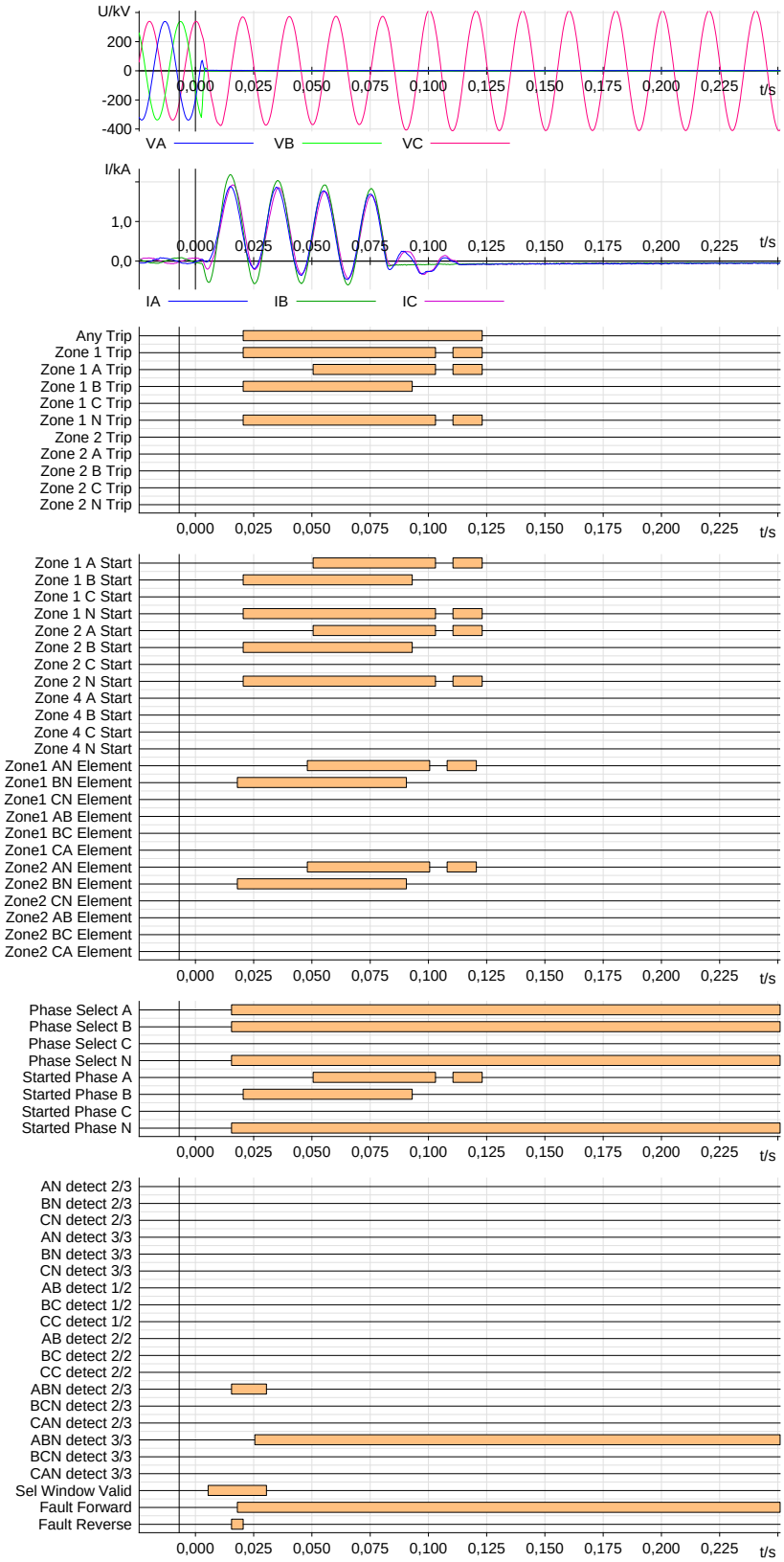

Figure 75. ABG fault at 0% of the line in the 40 MW scenario. Voltage, current and digital signals.

4.2.2 AB fault located at 100 % of the line length

In this case, the protection trips in zone 1 for the line to line faults located at 100 % of the line length, that is, in zone 2. In the oscillography from Figure 76, the impedance drops inside zone 1, although the fault is located at 100% of the line, which makes the protection trip, causing the overreach of the zone 1.

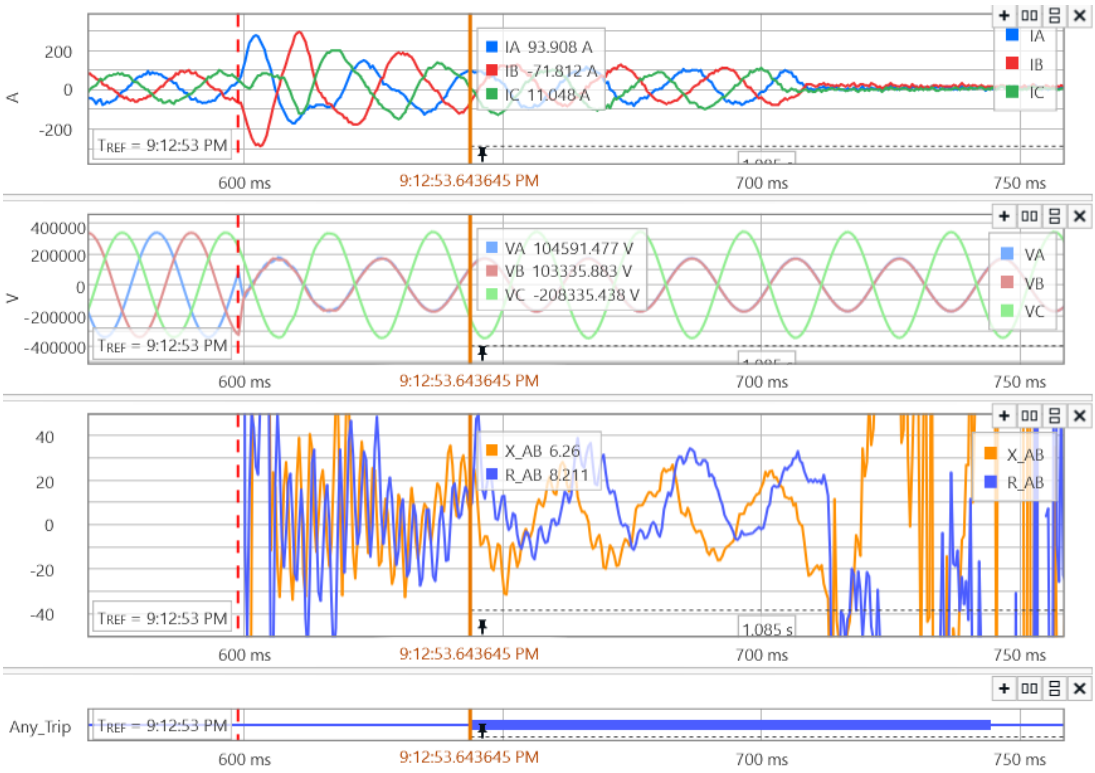

Figure 76. AB fault at 100% of the line in the 40 MW scenario. Currents, voltages, resistance and reactance values.

Apart from the wrong trip of the protection in zone 1 due to the impedance value, it is possible to observe in Figure 77 that the faulted phase algorithm works correctly.

Figure 77 also shows the reverse directionality activation. In the scenario with 40 MW generation level (which is a low current contribution) and mainly in line to line faults, the proposed directionality criterion is not 100% reliable because the positive and negative peaks of the scalar products of superimposed quantities are very similar between them. In the cases observed, fault current was around 70 A primary (i.e. 175 mA secondary for CT 2000/5), which is a very low current contribution. Nevertheless, the distance protection actuation follows the correct faulted phase selector supplied by the developed algorithm. For these cases, with such a low current contribution, it is recommended to use the impedance measurement to declare the directionality and in this way is implemented in the protection relay.

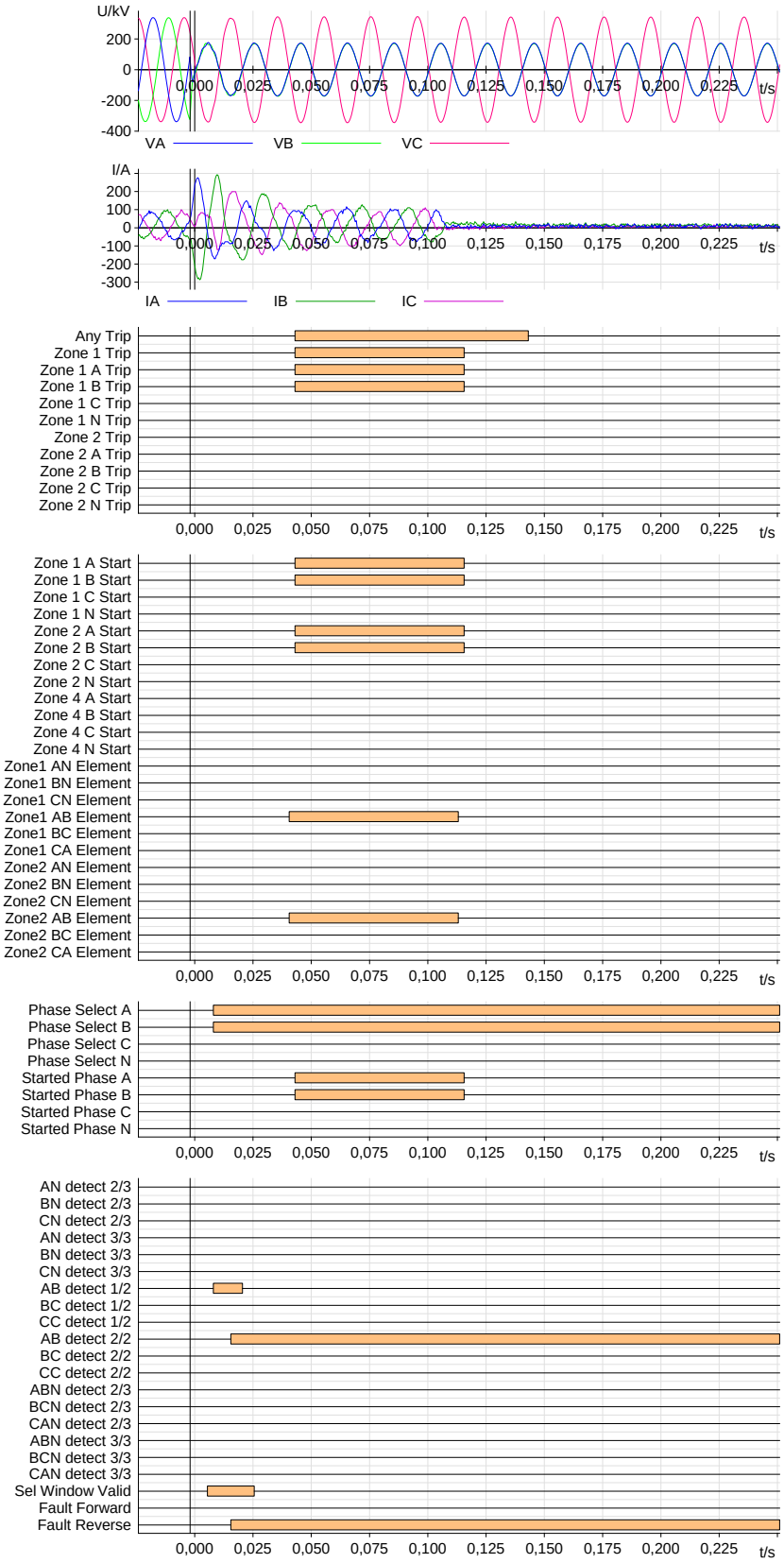

Figure 77. AB fault at 100% of the line in the 40 MW scenario.

4.3 Analysis of faults simulated in 200 MW scenario

In the 200 MW scenario, overreach of zone 1 for the line to line faults was detected for faults located at 90% and 100% of the line. Next, these faults are analyzed using the oscillagraphy of an AB fault.

4.3.1 AB faults at 100 % of the line length

The same phenomena seen in section 4.2, is observed for 200 MW with the fault at 100% of the line. Figure 78 shows that once the impedance drops in zone 1, protection relay trips, causing the overreach of the zone 1 for a fault located in zone 2. The impedance measurement less oscillating in this case than in the previous, as the generation level and current contribution to the fault are higher.

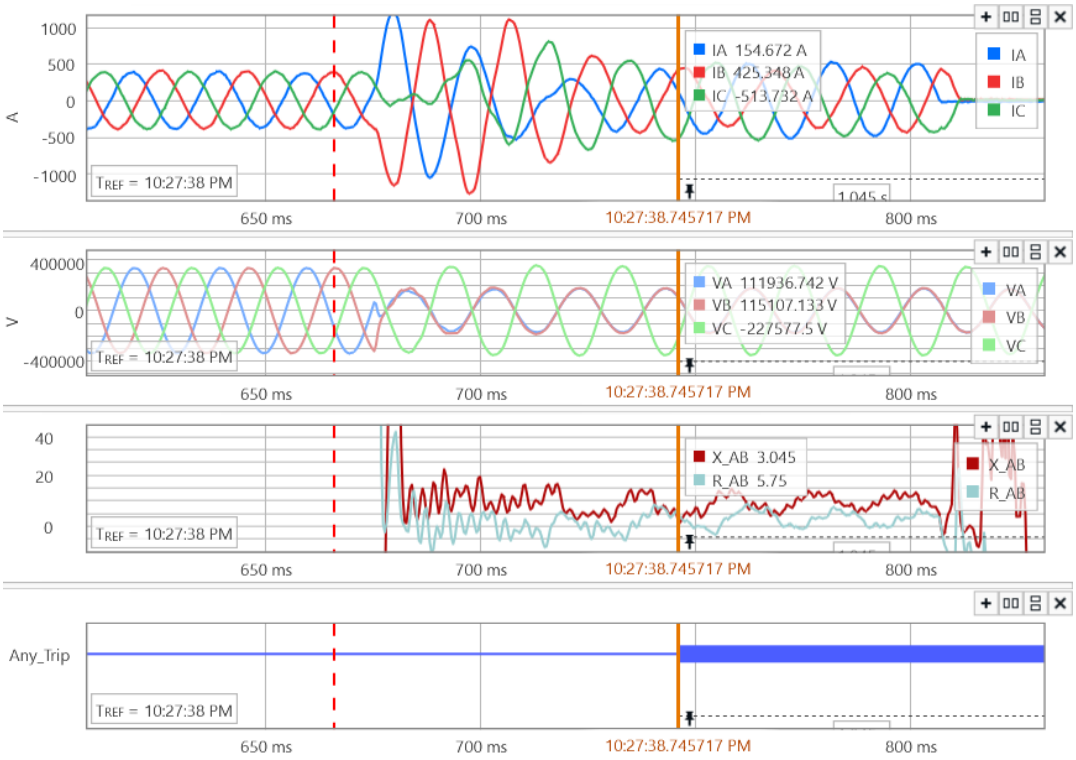

Figure 78. AB fault at 100% of the line in 200 MW scenario . Currents, voltages, resistance and reactance values and tripping signal.

Figure 79 shows that the behaviour of faulted phase selection is correct. However, when the impedance drops in zone 1, protection trips. Therefore, the overreach of zone 1 is caused by the impedance variability due to the current injection coming from renewables. The faulted phase selection algorithm works correctly since the AB fault is correctly identified. In this Figure 79, the start of the zone 2 impedance loop is activated after the fault inception and the AB 2/2 selection loop is also activated. The fault should have been tripped in 400 ms, but the drop of the impedance measurement in zone 1 causes the trip in about 80 ms, causing the overreach of zone 1.

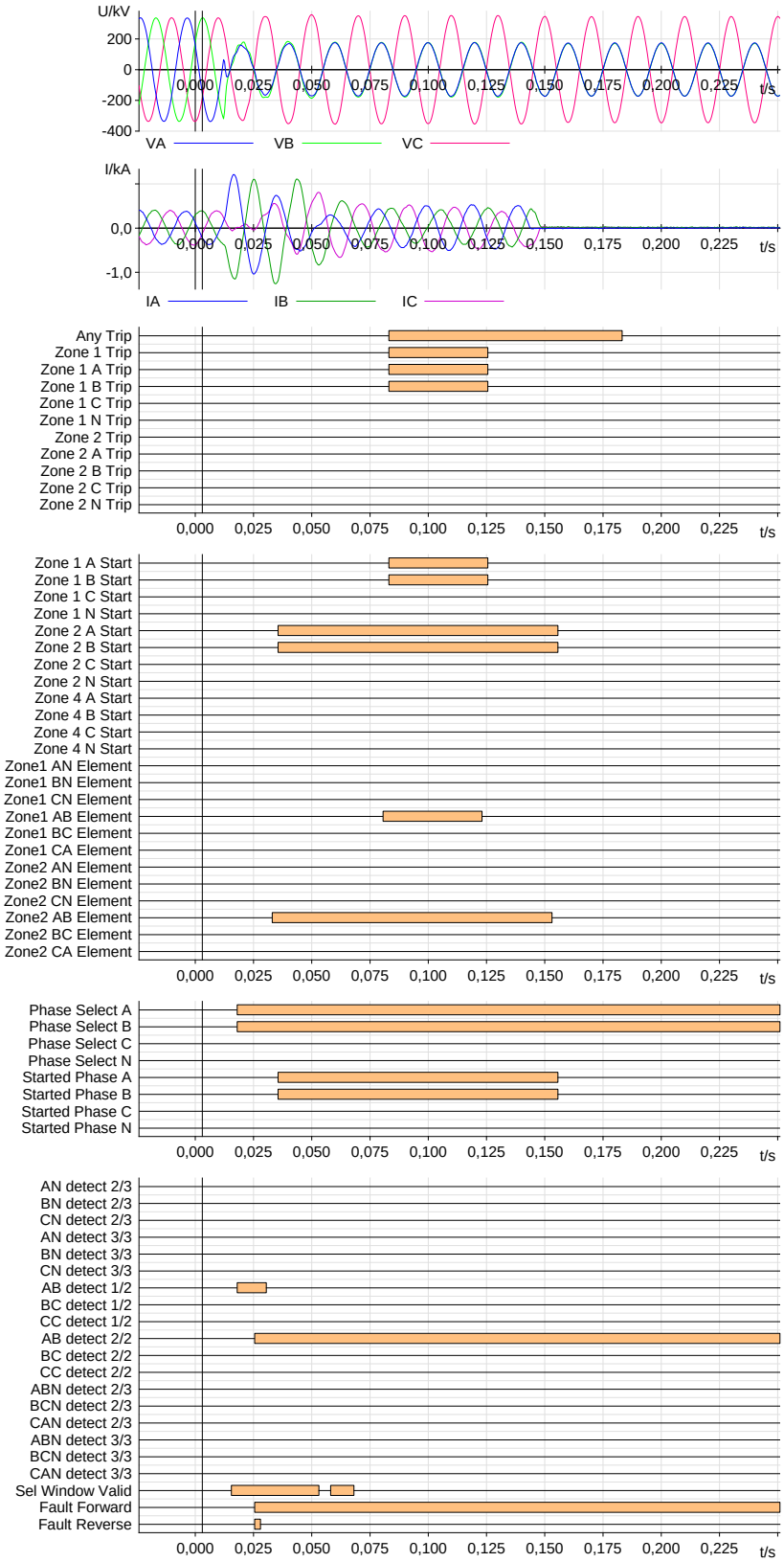

Figure 79. AB fault at 100% of the line in th e200 MW scenario. Voltages, currents and digital signals.

4.4 Results of IEC 60255-121:2014 functional tests

IEC 60255-121:2014 [65] standard defines a complete set of tests that commercial distance protection relays usually pass before its commercialization.

Tests with renewables were carried out following the same criteria as applied in Chapter 2 to demonstrate the improvement of the behaviour of distance protection with renewables. Additionally, to achieve a higher impact of the solutions and verify that these proposed solutions are close to the market, the tests contained in the standard IEC 60255-121:2014 were successfully completed.

This section gathers the results obtained during functional tests on the distance function when different distance protection algorithms are implemented in the MICOM P544 protection platform. These functional tests, described in section 6 of standard IEC 60255-121:2014, are classified as:

- Static tests
- Dynamic tests
- Performance with harmonics tests
- Performance during off-nominal frequency tests
- Double infeed tests

All these functional tests have been run two times: the first one for the commercial algorithm implemented in MICOM relay, the second one using the enhanced distance protection developed in this thesis including the developed faulted phase selector algorithm.

Due to the large number of tests from this standard, the results are shown briefly. The algorithm provides trip order in an average time of 25 ms. This time is a bit higher than the previous commercial solution because it is a bit more conservative to take into account the behaviour of renewables and the more conservative nature of the proposed faulted phase algorithm. In any case, this time can be considered good enough since it is only 5 ms higher than a cycle. Analyzing in detail the oscillographies, it can be noticed that the faulted phase selector detects the fault faster than the impedance is detected to enter the zone, so it can probably be due to the interaction between the impedance measurement loops and the faulted phase selection.

Table 11. Original P544 algorithm times according to IEC 60255-121.

Statistic	Time (ms)
Original P544 Algorithm	
Mode	18.50
Median	19.30
Mean	19.46

Table 12. Developed algorithm times according to IEC 60255-121.

Statistic	Time (ms)
Developed Algorithm	
Mode	23.50
Median	25.55
Mean	26.11

Results have been obtained with tripping times around 25 ms.

The times obtained are considered correct since they are clearly inside the time allowed to act in the protection criteria defined for the tests in Table 2.

4.5 Conclusions of the laboratory tests

Laboratory test results show that faulted phase selection problem detected in Chapter 2 and Chapter 3 has been successfully solved with the proposed algorithm because:

- The distance protection developed provides an enhanced behaviour regarding present distance protection algorithms under the current contribution to the fault of renewable energies, according to the fault study applied to the updated firmware of the protection.
- Faulted phase selector provides good performance for all the faults applied.
- There was no missed trip due to a wrong action of the faulted phase selector. Therefore, it is demonstrated that the developed algorithm for faulted phase selection, combined with the impedance measurement of the protection relay previously implemented in MICOM P544, enhances distance protection in scenarios with high penetration of renewables.

Once the faulted phase selector has been improved with the development of this thesis, some overreach problems have been detected because of impedance fluctuations due to power electronics and control systems. Therefore, the door is open to future developments for advanced methods that provide a more stable and reliable impedance measurement during the fault to avoid these problems. It has been observed that impedance calculation can cause malfunction of the distance protection such as:

  - In line to line faults at 0% of the line length, the impedance was seen backwards so that the protection did not trip.
  - In line to line faults at 0% of the line length, the impedance was seen backwards so that the protection did not trip.
  - For the line to line faults at 100% of the line, the impedance variation causes the protection to trip in zone 1, although those faults occurred in zone 2.

Chapter 5 Conclusions

The differences in the current contribution to short circuits by generators based on PE make it necessary to analyze the possible effects in the protection systems, which were designed based on the contribution provided by large generators synchronously connected to the electrical power system. these differen range from current levels, which are highly reduced during the fault, the current dynamic injected during the first milliseconds after the fault inception or the contribution before unbalanced faults.

To analyze how the protection relays behave with PE renewable sources, Hardware in the Loop (HiL) simulations were performed. In HiL experiments, the actual devices interact with a benchmark network modelled in RSCAD through RTDS interface. For this purpose, EMT models of type-4 wind turbines and PV generators were developed in the benchmark network to test two protection relays from different manufacturers before their current contribution.

The objective of these tests was to analyze the behaviour of protection algorithms commonly used in transmission networks: distance, line current differential and ground directional overcurrent. The following points summarize the main empirical conclusions from this part of the study:

- Distance protection was the function that presented the higher number of non-expected results in terms of missed trips, overreach of zone 1 for faults located at zone 2 and delayed trips for faults found both in zone 1 and zone 2.
- Detection of single line to ground and line to line fault was significantly affected due to the current contribution of renewables during the fault state.
- The lack of negative sequence current injection (even during asymmetrical faults) due to the control algorithms implemented on PV generator and Type-4 WT has been observed as problematic for distance protection algorithm in terms of directionality declaration and faulted phase selection
- Additional injection of negative sequence current during asymmetrical faults has improved fault detection in directionality declaration and fault selection.

- A transient period associated with the PV and Type-4 WT controls between the fault inception and the steady-state of the current during the fault can be defined. This transient period is especially problematic in algorithms associated with distance protection behaviour (mainly faulted phase selection).
- Faulted phase selector and declaration of directionality in the equipment analyzed presented a bad behavior, what meant a wrong performance of distance protection.
- Impedance measurement is correct during the steady-state period of the fault current, but it oscillates during the transient period. This fact leads the protection to overreach if the impedance enters zone 1 for some milliseconds during such oscillations, even when the fault is located in zone 2.
- Current contribution level during the steady-state of the fault can help the fault detection, but, considering that the minimum threshold has been reached, it is not the critical factor. Initial peak of the current, transient period of the control, directionality declaration and phase selection result more important than the current level for a correct fault identification.
- Line differential protection worked correctly for all the tests performed in this study, with the different kinds of renewable generators and types of fault. Then, the 87L function was not an object of the study to improve its behaviour in this thesis.
- Ground directional overcurrent protection detects the current through the system's grounding. Renewable generators are typically connected to the transmission network through a wye-grounded transformer on the high voltage side (delta connection on the low voltage side). This connection makes the circulation of current possible in case of fault involving ground.
- Renewable generation current injection did not affect 67N function behaviour, which depends on the connection of the neutral of the transformer. Then, the 67N function was not an object of the study to improve its behaviour in this thesis.

Because of these conclusions, this thesis focused on distance protection behaviour by enhancing the faulted phase selection and directionality algorithms.

After analyzing the behaviour of protection relays, a new faulted phase protection algorithm was developed and tested, obtaining improved results regarding the behaviour observed in present protection relays. This improved algorithm was developed as a multicriteria algorithm, introducing the novelty of adaptative window jointly with a multicriteria algorithm adapted to correctly work with renewable energies and power electronic.

This algorithm was implemented in a MICOM P544 relay. For this implementation, collaboration with Schneider Electric was needed to apply a firmware update to the equipment. Then, in this work, the same laboratory tests used for protection analysis in Chapter 2 were applied to validate the concepts of the implemented algorithm. The tests on this developed distance protection demonstrated improved behaviour with renewable generators current contribution. The behaviour with synchronous generation was also correct according to the standard IEC 60255:121 for distance protection.

Therefore, it has been shown that the theory of distance protection is still valid for protecting the network against fault current contribution coming from PE-based renewable sources by including appropriate modifications in the algorithms traditionally used with synchronous generation.

In addition to the distance protection improvement, to ensure the reliability of protection functions under high penetration of renewables, protection of transmission networks with high penetration of renewables can be achieved using:

- Line differential protection schemes when high speed communication is available.
- Ground directional overcurrent with the exception that it can be used for phase to ground and phase to phase to ground faults only.

These protection functions were tested in Chapter 2 showing a correct behavior.

The field of protection systems is currently in continuous evolution, so the following future research is recommended:

- Distance protection:
  - Improve time response of faulted phase selector to achieve an overall time response of distance protection below 20 ms.
  - Enhanced impedance measurement. It was observed during the tests that impedance measurements tend to be erratic during the transient period after the fault inception. This irregular measurement can cause an overreach of zone 1 due to the travel of the impedance. Therefore, it is interesting to analyze improved and immune solutions for the measurements received during a fault with contributions from renewable energies based on PE.

- Improve the reliability and speed of communication so that it is possible to connect different sides of the protected element (e.g. a line) and increase the reliability of the detection by using differential schemes.
- Analyze other methods to improve the system reliability against short circuits, such as wide-area protection based on synchrophasor measurement units (PMUs) for backup protection based on other actuation principles.

Chapter 6 References

[1] Red Eléctrica de España, "The Spanish Electricity System. Summary.," Madrid, 2020.

[2] Réseau de Transport d'Électricité, "Electricity report 2020," 2020. [Online]. Available: https://bilan-electrique-2020.rte-france.com/total-generation/?lang=en. [Accessed November 2021].

[3] Terna Driving Energy, "Provisional data on operation of the italian electricity system," 2020.

[4] Fraunhofer IEE, "The Four Control Areas," [Online]. Available: http://windmonitor.iee.fraunhofer.de/windmonitor_en/2_Netzintegration/2_netzbetrieb/1_Die_vier_Regelzonen/. [Accessed November 2021].

[5] K. Appunn, Y. Haas and J. Wettengel, "Germany's energy consumption and power mix in charts," *Clean Energy wire,* August 2021.

[6] Institute for Solar Energy Systems (ISE), "Public Net Electricity Generation in Germany 2020: Share from Renewables Exceeds 50 percent," 2021.

[7] Swiss Federal Office of Energy (SFOE), "Electricity production plants in Switzerland," Zurich, 2021.

[8] Agencija za energijo, "Report on the energy sector in Slovenia 2020," 2020.

[9] The Government of the Republic of Slovenia, "Integrated national energy and climate plan of the Republic of Slovenia," Liubliana, February 2020.

[10] International Energy Agency, "The Netherlands 2020. Energy Policy Review," 2020.

[11] Eirgrid Group, "Annual Report 2020," Dublin, 2020.

[12] Scottish renewables, "Statistics: Energy consumption by sector," Glasgow, 2019.

[13] International Atomic Energy Agency, "International Atomic Energy Agency," May 2019. [Online]. Available: https://www-pub.iaea.org/MTCD/publications/PDF/cnpp2019/countryprofiles/Finland/Finland.htm. [Accessed November 2021].

[14] Elering, "Security of supply. Report 2020 extract," Tallin, 2021.

[15] M. Altaf, M. Arif, S. Saha, S. Islam, M. E. Haque and A. Oo, "Renewable Energy Integration challenge on Power System Protection and its Mitigation for Reliable Operation," in *The 46th annual conference of the IEEE Industrial Electronics Society*, 2020.

[16] V. Telukunta, J. Pradhan, A. Agrawal, M. Singh and S. Srivani, "Protection challenges under bulk penetration of renewable energy resources in power systems: A review," *CEE Journal of Power and Energy Systems,* vol. 3, no. 4, pp. 365-379, 2017.

[17] J. C. Quispe , H. H. Villarroel-Gutiérrez and E. Orduña, "Analyzing Short-Circuit Current Behavior Caused by Inverter-Interfaced Renewable Energy Sources. Effects on Distance Protection," in *EE PES Transmission & Distribution Conference and Exhibition - Latin America (T&D LA)*, 2020.

[18] G. Missrani, N. Nabila, F. H. Jufri, D. R. Aryani and A. R. Utomo, "Study on Short Circuit Current Contribution after Photovoltaic Solar Plant Integration in Lombok' s Distribution Network," in *IEEE International Conference on Innovative Research and Development (ICIRD)*, 2019.

[19] A. Haddadi, M. Zhao, I. Kocar, U. Karaagac, K. Chan and E. Farantos, "Impact of Inverter-Based Resources on Negative Sequence Quantities-Based Protection Elements," *IEEE transactions on Power Delivery,* vol. 36, no. 1, pp. 289-298, 2021.

[20] "American National Standards Institute (ANSI)," [Online]. Available: https://www.ansi.org/.

[21] N. Fischer, H. J. Altuve, G. Benmouyal and B. Kasztenny, "Tutorial on Operating Characteristic of Microprocessor-Based Multiterminal Line Current Differetial Relays," in *Western Protective Relay Conference*, Spokane, 2011.

[22] Schneider Electric, Easergy Micom P54x Technical Manual, France, 2016.

[23] Siemens Power Academy, Principles of Distance Protection, Madrid, 2014.

[24] J. Roberts, A. Guzmán and E. Schweitzer, "Z=V/I does not make a distance relay," in *20th Annual Western Protective Relay Conference*, Spokane, 1993.

[25] D. Fentie, "Understanding the Dynamic Mho," in *69th Annual Western Conference for protective relay engineers*, Spokane, 2019.

[26] IEEE Working Working, "PES-TR7 Modeling and Analysis of System Transients Using Digital Programs Part 1," IEEE, 15.08.09.

[27] K. Ma, W. Chen, M. Liserre and F. Blaabjerg, "Power Controllability of a Three-Phase Converter With an Unbalanced AC Source," *IEEE Transactions on Power Electronics,* vol. 30, no. 3, pp. 1591-1604, March 2015.

[28] N. Chaudhuri, B. Chaudhuri, R. Majumder and A. Yazdani, Multi-terminal direct-current grids: Modeling, analysis, and control, John Wiley & Sons, 2014.

[29] Tennet, Requirements for Offshore Grid Connections in the Grid of Tennet, 2012.

[30] R.E.E., "Orden TED/749/2020, de 16 de julio, por la que se establecen los requisitos técnicos para la conexión a la red necesarios para la implementación de los códigos de red de conexión.," Madrid, 2020.

[31] H2020 MIGRATE Project, "Deliverable D1.6 Demonstration of Mitigation Measures and Clarification of Unclear Grid Code Requirements," 2019.

[32] M. Ndreko, M. Popov, A. A. van der Meer and v. d. Meijden, "The effect of the offshore VSC-HVDC connected wind power plants on the unbalanced faulted behavior of AC transmission systems," in *IEEE International Energy Conference (ENERGYCON)*, Leuven, 2016.

[33] B. Sen, D. Sharma and B. C. Babu, "DSRF and SOGI based PLL-two viable scheme for grid synchronization of DG systems during grid abnormalities," in *Engineering and Systems (SCES)*, Allahabad, Uttar Pradesh, 2012.

[34] M. L. Ke Ma and F. Blaabjerg, "Operating and Loading Conditions of a Three-Level Neutral-Point-Clamped Wind Power Converter Under Various Grid Faults," *IEEE Transactions on Industry Applications,* vol. 50, no. 1, pp. 520-530, Jan.-Feb. 2014.

[35] A. Yazdani and R. Iravani, Voltage-Sourced Converters in Power Systems: Modeling, Control and Applications, IEEE Press, Wiley, 2010.

[36] J. A. Suul, A. Luna and P. Rodríguez, "Power control of VSC HVDC converters for limiting the influence of AC unbalanced faults on multi-terminal DC grids," in *10th IET International Conference on AC and DC Power Transmission (ACDC 2012)*, Birmingham, 2012.

[37] J. Renedo, A. Garcia-Cerrada and L. Rouco, "Active Power Control Strategies for Transient Stability Enhancement of AC/DC Grids With VSC-HVDC Multi-Terminal Systems," *IEEE Transactions on Power Systems,* vol. 31, no. 6, pp. 4595-4604, 2016.

[38] L. He, C. C. Liu, A. Pitto and D. Cirio, "Distance Protection of AC Grid With HVDC-Connected Offshore Wind Generators," *IEEE Transactions on Power Delivery,* vol. 29, no. 2, pp. 493-501, 2014.

[39] S. K. Chaudhary, R. Teodorescu, P. Rodriguez, P. C. Kjaer and A. M. Gole, "Negative Sequence Current Control in Wind Power Plants With VSC-HVDC Connection," *IEEE Transactions on Sustainable Energy,* vol. 3, no. 3, pp. 535-544, July 2012.

[40] P. Rodriguez, J. Pou, J. C. J. I. Bergas, R. P. Burgos and D. Boroyevich, "Decoupled Double Synchronous Reference Frame PLL for Power Converters Control," *IEEE Transactions on Power Electronics,* vol. 22, no. 2, pp. 584-592, 2007.

[41] A. Luna, "Grid Voltage Synchronization for Distributed Generation Systems Under Grid Fault Conditions," *IEEE Transactions on Industry Applications,* vol. 51, no. 4, pp. 3414-3425, 2015.

[42] L. H. Liu, "Effects of HVDC connection for offshore wind turbines on AC grid protection," in *Power & Energy Society General Meeting*, Vancouver, BC, 2013.

[43] L. Zeni, H. Jóhannsson, A. D. Hansen, P. E. Sørensen, B. Hesselbæk and P. C. Kjær, "Influence of current limitation on voltage stability with Voltage Sourced Converter HVDC," in *IEEE PES ISGT Europe*, Lyngby, 2013.

[44] P. Zhang, H. Li, G. Wang and G. Zhu, "The Impact of HVDC Commutation Failure on the Distance Protection," in *Asia-Pacific Power and Energy Engineering Conference*, Chengdu, 2010.

[45] J. J. Grainger and W. D. Stevenson, Power System Analysis, North Carolina State University: McGraw-Hill, 1994.

[46] RTDS Technologies, RTDS User Manual, Winnipeg, 2018.

[47] Red Eléctrica de España; EDP HC Energía; Endesa; Estabanell Energía; Iberdrola; Unión Fenosa; Viesgo, Criterios de ajuste y coordinación de protecciones en la red peninsular de alta tensión de transporte y distribución, Madrid: Red Eléctrica de España, 2017.

[48] T. Neumann and I. Erlich, "Short Circuit Current Contribution of a Photovoltaic Power Plant," *Conference of power Plants and Power Systems Control,* 2012.

[49] B. Kasztenny and D. Finney, "Fundamentals of Distance Protection," in *61st annual conference for protective relay engineers*, Spokane, 2008.

[50] R. Walling, E. Gursoy and B. English, "Current contribution from Type 3 and Type 4 wind turbine generators during faults," *IEEE Power and Energy Society General Meeting,* 2011.

[51] J. Keller and B. Kroposki, "Understanding Fault Characteristics of Inverter-Based Distributed Energy Resources," in *Technical Report NREL/TP-550-46698*, 2010.

[52] M. Ndreko, M. Popov and M. A. M. M. van der Meijden, "Study on FRT compliance of VSC-HVDC connected offshore wind plants during AC faults including requirements for the negative sequence current control," *Electrical Power and Energy Systems,* pp. 97-116, 2017.

[53] Semikron, "Semikron Datasheet: IGBT SKM 50GB12T4 Rev," 2013. [Online]. Available: https://www.alliedelec.com/m/d/3e4d23912ec5bcceaf4b4ac4c24b2e72.pdf. [Accessed June 2017].

[54] S. Rijcke, P. S. Perez and J. Driesen, "Impact of wind turbines equipped with doubly fed induction generators on distance relaying," *IEEE Power Energy Soc. Gen Meeting ,* 2010.

[55] J. Blumschein, C. Dzienis and M. Kereit, "Directional Comparison based on High-Speed-Distance Protection using Delta Quantities".

[56] C. Dzienis, M. Kereit and J. Blumschein, "Analysis of High-Speed-Distance Protection," *The International Conference on Advanced Power System Automation and Protection,* 2011.

[57] P. Horton and S. Swain, "Using superimposed principles (delta) in protection techniques in an increasingly challenging power network".

[58] G. Benmouyal and J. Roberts, "Superimposed Quantities: Their True Nature and Application in Relays," in *26th Annual Western Protective Relay Conference*, Spokane, 1999.

[59] A. Guzmán, J. Mooney, G. Benmouyal, N. Fischer and B. Kasztenny, "Transmission Line Protection System for Increasing Power System Requirements," *International Symposium Modern Electric Power Systems (MEPS), Wroclaw, Poland,* September 20–22, 2010.

[60] G. Benmouyal and J. Mahseredjian, "A Combined Directional and Faulted Phase Selector Element Based on Incremental Quantities," *IEEE TRANSACTIONS ON POWER DELIVERY,* vol. 16, no. 4, pp. 478-484, OCTOBER 2001.

[61] D. Costello and K. Zimmerman, "Determining the Faulted Phase," in *36th Annual Western Protective Relay Conference*, Spokane, 2009.

[62] E. Martínez Carrasco, M. P. Comech Moreno, M. T. Villén Martínez and S. Borroy Vicente, "Improved Faulted Phase Selection Algorithm for Distance Protection under High Penetration of Renewable Energies," *Energies,* vol. 13, no. 3, p. 558, 2020.

[63] E. Martínez, S. Borroy and M. T. Villén, "Protection method of an electrical distribution and/or transmission network against short-circuits". European Patent Office Patent PCT/EP2020/053877, 2nd September 2020.

[64] E. Martinez, S. Borroy, M. T. Villén, D. López, M. Popov and H. Grasset, "New faulted phase selector solution for dealing with the effects of type-4 wind turbine on present protection relaying algorithms," in *CIRED Conference*, Madrid, 2019.

[65] International Electrotechnical Commission, IEC 60255-121:2014 Measuring relays and protection equipment - Part 121: Functional requirements for distance protection, 2014.

Appendix 1 Parameters of the grid model

This appendix shows the electrical parameters of the elements in the benchmark grid. Table 13 includes the parameters of the electrical data of the lines and Table 14 the electrical data of the transformers. The neutral point on 400 kV side is directly grounded.

Table 13. Electrical data of the lines.

LINE	SIDE 1	SIDE 2	Ur (kV)	Length (km)	R(Ω)	X(Ω)	B(μS)	R0(Ω)	X0(Ω)	B0(μS)
1	Bus 1	Bus 2	400	41.26	1.36	12.91	152.05	9.60	37.55	92.73
2	Bus 3	Bus 4	400	35.1	1.03	10.84	131.76	10.53	34.68	80.34
3	Bus 1	Bus 5	400	41.26	1.36	12.91	152.05	9.60	37.55	92.73
4	Bus 5	Bus 4	400	244.00	7.69	80.14	878.71	70.11	245.49	59.05
5	Bus 5	Bus 7	400	35.1	1.03	10.84	131.76	10.53	34.68	80.34
6	Bus 4	Bus 6	400	35.1	1.03	10.84	131.76	10.53	34.68	80.34
7	Bus 13	Bus 1	400	20	0.59	6.17	75.07	6	19.76	45.78
8	Bus 1	Bus 4	400	244.00	7.69	80.14	878.71	70.11	245.49	59.05

Table 14. Electrical data of the transformers.

Transformer	Vector group	Ur1(kV)	Ur2(kV)	Sn (MVA)	Z(%)	Loss (kW)
TR1H	Ynd11	400	14.5	225	12.49	759
TR2H	Ynd11	400	33	225	10	145,2
TR3H	Ynd11	400	33	225	10	145.2

Table 15 shows the electrical parameters of the external grid equivalent connected to bus 3 through line 13-1. Two scenarios are considered within the study depending on the strength fo the equivalent grid by using the two sets of parameters shown in the table.

Table 15. Electrical parameters of the infinite bus.

	R(Ω)	X(Ω)	R0(Ω)	X0(Ω)
Strong Network	1.45	6.47	0.55	6.85
Weak Network	7.211	33.02	3.765	34.97

The parameters used for the three synchronous generator used in parallel with the renewable generators are summarized in the table below.

Table 16. Parameters of the syncrhonous generators.

Generator	G1	G2	G3
Sn(MVA)	170	170	170
U(kV)	13.8	14.5	13.8
Inertia constant (H) (MWs/MVA)	7.6	7.6	7.6
Mechanical damping (D)	1	1	1
Xa	0.76	0.76	0.76
Ra (pu)	0.0125	0.0125	0.0125
Xd (pu)	2.06	2.06	2.06
Xq (pu)	1.85	1.85	1.85
Xd’ (pu)	0.19	0.19	0.19
Xq’(pu)	0.1901	0.1901	0.1901
Xd’’ (pu)	0.14	0.14	0.14
Xq’’(pu)	0.14	0.14	0.14
Tdo’	5.46	5.46	5.46
Tdo’’	0.018	0.018	0.018
Tqo’	0.64	0.64	0.64
Tqo’’	0.027	0.027	0.027
Frequency (hz)	50	50	50
Transformer Δ-Y LL voltage Primary/secondary (kV)	33/13.8		33/13.8

Appendix 2 Full Converter model test results

Once the Type-4 wind turbine model is developed, a set of tests have been performed with the aim of verifying the performance of the model simulation under a set of defined fault conditions.

All synchronous generators and PV models are disconnected during these tests, so only the Wind Turbine-Full Converter is connected in the benchmark model. The goal of these tests is to check the correct behaviour and the stability of the wind turbine-full converter model during the fault. The following situations have been simulated:

- Different generation levels of the type-4 wind turbine: 40 and 200 MW. These generation levels correspond to different scenarios of renewable energy penetration.
- Different types of faults applied: SLG, LL, LLG and LLLG. Such faults are applied in the middle of the line that evacuates the power from the Type-4 WT to the grid (line 5-7). The fault resistance used is zero (solid fault).
- The duration of all the faults is 500 ms.
- Different kind of current injection from the grid-side converters:
    - Negative sequence current equal to zero: Symmetrical current injection even with asymmetrical faults.
    - Negative sequence current proportional to negative sequence voltage. In this case, a k factor of 2.0 has been chosen.

Under these conditions, the following electrical variables were obtained in COMTRADE format. The following pages shows the voltage and current at high voltage side (Bus 7), belonging to the total current supplied by the type-4 wind turbine.

Without injection of negative sequence current

a Single line to ground fault

P=40 MW

Voltages and Currents at 400 kV side

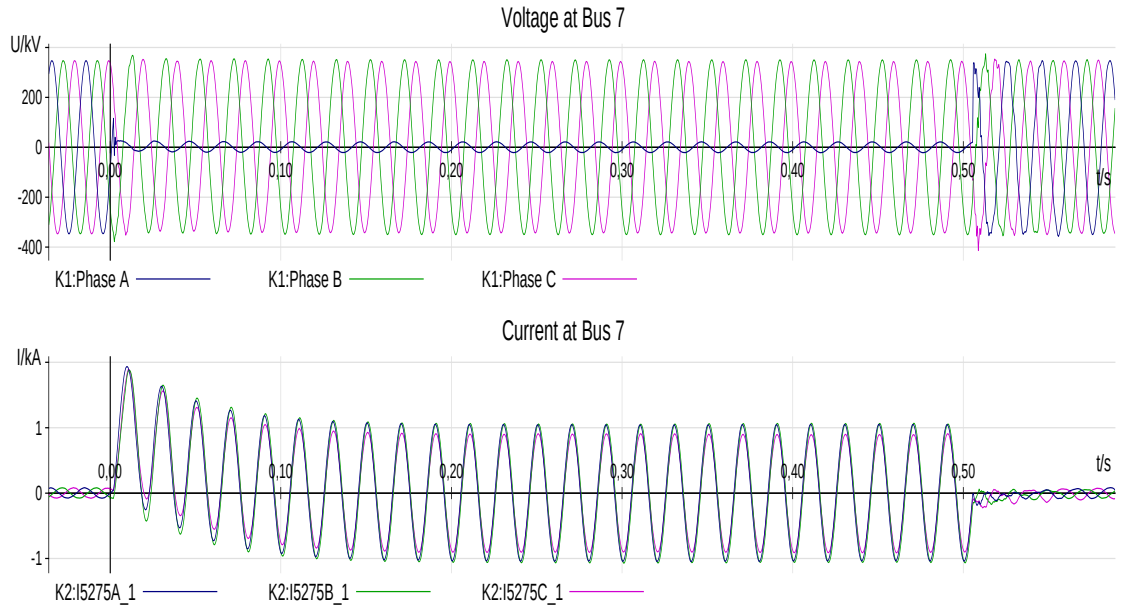

P=200 MW

Current and voltage at 400 kV side

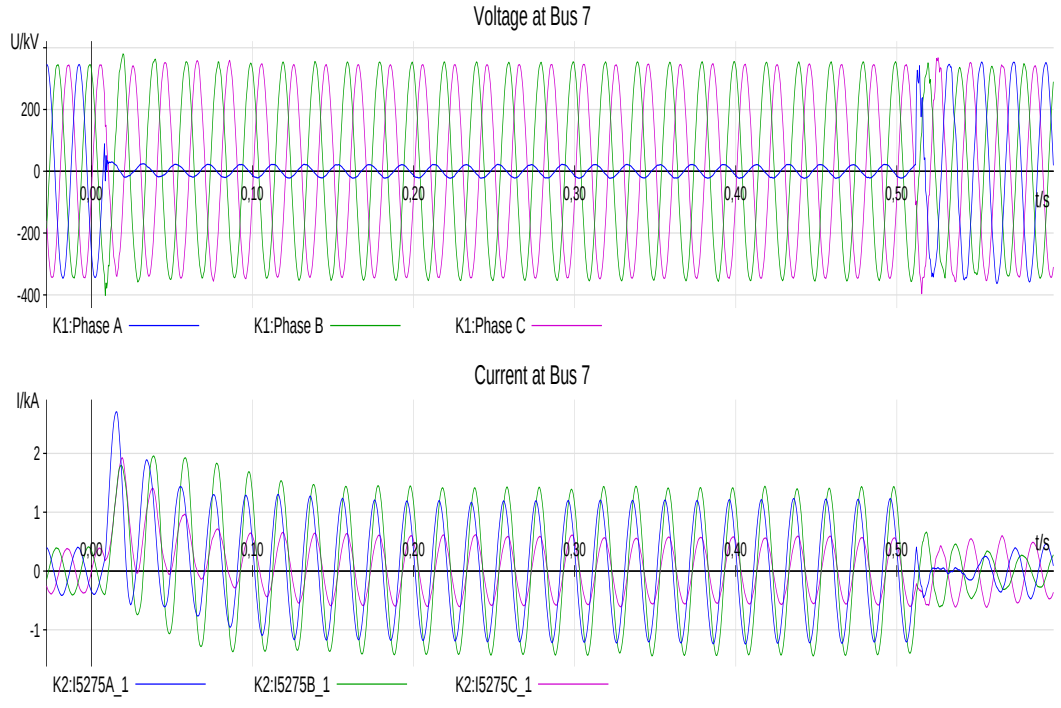

b Phase to phase to ground fault

P=40 MW

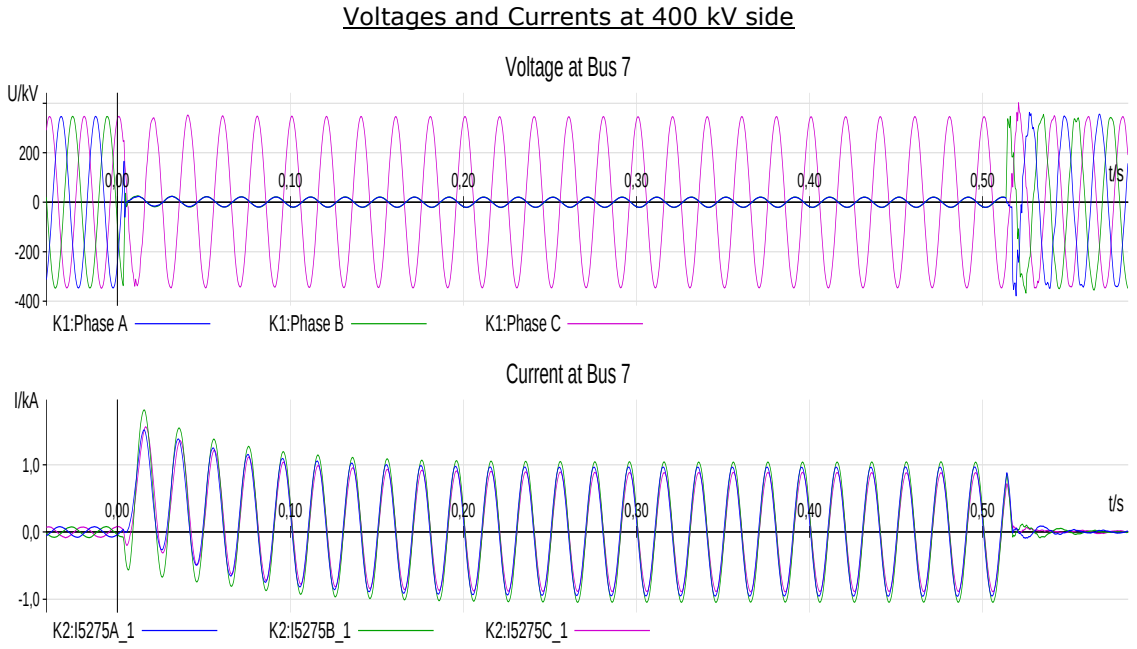

P=200 MW

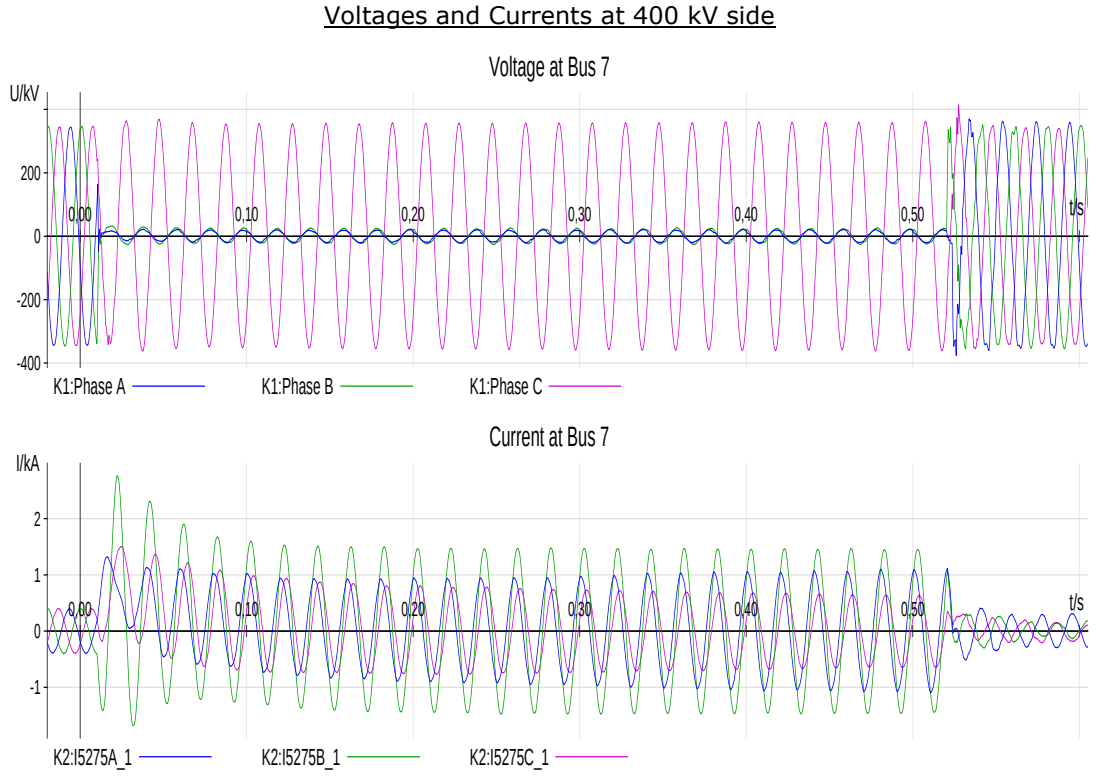

c Phase to phase fault

P=40 MW

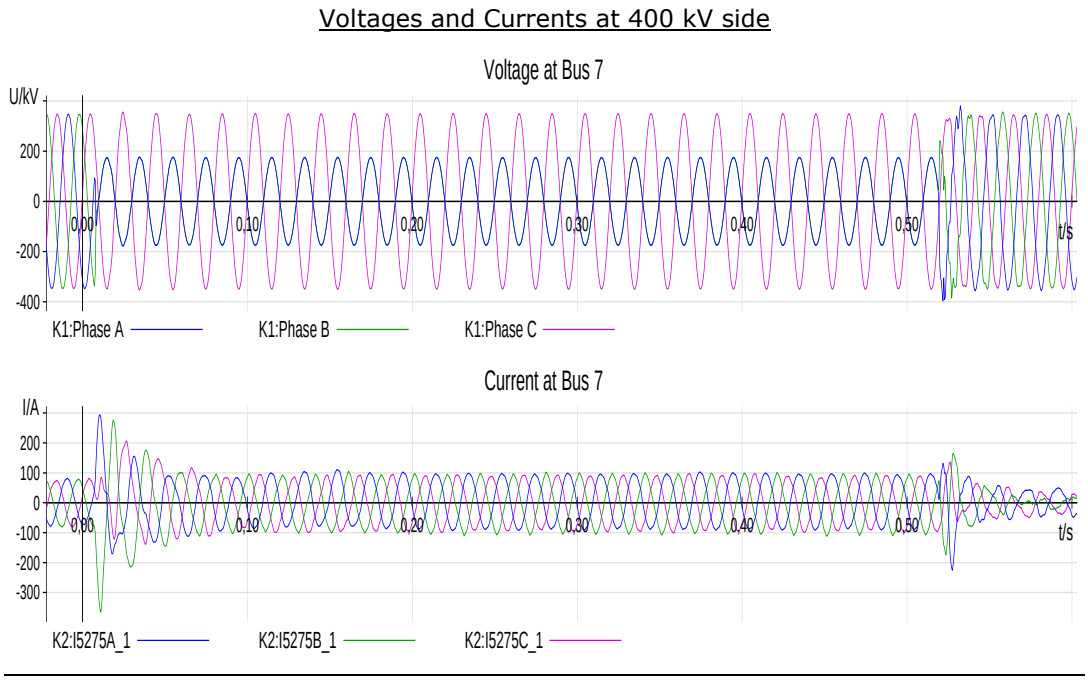

P=200 MW

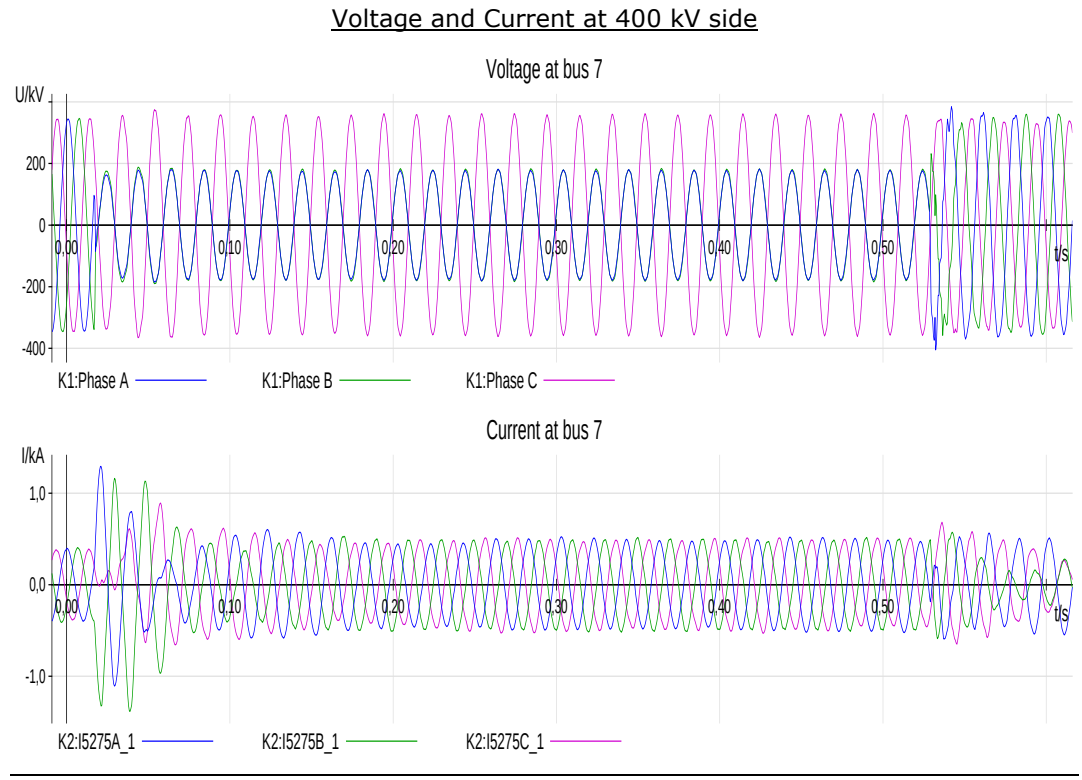

d Three phase fault to ground

P=40 MW

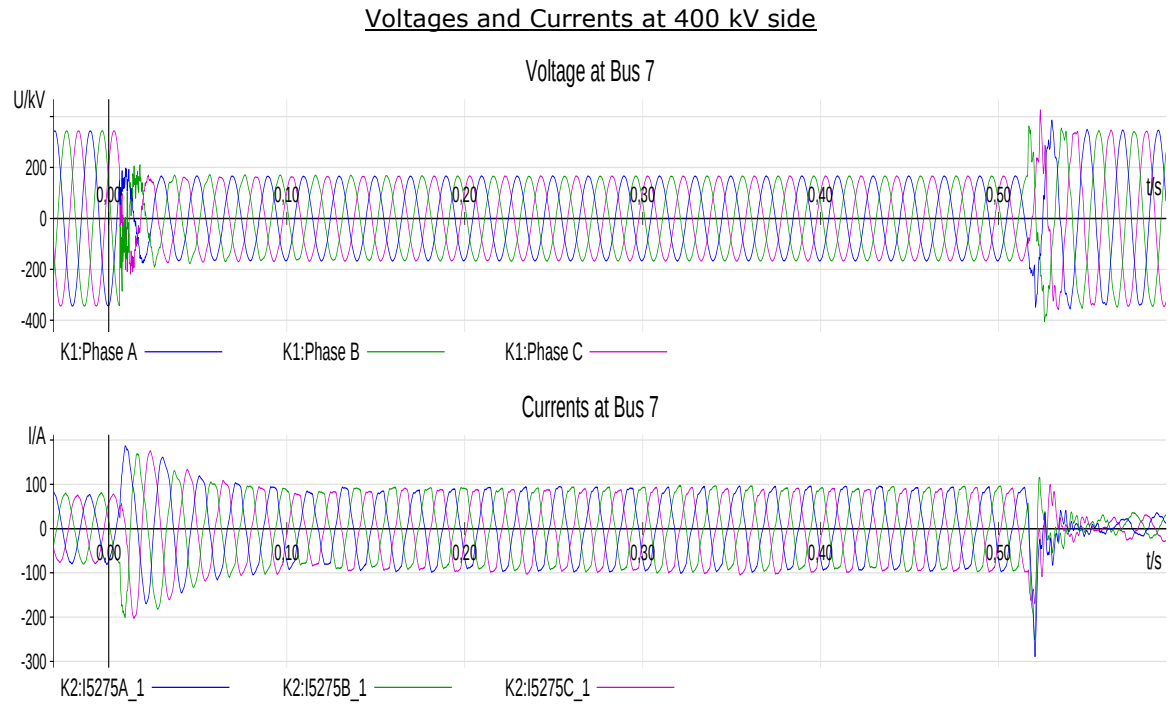

P=200 MW

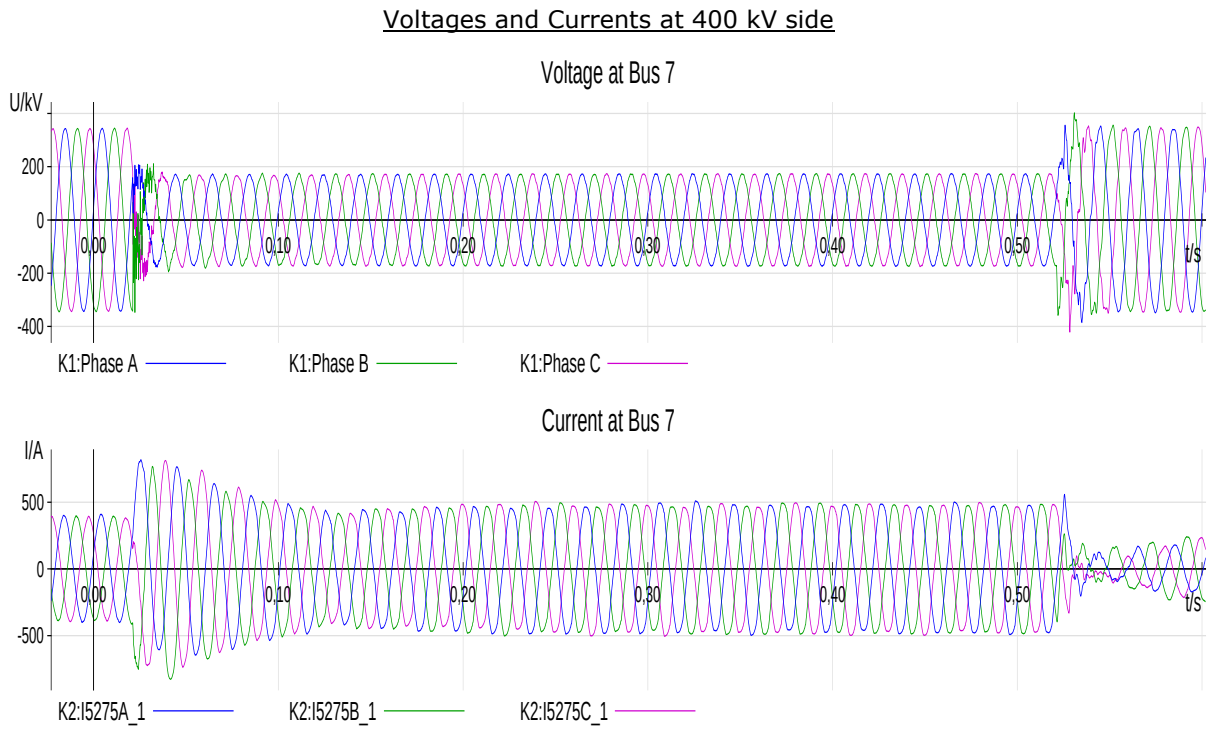

With the injection of negative sequence current

a Single line to ground fault

P=40 MW

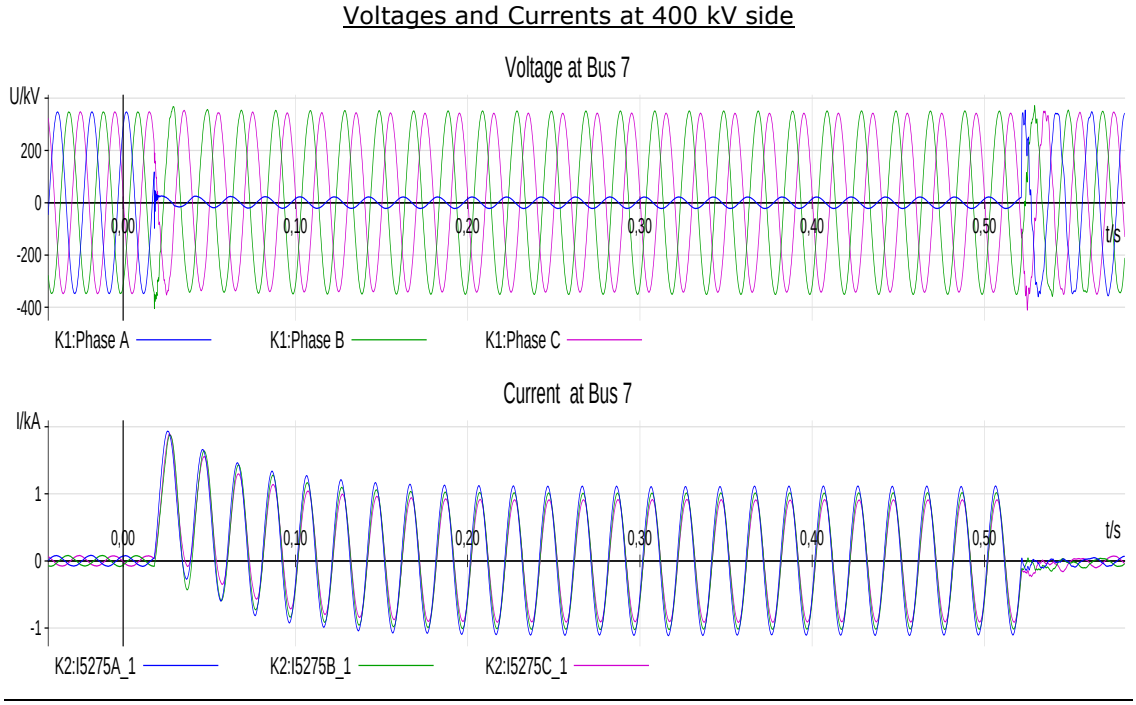

P=200 MW

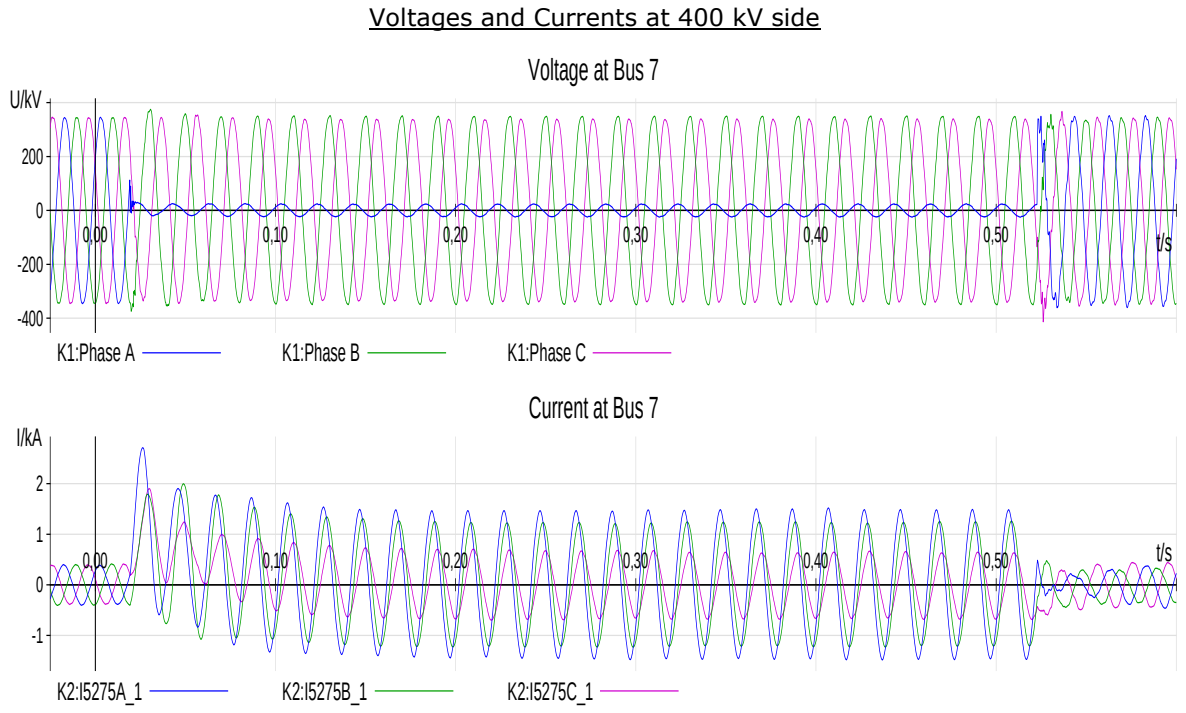

b Phase to phase fault

P=40 MW

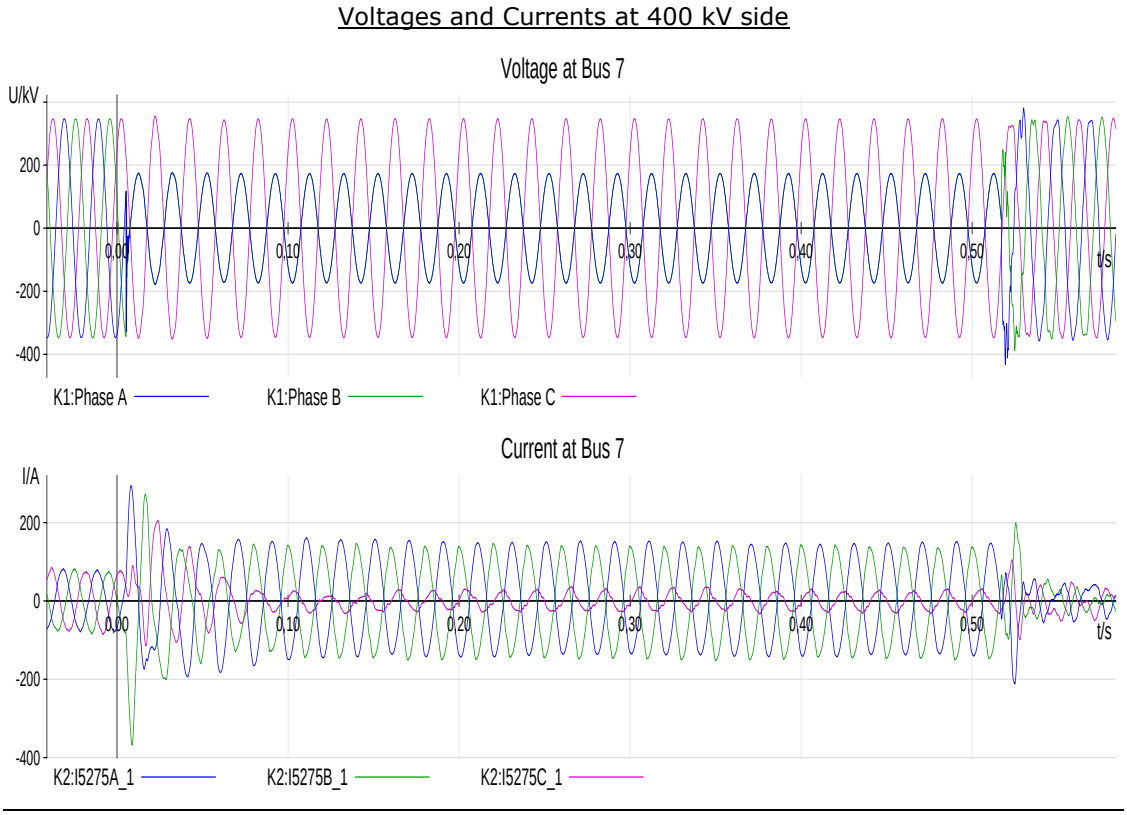

P=200 MW

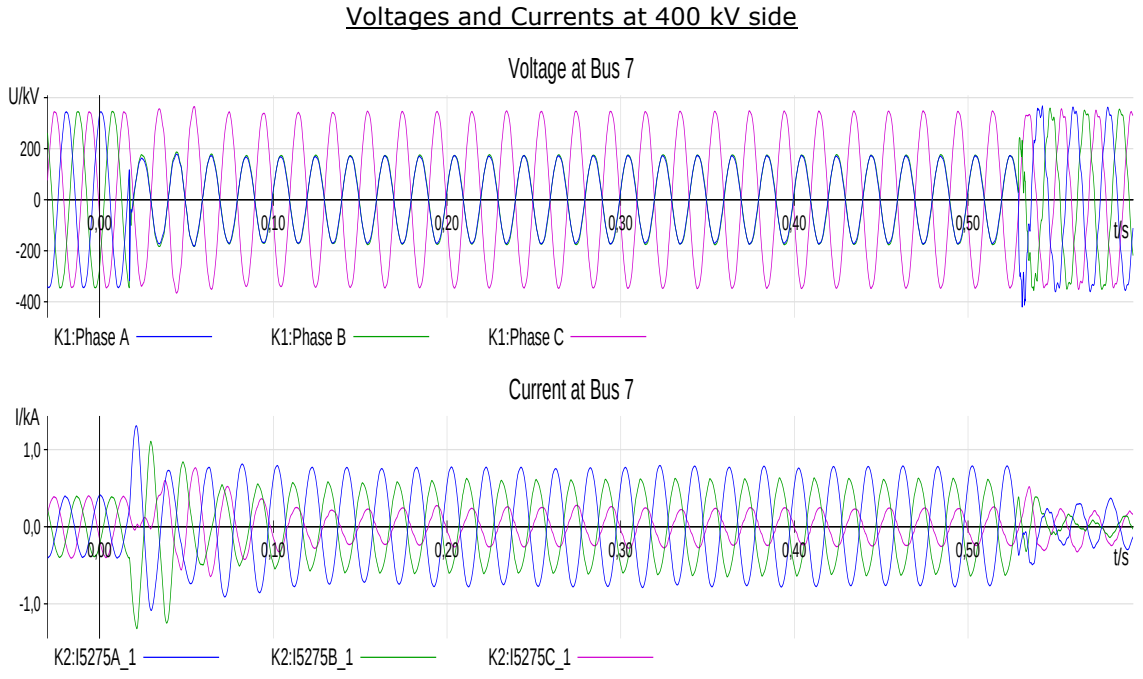

c Phase to phase to ground fault

P=40 MW

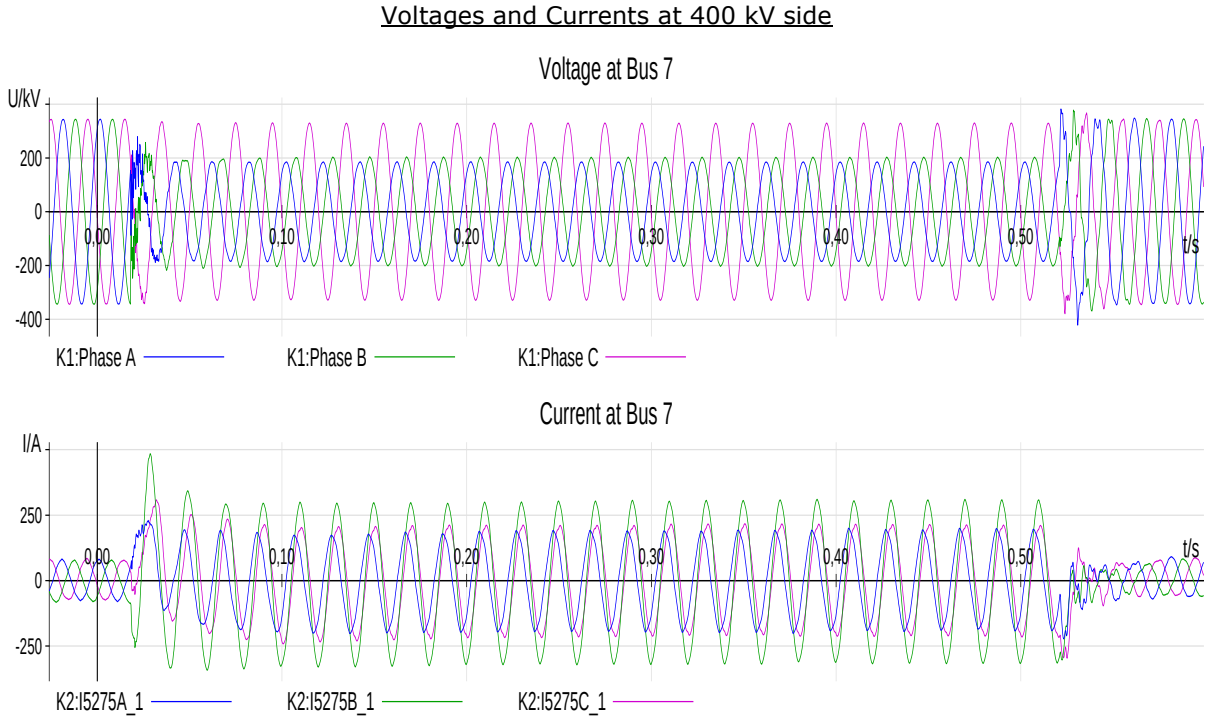

P=200 MW

Appendix 3 PV model test results

Once the PV model is developed, a set of tests have been performed with the aim of verifying the performance of the model simulation under a set of defined fault conditions.

All synchronous generators and the Type-4 WT models are disconnected during these tests, so only the PV model is connected in the benchmark model. The goal of these tests is to check the correct behaviour and the stability of the model during the fault. The following situations have been simulated:

- Different generation levels of the PV System are considered: 40, 200 MW. These generation levels correspond to different scenarios of PV System.
- Different types of faults applied: single-phase to ground, phase to phase, phase to phase to ground and three phase to ground. Such faults are applied in the middle of the line that evacuates the power from the PV system to the grid (line 4-5). The fault resistance used is zero (solid fault) with the goal of obtaining the maximum voltage dip.
- The duration of all the faults is 500 ms.
- Different kind of current injection from the grid-side converters:
    - Negative sequence current equal to zero: Symmetrical current injection even with asymmetrical faults.
    - Negative sequence current proportional to negative sequence voltage. In this case, a k factor of 2.0 has been chosen.

Under these conditions, the following electrical variables were obtained in COMTRADE format. The following pages shows the voltage and current at high voltage side (Bus 5), belonging to the total current supplied by the PV generator.

Without injection of negative sequence current

a Single line to ground fault

P=40 MW

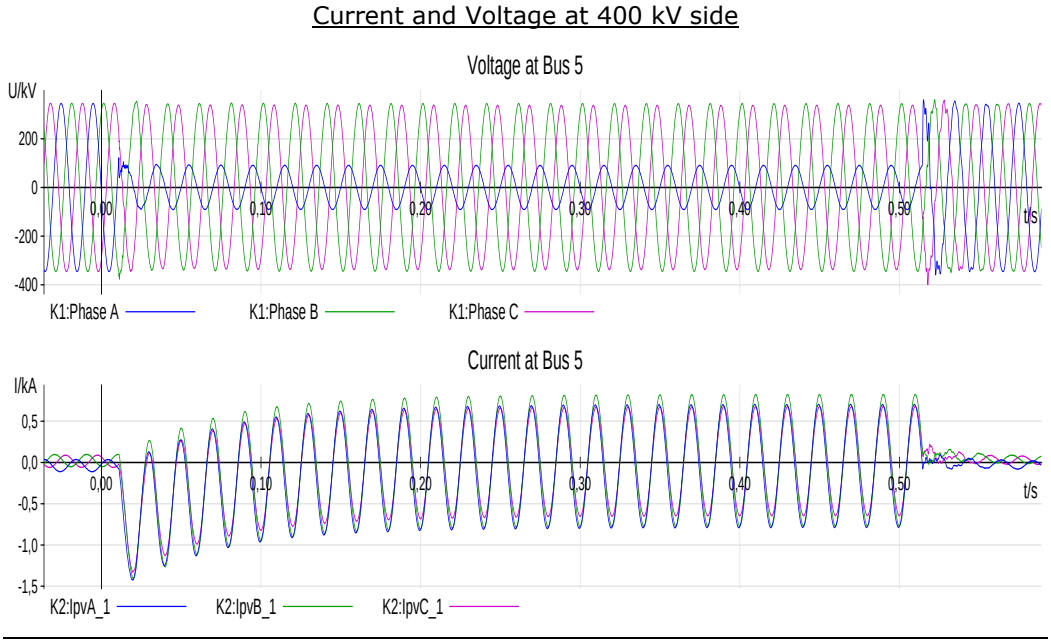

P=200 MW

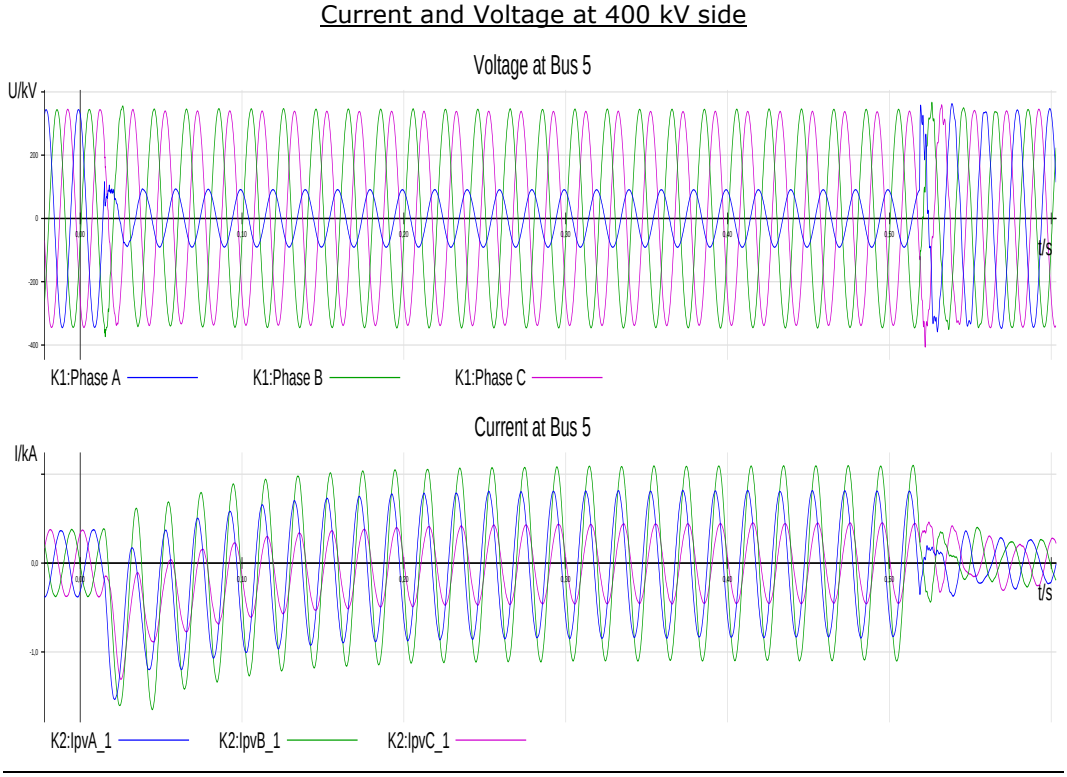

b Phase to phase fault

P=40 MW

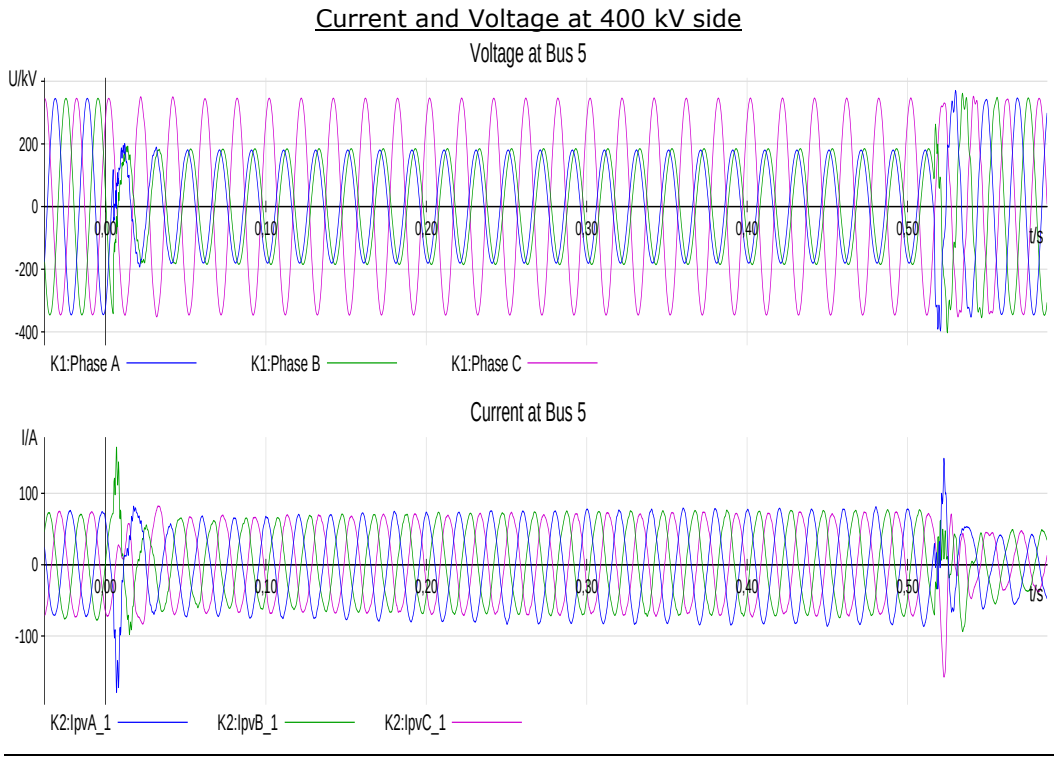

P=200 MW

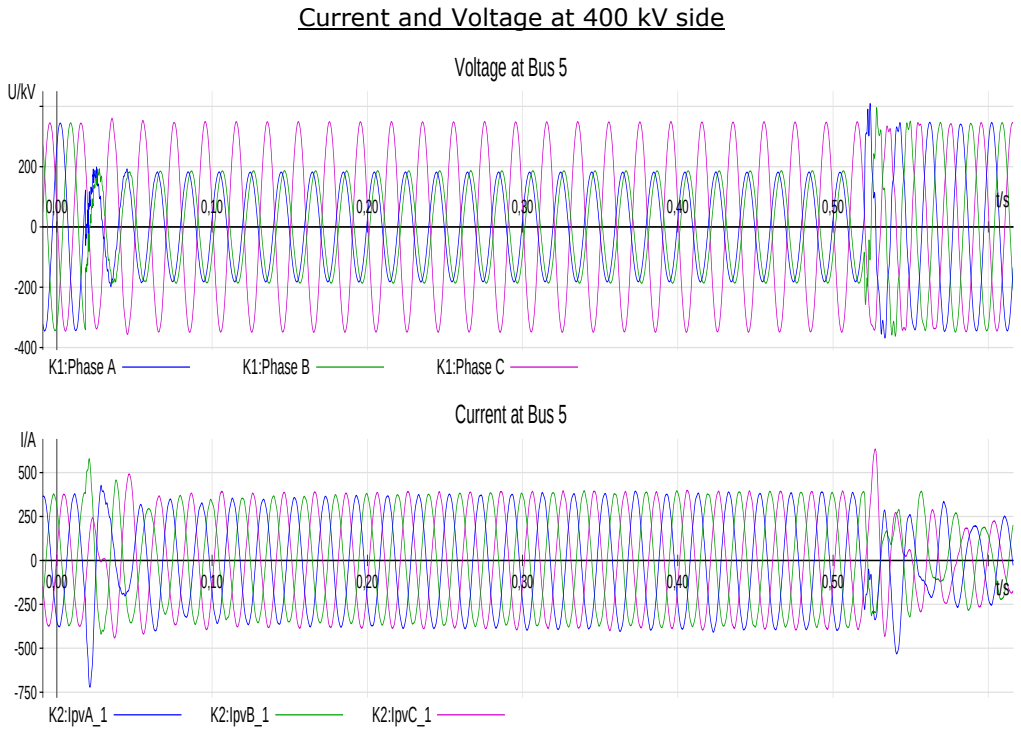

c Phase to phase to ground fault

P=40 MW

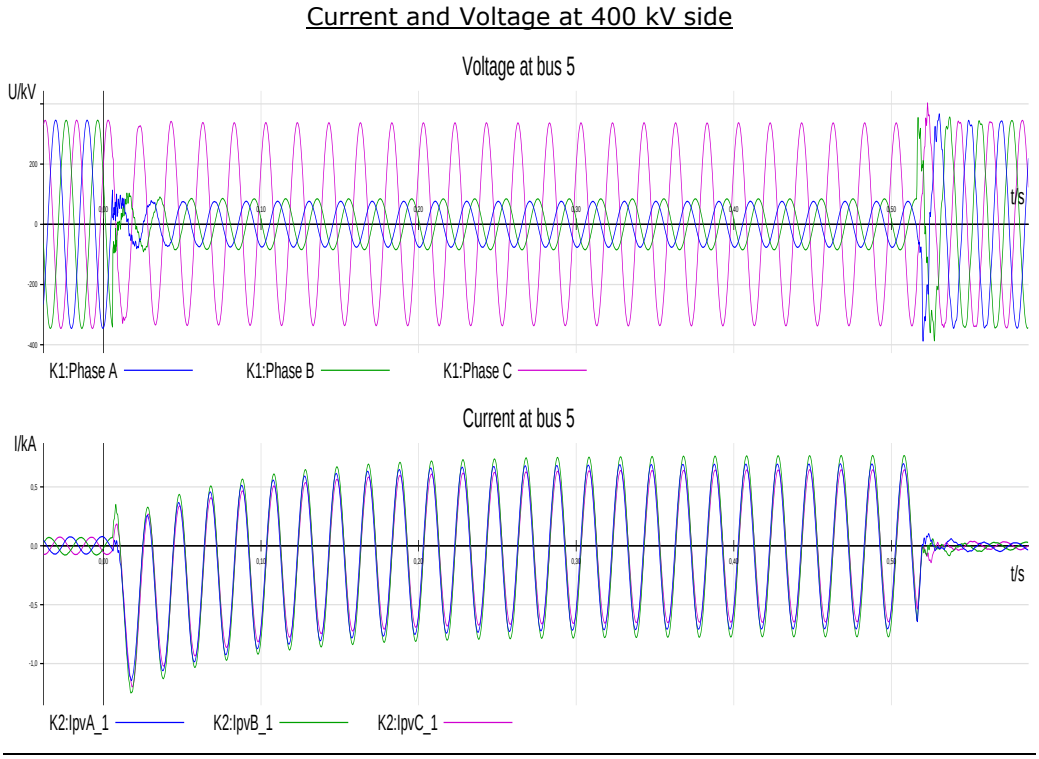

P=200 MW

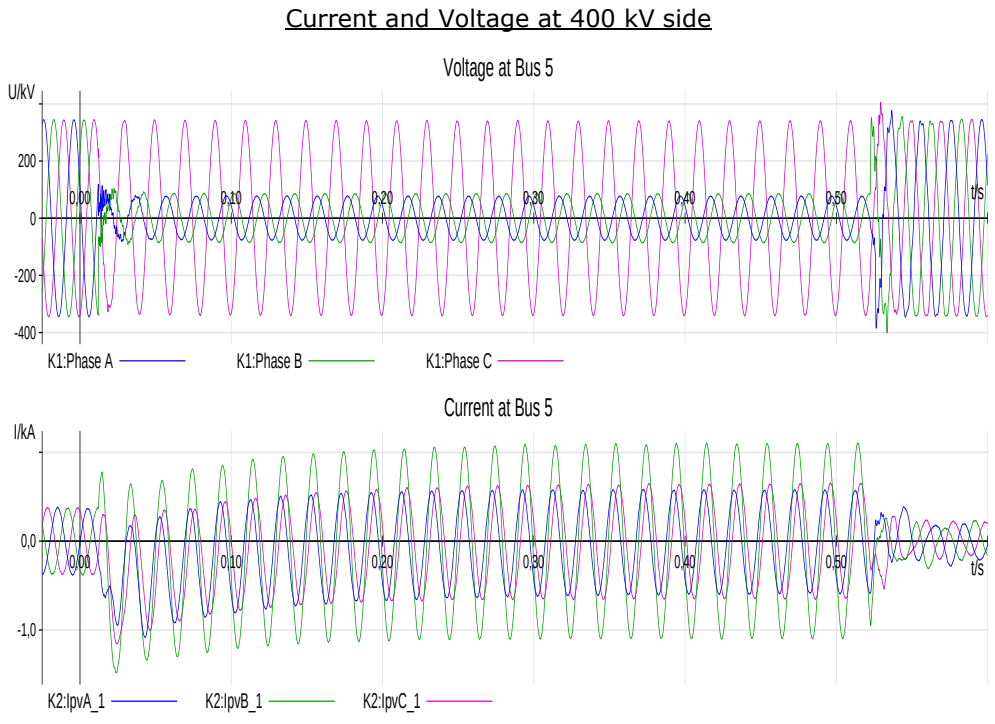

d Three phase fault to ground

P=40 MW

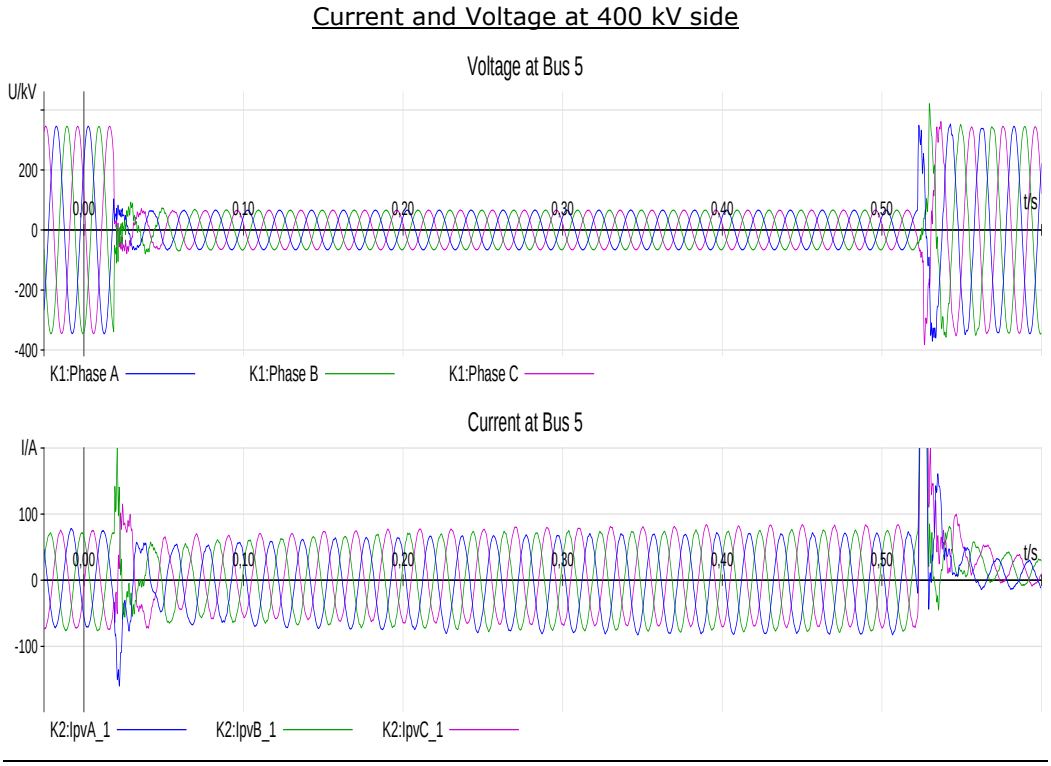

P=200 MW

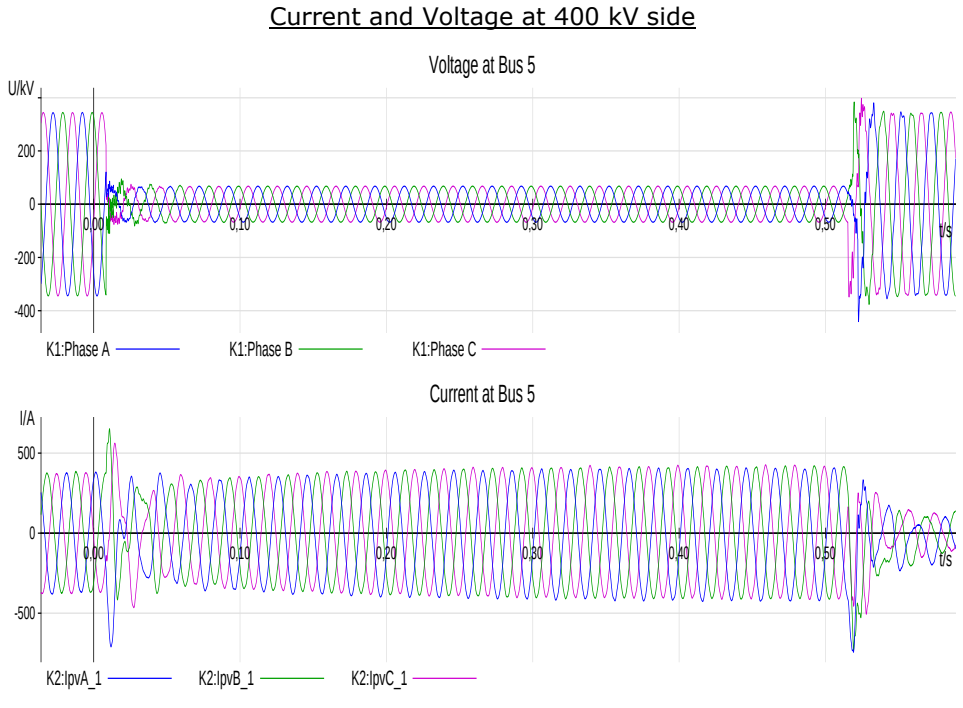

With the injection of negative sequence current

a Single line to ground fault

P=40 MW

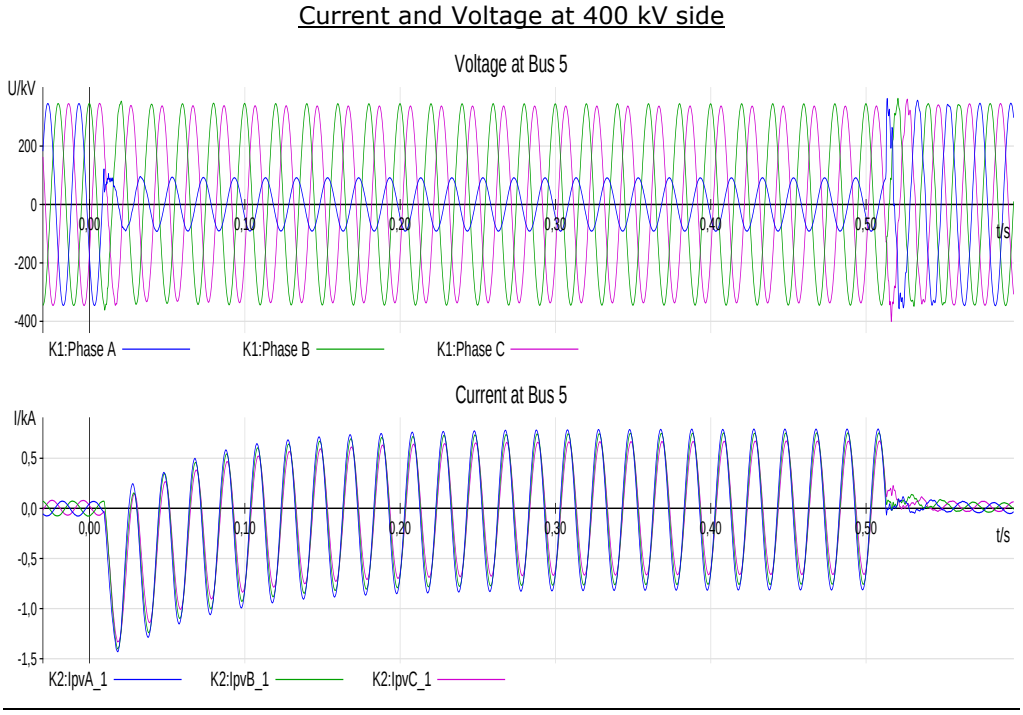

P=200 MW

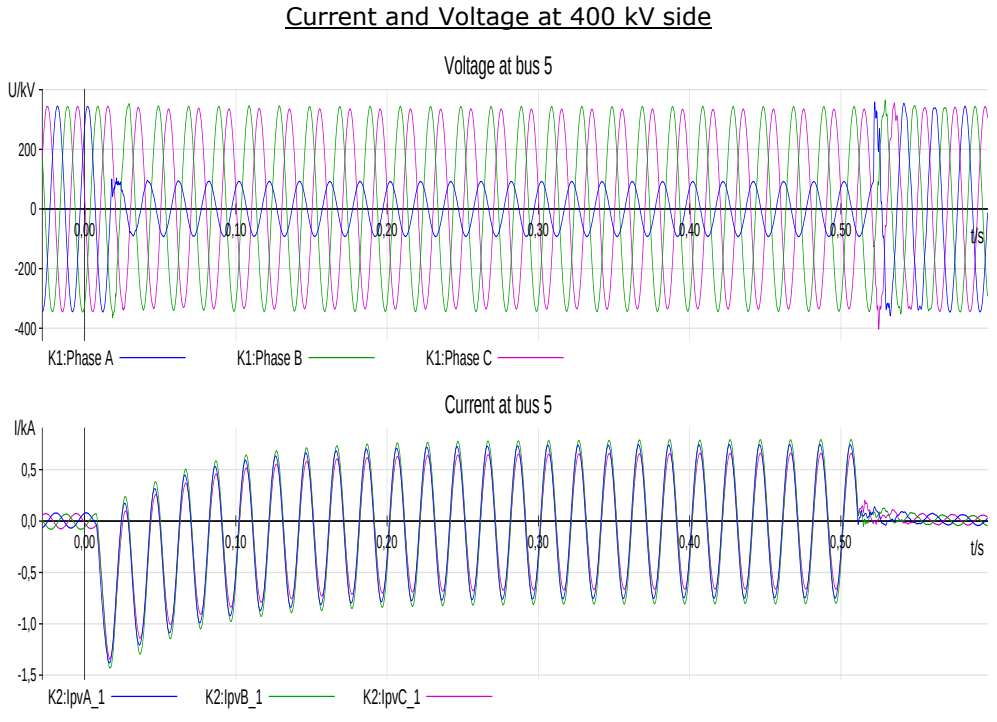

b Phase to phase fault

P=40 MW

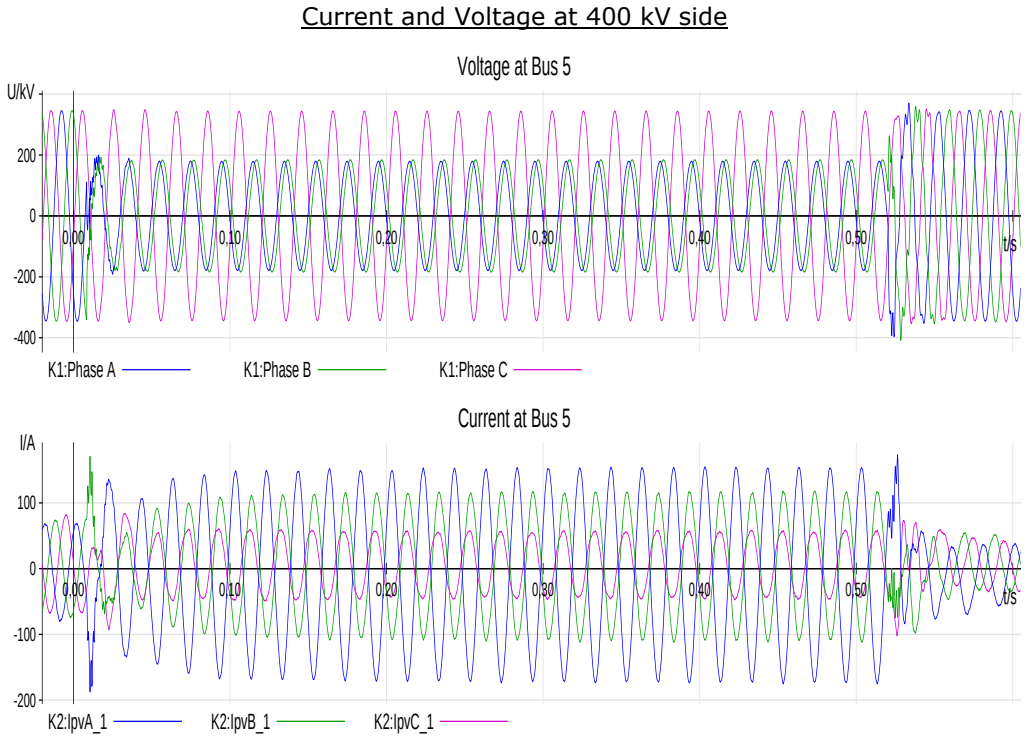

P=200 MW

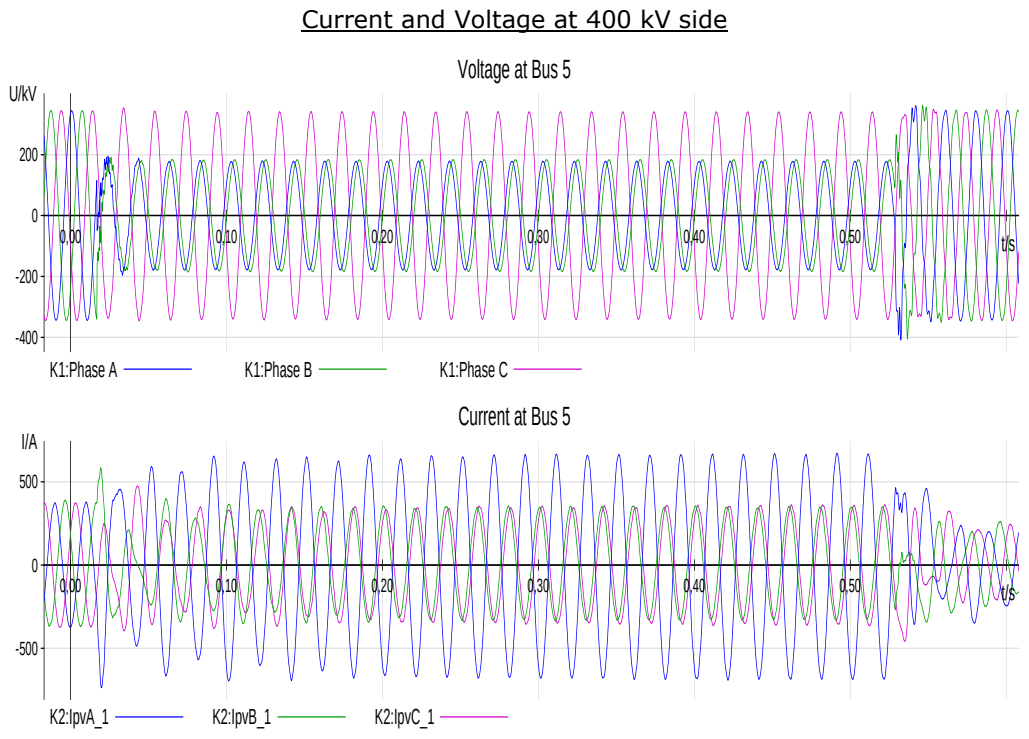

c Phase to phase to ground fault

P=40 MW

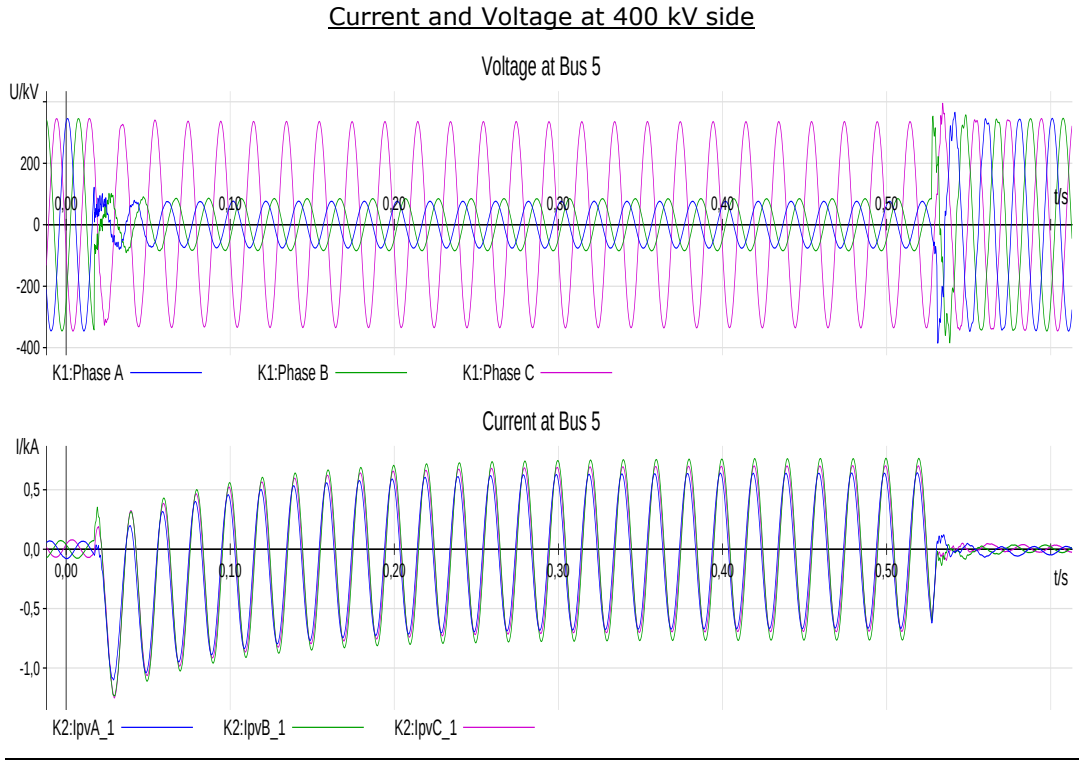

P=200 MW

Appendix 4 Protection relay test protocol

In this appendix, the protocol for assessing the performance of protection relays under high penetration levels of renewable energies and power electronic devices is defined. In the following pages, considerations for the testing process are described. This protocol aims at procuring the most efficient way to provide high quality results with an efficient use of the time.

Test environment definition

The behaviour of two protection relays from two different manufacturers has been assessed during under different penetration levels of renewable energy. The operation of these relays has been evaluated in different locations of the benchmark network described in section 1.1 and shown in the next figure.

Bus 13 is the grid equivalent that represents the slack bus for the simulation. As a reference for all the converters, it remains always connected during tests. This grid equivalent provides the voltage reference for the renewable generator models (Type-4 wind turbine and PV generator) and consumes the excess of power provided by each renewable generator and not consumed by the loads.

As shown in Figure 80, the lines chosen to evaluate the behaviour of protection relays are:

- **Line 5-7** to test the behaviour of protection functions before the Type-4 WT current. The model used includes all the lines connected, as shown in Figure 80. "Grid Side" bus is bus 5 while "Renewable Side" is bus 7.
- **Line 4-5** to test the behaviour of protection functions before the PV generator current. For the studies related to this line, line 1-5 is disconnected. Because of this disconnection, the whole (and only) current contribution seen by protection located at bus 5 during faults is provided from line 5-7. "Grid Side" bus is bus 4 while "Renewable Side" is bus 5.

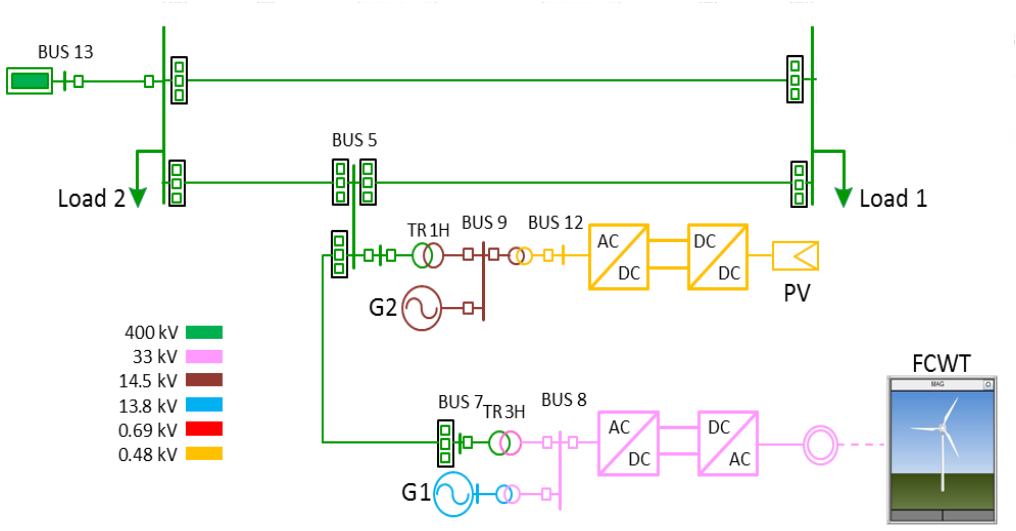

Figure 80. Benchmark model.

To evaluate relay operation, analog and digital signals must be exchanged between the benchmark model built in RSCAD and the relays in a Hardware in the Loop environment. In the following sections, the considerations needed to perform the study are included.

a Relays under test

In this thesis, the behaviour of two manufacturers is assessed: Henceforth Manufacturer A and Manufacturer B.

b Protection functions

The protection functions to be tested are:

- Distance protection (ANSI code 21)
- Differential protection (ANSI code 87L)
- Ground directional overcurrent (ANSI code 67N)

c List of exchanged signals

Two protection relays and RTDS. Table *17* shows the connection between RTDS signals and the protection relays.

Table 17. Signal exchange between RTDS and protection relays.

	Wiring in RTDS/Signal amplifiers	Protection Relays A and B
ANALOG INPUTS FOR PROTECTIONS	GTAO 7-GTAO 10 (SIDE S-SIDE R) to current amplifier	Current Phase A
	GTAO 8-GTAO 11 (SIDE S-SIDE R) to current amplifier	Current Phase B
	GTAO 9-GTAO 12 (SIDE S-SIDE R) to current amplifier	Current Phase C
	REFERENCE OF CURRENT AMPLIFIER SOURCE	Current Phase Star bridge
	GTAO 1-GTAO 4 (SIDE S-SIDE R) to voltage amplifier	Voltage Phase A
	GTAO 2-GTAO 5 (SIDE S-SIDE R) to voltage amplifier	Voltage Phase B
	GTAO 3-GTAO 6 (SIDE S-SIDE R) to voltage amplifier	Voltage Phase C
	REFERENCE OF VOLTAGE AMPLIFIER SOURCE	Voltage Phase Star bridge
DIGITAL INPUTS FOR PROTECTIONS	GTFPI HV PANEL 1-6 (SIDE S-SIDE R)	CB Closed Phase A
	GTFPI HV PANEL 2-7 (SIDE S-SIDE R)	CB Closed Phase B
	GTFPI HV PANEL 3-8 (SIDE S-SIDE R)	CB Closed Phase C
DIGITAL OUTPUTS FOR PROTECTIONS	DIGITAL INPUT 1-5/9-13 (SIDE S prot A(C)-SIDE S prot B(D) / SIDE R prot A(C)-SIDE R prot B(D))	Trip CB Phase A
	DIGITAL INPUT 2-6-10-14(SIDE S prot A(C)-SIDE S prot B(D) / SIDE R prot A(C)-SIDE R prot B(D))	Trip CB Phase B
	DIGITAL INPUT 3-7-11-15(SIDE S prot A(C)-SIDE S prot B(D) / SIDE R prot A(C)-SIDE R prot B(D))	Trip CB Phase C
	DIGITAL INPUT 4-8-12-16(SIDE S prot A(C)-SIDE S prot B(D) / SIDE R prot A(C)-SIDE R prot B(D))	Close CB

d Analog signals

GTAO cards supply the analog output signals (voltages and currents) generated by RTDS to the protection relays. Each GTAO card provides 12 analog outputs at the level of ±10 volts that must be amplified by the equipment called DOBLE F6350 to elevate such signals to the equivalent secondary voltage and current transformers.

These voltage and current signals are supplied to two protection relays simultaneously to optimize the time dedicated for testing and to ensure that the protection relays see the same fault values.

Amplifiers allow current injection of up to 60 and 70 RMS secondary amperes (24 and 28 primary kA). This injection level is enough to reproduce the fault current applied during the faults both on the grid and on the generator sides.

This parallel testing procedure does not increase the number of analog outputs needed. Parallel connections for voltage and series connections for current are made for the different protection relays.

e Digital signals

Besides the analog signals, additional information is exchanged between RTDS and protection devices. Digital inputs and outputs signals are needed for single-pole trip and breaker status signals.

The GTFPI (Front Panel Interface) Card is used for this goal. This card manages the digital inputs (16) and outputs (16) in the front panel of the RTDS simulator. For the digital inputs to RTDS (outputs for the protection relay), the front panel can detect when the dry-type contacts of the protection, which are in charge of sending trip orders, are activated or deactivated. For the digital outputs of RTDS (inputs for the protection), through the GTFPI, it is possible to send digital signals with voltages in the range of 0-250 Vdc, using an external voltage source. Therefore, RTDS is able to supply usual 125 V digital signals for protection inputs by using an external 125 V DC source.

Figure 81 shows the front panel interface. Digital inputs signals are in the upper side and the high voltage digital output signals are placed in the lower side.

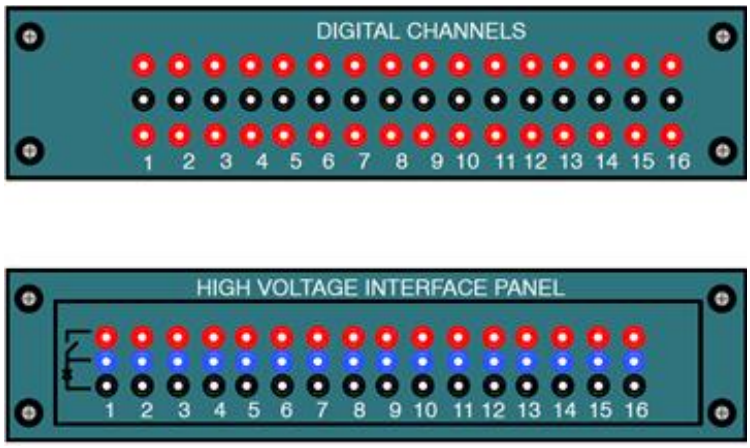

Figure 81. Low voltage (upper side) and High Voltage (lower side) Front Panel Interface (GTFPI)

Digital signal exchanged between RTDS and signal are:

1. Digital outputs from RTDS (Digital inputs to the protection device):
    - Breaker status pole A (signal of closed breaker)
    - Breaker status pole B (signal of closed breaker)
    - Breaker status pole C (signal of closed breaker)
2. Digital inputs to RTDS (Digital outputs from the protection device):
    - Single Pole Trip Phase A
    - Single Pole Trip Phase B
    - Single Pole Trip Phase C

In the case of testing differential protection or distance protection, for detecting the response of two manufacturers at the same time, RTDS needs to distinguish between the signals coming from each equipment. Therefore, since two manufacturers are tested in parallel, two equipment send digital signals to RTDS, so 8 digital inputs (4 signals from 2 equipment) are needed in RTDS.

Digital outputs from RTDS can be shared with the different protection relays under test. Therefore, three digital signals would be sufficient to define the state of each breaker. Therefore, six digital outputs define the state of two circuit breakers for every protection function under test.

Figure 82 shows the general diagram of the hardware in the loop test-bench that is used during the tests. The analog and digital signals are remarked in the diagram shown in Figure 82.

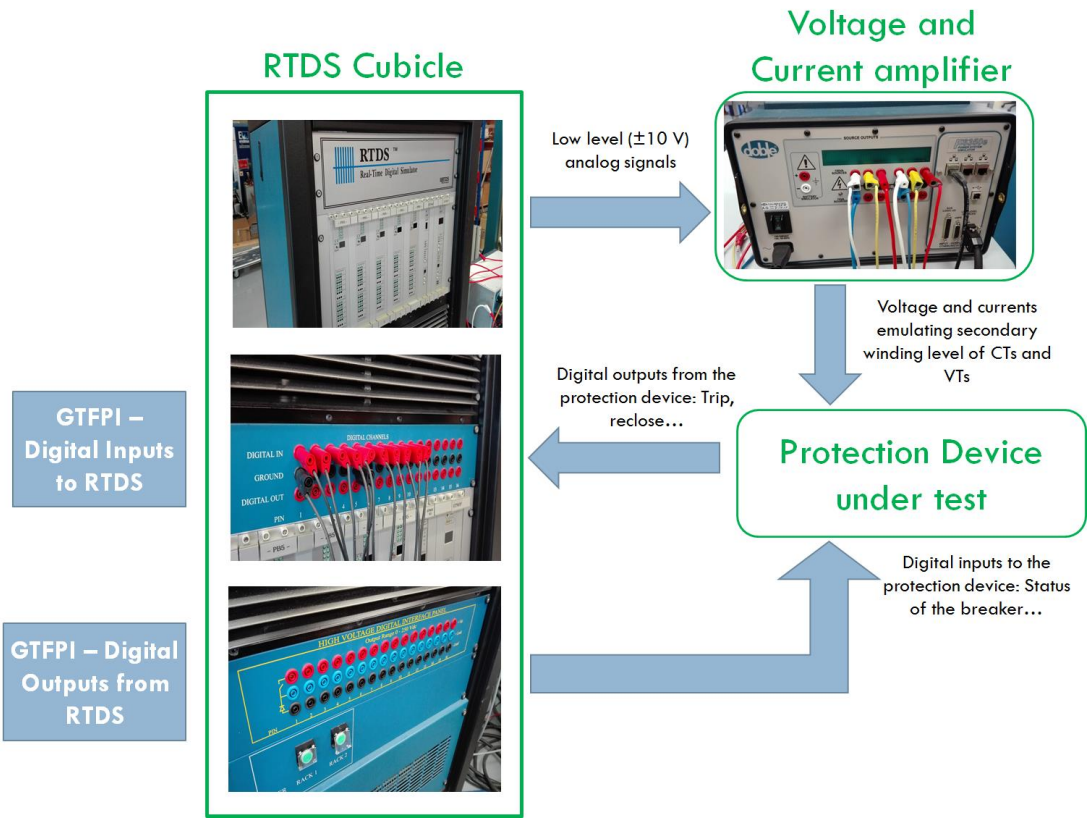

Figure 82. Hardware in the loop testing. Laboratory test-bench and signals exchanged.

f Waveforms and signals to save from protection relays and RTDS

Both protection relays and RTDS can store their oscillography results in COMTRADE files. These COMTRADE files contain relevant information which allows the analysis of the behaviour of protection relays under the different test conditions (defined in section Cases of study of the Appendix 4). This section describes the signals needed to analyze each study case.

- Signals collected at the protection relay:
    - Analog signals: Three voltages and three currents received at protection terminals, differential current internal calculation, impedance measurement from the relay (when possible).
    - Digital signals: Protection function start (21, 87, 67N), protective zone activated for distance protection, faulted phase detection, the breaker status, single pole tripping signal, directionality declaration, ground directional overcurrent thresholds, among many others that depend on each manufacturer.
- Signals collected at RTDS:
    - Analog signals: Voltages measured at 400 kV level for buses 1, 2, 3, 4, 5, 6, 7 and 13. Voltage and currents in MV level for buses 8, 9 and 10. Currents measured at lines: 1-2, 3-4, 4-6, 4-5, 5-7, 1-5, 1-4 and from the slack bus. Tripping time.
    - Digital signals: Tripping digital signals received from protection relays.
- Duration of the oscillography: The fault duration is set to 2.0 seconds to study possible problems with protection relays. Based on this fault duration, the length of the oscillography in RTDS is set to 2.5 seconds.

- Time between fault inception and the protection trip (tripping time) is registered. According to these values, it is possible to identify and classify the behaviour of the protection function under the different test conditions.
- For the initial mass tests, the oscillography generated by the protection is not initially downloaded. As explained in the following subsections, the idea is to perform the massive test process defined with RTDS and identify and register the problematic cases. Once these problematic cases are identified, the most interesting ones are repeated and the oscillography of the relays is downloaded and analyzed in detail from the beginning of the fault to study the cause of the abnormal behaviour of protection relays.

Cases of study

a Number of cases to be analyzed

The conditions fixed for the tests are listed below:

- The negative sequence current injected by PV and Type-4 Wind Turbine equals zero. This condition is considered the most restrictive from the point of view of protection relay performance. The injection of negative sequence current is considered in additional tests depending on the results obtained to analyze if its presence improves the performance of protection relays.
- Protection functions to be analyzed:
    - Distance protection
    - Differential protection
    - Ground directional overcurrent
- Lines where the protection relays are installed:
    - Line 5-7
    - Line 4-5
- Scenarios defined (scenarios shown graphically in section Grid configuration for testing of the Appendix 4):
    - Strong network with only synchronous generators, only renewable generators (always with the grid equivalent as the slack bus) and an intermediate scenario.
    - Weak network with only synchronous generators, only renewable generators and one intermediate scenario.
- Generation level from renewables: 40 MW and 200 MW.
- Generation level from synchronous: 40 MW and 170 MW.
- Point of the line where the fault is applied that depends on the protection function under test.
    - Distance protection: Tests in line 5-7 at 0 % (forward and backward), 50.0 %, 70.0 %, 90.0 % and 100 % (forward and backward). A repetitiveness of three times per point of the line is applied to check the consistency of the result.
    - Differential protection: Two faults inside the line (65 and 95 %) and one outside.
    - Ground directional overcurrent protection: Since 67N is a backup protection function, the same points used in distance protection are tested to ensure that in the case that

distance protection does not operate as expected, 67N represents a reliable backup protection function.

- Type of fault: Single line to ground, line to line, line to line to ground and three-phase.

Therefore, the total number of combinations is 4896. Table 18 shows the calculation with all the test parameters already defined.

Table 18. Initial estimation of total number of cases.

Priority	COMBINATIONS	DIFFERENTIAL PROTECTION	DISTANCE PROTECTION	GROUND DIRECTIONAL OVERCURRENT PROTECTION	EXPECTED NUMBER OF TESTS
1	Number of lines	2	2	2	
2	Scenarios	6	6	6	
3	Generation Level	2	2	2	
4	Point of the line	3	7	7	
5	Type of fault	4	4	4	
6	Fault Resistance	1	1	1	
7	Repetitiveness	3	3	3	
TOTAL NUMBER OF CASES		864	2016	2016	**4896**

b Conditions of the generation levels and power electronic converters

The cases of study, defined in the previous section a Number of cases to be analyzed, fix the conditions of the renewables and power electronic converters during faults. However, it is interesting to remark these conditions to clarify their contribution to the fault:

- Generation level: Two levels of active power generation during the pre-fault state: 40 MW and 200 MW.
- Current contribution during fault: Control for limiting the negative sequence current in the steady-state of the fault is set. Therefore, full converter topologies provide only positive sequence current. Besides, this current is limited to 1.1 p.u. approximately in PV and Type-4 wind turbine.
- Some additional faults are applied with injection of negative sequence current in combination with positive sequence current.

Logic implemented in RTDS model for trip

In the protection philosophy of transmission lines, an "OR" logic between the trip signals coming from protections working in parallel (primary and backup protection) is used to generate the final trip to the circuit breaker. In the case of tests carried out in this thesis, this "OR" gate is not

considered because if the primary protection does not act, the backup protection would trip the breaker hinding a possible problem.

Therefore, with the aim of not losing information about the behaviour of protection relays connected in parallel, "AND" logic gates have been used to trip the circuit breakers. With these logic gates, the breaker only opens when trip signals coming from both protection relays are received.

Consequently, if one of the protection relays does not send the trip signal, the breaker remains closed and the fault applied. In this way, it is possible to analyze the difference between the tripping times of each protection. The trip scheme described can be observed in Figure 83.

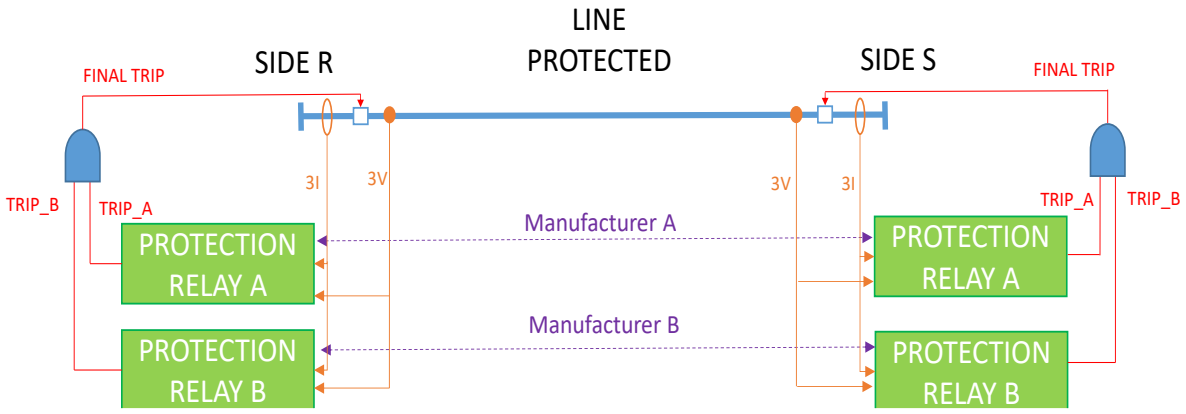

Figure 83. Trip scheme programmed in RTDS.

The logic used in RTDS model for tripping the circuit breaker of each side, according to the explained criteria, is shown in Figure 84.

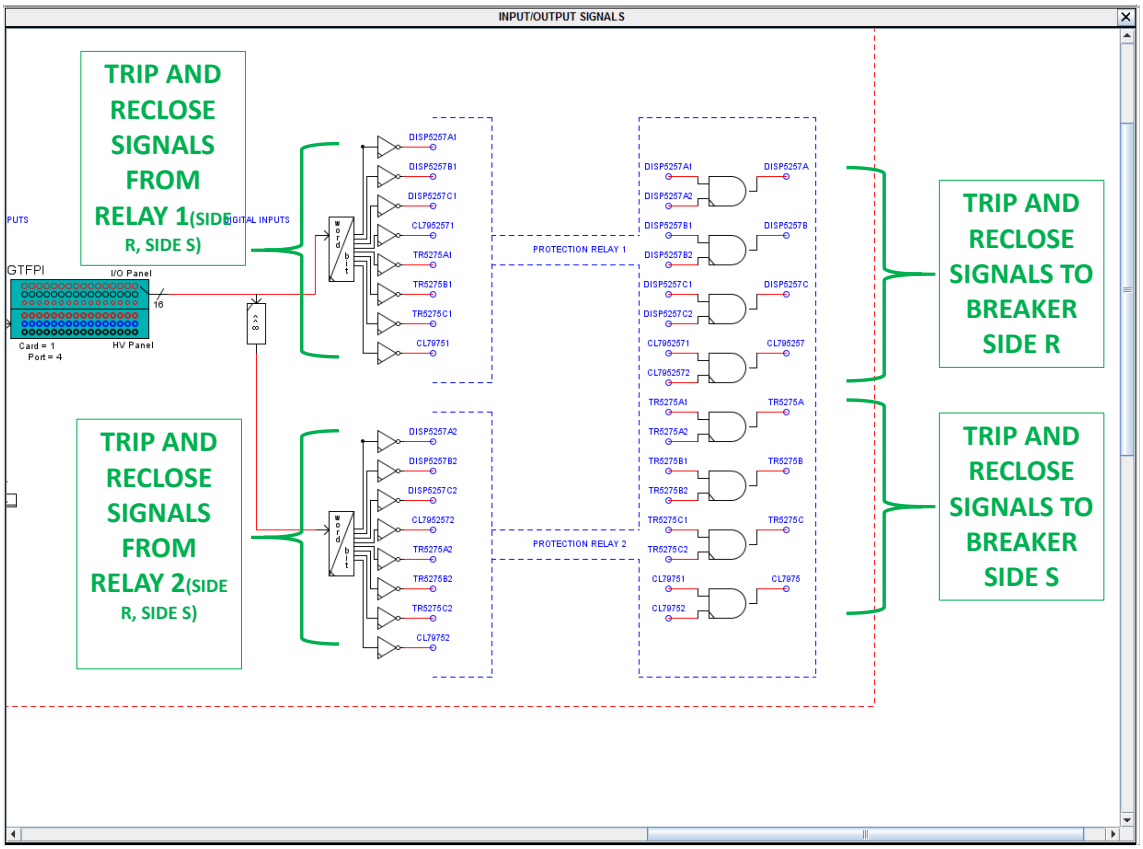

Figure 84. Logic implemented in RTDS for trip signals.

Benchmark model updates

Several changes have been applied to the original model to accommodate the test conditions described and make tests automatic. These changes are listed below:

- Automation of the change of impedance for the network equivalent. This update allows changing between strong and weak networks during the runtime. This parameter is directly operated by scripting. The RL values of the equivalent source that represents the slack bus are considered in parallel connection and shown in Table 19:

Table 19. Parameters of R//L for strong and weak network.

	Rp	Xp (Lp)	Rp0	Xp0 (Lp0)
Strong Network	30.319 Ω	6.795 Ω (0.02163 H)	85.864 Ω	6.894 Ω (0.02194 H)
Weak Network	158.413 Ω	34.595 Ω (0.11012 H)	328.570 Ω	35.375 Ω (0.11260 H)

- Tripping signals coming from the protection relay have been included in the model.
- Timers for recording tripping signals. The tripping times are needed to evaluate the behaviour of the protection. The tripping times are recorded for the two protection relays on each side of the line under test. Consequently, there are four timers to measure the tripping times.
- GTAO and GPFPI blocks for sending analog signals and for sending/receiving digital signals. Table *17* contains the list of signals exchanged between RTDS and protection relays.
- Conversion factors inserted in GTAO for current and voltage signals are applied to DOBLE F6350.
- Enable/Disable the voltage and current signals injection sent by GTAO to the amplifiers.
- Status of the breaker signals (pole by pole) are provided to protection relays.
- Additional breaker in line 1-5, in bus 5 side with the idea of eliminating grid contribution to faults in line 4-5 (as described previously).
- Fault clearing after the breakers have opened in both sides of the faulted line. With this modification, once the circuit breakers at the two sides of the protected line have been tripped, the fault disappears (as in real systems in case of transient faults).
- Two protections of manufacturers A and B are installed in laboratory, connected to RTDS via digital signals and receiving analog signals from Doble F6350 Amplifiers.

Actions for testing protection devices: Scripting

To make the study feasible, as well as replicable, it is necessary to develop ad-hoc tools for automatically applying the vast amount of tests described in Appendix 4. Script code for RTDS has been designed to deal with this number of tests. It is remarkable that along with changing test conditions according to test cases defined, the script performs an automated initial fault analysis to identify relevant situations to be studied in deeper detail, as it is explained in following subsections.

This section describes the steps followed to perform and automate the tests.

1. The tests start with transmission lines 5-7 and 4-5.
2. On each line, distance protection is tested first, then differential and finally ground directional overcurrent.
3. Based on the flow charts shown in the next section, the script automatically perform the different tests changing automatically the parameters to set the cases of study and classify the behaviour of the protection system automatically. Script files provide the following information:
    a. Excel file (one file for each side of the line under test, example in Figure 85), including:
        i. The number of tests to have a unique reference for each one.
        ii. The type of the fault: single-line to ground, line to line, line to line to ground and three-phase.
        iii. The generation scenario: Synchronous or renewable for weak and strong grid defined in the slack bus conditions.
        iv. The point of the line (in %) where the fault is applied.
        v. Trip signal reception from the two protection devices phase A, B and C tested.
        vi. The tripping time associated to the trip signals. Two tripping times in total: one for each protection device at each side of the protection line. The timer starts when the fault is applied and finishes when the trip signal is received.
        vii. Behaviour expected or unexpected based on the action of the protection, the correct pole operation and trip time. The conditions for declaring a unexpected behaviour are summarized in section Flowcharts for scripting and testing in Appendix 4.

Point of the fault	Type of fault	Generation level	Scenario	Trip_A	Trip_B	Trip_C	Close	Behaviour not expected	Delayed trip	Under reach	Over reach	tripping time Prot_A	reclose time Prot_A	tripping time Prot_B	reclose time Prot_B	TripA Prot_A	TripB Prot_A	TripC Prot_A	Reclose Prot_A	TripA Prot_B	TripB Prot_B	TripC Prot_B	Reclose-Prot_B
5.0%	SLG	40MW	SG_SG	1	0	0	1	0	0	0	0	0.025	1.042	0.026	1.022	1	0	0	1	1	0	0	1
5.0%	SLG	200MW	SG_SG	1	0	0	1	0	0	0	0	0.025	1.042	0.026	1.023	1	0	0	1	1	0	0	1
5.0%	SLG	40MW	SG_WG	1	0	0	1	0	0	0	0	0.025	1.036	0.027	1.022	1	0	0	1	1	0	0	1
5.0%	SLG	200MW	SG_WG	1	0	0	1	0	0	0	0	0.025	1.038	0.025	1.025	1	0	0	1	1	0	0	1
50.0%	SLG	40MW	SG_SG	1	0	0	1	1	0	1	0	0.025	1.039	0.038	1.024	1	0	0	1	1	0	0	1
50.0%	SLG	200MW	SG_SG	1	0	0	1	0	0	0	0	0.026	1.030	0.026	1.020	1	0	0	1	1	0	0	1
50.0%	SLG	40MW	SG_WG	1	0	0	1	1	0	1	0	0.026	1.040	0.037	1.021	1	0	0	1	1	0	0	1
50.0%	SLG	200MW	SG_WG	1	0	0	1	0	0	0	0	0.026	1.030	0.023	1.022	1	0	0	1	1	0	0	1

Figure 85. Example of information gathered in the Excel File (protection manufacturer A and B). Synchronous generation and strong/weak grid.

    b. In the case of obtaining an unexpected behaviour, the script saves oscillography, in COMTRADE file, from RTDS: Voltages and Currents for each node of the system are stored on directories, classified by scenario, type of fault, generation level and point

of the line. One COMTRADE file is created for all voltages, one COMTRADE file for all currents and one more COMTRADE file for tripping and time signals.

The excel sheet provides information to the user about which tests do not have an expected result. In this way, the user can filter those results most interesting to repeat and analyze by means of protection oscillography download.

The flowcharts for scripting (Flowcharts for scripting and testing in Appendix 4) show, after the fault inception, an oscillography conditional saving box based on the automated behaviour analysis. The function of this oscillography conditional saving option is to store only the signals of those tests where the behaviour of the protection relay is considered wrong (behaviour unexpected). This algorithm evaluates if the protection function passes or fails the test.

The test is considered *passed* if all the following conditions are accomplished, based on TSO criteria:

- The protection must trip within the expected time:
    - For distance protection:
        - Fault within zone 1: Less than 45 ms
        - Fault within zone 2: Between 400 ms and 440 ms
    - For differential protection:
        - Fault inside the protected line: Less than 45 ms
    - For directional protection:
        - Fault forward in the time defined by settings. The time setting is definite time: 200 ms for first step and 600 ms for second step of setting.
- The protection must not to trip when:
    - For distance protection:
        - Fault backwards
    - For differential protection:
        - Fault outside the line
    - For directional protection
        - Fault backwards
- The pole operation of the protection works correctly. A correct behaviour is considered when the protection relay opens the correct pole (or poles) of the breaker, depending on if the fault is single-phase, phase to phase or three-phase.

In other circumstances, the test is considered *failed,* and the oscillography data is saved.

Flowcharts for scripting and testing

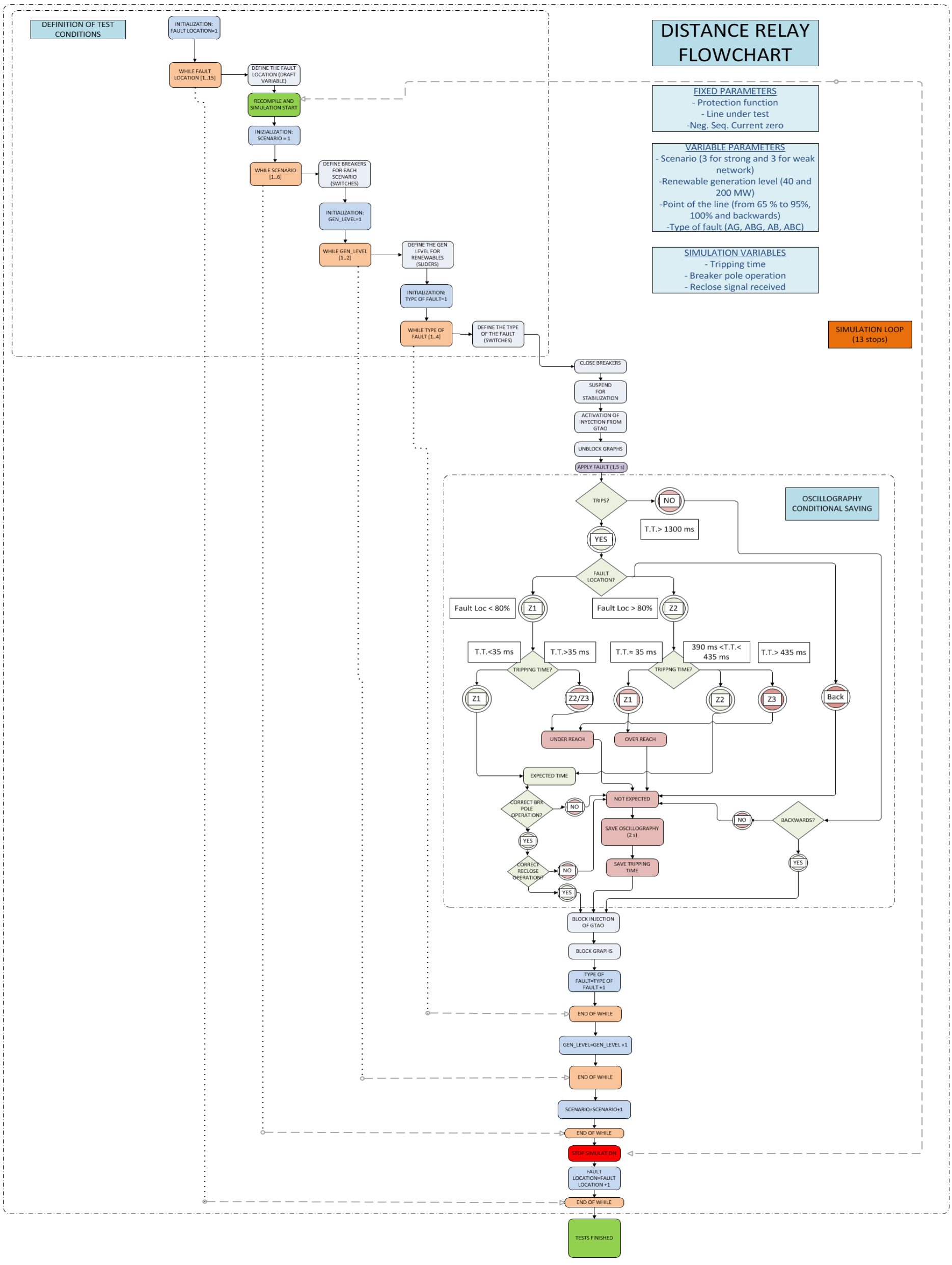

Figure 86. Flowchart for distance function testing.

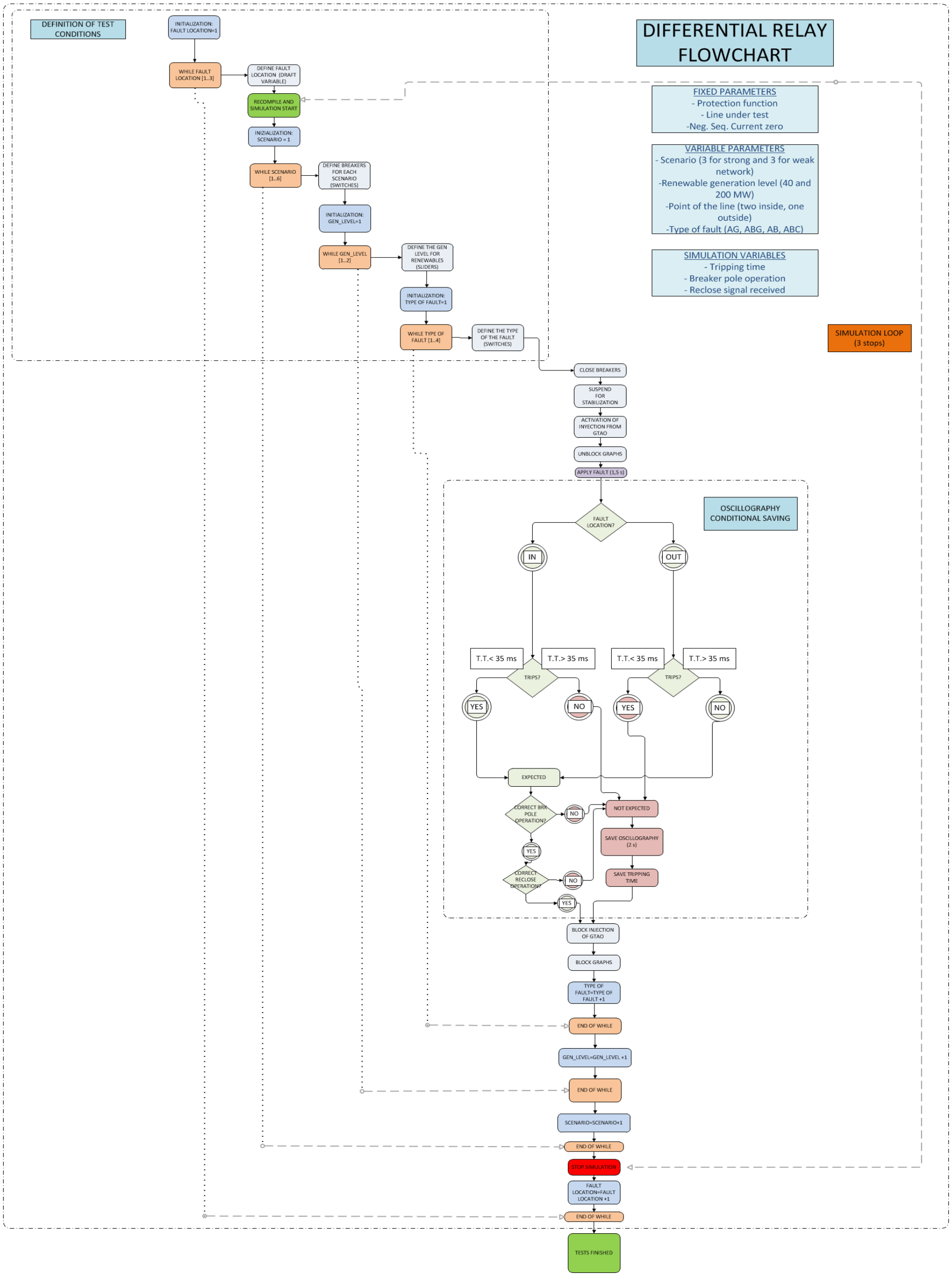

Figure 87. Flowchart for line differential function testing.

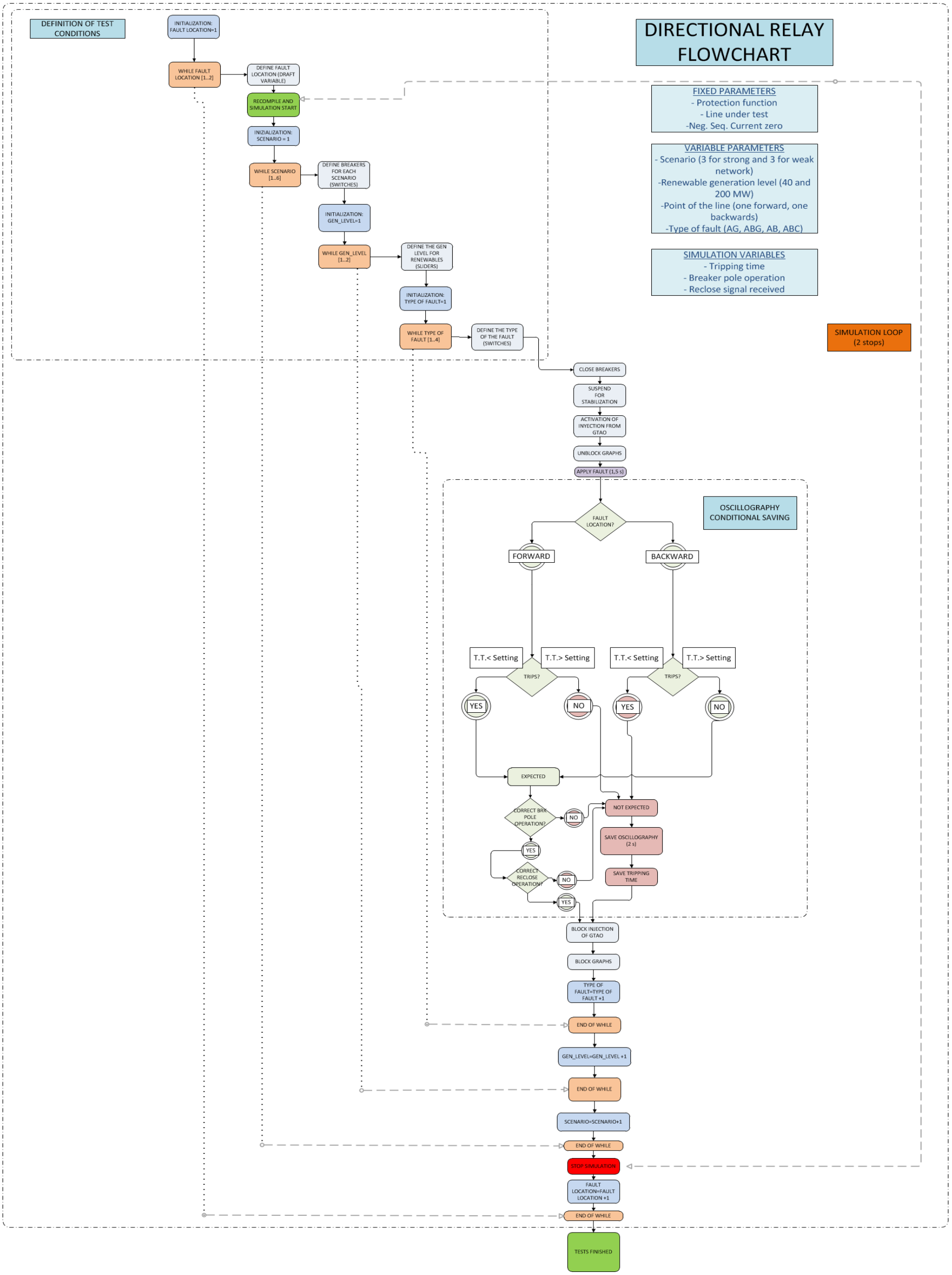

Figure 88. Flowchart for ground directional overcurrent function testing.

Grid configuration for testing

This section explains the different grid configurations used during the test process for the three protection functions.

a Testing line 5-7

Figure 89 and Figure 90 show the grid configuration for tests in line 5-7.

100 % synchronous generation scenario. Grid side: Bus 5. Synchronous Generator Side: Bus 7.

Bus 7: Synchronous Generator

Bus 5: Synchronous Generator

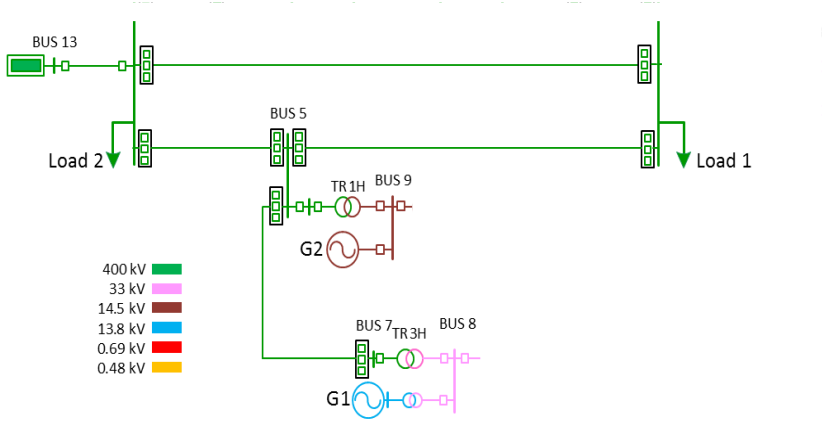

Figure 89. Tests applied to line 5-7: 100% Synchronous generation.

100 % renewable energy scenario. Grid side: Bus 5. Renewable Generator Side: Bus 7.

Bus 7: Type-4 WT

Bus 5: PV generator

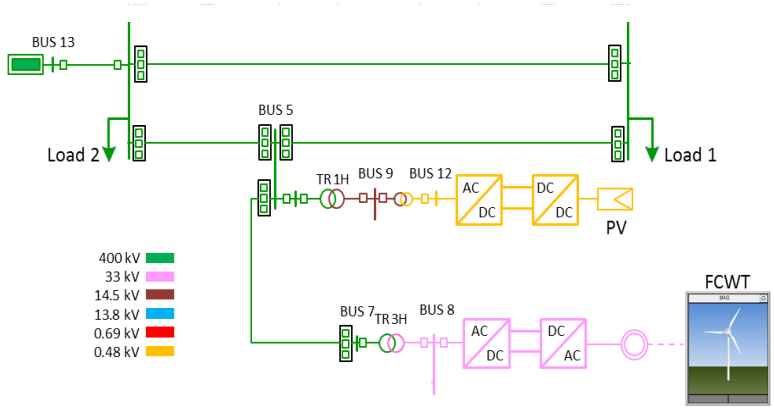

Figure 90. Tests applied to line 5-7: 100% renewable generators(*)[4].

[4] Even when all synchronous generators are disconnected, the slack bus remains connected

b Testing line 4-5 (line 1-5 removed for all the tests)

Figure 91 and Figure 92 show the grid configuration for tests in line 4-5.

100 % synchronous generation scenario. Grid side: Bus 5. Synchronous Generator Side: Bus 4.

Bus 7: Synchronous Generator

Bus 5: Synchronous Generator

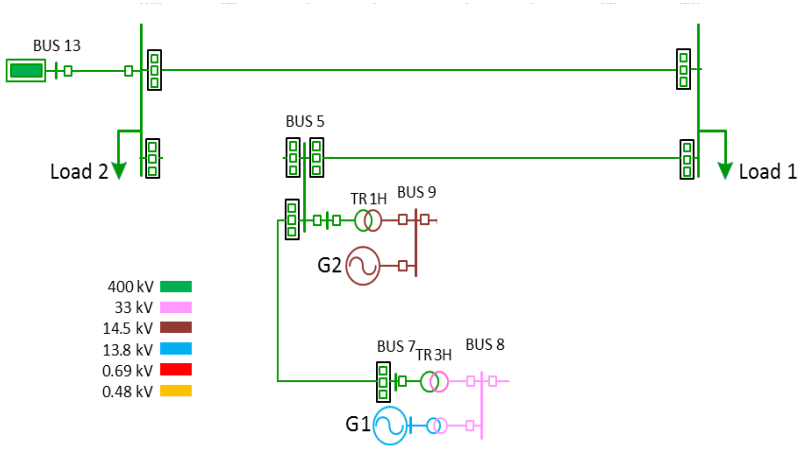

Figure 91. Tests applied to line 4-5. 100% Synchronous generators.

100 % renewable energy scenario. Grid side: Bus 5. Renewable Generator Side: Bus 4.

Bus 7: No generation

Bus 5: PV generator

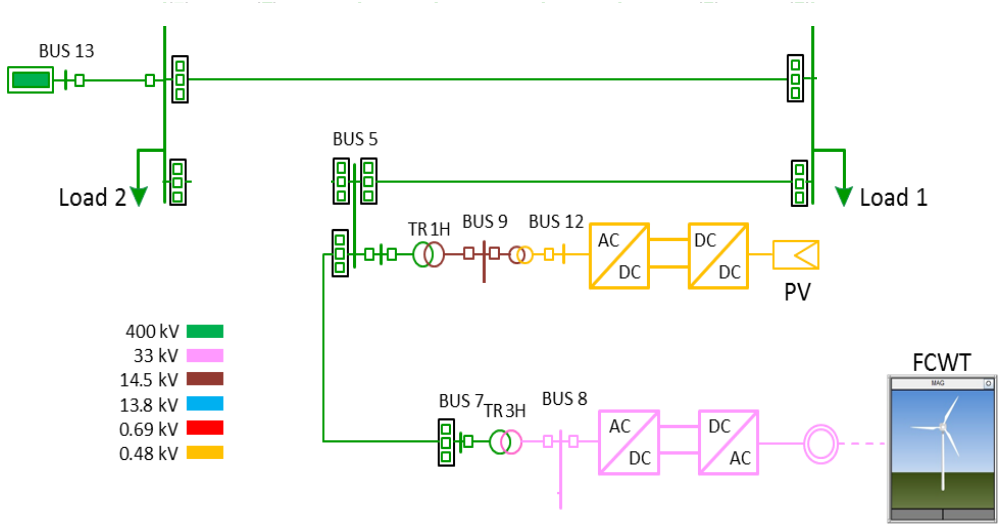

Figure 92. Tests applied to line 4-5. 100% Renewable generators.

Protection Function Settings

To test protection functions, settings are implemented according to standard criteria followed by TSO.

In this chapter the general settings criteria adopted are described.

a Distance Protection (21) Settings

In Distance Protection Function (21), three different zones have been implemented in the two relay manufacturers under test. Note that every manufacturer has its own parameter set, which is implemented differently in each relay. The general settings criteria for each zone are explained below:

Zone 1:

$Zone\ 1\ Reach = 0{,}8\ x\ Zline$

$Zone\ 1\ Time\ Delay = 0ms$

$Zone\ 1\ Directionality = Forward$

Zone 2:

$Zone\ 2\ Reach = 1{,}2\ x\ ZLine$

$Zone\ 2\ Time\ Delay = 400ms$

$Zone\ 2\ Directionality = Forward$

Zone 3:

$Zone\ 3\ Reach = 0{,}65\ x\ Z\_Shortest\_Line\_Connected\_To\_Local\_Busbar$

$Zone\ 3\ Time\ Delay = 1{,}5\ seg$

$Zone\ 3\ Directionality = Reverse$

b Line Differential Protection (87L) Settings

In the Line Differential Protection (87L), the majority of the settings regarding magnitudes of the 87L characteristic (slopes, operation angles…) has been set up with default values, which are valid for the tests developed.

The pickup value for 87L in the traditional algorithm, has been calculated for the maximum capacitive current expected for the line under test:

$I\ Pickup\ 87L = 1{,}1\ x\ I\ Capacitive \rightarrow If\ 1{,}1\ x\ I\ Capacitive > 0{,}2\ x\ I\ Nominal\ Primary\ Current$

$I\ Pickup\ 87L = 0{,}2\ x\ I\ Nominal\ Primary\ Current \rightarrow If\ 1{,}1\ x\ I\ Capacitive < 0{,}2\ x\ I\ Nominal\ Primary\ Current$

c Directional Earth Fault Protection (67N) Settings

Two time delayed steps have been implemented in Directional Earth Fault Protection. The general setting criteria established for these two steps are:

$67N\ Step\ 1\ Pickup = 1{,}1\ x\ 3I0_{Max}\ for\ Ground\ Faults\ at\ 70\%\ of\ Line\ Length$

$67N\ Step\ 1\ Time\ Delay = 200ms$

$67N\ Step\ 2\ Pickup = 0{,}2\ x\ I\ Primary\ Nominal\ Current$

$67N\ Step\ 2\ Time\ Delay = \ 600ms$

Zero sequence voltage (-3V0) has been used as polarizing magnitude, although each manufacturer offers different magnitudes as polarizing quantities, and in some cases, the selection is adaptive.

Validation of settings

For the initial validation of settings for distance protection, the following tests are done using the line 5-7:

- Scenario: Strong and weak network with 100% synchronous generation.
- Type of faults to be applied:
    - Single line to ground (AG):
        - Point of the line: 0% and 50 %
        - Point of the wave: 0 and 90 degrees
        - Fault resistance: 15 ohm
    - Line to line (AB):
        - Point of the line: 0% and 50 %
        - Point of the wave: 0 and 90 degrees
        - Fault resistance: 10 ohm

These test parameters used for validation of distance protection are based on IEC 62055-121:2014 standard for distance protection testing. These conditions apply for radial configurations with current supplied from only one side with the other side without contribution. According to this statement, this way of testing suits for protection relay located at grid side position but not for relay located at synchronous or renewable generator side protection. I.e., according to the network topology, validation according to the standard is applied to a fault inside line 5-7 with protection seeing the current provided by the grid-side (bus 5). This validation for grid-side according to the IEC 62055-121:2014 Standard is applied only once since the criteria followed for grid side protection relay is always the same.

Once this validation is done, the process followed with the three lines under test is based on comparing of protection relay behaviour between the scenarios with only synchronous and with renewable generators based on power electronic converters.

For the *"generator side"*, the the setting validation is done by comparing the renewable scenario results with synchronous generator behaviour. That is, for each line, there is a base scenario with only synchronous generators connected. With the settings provided with TSO criteria, based on usual settings calculation practices, the behaviour of the protection must be:

- For distance protection: Faults within zone 1 must be tripped in less than 45 ms. Faults in zone 2 must be tripped in less than 440 ms.
- For line differential protection: Faults inside the line must be tripped in less than 45 ms. Faults outside the protected line must not trip.
- For ground directional overcurrent: Line to Line faults and three-phase faults must not make the protection trip since there is no ground current flowing. Single line to ground and line to line to ground faults must be tripped by the protection since there is ground current flowing. There are two different tripping times set depending on the current value through the neutral point.

- Once the protection relays are working correctly with 100% synchronous scenario, the base case for the comparison to the renewable scenario is established.

Settings are made according to TSO Criteria used on their own lines for protection. That is, settings used are in line with present practices in the industry.

To validate the settings for each study with renewables, firstly the tests are done for distance (solid faults), line differential (150 ohm phase to ground resistance) and ground directional overcurrent (150 ohm phase to ground) only with synchronous generators connected and renewable ones disconnected. These first results with only synchronous generation must accomplish the actuation times for distance (zone 1 and zone 2), line differential (tripping faults inside and no tripping faults outside) and ground directional overcurrent (tripping faults involving ground and no tripping faults isolated from the ground). Once the protection operates correctly with synchronous generators, there is already a base case where the protection relays are working correctly. This case is compared with the protection relay behaviour when connecting renewable generators instead of synchronous.

Agradecimientos

A mis compañeros de CIRCE donde he tenido la oportunidad de crecer profesionalmente y poder desarrollar la tesis doctoral. Tengo tantas personas a las que debo agradecimiento que no sería justo nombrar a ninguna en concreto. Por ello, muchas gracias a todos los que tengo diariamente la suerte de trabajar codo con codo.

A los compañeros de Red Eléctrica de España (David López, Rubén Andrino, Lucía Pidado y Santiago López), TU Delft (Marjan Popov, José Chavez), Universidad de Manchester (Vladimir Terzija, Sadegh Azizi), Schneider Electric (Henri Grasset, Mike Browne, Christophe Casadoumecq), RTE (Christian Guibout, Aurelien Watare), Elering (Jako Kilter, Andrus Reinson, Marko Tealane); por el periodo de aprendizaje y crecimiento durante las actividades del WP4 del proyecto MIGRATE.

A Mari Paz, mi directora de tesis por la ayuda en el largo camino hasta llegar aquí.

A mi familia quienes, sin duda, serán los que más se alegren del logro que supone finalizar una tesis. En especial a Cris y a Ixeya, quienes más han sufrido este proceso y que con su apoyo en el día a día he conseguido finalizar esta tesis.

Gracias a todos.

Disclaimer

Disclaimer: This thesis reflects the view of the author, based on the results with MIGRATE consortium.

The information, documentation and figures in this thesis are written by the author as a part of MIGRATE project consortium under EC grant agreement No 691800 and do not necessarily reflect the views of the European Commission. The European Commission is not liable for any use that may be made of the information contained herein.

This project has received funding from the European Union's Horizon 2020 research and innovation programme under grant agreement No 691800.